

University of Warwick institutional repository: <http://go.warwick.ac.uk/wrap>

A Thesis Submitted for the Degree of PhD at the University of Warwick

<http://go.warwick.ac.uk/wrap/66673>

This thesis is made available online and is protected by original copyright.

Please scroll down to view the document itself.

Please refer to the repository record for this item for information to help you to cite it. Our policy information is available from the repository home page.

**Amphipathic α -helix mimetics through asymmetric
self-assembly on a metal scaffold**

by

Rebecca Ann Kaner

A thesis submitted in partial fulfilment of the requirements of the degree of
Doctor of Philosophy in Chemistry

Department of Chemistry, University of Warwick

September 2014

Table of Contents

Chapter 1: Anticancer cationic α-helices and their mimetics	1
1.1 Efficacy of DNA damage agents in chemotherapy	2
1.2 Anticancer cationic α -helical peptides	3
1.3 Synthetic mimics of α -helical peptides	7
1.4 Metallohelices	10
1.4.1 Helicates	11
1.4.2 Flexicates	13
1.5 Project aims	15
1.6 References for Chapter 1	17
 Chapter 2: Functionalised symmetrical flexicates	 26
2.1 Introduction	26
2.2 Synthesis of a range of functionalised flexicates	28
2.2.1 Synthesis of functionally diverse dialdehyde units	28
2.2.2 Synthesis of zinc (II) flexicates	31
2.2.3 Synthesis of flexicates with functionalised amine units	40
2.2.4 Synthesis of highly water soluble complexes	42
2.2.5 Water of crystallisation	44
2.2.6 Synthesis of the Hannon helicate	45
2.2.7 Complex stability in aqueous media	46
2.3 Antimicrobial activity	50
2.4 Anticancer activity	52
2.4.1 Cytotoxicity in cancer cells	53
2.4.2 Toxicity in non-cancerous human cells and selectivity	56
2.5 Mode of action	58
2.5.1 Denaturation of ct-DNA	58
2.5.2 Potency over 24 h in HCT116 p53 ^{+/+}	59
2.5.3 Induction of DNA damage	60
2.5.4 Effects on the cell cycle	62
2.5.5 Induction of apoptosis	64
2.6 Summary	66

2.7 References for Chapter 2	67
Chapter 3: Asymmetric triplex metallohelices with high and selective activity against cancer cells	69
3.1 Introduction	69
3.1.1 Design of the structure of a triplex metallohelix	69
3.2 Assembly of triplex metallohelices	72
3.2.1 Molecular modelling of $[M_2(AB-CD)_3]^{4+}$	72
3.2.2 Synthesis of triplex metallohelices	74
3.2.3 Synthesis of highly water soluble triplex metallohelices	80
3.2.4 Water of crystallisation	83
3.2.5 Complex stability in aqueous media	85
3.3 Antimicrobial activity	88
3.4 Anticancer activity	89
3.4.1 MDA-MB-468	89
3.4.2 HCT116 p53 ^{+/+}	90
3.4.3 HCT116 p53 ^{-/-}	91
3.4.4 Toxicity against non-cancerous human cells and selectivity	92
3.5 Mode of action	93
3.5.1 Denaturation of ct-DNA	93
3.5.2 Induction of DNA damage	94
3.5.3 Effects on the cell division cycle	96
3.5.4 Induction of apoptosis	97
3.5.5 Cell localisation	98
3.6 Summary	101
3.7 References for Chapter 3	102
Chapter 4: Progress towards α-helix mimetic metallohelices	104
4.1 Progress through this research project	105
4.2 Potential future developments	107
4.5 References for Chapter 4	109

Chapter 5: Experimental details	110
5.1.1 Solvents and chemicals	110
5.1.2 Equipment and instrumentation	110
5.2 5-hydroxypicolinaldehyde	112
5.3 Dipicolinaldehyde units	116
5.4 Phenylglycinol and derived ethers	128
5.4.1 Phenylglycinol	128
5.4.2 Phenylglycinol derived ethers	130
5.5 Functionalised flexicates	136
5.5.1 $[\text{Zn}_2\text{L}^{2-10}_3][\text{ClO}_4]_4$	136
5.5.2 $[\text{Fe}_2\text{L}^{11-20}_3][\text{ClO}_4]_4$	145
5.5.3 $[\text{Fe}_2\text{L}_3]\text{Cl}_4$	154
5.6 5-(2,2'-bipyridin-5-ylmethoxy)picolinaldehyde	161
5.7 Triplex metallohelices	167
5.7.1 $[\text{Zn}_2\text{L}^{20-26}_3][\text{ClO}_4]_4$	167
5.7.2 $[\text{Fe}_2\text{L}_3]\text{Cl}_4$	175
5.8 Molecular modelling	183
5.9 Biophysical analysis	184
5.9.1 Circular dichroism	184
5.9.2 Thermogravimetric analysis	184
5.9.3 Absorbance spectroscopy and stability	184
5.9.4 Denaturation of ct-DNA	185
5.10 Antimicrobial activity	186
5.11 Pharmacology	187
5.11.1 MTT assay	187
5.11.2 Single cell gel electrophoresis (comet assay)	188
5.11.3 FACS assay ($\gamma\text{-H}_2\text{AX}$ expression and cell cycle analysis)	189
5.11.4 Flow cytometry (apoptosis induction)	190
5.11.5 Cell localisation assay	191
5.12 References for Chapter 5	192
 Appendix A	 193
A.1 Absorbance spectroscopy	193

A.1.1 Circular dichroism spectra	193
A.1.2 Water stability studies	194
A.1.3 Dilute acid stability studies	195
A.2 Thermogravimetric analysis	198
A.3 IC ₅₀ values	200
Appendix B	201
B.1 Optically pure heterobimetallic helicates	201
B.2 Experimental details	203

List of Figures

Figure 1.1	Solution structure of magainin II with labelled hydrophilic (blue) and hydrophobic (green) side chains	4
Figure 1.2	Solution structure of the active core of LL-37, corresponding to residues 13-17	5
Figure 1.3	Solution structure of a stapled peptide, hydrocarbon tether shown in yellow	7
Figure 1.4	Structure of an example hairpin pyrrole-imidazole polyamide	8
Figure 1.5	Structure of a ruthenium (II) metallopeptide	9
Figure 1.6	Schematic diagram of a bimetallic triple helicate $\Delta_M-[M_2(AB-BA)_3]^{n+}$	10
Figure 1.7	Structure of ligand L^B (R and R' range from small polar groups to larger aromatic moieties) and structure of $[Ln_2L^B_3]^{n+}$	11
Figure 1.8	Structure of ligand L^H and structure of $[Fe_2L^H_3]Cl_4$	11
Figure 1.9	Structure of ligand L^V and computed structure $[Fe_2L^V]^{4+}$	12
Figure 1.10	Structure of ligand L^S and structure of a class Ia $\Delta_{Fe}-[Fe_2L^S_3]Cl_4$	13
Figure 1.11	Ligand structure of L^1 and structure of class Ib $\Lambda_{Fe}-[Fe_2L^1_3]Cl_4$	14
Figure 2.1	Cartoon of the strategy to alter the flexicate ligand with a view to producing a library of architectures	27
Figure 2.2	Structure of L^2-L^4 synthesised with flexible aliphatic linkers and structures of the assembled flexicates $\Lambda_{Zn}-[Zn_2L^x_3][ClO_4]_4 \cdot 4H_2O$ ($x = 2-4$)	32
Figure 2.3	(i) Structure of L^5 and L^6 and structures of the assembled flexicates $\Lambda_{Zn}-[Zn_2L^5_3][ClO_4]_4 \cdot 4H_2O$ and $\Delta_{Zn}-[Zn_2L^6_3][ClO_4]_4 \cdot 4H_2O$ (ii) 1H NMR spectrum of $\Lambda_{Zn}-[Zn_2L^6_3][ClO_4]_4 \cdot 4H_2O$ at 298 K in d^3 -acetonitrile (δ_H 1.95, water present δ_H 2.19), recorded using 400 MHz spectrometer	33
Figure 2.4	(i) Structure of L^7 and structures of the assembled flexicates $\Lambda_{Zn}-[Zn_2L^7_3][ClO_4]_4 \cdot 4H_2O$ (ii) 1H NMR spectrum of $\Lambda_{Zn}-[Zn_2L^7_3][ClO_4]_4 \cdot 4H_2O$ at 298 K in d^3 -acetonitrile (δ_H 1.95, water present δ_H 2.19), recorded using 400 MHz spectrometer at 298 K	34
Figure 2.5	(i) Structure of L^8 and structures of the assembled flexicate $\Lambda_{Zn}-[Zn_2L^8_3][ClO_4]_4 \cdot 4H_2O$. (ii) 1H NMR spectra of $\Lambda_{Zn}-[Zn_2L^8_3]$	35

	[ClO ₄] ₄ .4H ₂ O at 253 – 353 K in <i>d</i> ³ -acetonitrile (δ_{H} 1.95, water present δ_{H} 2.19), recorded using 400 MHz spectrometer at 298 K, with magnified area shown in red depicting increasing population of second asymmetric conformer	
Figure 2.6	Structure of L ⁹ and structure of the assembled flexicate Λ_{Zn} -[Zn ₂ L ⁹] ₃ [ClO ₄] ₄ .4H ₂ O	38
Figure 2.7	(i) Structure of L ¹⁰ and structure of the assembled flexicate Λ_{Zn} -[Zn ₂ L ¹⁰] ₃ [ClO ₄] ₄ .4H ₂ O. (ii) ¹ H NMR spectrum of Λ_{Zn} -[Zn ₂ L ¹⁰] ₃ [ClO ₄] ₄ .4H ₂ O at 298 K in <i>d</i> ³ -acetonitrile (δ_{H} 1.95, water present δ_{H} 2.19), recorded using 400 MHz spectrometer at 298 K	39
Figure 2.8	Structure of L ¹¹⁻²⁰ with differing functionality at position R and R' and structures of the assembled flexicates Λ_{Fe} -[Fe ₂ L ^x] ₃ [ClO ₄] ₄ .4H ₂ O (x = 11 – 20)	40
Figure 2.9	Partially resolved crystal structure of Δ_{Fe} -[Fe ₂ L ¹⁴] ₃ [ClO ₄] ₄ .4H ₂ O with acetonitrile molecule occupying the cavity	41
Figure 2.10	(i) Structure of L ⁶ and structure of the assembled flexicate Δ_{Fe} -[Fe ₂ L ⁶] ₃ [Cl ₄] (ii) ¹ H-NMR spectrum (iii) ¹³ C{ ¹ H}-NMR spectrum of Δ_{Fe} -[Fe ₂ L ⁶] ₃ [Cl ₄] in <i>d</i> ⁴ -methanol (δ_{H} 3.31, δ_{C} 49, water present δ_{H} 4.87), recorded using 400 MHz spectrometer at 298 K	43
Figure 2.11	CD spectra of Λ_{Fe} -[Fe ₂ L ⁴] ₃ [Cl ₄] and Δ_{Fe} -[Fe ₂ L ⁴] ₃ [Cl ₄] (0.03 mM) in H ₂ O, showing each pair of enantiomers having equal and opposite spectra	44
Figure 2.12	Infra-red spectrum of Λ_{Fe} -[Fe ₂ L ⁵] ₃ [Cl ₄].9H ₂ O	44
Figure 2.13	Thermogravimetric spectra of Λ_{Fe} -[Fe ₂ L ⁵] ₃ [Cl ₄].9H ₂ O and Δ_{Fe} -[Fe ₂ L ⁵] ₃ [Cl ₄].9H ₂ O, indicating mass lost due to water of crystallisation and thermal decomposition	45
Figure 2.14	(i) Photograph of a 96 well plate containing MDA-MB-468 cells after treatment with Δ_{Fe} -[Fe ₂ L ¹] ₃ [Cl ₄] and addition of MTT. (ii) Photograph of the same 96 well plate after incubation with MTT for 4 h and dissolution of the formazan produced in dimethyl sulfoxide	53
Figure 2.15	IC ₅₀ values of cisplatin (Pt , white), [Fe ₂ L ^H] ₃ [Cl ₄].4H ₂ O (H , hashed) and flexicates [Fe ₂ L ^x] ₃ [Cl ₄] (x = S , 1 , 4 , 5 , 6 , 8) (Δ_{Fe} - light grey, Λ_{Fe} - dark grey) against MDA-MB-468, HCT116 p53 ^{+/+} and HCT116 p53 ^{-/-} cells over 96 h and ligand structure key	54
Figure 2.16	(i) IC ₅₀ values of cisplatin (Pt , white), [Fe ₂ L ^H] ₃ [Cl ₄].4H ₂ O (H , hashed) and flexicates [Fe ₂ L ^x] ₃ [Cl ₄] (x = S , 1 , 4) (Δ_{Fe} - light grey, Λ_{Fe} - dark grey) against ARPE19 over 96 h (ii) comparison of activity of cisplatin (black), Λ_{Fe} -[Fe ₂ L ^S] ₃ [Cl ₄] (red) and Δ_{Fe} -	57

	[Fe ₂ L ⁶ ₃]Cl ₄ (blue) in cancerous HCT116 p53 ^{-/-} and non-cancerous ARPE19 cells, on a logarithmic scale	
Figure 2.17	Effect on T_m of linear ct-DNA (DNA , white) from interactions with [Fe ₂ L ^H ₃]Cl ₄ ·4H ₂ O (H , hashed) and flexicates [Fe ₂ L ^X ₃]Cl ₄ (Δ_{Fe} - light grey, Λ_{Fe} - dark grey) in 1mM Trizma base (10:1 base pair to complex)	59
Figure 2.18	IC ₅₀ values of cisplatin (Pt , white), [Fe ₂ L ^H ₃]Cl ₄ ·4H ₂ O (H , hashed) and flexicates (Δ_{Fe} - light grey, Λ_{Fe} - dark grey) against HCT116 p53 ^{+/+} over 24 h	59
Figure 2.19	Mean γ -H2AX expression of HCT116 p53 ^{+/+} cells (untreated control – white) after treatment with flexicates (10 μ M, Δ_{Fe} - light grey, Λ_{Fe} - dark grey) for 24 h	62
Figure 2.20	% population of HCT116 p53 ^{+/+} cells in each of the phases of the cell cycle after treatment with flexicates (10 μ M) for 24 h compared to a control of untreated cells	63
Figure 2.21	Amount of early apoptotic (dark grey) and late apoptotic / necrotic (light grey) HCT116 p53 ^{+/+} cells after treatment with flexicates (20 μ M) for 72 h, along with an untreated control	65
Figure 3.1	Schematic diagrams of (i) the highly symmetrical Δ_M -[M ₂ (AB-BA) ₃] configuration, (ii) the symmetric $\Delta_\alpha\Delta_\beta$ -Head-to-Head-to-Head [M ₂ (AB-CD) ₃], and (iii) the asymmetric $\Delta_\alpha\Delta_\beta$ -Head-to-Head-to-Tail [M ₂ (AB-CD) ₃] configurations	70
Figure 3.2	structure of L ²¹ and L ^{F1}	72
Figure 3.3	(i) Structure of L ²⁰ and structure of the assembled triplex metallohelix Λ_{Zn} -[Zn ₂ L ²⁰ ₃][ClO ₄] ₄ (ii) ¹ H (500 MHz) and (iii) ¹³ C{ ¹ H} (126 MHz) NMR spectra of $\Lambda_{Zn,HHT}$ -[Zn ₂ L ²⁰ ₃][ClO ₄] ₄ in d ³ -acetonitrile (δ_H 1.95, δ_C 117, water present δ_H 2.19) at 298 K, with some key assignments. * indicates the presence of the HHH-isomer, <i>ca</i> 3%	76
Figure 3.4	(i) Structure of L ²¹ and structure of the assembled triplex metallohelix Λ_{Zn} -[Zn ₂ L ²¹ ₃][ClO ₄] ₄ (ii) ¹ H (500 MHz) and (iii) ¹³ C{ ¹ H} (126 MHz) NMR spectra of $\Lambda_{Zn,HHT}$ -[Zn ₂ L ²¹ ₃][ClO ₄] ₄ in d ³ -acetonitrile (δ_H 1.95, δ_C 117, water present δ_H 2.19) at 298 K, with some key assignments	78
Figure 3.5	Structure of L ²² and structure of the assembled triplex metallohelix $\Lambda_{Zn,HHT}$ -[Zn ₂ L ²² ₃][ClO ₄] ₄	79
Figure 3.6	Structure of L ²³ and structure of the assembled triplex metallohelix $\Lambda_{Zn,HHT}$ -[Zn ₂ L ²³ ₃][ClO ₄] ₄	79

Figure 3.7	Ligand structure of \mathbf{L}^{24} and \mathbf{L}^{25} and structures of the assembled triplex metallohelices $\Lambda_{\text{Zn,HHT}}\text{-}[\text{Zn}_2\mathbf{L}^n_3][\text{ClO}_4]_4$ ($n = \mathbf{24}, \mathbf{25}$)	80
Figure 3.8	Ligand functionality of water soluble iron (II) chloride triplex metallohelices	81
Figure 3.9	(i) Structure of \mathbf{L}^{20} and structure of the assembled triplex metallohelix $\Lambda_{\text{Fe}}\text{-}[\text{Fe}_2\mathbf{L}^{20}_3][\text{Cl}_4]$ (ii) ^1H (500 MHz) and $^{13}\text{C}\{^1\text{H}\}$ (126 MHz) NMR spectra of $\Lambda_{\text{Fe,HHT}}\text{-}[\text{Fe}_2\mathbf{L}^{20}_3]\text{Cl}_4$ in d^4 -methanol (δ_{H} 3.31, δ_{C} 49, water present δ_{H} 4.87) at 298 K, with some key assignments	82
Figure 3.10	CD spectra of $\text{HHT}\text{-}[\text{Fe}_2\mathbf{L}^{20}_3]\text{Cl}_4$ (0.03 mM) in H_2O , each of the pair of enantiomers display an equal and opposite spectrum	83
Figure 3.11	infra-red spectrum of $\Lambda_{\text{Fe,HHT}}\text{-}[\text{Fe}_2\mathbf{L}^{22}_3]\text{Cl}_4$	83
Figure 3.12	Thermogravimetric spectra of $\Lambda_{\text{Fe,HHT}}\text{-}[\text{Fe}_2\mathbf{L}^{20}_3]\text{Cl}_4$ and $\Delta_{\text{Fe,HHT}}\text{-}[\text{Fe}_2\mathbf{L}^{20}_3]\text{Cl}_4$, indicating mass lost due to water of crystallisation and thermal decomposition	84
Figure 3.13	(i) Absorbance spectra of $\Lambda_{\text{Fe,HHT}}\text{-}[\text{Fe}_2\mathbf{L}^{20}_3]\text{Cl}_4$ (0.03 mM in 0.2 M HCl) at 0, 12 and 24 h. (ii) $\ln(\epsilon)$ at 540 nm (corresponding to MLCT band) of $\Delta_{\text{Fe,HHT}}\text{-}[\text{Fe}_2\mathbf{L}^{20}_3]\text{Cl}_4$ (0.03 mM in 0.2 M HCl)	86
Figure 3.14	IC_{50} values of cisplatin (Pt , white), $[\text{Fe}_2\mathbf{L}^{\text{H}}_3]\text{Cl}_4 \cdot 4\text{H}_2\text{O}$ (H , hashed) and the panel of triplex metallohelices (Δ_{Fe} - light grey, Λ_{Fe} - dark grey) against MDA-MB-468 over 96 h	89
Figure 3.15	IC_{50} values of cisplatin (Pt , white), $[\text{Fe}_2\mathbf{L}^{\text{H}}_3]\text{Cl}_4 \cdot 4\text{H}_2\text{O}$ (H , hashed) and the panel of triplex metallohelices (Δ_{Fe} - light grey, Λ_{Fe} - dark grey) against HCT116 p53 ^{+/+} over 96 h	90
Figure 3.16	IC_{50} values of cisplatin (Pt , white), $[\text{Fe}_2\mathbf{L}^{\text{H}}_3]\text{Cl}_4 \cdot 4\text{H}_2\text{O}$ (H , hashed) and $\text{HHT}\text{-}[\text{Fe}_2\mathbf{L}^x_3]\text{Cl}_4$ ($x = \mathbf{21}\text{-}\mathbf{24}, \mathbf{26}$) (Δ_{Fe} - light grey, Λ_{Fe} - dark grey) against HCT116 p53 ^{-/-} over 96 h	91
Figure 3.17	(i) IC_{50} values of cisplatin (Pt , white), $[\text{Fe}_2\mathbf{L}^{\text{H}}_3]\text{Cl}_4 \cdot 4\text{H}_2\text{O}$ (H , hashed) and the most active of the panel of triplex metallohelices against ARPE19 cells over 96 h, presented on a logarithmic scale. (ii) Comparison of activity of Cisplatin, $\Delta_{\text{Fe,HHT}}\text{-}[\text{Fe}_2\mathbf{L}^{20}_3]\text{Cl}_4$ and $\Lambda_{\text{Fe,HHT}}\text{-}[\text{Fe}_2\mathbf{L}^{25}_3]\text{Cl}_4$ in HCT116 p53 ^{-/-} and ARPE19 cells	92
Figure 3.18	Effect on T_{m} of linear ct-DNA (DNA , white) from interactions with $[\text{Fe}_2\mathbf{L}^{\text{H}}_3]\text{Cl}_4 \cdot 4\text{H}_2\text{O}$ (H , hashed) and triplex metallohelices in 1mM Trizma base (10:1 base pair to complex)	93
Figure 3.19	Fluorescence microscopy images of single untreated control HCT116 p53 ^{+/+} cells, those exposed to $\Lambda_{\text{Fe,HHT}}\text{-}[\text{Fe}_2\mathbf{L}^{20}_3]\text{Cl}_4$ (20 μM) for 24 h, those exposed to H_2O_2 for 30 min and those exposed	94

	to both $\Lambda_{\text{Fe,HHT}}\text{-}[\text{Fe}_2\text{L}^{20}]_3\text{Cl}_4$ and H_2O_2	
Figure 3.20	Mean $\gamma\text{-H2AX}$ expression of HCT116 $\text{p53}^{+/+}$ cells (untreated control – white) after treatment with $\text{HHT-}[\text{Fe}_2\text{L}^{20}]_3\text{Cl}_4$ or $\text{HHT-}[\text{Fe}_2\text{L}^{\text{F1}}]_3\text{Cl}_4$ (10 μM , Δ_{Fe} – light grey, Λ_{Fe} – dark grey) for 24 h	95
Figure 3.21	Cell Cycle FACS Assay showing the % population of HCT116 $\text{p53}^{+/+}$ cells when treated with $\Lambda_{\text{Fe,HHT}}\text{-}[\text{Fe}_2\text{L}^{21}]_3\text{Cl}_4$ and $\Delta_{\text{Fe,HHT}}\text{-}[\text{Fe}_2\text{L}^{\text{F1}}]_3\text{Cl}_4$ (10 μM) for 24 h and a control of untreated cells	96
Figure 3.22	Amount of early apoptotic (annexin-v positive, propidium iodide negative) and late apoptotic / necrotic (annexin-v positive, propidium iodide positive) HCT116 $\text{p53}^{+/+}$ cells after incubation for 72 h with 20 μM of each compound, compared to an untreated control	97
Figure 3.23	Fluorescence microscopy images of HCT116 $\text{p53}^{-/-}$ cells treated with different concentrations – (a) 1 μM , (b) 3 μM , (c) 10 μM , (d) 30 μM – of $\Delta_{\text{Fe,HHT}}\text{-}[\text{Fe}_2\text{L}^{25}]_3\text{Cl}_4$ for 48 h and stained with AlexaFluor® 555 azide	99
Figure 4.1	Schematic diagram of a symmetrical flexicate metallohelix	105
Figure 4.2	Schematic diagram of an asymmetric HHT triplex metallohelix	106
Figure 4.3	Schematic diagram of a hairpin-tethered HHT metallohelix	107
Figure A.1	Circular Dichroism spectra of each pair of $[\text{Fe}_2\text{L}_3]\text{Cl}_4$ enantiomers in water (0.03 mM)	193
Figure A.2	$\ln(\epsilon)$ at 540 nm (corresponding to MLCT band) of iron (II) chloride triplex metallohelices (0.03 mM in water)	194
Figure A.3	$\ln(\epsilon)$ at 540 nm (corresponding to MLCT band) of iron (II) chloride flexicates and triplex metallohelices (0.03 mM in 0.2 M HCl)	195
Figure A.4	Thermogravimetric analysis of iron (II) chloride flexicates and triplex metallohelices, indicating mass lost due to water of crystallisation and thermal decomposition	198
Figure B.1	Structure of L^{26} designed for formation of a heterobimetallic complex	201
Figure B.2	Structure of the cation in the asymmetric unit of $\text{fac},\Lambda_{\text{Fe}},R_{\text{C}}\text{-}[\text{FeL}^{26}]_3(\text{ClO}_4)_2\cdot\text{CH}_3\text{CN}$ (H atoms, counterions and solvent molecules omitted for clarity)	202

List of Schemes

Scheme 2.1	Synthesis of dipicolinaldehyde units 5-7 via 5-hydroxy picolinaldehyde (4)	28
Scheme 2.2	Synthesis of 5,5'-(2,2'-oxybis(ethane-2,1-diyl)bis(oxy)) dipicolinaldehyde (9) via 1-bromo-2-(2-bromoethoxy)ethane (8)	29
Scheme 2.3	Synthesis of 5,5'-(but-2-yne-1,4-diylbis(oxy))dipicolinaldehyde (11) via 1,4-dibromobut-2-yne (10) and (E)-5,5'-(but-2-ene-1,4-diylbis(oxy))dipicolinaldehyde (12)	29
Scheme 2.4	Synthesis of 5,5'-(1,4-phenylenebis(methylene))bis(oxy) dipicolinaldehyde (13), 5,5'-(1,3-phenylenebis(methylene))bis(oxy) dipicolinaldehyde (14) and 5,5'-(4,4'-methylenebis(4,1-phenylene)bis(methylene))bis(oxy) dipicolinaldehyde (16) via bis(4-(bromomethyl)phenyl)methane (15)	30
Scheme 2.5	Synthesis of bis(6-formylpyridin-3-yl) glutarate (17)	31
Scheme 2.6	Self-assembly of flexicate $\Lambda_{\text{Zn}}\text{-}[\text{Zn}_2\text{L}^1_3][\text{ClO}_4]_4\cdot 4\text{H}_2\text{O}$	31
Scheme 2.7	Reduction of phenylglycene to phenylglycinol and subsequent modified ether synthesis	40
Scheme 2.8	Self-assembly of the known helicate, $[\text{Fe}_2\text{L}^{\text{H}}_3]\text{Cl}_4\cdot 4\text{H}_2\text{O}$	46
Scheme 2.9	Cellular reduction of soluble yellow 3-(4,5-dimethylthiazol-2-yl)-2,5-diphenyltetrazolium bromide (MTT) to insoluble purple formazan	52
Scheme 3.1	Synthesis of 5-(2,2'-bipyridin-5-ylmethoxy)picolinaldehyde (30) via 5-(chloromethyl)-2,2'-bipyridine (29)	74
Scheme 3.2	Self-assembly of a triplex metallohelix $\Lambda_{\text{Zn,HHT}}\text{-}[\text{Zn}_2\text{L}^{20}_3][\text{ClO}_4]_4$	75
Scheme 3.3	Copper (II) mediated click azide-alkyne reaction between $\Delta_{\text{Fe,HHT}}\text{-}[\text{Fe}_2\text{L}^{26}_3]\text{Cl}_4$ and AlexaFluor® 555 (structure not yet published by Invitrogen)	98

List of Tables

Table 2.1	Calculated structures, relative energies (compared to <i>endo1</i>) and Zn-Zn distances of the six conformational isomers of $\Lambda_{\text{Zn}}\text{-}[\text{Zn}_2\text{L}^8_3][\text{ClO}_4]$	37
Table 2.2	Recorded and theoretical elemental analysis of $\Lambda_{\text{Fe}}\text{-}[\text{Fe}_2\text{L}^5_3]\text{Cl}_4\cdot 9\text{H}_2\text{O}$ and $\Delta_{\text{Fe}}\text{-}[\text{Fe}_2\text{L}^5_3]\text{Cl}_4\cdot 9\text{H}_2\text{O}$	45
Table 2.3	Solution half-life ($t_{1/2}$) of MLCT band (540 nm) for the iron (II) chloride flexicates, 0.03 mM in 0.2 M hydrochloric acid (pH 1.0) at 20°C	47
Table 2.4	% integrity in MLCT band (540 nm) after 96 h in RPMI-1640 cell culture medium at 37°C	48
Table 2.5	MIC values for ampicillin, class Ia ($\Lambda_{\text{Fe}}\text{-}[\text{Fe}_2\text{L}^S_3]\text{Cl}_4$) and class Ib ($\Lambda_{\text{Fe}}\text{-}[\text{Fe}_2\text{L}^x_3]\text{Cl}_4$, $x = 1, 4\text{-}6$) flexicates, and $[\text{Fe}_2\text{L}^H_3]\text{Cl}_4\cdot 4\text{H}_2\text{O}$ against <i>Staphylococcus aureus</i> , USA300 (MRSA) and <i>Escherichia coli</i> , TOP10 (<i>E. Coli</i>) over 20 h at 37°C in Mueller-Hinton broth	50
Table 2.6	Mean tail moments of 50 comets, indicating the level of SSB X-link DNA damage caused by 20 μM flexicates to HCT116 p53 ^{+/+} cells after 24 h exposure, with an untreated control (0% SSB) and H ₂ O ₂ (100% SSB, 0% X-link)	59
Table 3.1	Relative energies (compared to $\Delta_\alpha\Delta_\beta\text{-HHT}$) of calculated structures of $[\text{M}_2(\text{S})\text{-L}^{21}_3]^{4+}$ ($\text{M} = \text{Zn(II)}, \text{Fe(II)}$) and predicted percentage Boltzmann population of each isomer at 298 K (calculated from the energy difference between each isomer and the lowest energy isomer, including a statistical correction term)	73
Table 3.2	Recorded and theoretical elemental analysis of $\Lambda_{\text{Fe},\text{HHT}}\text{-}[\text{Fe}_2\text{L}^{20}_3]\text{Cl}_4$ and $\Delta_{\text{Fe},\text{HHT}}\text{-}[\text{Fe}_2\text{L}^{20}_3]\text{Cl}_4$	85
Table 3.3	Solution half-life ($t_{1/2}$) of MLCT band (540 nm) for triplex metallohelices and $[\text{Fe}_2\text{L}^H_3]\text{Cl}_4\cdot 4\text{H}_2\text{O}$ (0.03 mM) in water (pH 7.0), <i>a</i> Complete hydrolysis observed in 19 days	85
Table 3.4	Solution half-life ($t_{1/2}$) of MLCT band (540 nm) for triplex metallohelices and $[\text{Fe}_2\text{L}^H_3]\text{Cl}_4\cdot 4\text{H}_2\text{O}$ (0.03 mM), 0.2 M hydrochloric acid (pH 1.0) <i>a</i> No hydrolysis observed over the time period of the experiment (10 days)	87
Table 3.5	% integrity in MLCT band (540 nm) of triplex metallohelices and $[\text{Fe}_2\text{L}^H_3]\text{Cl}_4\cdot 4\text{H}_2\text{O}$, (0.03 mM) after 96 h in RPMI-1640 cell culture medium at 37°C	87

Table 3.6	MIC values for triplex metallohelices, along with positive controls, $\Lambda_{\text{Fe}}\text{-}[\text{Fe}_2\text{L}^{\text{S}}_3]\text{Cl}_4$, the helicate racemate and ampicillin against gram-positive <i>Staphylococcus aureus</i> , USA300 (MRSA) and gram-negative <i>Escherichia coli</i> , TOP10 (<i>E. Coli</i>) over 20 h at 37°C in Mueller-Hinton broth	88
Table 3.7	Mean tail moments of 50 comets, indicating the level of SSB X-link DNA damage caused by triplex metallohelices (20 μM , 24 h) to HCT116 p53 ^{+/+} cells, with an untreated control (0% SSB) and H ₂ O ₂ (100% SSB, 0% X-link)	95
Table A.1	IC ₅₀ values of cisplatin, $[\text{Fe}_2\text{L}^{\text{H}}_3]\text{Cl}_4$ and all iron (II) chloride complexes against MDA-MB-468, HCT116 p53 ^{+/+} , HCT116 p53 ^{-/-} and ARPE19 cells over 96 h, and HCT116 p53 ^{+/+} cells over 24 h	200

Acknowledgements

Firstly, I would like to thank my supervisor Professor Peter Scott for giving me the opportunity to work on this project as well as for all the guidance, support and knowledge over the last four years. Many thanks go to Warwick University for funding this project throughout my PhD. I would particularly like to thank Scott group members Dr Suzanne Howson, Dr Alan Faulkner, Daniel Simpson and Pratik Gurnani for their invaluable contributions to this project.

Thanks also go to other members of the Chemistry Department at Warwick and those at the Institute of Cancer Therapeutics for their help with this project: Dr Roger Philips, Dr Qasem Abdallah, Dr Simon Philips and the rest of ICT for the guidance and opportunity to work alongside them in the anticancer studies; Dr Ivan Prokes for help with NMR spectrometry; Dr Lijiang Song and Philip Aston for help with mass spectrometry; Dr Guy Clarkson for all the crystallography; Professor Alison Rodger and Dr Nikola Chmel for allowing me to use their facilities and for all the help with the spectroscopic studies; Professor Peter Sadler and Dr Paul Taylor for being on my advisory panel and giving me helpful suggestions.

Special thanks must go to all of the other Scott group members, past and present for all of their help and involvement in my project especially Dr Christopher Kay, Connah Burnett and Paul Goring for helping me enjoy everyday life in the lab. I would like to thank all my family; my Mum, my Dad and Robert, as well as all my friends for all their support and encouragement. Finally I would like to thank my long suffering boyfriend Dom for saving my sanity a thousand times during my PhD.

Publications

Chapter 2

“Metallohelices with activity against cisplatin-resistant cancer cells; does the mechanism involve DNA binding?” V. Brabec, S. E. Howson, **R. A. Kaner**, R. M. Lord, J. Malina, R. M. Phillips, Q. M. A. Abdallah, P. C. McGowan, A. Rodger and P. Scott, *Chem. Sci.*, 2013, **4**, 4407-4416.

Chapter 3

“Asymmetric triplex metallohelices with high and selective activity against cancer cells” A. D. Faulkner,[†] **R. A. Kaner**,[†] Q. M. A. Abdallah, G. Clarkson, D. J. Fox, P. Gurnani, S. E. Howson, R. M. Phillips, D. I. Roper, D. H. Simpson and P. Scott, *Nat. Chem.*, 2014, **6**, 797-803 ([†]contributed equally to this work).

Others (Appendix B)

“Optically pure heterobimetallic helicates from self-assembly and click strategies” S. E. Howson, G. J. Clarkson, A. D. Faulkner, **R. A. Kaner**, M. J. Whitmore & P. Scott, *Dalton Trans*, 2013, **42**, 14967-14981.

Declaration

The work performed in this thesis was carried out in the Department of Chemistry, University of Warwick between October 2010 and September 2014. Unless otherwise stated it is the work of the author and has not been submitted in whole or in part for any degree at this or any other university.

Summary

Chapter 1 | Reviews innate host-defence α -helices and their mimetics as potential anticancer chemotherapeutics. Introduces biologically relevant bimetallic triple metallohelices as potential non-peptide mimics, and reviews the known flexicates. Discusses the criteria such compounds would need to satisfy in order to be successful anticancer agents.

Chapter 2 | Describes the discovery, synthesis and characterisation of nineteen new class Ib flexicates with varying ligand functionality. These compounds are found to be highly active and selective in cancer, with no observed activity in bacteria. Preliminary modes of action studies indicate that they do not act through DNA interactions, but cause changes to the cell cycle and induce programmed cell death.

Chapter 3 | Describes the conception, synthesis and characterisation of a new asymmetric type of architecture, named a triplex metallohelix. A range of these novel complexes are found to be highly active and selective in several cancer cell lines. Possible modes of action found the triplex metallohelices do not bind or damage DNA, but do cause changes to the cell cycle, induce programmed cell death and appear to localise on the cellular membrane of colon cancer cells.

Chapter 4 | Summarises the aims and results of this research project and concludes this work by discussing the perspectives of the novel metallohelices described as α -helix mimetics. Final remarks consider some possible directions that this research could take in the future.

Chapter 5 | Provides details of the experimental procedures used to carry out the work in this thesis.

Glossary and Abbreviations

Most of the abbreviations and symbols used in this thesis are in common use within the scientific community. Necessary abbreviations and a glossary of terms used in this work are given below:

Adenocarcinoma	Cancerous gland cells
Albumin	Water soluble globulin protein found in blood plasma
AlexaFluor 555® azide	Orange-fluorescent tag designed to only fluoresce after reacting with an alkyne group in a copper (II) catalysed click reaction
Alkylator	Compound which covalently adds alkyl groups to nucleic acids
Amphipathic	Molecule containing both hydrophobic and hydrophilic groups or surfaces
Amphiphilic	Molecule containing groups that enable it to interact favourably with both hydrophobic and hydrophilic environments
Amyloid-β	Small peptide with a crucial role in Alzheimer's disease
Annexin-V-FLUOS	Fluorescent-conjugated anticoagulant for the detection of phosphatidylserine on the cell membrane of apoptotic cells
Antimetabolite	Chemical which interferes with the function of a metabolite
Apoptosis	The process of programmed cell death
ARPE19	Human retinal pigment epithelial cells (non-cancerous)
bpy	2,2'-bipyridine
CAP18	Example cathelicidin protein
Carcinogenesis	The process by which cancerous tumours form
Carcinoma	Cancerous epithelial cells
Cathelicidin	Family of innate proteins with a role in host-defence

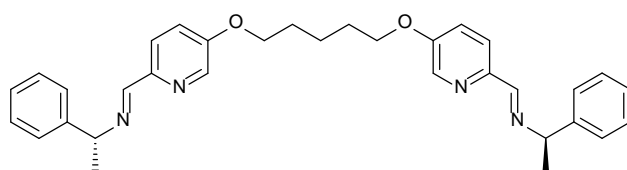
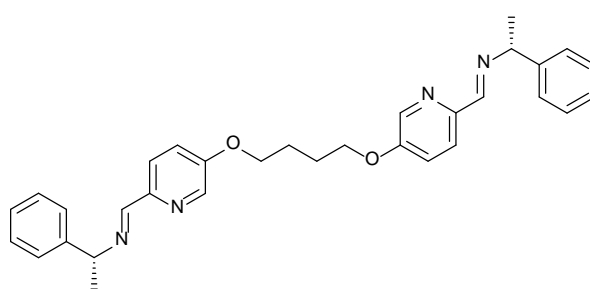
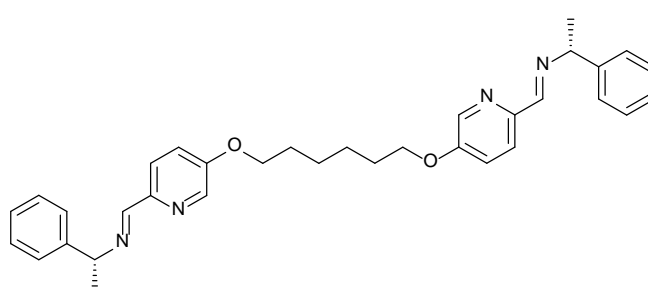
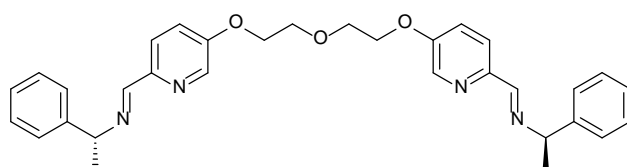
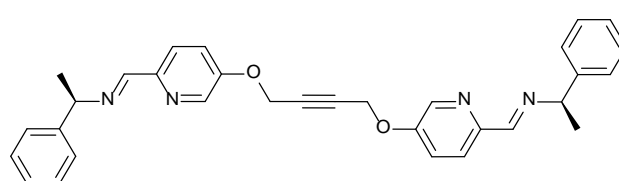
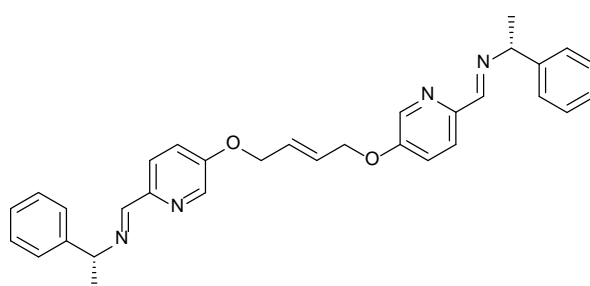
CD	Circular dichroism
Cell cycle	The series of processes by which a cell divides itself to form two daughter cells by duplicating its DNA ($N_{\text{DNA}} =$ amount of DNA compared to a cell at rest)
ct-DNA	Calf thymus DNA, a heterogeneous mixture of linear DNA fragments
Sub G₁ phase	Cells in the cell cycle which are considered apoptotic ($N_{\text{DNA}} < 1$)
G₁ phase	Gap 1: cells in the cell cycle which have increased in size but not begun to synthesise duplicate DNA ($N_{\text{DNA}} = 1$)
S phase	Synthesis: cells in the cell cycle which are replicating their DNA ($1 < N_{\text{DNA}} < 2$)
G₂/M phase	Gap 2: checkpoint in the cell cycle between synthesis of DNA and cell division. Mitosis: cells in the cell cycle are dividing into two daughter cells ($N_{\text{DNA}} = 2$)
Chemotherapy	Treatment of cancer by the use of anti-cancer drugs
Click reaction	1,3-dipolar reaction between a molecule with a terminal azide and a molecule with a terminal alkyne to give a 1,2,3-triazole
Click-iT	Click labelling reaction assay kit from Life Technologies
Cytotoxicity	The measure the toxicity of a compound towards a cell
Down-regulated	Reduced production of an innate compound compared to the expected normal amount
DSB	Double strand DNA breaks
Epithelial	Cells which line the membranes of an animal
FACS	Fluorescence-activated cell sorting
Fibroblast	Cells which form connective tissue in animals
FK-16	Fragment of LL-37, corresponding to residues 13-37
Flexicate	Bimetallic complex formed of two independent, optically pure, monometallic, octahedral iron (II) or

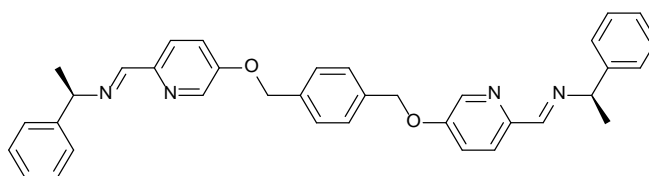
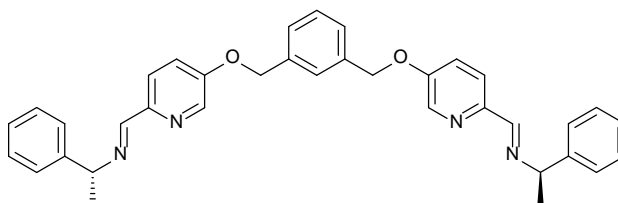
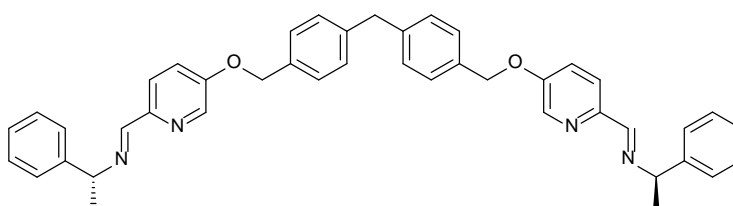
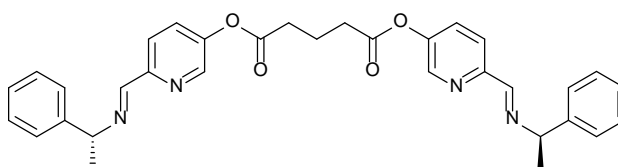
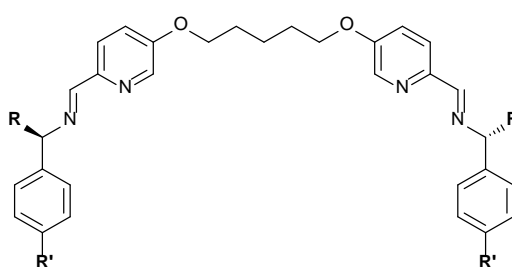
	zinc (II) iminopyridine subunits, connected by three linear linkers
Class Ia	Flexicate where the two subunits are connected by the imine side of the chiral imino-pyridine
Class Ib	Flexicate where the two subunits are connected by the pyridine side of the chiral imino-pyridine
Flow cytometry	Method of cell sorting or counting
Gel electrophoresis	Method for the separation and analysis of biological macromolecules by applying a potential gradient
HCT116 p53^{+/+}	Colon carcinoma cells with wild type (non-mutated) p53
HCT116 p53^{-/-}	Colon carcinoma cells with mutated p53
Helicand	Sufficiently short or rigid ligand capable of mechanically coupling the stereochemistry of two or more metal centres in a multimetallic complex
Helicate	Multimetallic complex connected by linear linkers which mechanically couple the stereochemistries of the metal centres to each other
HHH	Head to Head to Head constitution of a bimetallic complex with directional linkers
HHT	Head to Head to Tail constitution of a bimetallic complex with directional linkers
HMQC	Heteronuclear multiple quantum coherence $^1\text{H} - ^{13}\text{C}$ coupling NMR experiment
Host-defence	The process by which an organism protects itself from microbial invasion
IC₅₀	Half maximal inhibitory concentration
Immunostimulant	Molecule which promotes the immune ability of a host
Intercalator	Molecule which can insert flat aromatic groups between base pairs of a DNA strand
LL-37	The active α -helical peptide from human cathelicidin hCAP18

Lysis	The breaking down of a cell through disintegration of the cell membrane
MDA-MB-468	Breast adenocarcinoma cell line
<i>m</i>-xylenyl	Derived from 1,3-bis(bromomethyl)benzene
MIC	Minimum inhibitory concentration
Microvilli	Cellular membrane protrusions which increases the surface area of a cell
MLCT	Metal-ligand charge transfer
MTT	3-(4,5-dimethylthiazol-2-yl)-2,5-diphenyltetrazolium salt, a yellow tetrazole dye
MTT assay	Quantitative colorimetric assay to assess cell viability after treatment with a chemical agent
Necrosis	Premature cell death caused by external factors
p53	Protein which is involved in cell cycle regulation and activation of apoptosis in cells
<i>p</i>-xylenyl	Derived from 1,4-bis(bromomethyl)benzene
PBS	Phosphate buffered saline
Pharmacokinetics	How a drug is affected and metabolised by a cell or animal after treatment
Proteolytic cleavage	The breaking of peptide bonds
Quadruplex DNA	A structure of four strands of DNA stabilised by a cation
RPMI-1640	Roswell Park Memorial Institute phosphate rich cell culture medium
Serum	From clotted blood
SSB	Single strand DNA breaks
$t_{1/2}$	Half-life
TGA	Thermogravimetric analysis
T_m	Temperature at which DNA unwinds from a double helix to random coil state

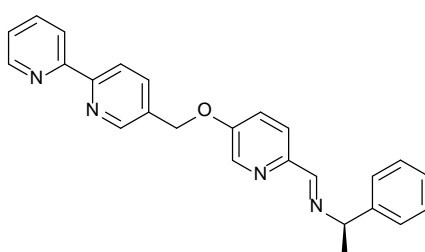
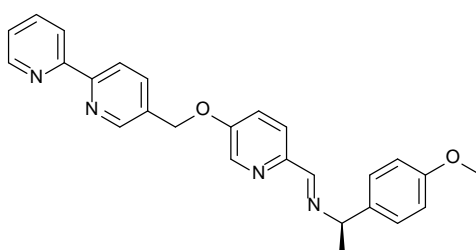
Transcription	The act of copying a strand of DNA to RNA
Triplex DNA	Triple helix architecture of DNA
Triplex metallohelix	Bimetallic complex where two optically pure iron (II) or zinc (II) metal centres scaffold three linear directional ligands in an HHT constitution
Triton-X	Non-ionic surfactant that permeabilises cell membranes
Up-regulated	Increased production of an innate compound compared to the expected normal amount
X-link	DNA cross link
Zwitterionic	A molecule containing both positive and negative charges
β-lactam	Four-membered cyclic amide where the nitrogen is attached to the β -carbon, which makes up the core structure of many antibiotics
γ-H₂AX	Primary rabbit anti-human phosphor histone

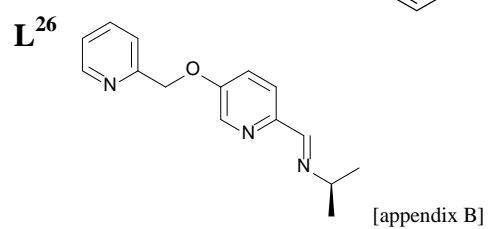
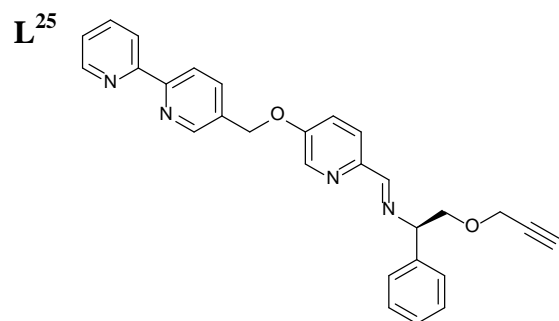
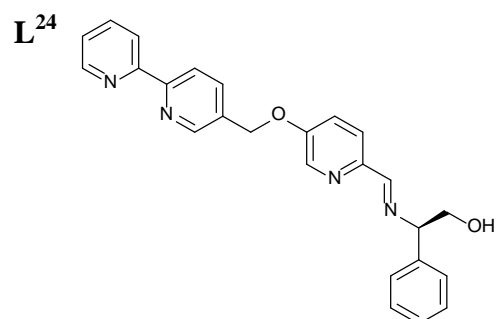
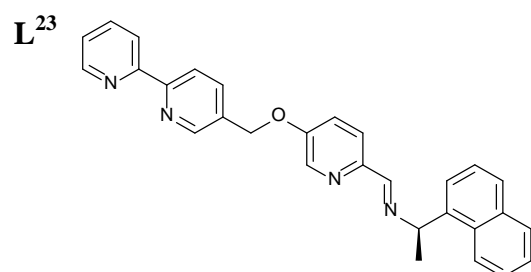
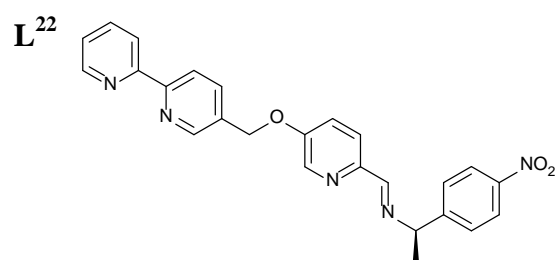
Ligands used in this Thesis

L¹**L²****L³****L⁴****L⁵****L⁶**

L⁷**L⁸****L⁹****L¹⁰****L¹¹-L¹⁹**

L¹¹-L¹⁵ R': H	L¹⁶-L¹⁹ R: H
L¹¹ R: CH₃	L¹⁶ R': CH₃
L¹² R: OCH₃	L¹⁷ R: OCH₃
L¹³ R: OCH₂CHCH₂	L¹⁸ R: NO₂
L¹⁴ R: OCH₂Ph	L¹⁹ R: Cl
L¹⁵ R: OCH₂Naph	

L²⁰**L²¹**



Chapter 1

Anticancer cationic α -helices and their mimetics

There is a need to develop new cancer chemotherapeutic drugs¹ which are selective against tumour cells, with a particular drive to discover systems that exhibit different modes of action to traditional DNA damage agents.^{2, 3} Host-defence peptides have been investigated as potential anticancer agents with this aim.⁴⁻⁶ However these innate proteins are not ideal chemotherapeutic candidates as they tend to suffer from poor selectivity and pharmacokinetics.⁷⁻¹⁰ The design of mimetic systems with more desirable drug-like properties is an area of intense investigation.¹¹ Successful strategies include the synthesis of peptidic foldamers,¹² stapled peptides,¹² non-peptide oligomers¹³⁻¹⁵ and metallopeptides;^{16, 17} all of which seek to imitate some of the function and structure of α -helices.

Following early comments on the matter by Lehn,¹⁸ helicates – formed when rigid linear organic ligands are arranged around a metal scaffold – have received significant attention.¹⁹⁻²³ Some of these assemblies are of a similar size to peptidic α -helices,²⁴⁻²⁶ and the advancement of the paradigm that metallohelices may function as peptidomimetics is the subject of this thesis.

In this chapter the current outlook for cationic peptidic α -helices and their synthetic analogues as chemotherapeutic agents in cancer are reviewed. Some examples of metallohelices are described in this context.

1.1 Efficacy of DNA damage agents in chemotherapy

Cancerous cells are typically genetically unstable, arising from a loss of regulation of the cell cycle and an absence of DNA repair.²⁷ These phenomena can be exploited by chemotherapeutic agents in several ways. Irreversible damage of DNA within the cancer cell by alkylators,^{2, 3} cyclophosphamide²⁸ and cisplatin,^{29, 30} induces apoptosis.³¹ Antimetabolites, such as 5-fluorocil,³² act by preventing the replication of DNA, which inhibits cell reproduction.³³ Doxorubicin³⁴ and other anthracyclines are so called anticancer antibiotics which act by intercalating DNA and preventing transcription, which can then lead to cell death.³⁵ These DNA damage agents often show little or no selectivity towards cancerous over non-cancerous cells, leading to off-target interactions and undesirable side effects.³⁶

The genetic instability of cancer cells means they are also able to build up multidrug resistance.²⁷ An example of this is the mutation of p53,^{37, 38} a protein which is key in the activation of some apoptotic pathways.^{39, 40} Stimulation of p53 associated cell death is often part of the mode of action of a DNA damage agent and mutations which prevent this could cause the cell to become resistant to such a mechanism.⁴¹

Alternative chemotherapeutic agents which target different modes of action, such as interactions with cell membranes or other biomolecules and cellular machinery, may be able to act in a potent manner towards cancer cells that are resistant towards DNA damage agents.

1.2 Anticancer cationic α -helical peptides

Innate immunity peptides are produced in many organisms, primarily to fight microbial invasion.⁴²⁻⁴⁵ They are also involved in the natural ability of the host to recognise and destroy cancer cells.^{46, 47} For this reason host-defence peptides have been investigated as anticancer agents.⁴⁻⁶ They are α -helical in shape, small (≤ 50 residues), cationic (contain arginine, lysine and histidine residues),^{26, 27} and amphiphilic.^{8, 42}

Normal cell membranes are zwitterionic.^{5, 8} Cancer cell membranes are more negatively charged, due to an overexpression of molecules like phosphatylserine and glycoproteins.^{48, 49} This can cause the cationic peptides, which act by aggregating on the extracellular membrane, to interact more strongly with cancerous cells compared to healthy ones.^{4, 19} Tumour cell membranes also have more microvilli which increase the surface area available.^{50, 51} Furthermore, most cancer cells have increased susceptibility to membrane destabilisation.^{52, 53} Membrane interactions with host-defence peptides can trigger necrosis through lysis and apoptosis resulting from disruption of mitochondria,^{6, 54-58} although other modes of action have been suggested.⁵⁹⁻⁶¹

There is a lower of risk of cancer cell resistance⁶² towards these peptides as they act by different modes of action to anticancer alkylators.⁷ This can also cause lower intrinsic cytotoxicity towards healthy host cells.^{5, 63}

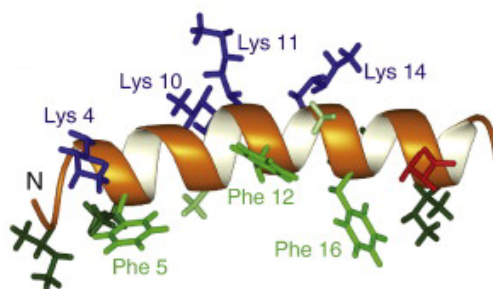


Figure 1.1 | Solution structure of magainin II with labelled hydrophilic (blue) and hydrophobic (green) side chains.⁶⁴

Cecropins (host defence peptides from cecropia moths)⁶⁵ and magainins (from the skin of frogs)^{66, 67} have shown activity in cancerous lung,^{68, 69} bladder,^{70, 71} colon⁷² and leukaemia⁷³ cells by triggering apoptosis through cell membrane lysis.^{71, 74-76} They show some selectivity towards cancer cells over normal fibroblasts,^{77, 78} but display reduced efficacy in *in vivo* studies.⁶⁸

Cathelicidins, such as CAP18,⁷⁹ make up another class of proteins which have a wide range of activity in host defence.⁸⁰⁻⁸⁸ LL-37⁸⁹ is the active domain of the human cathelicidin (hCAP18).⁸³ It is a cationic (net +6), 37 residue, amphipathic⁹ peptide, found in human skin and gut epithelial cells, and breast tissue.⁹⁰⁻⁹² It has been found to have many inherent roles within the cell⁹³ such as antimicrobial,⁹⁴⁻⁹⁶ antifungal^{92, 97, 98} and antiviral⁹⁹⁻¹⁰⁴ activity. It appears to act in a tissue- and disease-specific manner.^{105, 106} LL-37 has been found to act as an immunostimulant, promoting the ability of the host to fight cancerous cells,¹⁰⁷ and to induce apoptosis in colon,¹⁰⁵ oral^{30, 31} and blood¹⁰⁸ cancer cells, as well as preventing regrowth of some ovarian cancers.¹⁰⁹ In gastric and colorectal cancer, native LL-37 is found to be down-regulated and so treatment with exogenous LL-37 has a potential for tumour suppression. Indeed, it is found to induce cell cycle arrest and mitochondria-associated pathways to apoptosis.^{17, 29, 30} However, LL-37 is also found to be

uncontrollably up-regulated in some cancers and can act as an oncogene. It is reported to promote carcinogenesis in ovarian,^{110, 111} breast^{112, 113} and lung^{9, 114} cancer, and the migration of malignant cells.¹¹⁵

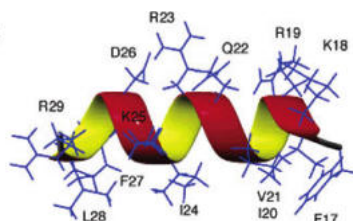


Figure 1.2 | Solution structure of the active core of LL-37, corresponding to residues 13-17.¹¹⁶

FK-16 is a fragment of LL-37.¹¹⁶ It has been identified as having greater antimicrobial¹¹⁷ and anticancer¹¹⁸ potential than the full peptide. In colon carcinoma cells (LoVo and HCT116) it has been found to be active (IC₅₀ 40μM in HCT116) and to induce apoptosis, more selectively than complete LL-37. It also appears to be highly selective; no activity was observed in normal colon mucosal epithelial cells (NCM460).¹¹⁸

Unfortunately such cationic host defence peptides often exhibit undesirable metabolism mechanisms, which means they are not viable drug candidates.⁸ For example they suffer from proteolytic cleavage which reduces their half-life in serum and limits their bioavailability. They are also found to interact with negatively charged components of serum, such as albumin, which also reduces efficacy.¹⁰ Some are found to closely resemble human peptides and so treatment with them may compromise natural host-defence responses and cause unwanted off-target interactions.^{7, 9}

The challenge is to design synthetic mimics of these peptides which display improved delivery to tumours while maintaining toxicity towards cancer cells, increased selectivity and improved production viability.¹¹⁹ This could be achieved by

manipulating the peptide sequence, net charge, secondary structure, amphipathicity¹²⁰ and stability.¹²¹ Identifying active sequences within the peptide would allow the synthesis of less expensive shorter oligomers and may improve stability and bioavailability.¹²² Exchanging L-amino acids for D- has been found not to reduce cytotoxicity, but can avoid proteolytic cleavage and so increases the stability of the peptide in serum.⁶⁸ Utilising a system such as vector mediated delivery⁶¹ or conjugation to a homing peptide¹²³⁻¹²⁶ can reduce unwanted off-target interactions and improve peptide stability. It is also possible to gain synergistic effects if these cationic α -helical peptides are combined with other anticancer drugs.⁶

1.3 Synthetic mimics of α -helical peptides

Significant progress has been made in the development of synthetic analogues of peptidic α -helices,¹¹ with improved structural integrity and relevant biological properties.¹²⁷ Several key examples are described here. Peptidic foldamers,¹² such as β -peptides,¹²⁸⁻¹³⁰ can be designed and synthesised to support an α -helical structure.¹³¹⁻¹³⁴ Some are found to mimic host-defence peptides¹³⁵ and they often display reduced susceptibility to proteolytic cleavage.¹³⁶

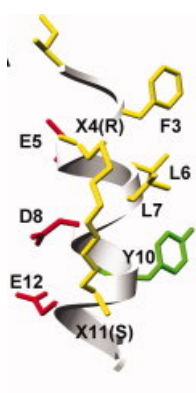


Figure 1.3 | Solution structure of a stapled peptide, hydrocarbon tether shown in yellow.¹³⁷

α -Helical architectures can be stabilised by the inclusion of labile polar^{138, 139} or inert hydrocarbon¹⁴⁰ intramolecular cross-linking moieties, to form stapled peptides.¹⁴¹ These highly stabilised oligomers have been investigated for their potential therapeutic effects.¹⁴² They are found to have increased cell permeability and selectivity towards specific targets.¹⁴³ Walensky reports stapled peptides derived from the protein BH3 that are found to be active in a range of leukaemia cells (*e.g.* IC₅₀ 2.2 μ M in Jurkat leukaemia) and are reported to activate apoptotic pathways *in vivo*.¹⁴⁴⁻¹⁴⁶

Several non-peptide synthetic scaffolds have also been put forward,¹³⁻¹⁵ including indanes,¹⁴⁷⁻¹⁴⁹ terphenyls,¹⁵⁰⁻¹⁵² oligophenyls,¹⁵³ and chalcones.¹⁵⁴ These

molecules are not formed of amino acid residues, but are designed to mimic the structure of natural α -helices.¹⁵ They can imitate some protein-protein interactions, though certain chalcones are reported by Holak to exhibit marginal antitumour activity (IC_{50} *ca* 200 μ M).¹⁵⁴ However they can suffer from poor solubility. This tempers their viability for use in the biological regime.^{13, 155, 156}

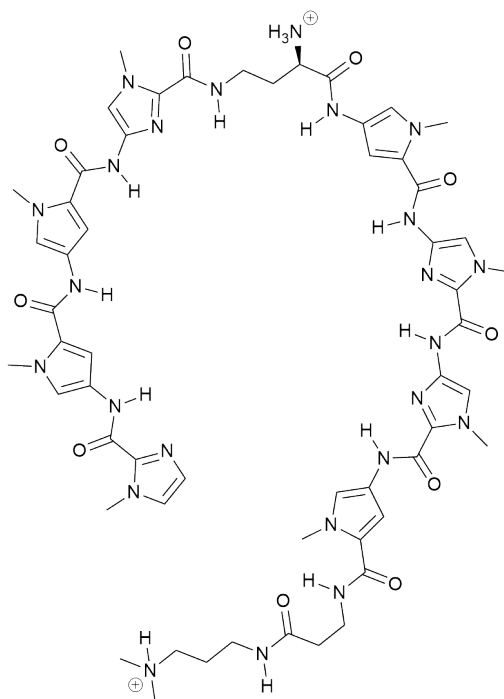


Figure 1.4 | Structure of an example hairpin pyrrole-imidazole polyamide.¹⁵⁷

Dervan reports hairpin pyrrole-imidazole polyamides that can selectively bind the minor groove of DNA.¹⁵⁷⁻¹⁶² These polyamides have been reported to gain access to the intracellular environment¹⁶³⁻¹⁶⁵ and appear to have favourable pharmacokinetic properties in *in vivo* studies.¹⁶⁶⁻¹⁶⁸ They are found to be active in cancer cells (*e.g.* IC_{50} 7.0 ± 2.8 μ M in LNCaP prostate adenocarcinoma)¹⁶⁹ and appear to act by perturbing DNA-dependant cellular processes, similarly to other anticancer alkylators.^{170, 171}

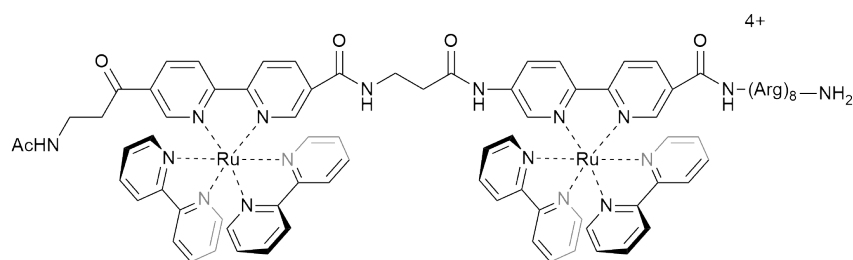


Figure 1.5 | Structure of a ruthenium(II) metalloprotein.¹⁷²

It is possible to build synthetic oligomers that incorporate metal-chelating units, such as 2,2'-bipyridine, to preferentially capture specific metal cations and stabilise secondary structures.^{16, 17} This can allow for the precise control of chirality and functional group placement upon the peptide architecture.¹⁷³ Some synthetic metalloproteins have been found to interact with the minor groove of DNA¹⁷⁴⁻¹⁷⁷ and can exhibit cytotoxicity.¹⁷⁸ Vázquez reports a bimetallic ruthenium(II) example (Fig 1.5) that is found to kill cisplatin resistant ovarian carcinoma (IC₅₀ 7 μ M in A2780cis).¹⁷²

The cost and difficulty of synthesis of oligomeric mimics,¹⁷⁹ and some of their biophysical properties, such as low solubility in aqueous media, could cause compounds of this type to be less suitable as a class of anticancer therapeutics. Another approach to access the size and structural stability required of an α -helix mimetic would be to utilise metallohelices, where linear organic ligands are supported by metal scaffolds.

1.4 Metallohelices

A bimetallic triple helicate is an assembly where three organic ligands **AB–BA** arrange about two metal centres; a schematic example is shown in Fig 1.6.^{18, 24, 180-185}

Some examples are of a similar diameter to peptidic α -helices (*ca* 1.2 nm); synthetic and biophysical studies investigating their potential in the biological regime are being carried out by groups worldwide.²⁴⁻²⁶ Nevertheless, the biological impact of these systems will be limited unless certain criteria can be achieved, detailed in a recent review by Scott and Howson.¹⁹ They must be: optically pure and non-racemising for use in human systems; soluble and both chemically and enantiomerically stable in aqueous solutions; readily available on a practical scale; and synthetically flexible so that drug-like properties can be designed or optimised.

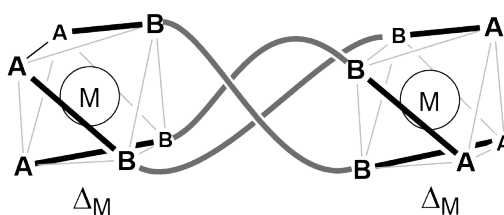


Figure 1.6 | Schematic diagram of a bimetallic triple helicate $\Delta_M\text{-}[M_2(\text{AB-BA})_3]^{n+}$

Some examples of bimetallic triple helicates of the type $[M_2(\text{AB-BA})_3]^{n+}$ are reported to have interesting properties in the biological regime. An overview of the current and potential outlook of bimetallic triple helicates with biological activity is given here.

1.4.1 Helicates

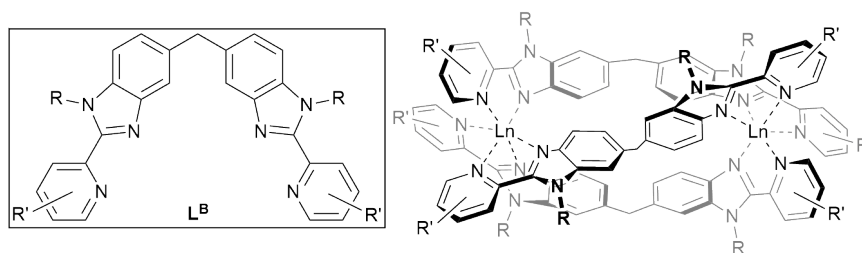


Figure 1.7 | Structure of L^B (R and R' range from small polar groups to larger aromatic moieties) and structure of $[Ln_2L^B_3]^{n+}$.¹⁸⁶

Bünzli reports bimetallic lanthanide triple helicates, $[Ln_2L^B_3]^{n+}$ as bioluminescent probes, such as for MRI or protein labelling.¹⁸⁶⁻¹⁹¹ They are formed of three rigid ligands (L^B) that encapsulate two lanthanide ions ($Ln(III)$).^{186, 192} The functionality of the ligands can tune the properties of the helicate, by manipulating selectivity towards particular $Ln(III)$ cations and protecting them from de-excitation through high energy vibrations and low energy ligand-to-metal charge-transfer states.¹⁹³⁻¹⁹⁶

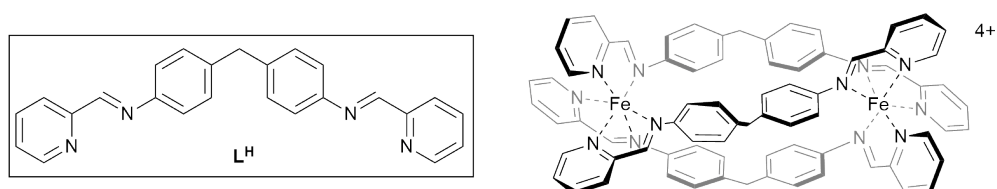


Figure 1.8 | Structure of Ligand L^H and structure of the complex $[Fe_2L^H_3]Cl_4$.¹⁹⁷

Hannon reports a bimetallic iron(II) triple helicate,¹⁹⁷ $[Fe_2L^H_3]Cl_4$. It binds in the major groove of DNA with some sequence-selectivity.¹⁹⁸ It induces intramolecular coiling¹⁹⁹ and has some antimicrobial²⁰⁰ and anticancer activity.^{201, 202} Qu has discovered that the same iron(II) compound recognises human telomeric G-quadruplex DNA²⁰³⁻²⁰⁵ and targets the amyloid- β peptide, reducing cytotoxicity and ameliorating memory deficits in a transgenic mouse model.²⁰⁶ Nevertheless, the compound is prepared as a racemate and requires chromatographic resolution, which

reduces the appeal of such systems to medicinal chemistry.^{207, 208} As far as we are aware, no details of the synthesis or characterisation of the chloride salt have appeared, although the hexafluorophosphate salt is known.¹⁹⁷

Some analogues of the iron(II) complex have been reported²⁰⁹⁻²¹² and an anticancer racemic ruthenium(II) compound was isolated, though in very low yield (IC_{50} 22 μ M in HB100 breast carcinoma).²⁰¹ Recently a derivative of $[Fe_2L^H_3]^{4+}$ containing arginine units showed improved separation of enantiomers and greater cytotoxicity against A2780 ovarian cancer cells (IC_{50} ca 7 μ M).²¹³

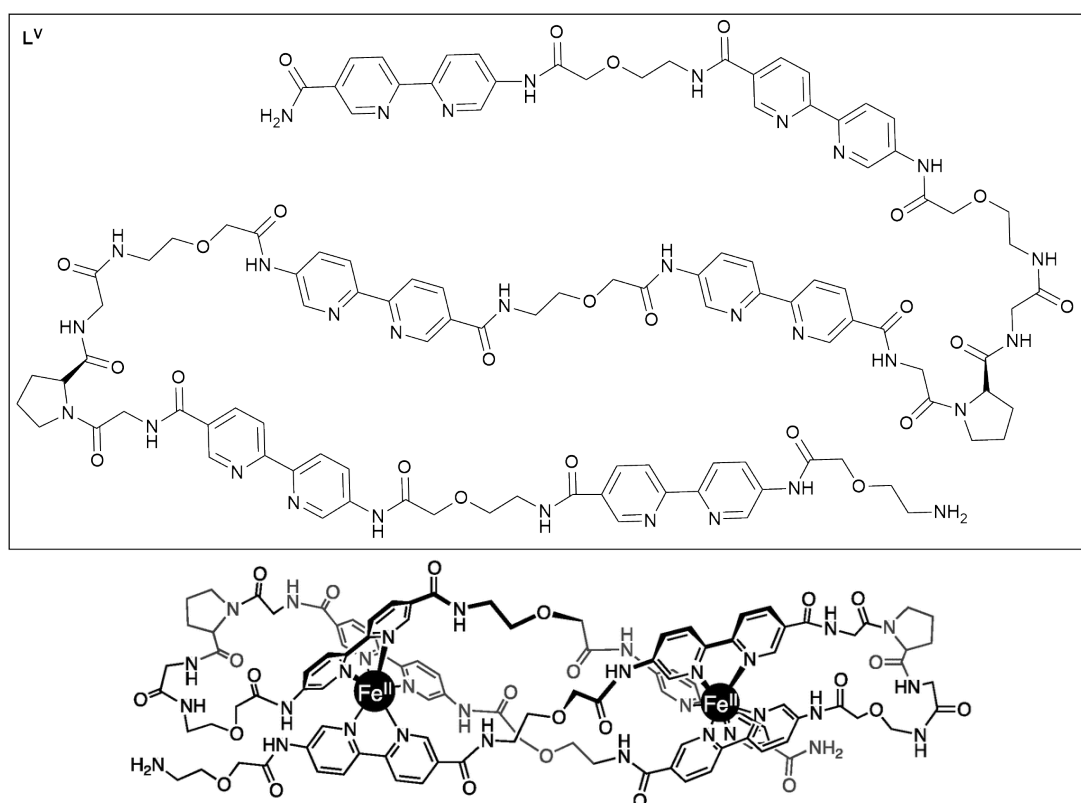


Figure 1.9 | Structure of Ligand L^V and computed structure of the complex $[Fe_2L^V]^{4+}$.¹⁷⁷

Vázquez has recently reported a helical metallopeptide $[Fe_2L^V]^{4+}$, where an optically pure ligand containing two hairpin turns, predisposes the formation of a homochiral iron(II) helix according to calculations.¹⁷⁷ The complex is assembled *in situ* on a small scale and is not isolated, but is detected by mass spectrometry. In this

preliminary communication it is suggested that the helical complex may bind to DNA and there is evidence that it accessed the intracellular environment of Vero cells.

1.4.2 Flexicates

Previous members of the Scott group have developed a route to thermodynamically stable, optically pure octahedral monometallic complexes from simple chiral bidentate ligands and iron(II).^{214, 215} Two of these monometallic species can be connected together with linear linkers, to form bimetallic species known as flexicates.²⁰⁻²³ Lehn's strategy for helicate synthesis¹⁸ – mechanical coupling of chirality between metal centres by short or rigid linkers – is not used here, and it is possible to create the assemblies to incorporate linkers with different degrees of flexibility.

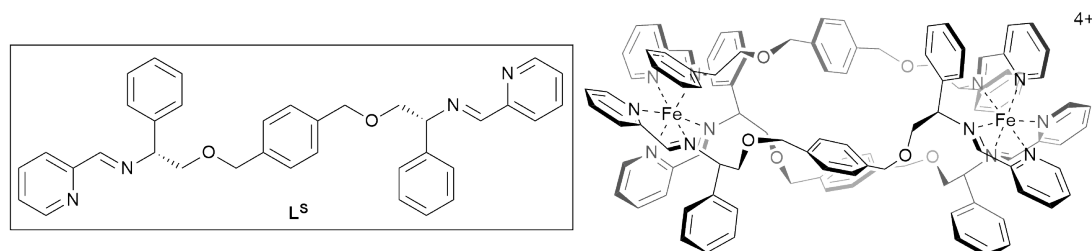


Figure 1.10 | Structure of L^S and structure of a class Ia Δ_{Fe} - $[Fe_2L^S_3]Cl_4$.²¹

The class Ia iron(II) flexicate, $[Fe_2L^S_3]Cl_4$, is formed in a highly diastereoselective manner ($dr > 99.5$ either Λ_{Fe} or Δ_{Fe}) dependent on the chirality of the ligand (L^S). The compound is readily water-soluble and remarkably stable in a variety of media. It interacts with DNA, showing selectivity for 5'-CACATA and 5'-CACTAT segments, as well as stabilising different three- and four- way oligonucleotide junctions.²² Overall the Λ_{Fe} enantiomer has been found to be a stronger DNA binder and more active compound than its Δ_{Fe} enantiomer.^{21, 22} These flexicates have shown very promising antimicrobial activity towards methicillin-resistant *Staphylococcus*

aureus (MRSA) (MIC $8 \mu\text{g ml}^{-1}$) and *Escherichia coli* (*E. Coli*) (MIC $4 \mu\text{g ml}^{-1}$) alongside low toxicity to the non-mammalian model organism *Caenorhabditis elegans* (LC₅₀ *ca* $450 \mu\text{g ml}^{-1}$).²¹ In a preliminary study, the author and co-workers found that these compounds exhibit potent cytotoxicity in cisplatin-resistant ovarian carcinoma cells (IC₅₀ *ca* $2.5 \mu\text{M}$ in A2780cis).²²

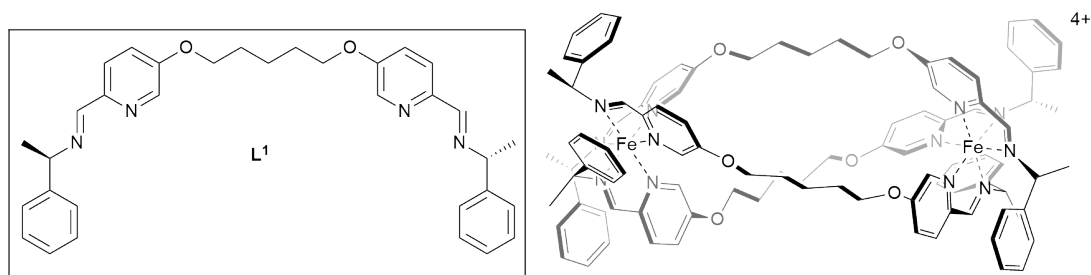


Figure 1.11 | Ligand structure of **L¹** and structure of class Ib $\Lambda_{\text{Fe}}\text{-}[\text{Fe}_2\text{L}_3]\text{Cl}_4$

The class Ib iron(II) flexicate $[\text{Fe}_2\text{L}_3]\text{Cl}_4$ forms in a similar diastereoselective manner to the previous example, but is connected *via* a flexible aliphatic linker. It is also found to be soluble in aqueous media, but with somewhat lower stability than the previous example. Neither enantiomer is observed to bind significantly to DNA selectively or to act as an antimicrobial agent.^{21, 22} These compounds have, however, been found to be active in ovarian cancer (IC₅₀ *ca* $3.5 \mu\text{M}$ in A2780).²² Recently Qu and Scott have reported that both class Ia and class Ib flexicates interact with proteins and can enantioselectively target and inhibit amyloid- β , a therapeutic target in Alzheimer's disease.²³

In using the flexicate system,²¹ many of the associated drawbacks of more traditional helicates are avoided. These compounds form as single diastereoisomers, stabilised by interligand π -stacking between the aromatic groups about each monometallic subunit. Unlike natural peptides and other metallohelices, they are found to be chemically and enantiomerically stable in solution (*vide infra*).

1.5 Project aims

The promising flexicate system was based on few analogues, therefore a range of class Ib flexicates were investigated as non-peptide α -helix mimetics. This system was chosen over the other class of flexicate as it displayed potent anticancer activity but was inactive in bacteria. It was hoped that the range of complexes synthesised would be found to satisfy the previously described requirements of an ideal system and would exhibit potent anticancer activity.

Alongside the criteria set out by Scott and Howson, to be able to approach the precision of functional group placement and topology seen in a natural α -helix, the use of high symmetry systems could be considered restricting. We therefore suggested that a model amphipathic α -helix mimetic should have the following characteristics:

- (a) many analogues available on a practical scale
- (b) optically pure and non-racemising
- (c) soluble, and resistant to deterioration in biological media
- (d) potent and selective biological activity
- (e) precise and deliberate placement of functional groups

At the outset of the work described in this thesis, a few analogues of class Ia and Ib flexicates had been synthesised in an optically pure form with good solubility and stability.²¹ Some promising antimicrobial activity had been noted.

In chapter 2 we describe the synthesis and characterisation of a range of class Ib flexicates, their biophysical properties and potential as active and selective anticancer therapeutics, as well as investigations into their possible mode of action.²²

In chapter 3 we make the first advances towards to the ambitious objective (e) and report the highly diastereoselective synthesis of amphipathic metallohelicenes with potent and selective anticancer activity.²¹⁶

1.6 References

1. L. Novotny and T. Szekeres, *Expert. Opin. Ther. Targets.*, 2005, **9**, 343-357.
2. A. Garnier-Suillerot, C. Marbeuf-Gueye, M. Salerno, C. Loetchutinat, I. Fokt, M. Krawczyk, T. Kowalczyk and W. Priebe, *Curr. Med. Chem.*, 2001, **8**, 51-64.
3. R. Perez-Tomas, *Curr. Med. Chem.*, 2006, **13**, 1859-1876.
4. M.-D. Seo, H.-S. Won, J.-H. Kim, T. Mishig-Ochir and B.-J. Lee, *Molecules*, 2012, **17**, 12276-12286.
5. D. W. Hoskin and A. Ramamoorthy, *Biochim. Biophys. Acta*, 2008, **1778**, 357-375.
6. F. Schweizer, *Eur. J. Pharmacol.*, 2009, **625**, 190-194.
7. C. Chen, J. Hu, S. Zhang, P. Zhou, X. Zhao, H. Xu, X. Zhao, M. Yaseen and J. R. Lu, *Biomaterials*, 2012, **33**, 592-603.
8. R. E. W. Hancock and H.-G. Sahl, *Nat. Biotechnol.*, 2006, **24**, 1551-1557.
9. W. K. K. Wu, G. Wang, S. B. Coffelt, A. M. Betancourt, C. W. Lee, D. Fan, K. Wu, J. Yu, J. J. Y. Sung and C. H. Cho, *Int. J. Cancer*, 2010, **127**, 1741-1747.
10. A. Lichtenstein, T. Ganz, M. Selsted and R. Lehrer, *Blood*, 1986, **68**, 1407-1410.
11. C. Adessi and C. Soto, *Curr. Med. Chem.*, 2002, **9**, 963-978.
12. D.-W. Zhang, X. Zhao, J.-L. Hou and Z.-T. Li, *Chem. Rev.*, 2012, **112**, 5271-5316.
13. J. M. Davis, L. K. Tsou and A. D. Hamilton, *Chem. Soc. Rev.*, 2007, **36**, 326-334.
14. V. Azzarito, K. Long, N. S. Murphy and A. J. Wilson, *Nat. Chem.*, 2013, **5**, 161-173.
15. V. Haridas, *Eur. J. Org. Chem.*, 2009, **2009**, 5112-5128.
16. R. P. Cheng, S. L. Fisher and B. Imperiali, *J. Am. Chem. Soc.*, 1996, **118**, 11349-11356.
17. Y. Q. Shi and S. Sharma, *Bioorg. Med. Chem. Lett.*, 1999, **9**, 1469-1474.
18. J. M. Lehn, A. Rigault, J. Siegel, J. Harrowfield, B. Chevrier and D. Moras, *Proc. Natl. Acad. Sci. USA.*, 1987, **84**, 2565-2569.
19. S. E. Howson and P. Scott, *Dalton Trans.*, 2011, **40**, 10268-10277.
20. S. E. Howson, *Ph.D. Thesis, University of Warwick*, 2011.
21. S. E. Howson, A. Bolhuis, V. Brabec, G. J. Clarkson, J. Malina, A. Rodger and P. Scott, *Nat. Chem.*, 2012, **4**, 31-36.
22. V. Brabec, S. E. Howson, R. A. Kaner, R. M. Lord, J. Malina, R. M. Phillips, Q. M. A. Abdallah, P. C. McGowan, A. Rodger and P. Scott, *Chem. Sci.*, 2013, **4**, 4407-4416.
23. M. Li, S. E. Howson, K. Dong, N. Gao, J. Ren, P. Scott and X. Qu, *J. Am. Chem. Soc.*, 2014, **136**, 11655-11663.
24. M. Albrecht, *Chem. Rev.*, 2001, **101**, 3457-3498.
25. C. Piguet, G. Bernardinelli and G. Hopfgartner, *Chem. Rev.*, 1997, **97**, 2005-2062.
26. M. J. Hannon, *Chem. Soc. Rev.*, 2007, **36**, 280-295.
27. B. Alberts, A. Johnson, J. Lewis, M. Raff, K. Roberts and P. Walter, *Molecular Biology of the Cell*, fifth edn., Garland Science, New York, 2008.

28. A. R. Ahmed and S. M. Hombal, *J. Am. Acad. Dermatol.*, 1984, **11**, 1115-1126.
29. B. Rosenberg, *Plat. Met. Rev.*, 1971, **15**, 42-51.
30. J. Reedijk, *Pure Appl. Chem.*, 1987, **59**, 181-192.
31. J. F. R. Kerr, C. M. Winterford and B. V. Harmon, *Cancer*, 1994, **73**, 2013-2026.
32. D. B. Longley, D. P. Harkin and P. G. Johnston, *Nat. Rev. Cancer*, 2003, **3**, 330-338.
33. G. J. Peters, C. L. van der Wilt, C. J. A. van Moorsel, J. R. Kroep, A. M. Bergman and S. P. Ackland, *Pharmacol. Ther.*, 2000, **87**, 227-253.
34. R. B. Weiss, *Semin. Oncol.*, 1992, **19**, 670-686.
35. G. Minotti, P. Menna, E. Salvatorelli, G. Cairo and L. Gianni, *Pharmacol. Rev.*, 2004, **56**, 185-229.
36. L. L. Smith, K. Brown, P. Carthew, C. K. Lim, E. A. Martin, J. Styles and I. N. White, *Crit. Rev. Toxicol.*, 2000, **30**, 571-594.
37. S. E. Kern, K. W. Kinzler, A. Bruskin, D. Jarosz, P. Friedman, C. Prives and B. Vogelstein, *Science*, 1991, **252**, 1708-1711.
38. D. P. Lane, *Nature*, 1992, **358**, 15-16.
39. M. Hollstein, D. Sidransky, B. Vogelstein and C. C. Harris, *Science*, 1991, **253**, 49-53.
40. S. J. Baker, E. R. Fearon, J. M. Nigro, S. R. Hamilton, A. C. Preisinger, J. M. Jessup, P. VanTuinen, D. H. Ledbetter, D. F. Barker, Y. Nakamura, R. White and B. Vogelstein, *Science*, 1989, **244**, 217-221.
41. J. M. Brown and B. G. Wouters, *Cancer Res.*, 1999, **59**, 1391-1399.
42. M. Zaslhoff, *Nature*, 2002, **415**, 389-395.
43. H. G. Boman, *Cell*, 1991, **65**, 205-207.
44. A. Tossi, L. Sandri and A. Giangaspero, *Biopolymers*, 2000, **55**, 4-30.
45. A. Giangaspero, L. Sandri and A. Tossi, *Eur. J. Biochem.*, 2001, **268**, 5589-5600.
46. K. C. Dunn, A. E. Aotaki-Keen, F. R. Putkey and L. M. Hjelmeland, *Exp. Eye Res.*, 1996, **62**, 155-170.
47. S. Mocellin, C. R. Rossi and D. Nitti, *Exp. Cell Res.*, 2004, **299**, 267-278.
48. T. Utsugi, A. J. Schroit, J. Connor, C. D. Bucana and I. J. Fidler, *Cancer Res.*, 1991, **51**, 3062-3066.
49. I. Dobrzyńska, B. Szachowicz-Petelska, S. Sulkowski and Z. Figaszewski, *Mol. Cell. Biochem.*, 2005, **276**, 113-119.
50. R. F. Zwaal and A. J. Schroit, *Blood*, 1997, **89**, 1121-1132.
51. S. C. Chan, L. Hui and H. M. Chen, *Anticancer Res.*, 1998, **18**, 4467-4474.
52. K. Kozłowska, J. Nowak, B. Kwiatkowski and M. Cichorek, *Exp. Toxicol. Pathol.*, 1999, **51**, 89-92.
53. M. Sok, M. Šentjurc and M. Schara, *Cancer Lett.*, 1999, **139**, 215-220.
54. M. Shadidi and M. Sioud, *Drug Resist. Updat.*, 2003, **6**, 363-371.
55. C. Leuschner and W. Hansel, *Curr. Pharm. Des.*, 2004, **10**, 2299-2310.
56. N. Papo, M. Shahr, L. Eisenbach and Y. Shai, *J. Biol. Chem.*, 2003, **278**, 21018-21023.
57. Z. Oren and Y. Shai, *Biopolymers*, 1998, **47**, 451-463.
58. Y. Shai, *Biochim. Biophys. Acta*, 1999, **1462**, 55-70.
59. S. V. Sharma, *Oncogene*, 1992, **7**, 193-201.

60. M. Wachinger, A. Kleinschmidt, D. Winder, N. von Pechmann, A. Ludvigsen, M. Neumann, R. Holle, B. Salmons, V. Erfle and R. Brack-Werner, *J. Gen. Virol.*, 1998, **79**, 731-740.
61. D. Winder, W. H. Gunzburg, V. Erfle and B. Salmons, *Biochem. Biophys. Res. Commun.*, 1998, **242**, 608-612.
62. A. Giuliani, G. Pirri, A. Bozzi, A. Di Giulio, M. Aschi and A. C. Rinaldi, *Cell. Mol. Life Sci.*, 2008, **65**, 2450-2460.
63. N. Papo and Y. Shai, *Cell. Mol. Life Sci.*, 2005, **62**, 784-790.
64. E. F. Haney, H. N. Hunter, K. Matsuzaki and H. J. Vogel, *Biochim. Biophys. Acta, Biomembr.*, 2009, **1788**, 1639-1655.
65. H. Steiner, D. Hultmark, A. Engstrom, H. Bennich and H. G. Boman, *Nature*, 1981, **292**, 246-248.
66. M. Zasloff, *Proc. Natl. Acad. Sci. USA*, 1987, **84**, 5449-5453.
67. M. Zasloff, *Curr. Opin. Immunol.*, 1992, **4**, 3-7.
68. M. A. Baker, W. L. Maloy, M. Zasloff and L. S. Jacob, *Cancer Res.*, 1993, **53**, 3052-3057.
69. Y. Ohsaki, A. F. Gazdar, H.-C. Chen and B. E. Johnson, *Cancer Res.*, 1992, **52**, 3534-3538.
70. H. Suttman, M. Retz, F. Paulsen, J. Harder, U. Zwergel, J. Kamradt, B. Wullich, G. Unteregger, M. Stockle and J. Lehmann, *BMC Urol.*, 2008, **8**, 5-5.
71. J. Lehmann, M. Retz, S. S. Sidhu, H. Suttman, M. Sell, F. Paulsen, J. Harder, G. Unteregger and M. Stockle, *Eur. Urol.*, 2006, **50**, 141-147.
72. W.-m. Zhang, Z.-s. Lai, M.-r. He, G. Xu, W. Huang and D.-y. Zhou, *Diyi Junyi Daxue Xuebao*, 2003, **23**, 1066-1068.
73. L. Hui, K. Leung and H. M. Chen, *Anticancer Res.*, 2002, **22**, 2811-2816.
74. D. I. Chan, E. J. Prenner and H. J. Vogel, *Biochim. Biophys. Acta.*, 2006, **1758**, 1184-1202.
75. H. Jenssen, P. Hamill and R. E. Hancock, *Clin. Microbiol. Rev.*, 2006, **19**, 491-511.
76. K. A. Brogden, *Nat. Rev. Microbiol.*, 2005, **3**, 238-250.
77. S. Y. Shin, S. H. Lee, S. T. Yang, E. J. Park, D. G. Lee, M. K. Lee, S. H. Eom, W. K. Song, Y. Kim, K. S. Hahm and J. I. Kim, *J. Pept. Res.*, 2001, **58**, 504-514.
78. R. A. Cruciani, J. L. Barker, M. Zasloff, H. C. Chen and O. Colamonici, *Proc. Natl. Acad. Sci. USA*, 1991, **88**, 3792-3796.
79. J. W. Larrick, J. G. Morgan, I. Palings, M. Hirata and M. H. Yen, *Biochem. Biophys. Res. Commun.*, 1991, **179**, 170-175.
80. T. Ganz and R. I. Lehrer, *Curr. Opin. Immunol.*, 1998, **10**, 41-44.
81. H. G. Boman, *J. Intern. Med.*, 2003, **254**, 197-215.
82. R. Bals, *Resp. Res.*, 2000, **1**, 141-150.
83. M. Zaiou and R. Gallo, *J. Mol. Med.*, 2002, **80**, 549-561.
84. M. Zanetti, *J. Leukocyte Biol.*, 2004, **75**, 39-48.
85. C. Herr, R. Shaykhiev and R. Bals, *Expert Opin. Biol. Ther.*, 2007, **7**, 1449-1461.
86. J. H. Wong, X. J. Ye and T. B. Ng, *Curr. Protein Pept. Sci.*, 2013, **14**, 504-514.
87. J. W. Larrick, M. Hirata, Y. Shimomoura, M. Yoshida, H. Zheng, J. Zhong and S. C. Wright, *Antimicrob. Agents Chemother.*, 1993, **37**, 2534-2539.
88. Y. P. Lai and R. L. Gallo, *Trends Immunol.*, 2009, **30**, 131-141.

89. J. W. Larrick, M. Hirata, R. F. Balint, J. Lee, J. Zhong and S. C. Wright, *Infect. Immun.*, 1995, **63**, 1291-1297.
90. G. H. Gudmundsson, B. Agerberth, J. Odeberg, T. Bergman, B. Olsson and R. Salcedo, *Eur. J. Biochem.*, 1996, **238**, 325-332.
91. M. Murakami, R. A. Dorschner, L. J. Stern, K. H. Lin and R. L. Gallo, *Pediatr. Res.*, 2005, **57**, 10-15.
92. K. Hase, M. Murakami, M. Iimura, S. P. Cole, Y. Horibe, T. Ohtake, M. Obonyo, R. L. Gallo, L. Eckmann and M. F. Kagnoff, *Gastroenterology*, 2003, **125**, 1613-1625.
93. D. Vandamme, B. Landuyt, W. Luyten and L. Schoofs, *Cell. Immunol.*, 2012, **280**, 22-35.
94. J. B. Cowland, A. H. Johnsen and N. Borregaard, *FEBS Lett.*, 1995, **368**, 173-176.
95. J. Turner, Y. Cho, N.-N. Dinh, A. J. Waring and R. I. Lehrer, *Antimicrob. Agents Chemother.*, 1998, **42**, 2206-2214.
96. S. Joly, C. Maze, P. B. McCray and J. M. Guthmiller, *J. Clin. Microbiol.*, 2004, **42**, 1024-1029.
97. M. Murakami, B. Lopez-Garcia, M. Braff, R. A. Dorschner and R. L. Gallo, *J. Immunol.*, 2004, **172**, 3070-3077.
98. J. H. Wong, T. B. Ng, A. Legowska, K. Rolka, M. Hui and C. H. Cho, *Peptides*, 2011, **32**, 1996-2002.
99. H. Bock, S. Mohmand, T. Hirabayashi and A. Semkow, *J. Am. Chem. Soc.*, 1982, **104**, 312-313.
100. M. D. Howell, J. F. Jones, K. O. Kisich, J. E. Streib, R. L. Gallo and D. Y. M. Leung, *J. Immunol.*, 2004, **172**, 1763-1767.
101. Y. J. Gordon, L. C. Huang, E. G. Romanowski, K. A. Yates, R. J. Proske and A. M. McDermott, *Curr. Eye Res.*, 2005, **30**, 385-394.
102. J. H. Wong, A. Legowska, K. Rolka, T. B. Ng, M. Hui, C. H. Cho, W. W. L. Lam, S. W. N. Au, O. W. Gu and D. C. C. Wan, *Peptides*, 2011, **32**, 1117-1122.
103. G. Wang, K. M. Watson and R. W. Buckheit, Jr., *Antimicrob. Agents Chemother.*, 2008, **52**, 3438-3440.
104. M. E. Quinones-Mateu, M. M. Lederman, Z. Feng, B. Chakraborty, J. Weber, H. R. Rangel, M. L. Marotta, M. Mirza, B. Jiang, P. Kiser, K. Medvik, S. F. Sieg and A. Weinberg, *AIDS*, 2003, **17**, F39-48.
105. J. Y. C. Chow, Z. J. Li, W. K. Kei and C. H. Cho, *World J. Gastroenterol.*, 2013, **19**, 2731-2735.
106. P. Elsbach, *J. Clin. Invest.*, 2003, **111**, 1643-1645.
107. A. S. Büchau, S. Morizane, J. Trowbridge, J. Schaubert, P. Kotol, J. D. Bui and R. L. Gallo, *J. Immunol.*, 2010, **184**, 369-378.
108. J. Aarbiou, G. S. Tjabringa, R. M. Verhoosel, D. K. Ninaber, S. R. White, L. T. Peltenburg, K. F. Rabe and P. S. Hiemstra, *Inflam. Res.*, 2006, **55**, 119-127.
109. C. M. Chuang, A. Monie, A. Wu, C. P. Mao and C. F. Hung, *Hum. Gene. Ther.*, 2009, **20**, 303-313.
110. S. B. Coffelt, F. C. Marini, K. Watson, K. J. Zvezdaryk, J. L. Dembinski, H. L. LaMarca, S. L. Tomchuck, K. H. zu Bentrup, E. S. Danko, S. L. Henkle and A. B. Scandurro, *Proc. Natl. Acad. Sci. USA*, 2009, **106**, 3806-3811.
111. S. B. Coffelt, S. L. Tomchuck, K. J. Zvezdaryk, E. S. Danko and A. B. Scandurro, *Mol. Cancer Res.*, 2009, **7**, 907-915.

-
112. J. D. Heilborn, M. F. Nilsson, C. I. C. Jimenez, B. Sandstedt, N. Borregaard, E. Tham, O. E. Sørensen, G. Weber and M. Ståhle, *Int. J. Cancer*, 2005, **114**, 713-719.
 113. G. Weber, C. I. Chamorro, F. Granath, A. Liljegren, S. Zreika, Z. Saidak, B. Sandstedt, S. Rotstein, R. Mentaverri, F. Sanchez, A. Pivarcsi and M. Stahle, *Breast Cancer Res.*, 2009, **11**, R6.
 114. J. von Haussen, R. Koczulla, R. Shaykhiev, C. Herr, O. Pinkenburg, D. Reimer, R. Wiewrodt, S. Biesterfeld, A. Aigner, F. Czubayko and R. Bals, *Lung Cancer*, 2008, **59**, 12-23.
 115. A. Girnita, H. Zheng, A. Gronberg, L. Girnita and M. Stahle, *Oncogene*, 2012, **31**, 352-365.
 116. X. Li, Y. Li, H. Han, D. W. Miller and G. Wang, *J. Am. Chem. Soc.*, 2006, **128**, 5776-5785.
 117. G. Wang, *J. Biol. Chem.*, 2008, **283**, 32637-32643.
 118. S. X. Ren, J. Shen, A. S. L. Cheng, L. Lu, R. L. Y. Chan, Z. J. Li, X. J. Wang, C. C. M. Wong, L. Zhang, S. S. M. Ng, F. L. Chan, F. K. L. Chan, J. Yu, J. J. Y. Sung, W. K. K. Wu and C. H. Cho, *PLoS One*, 2013, **8**, e63641.
 119. J. Hu, C. Chen, S. Zhang, X. Zhao, H. Xu, X. Zhao and J. R. Lu, *Biomacromolecules*, 2011, **12**, 3839-3843.
 120. Y. B. Huang, X. F. Wang, H. Y. Wang, Y. Liu and Y. Chen, *Mol. Cancer. Ther.*, 2011, **10**, 416-426.
 121. D. Gaspar, A. S. Veiga and M. A. R. B. Castanho, *Front. Microbiol.*, 2013, **4**.
 122. B. Fadnes, L. Uhlin-Hansen, I. Lindin and O. Rekdal, *BMC Cancer*, 2011, **11**, 116.
 123. E. Ruoslahti, T. Duza and L. Zhang, *Curr. Pharm. Des.*, 2005, **11**, 3655-3660.
 124. W. Arap, R. Pasqualini and E. Ruoslahti, *Curr. Opin. Oncol.*, 1998, **10**, 560-565.
 125. A. Sacchi, A. Gasparri, F. Curnis, M. Bellone and A. Corti, *Cancer Res.*, 2004, **64**, 7150-7155.
 126. A. Sacchi, A. Gasparri, C. Gallo-Stampino, S. Toma, F. Curnis and A. Corti, *Clin. Cancer Res.*, 2006, **12**, 175-182.
 127. L. Gentilucci, A. Tolomelli and F. Squassabia, *Curr. Med. Chem.*, 2006, **13**, 2449-2466.
 128. R. P. Cheng, S. H. Gellman and W. F. DeGrado, *Chem. Rev.*, 2001, **101**, 3219-3232.
 129. D. H. Appella, L. A. Christianson, I. L. Karle, D. R. Powell and S. H. Gellman, *J. Am. Chem. Soc.*, 1996, **118**, 13071-13072.
 130. L. M. Johnson and S. H. Gellman, in *Methods in Protein Design*, ed. A. E. Keating, 2013, vol. 523, pp. 407-429.
 131. D. Seebach, A. K. Beck and D. J. Bierbaum, *Chem. Biodiversity*, 2004, **1**, 1111-1239.
 132. S. H. Gellman, *Acc. Chem. Res.*, 1998, **31**, 173-180.
 133. L. Guo, Y. Chi, A. M. Almeida, I. A. Guzei, B. K. Parker and S. H. Gellman, *J. Am. Chem. Soc.*, 2009, **131**, 16018-16020.
 134. C. M. Goodman, S. Choi, S. Shandler and W. F. DeGrado, *Nat. Chem. Biol.*, 2007, **3**, 252-262.
 135. E. A. Porter, B. Weisblum and S. H. Gellman, *J. Am. Chem. Soc.*, 2002, **124**, 7324-7330.
 136. T. Beke, C. Somlai and A. Perczel, *J. Comput. Chem.*, 2006, **27**, 20-38.
-

-
137. S. Bhattacharya, H. Zhang, D. Cowburn and A. K. Debnath, *Biopolymers*, 2012, **97**, 253-264.
 138. A. M. Leduc, J. O. Trent, J. L. Wittliff, K. S. Bramlett, S. L. Briggs, N. Y. Chirgadze, Y. Wang, T. P. Burris and A. F. Spatola, *Proc. Natl. Acad. Sci. USA*, 2003, **100**, 11273-11278.
 139. B. Yang, D. Liu and Z. Huang, *Bioorg. Med. Chem. Lett.*, 2004, **14**, 1403-1406.
 140. C. E. Schafmeister, J. Po and G. L. Verdine, *J. Antimicrob. Chemother.*, 2000, **122**, 5891-5892.
 141. L. K. Henchey, A. L. Jochim and P. S. Arora, *Curr. Opin. Chem. Biol.*, 2008, **12**, 692-697.
 142. G. L. Verdine and G. J. Hilinski, *Methods Enzymol.*, 2012, **503**, 3-33.
 143. J. A. Kritzer, *Nat. Chem. Biol.*, 2010, **6**, 566-567.
 144. L. D. Walensky, A. L. Kung, I. Escher, T. J. Malia, S. Barbuto, R. D. Wright, G. Wagner, G. L. Verdine and S. J. Korsmeyer, *Science*, 2004, **305**, 1466-1470.
 145. E. Gavathiotis, M. Suzuki, M. L. Davis, K. Pitter, G. H. Bird, S. G. Katz, H.-C. Tu, H. Kim, E. H. Y. Cheng, N. Tjandra and L. D. Walensky, *Nature*, 2008, **455**, 1076-1081.
 146. L. Zhang, L. Ming and H. Yu, *Drug Resist. Updates*, 2007, **10**, 207-217.
 147. D. C. Horwell, W. Howson, W. P. Nolan, G. S. Ratcliffe, D. C. Rees and H. M. G. Willems, *Tetrahedron*, 1995, **51**, 203-216.
 148. D. C. Horwell, W. Howson, G. S. Ratcliffe and H. M. Willems, *Bioorg. Med. Chem.*, 1996, **4**, 33-42.
 149. D. C. Horwell, W. Howson, G. Ratcliffe and H. Willems, *Bioorg. Med. Chem. Lett.*, 1994, **4**, 2825-2830.
 150. H. Yin and A. D. Hamilton, *Angew. Chem.-Int. Edit. Engl.*, 2005, **44**, 4130-4163.
 151. O. Kutzki, H. S. Park, J. T. Ernst, B. P. Orner, H. Yin and A. D. Hamilton, *J. Am. Chem. Soc.*, 2002, **124**, 11838-11839.
 152. I. C. Kim and A. D. Hamilton, *Org. Lett.*, 2006, **8**, 1751-1754.
 153. S. Litvinchuk and S. Matile, *Supramol. Chem.*, 2005, **17**, 135-139.
 154. R. Stoll, C. Renner, S. Hansen, S. Palme, C. Klein, A. Belling, W. Zeslawski, M. Kamionka, T. Rehm, P. Mühlhahn, R. Schumacher, F. Hesse, B. Kaluza, W. Voelter, R. A. Engh and T. A. Holak, *Biochemistry*, 2001, **40**, 336-344.
 155. J. M. Davis, A. Truong and A. D. Hamilton, *Org. Lett.*, 2005, **7**, 5405-5408.
 156. H. Yin, G.-i. Lee, K. A. Sedey, J. M. Rodriguez, H.-G. Wang, S. M. Sebt and A. D. Hamilton, *J. Am. Chem. Soc.*, 2005, **127**, 5463-5468.
 157. C. F. Hsu, J. W. Phillips, J. W. Trauger, M. E. Farkas, J. M. Belitsky, A. Heckel, B. Z. Olenyuk, J. W. Puckett, C. C. Wang and P. B. Dervan, *Tetrahedron*, 2007, **63**, 6146-6151.
 158. C. L. Kielkopf, S. White, J. W. Szewczyk, J. M. Turner, E. E. Baird, P. B. Dervan and D. C. Rees, *Science*, 1998, **282**, 111-115.
 159. S. White, J. W. Szewczyk, J. M. Turner, E. E. Baird and P. B. Dervan, *Nature*, 1998, **391**, 468-471.
 160. P. B. Dervan, *Bioorgan. Med. Chem.*, 2001, **9**, 2215-2235.
 161. P. B. Dervan and R. W. Bürli, *Curr. Opin. Chem. Biol.*, 1999, **3**, 688-693.
 162. P. B. Dervan and B. S. Edelson, *Curr. Opin. Struc. Biol.*, 2003, **13**, 284-299.
 163. J. M. Belitsky, S. J. Leslie, P. S. Arora, T. A. Beerman and P. B. Dervan, *Bioorgan. Med. Chem.*, 2002, **10**, 3313-3318.
-

-
164. T. P. Best, B. S. Edelson, N. G. Nickols and P. B. Dervan, *Proc. Natl. Acad. Sci. USA*, 2003, **100**, 12063-12068.
 165. B. S. Edelson, T. P. Best, B. Olenyuk, N. G. Nickols, R. M. Doss, S. Foister, A. Heckel and P. B. Dervan, *Nucleic Acids Res.*, 2004, **32**, 2802-2818.
 166. J. L. Meier, D. C. Montgomery and P. B. Dervan, *Nucleic Acids Res.*, 2012, **40**, 2345-2356.
 167. J. A. Raskatov, A. E. Hargrove, A. Y. So and P. B. Dervan, *J. Am. Chem. Soc.*, 2012, **134**, 7995-7999.
 168. T. W. Synold, B. Xi, J. Wu, Y. Yen, B. C. Li, F. Yang, J. W. Phillips, N. G. Nickols and P. B. Dervan, *Cancer Chemother. Pharmacol.*, 2012, **70**, 617-625.
 169. F. Yang, N. G. Nickols, B. C. Li, G. K. Marinov, J. W. Said and P. B. Dervan, *Proc. Nat. Am. Sci. USA*, 2013, **110**, 1863-1868.
 170. H. Matsuda, N. Fukuda, T. Ueno, M. Katakawa, X. Wang, T. Watanabe, S.-I. Matsui, T. Aoyama, K. Saito, T. Bando, Y. Matsumoto, H. Nagase, K. Matsumoto and H. Sugiyama, *Kidney Int.*, 2011, **79**, 46-56.
 171. J. A. Raskatov, N. G. Nickols, A. E. Hargrove, G. K. Marinov, B. Wold and P. B. Dervan, *Proc. Nat. Am. Sci. USA*, 2012, **109**, 16041-16045.
 172. I. Gamba, I. Salvadó, G. Rama, M. Bertazzon, M. I. Sánchez, V. M. Sánchez-Pedregal, J. Martínez-Costas, R. F. Brissos, P. Gamez, J. L. Mascareñas, M. Vázquez López and M. E. Vázquez, *Chem.-Eur. J.*, 2013, **19**, 13369-13375.
 173. G. Rama, A. Ardá, J.-D. Maréchal, I. Gamba, H. Ishida, J. Jiménez-Barbero, M. E. Vázquez and M. Vázquez López, *Chem.-Eur. J.*, 2012, **18**, 7030-7035.
 174. E. C. Long, P. D. Eason and Q. Liang, *Metal Ions in Biological Systems, Vol 33*, 1996, **33**, 427-452.
 175. D. F. Shullenberger, P. D. Eason and E. C. Long, *J. Am. Chem. Soc.*, 1993, **115**, 11038-11039.
 176. D. F. Shullenberger and E. C. Long, *Bioorg. Med. Chem. Lett.*, 1993, **3**, 333-336.
 177. I. Gamba, G. Rama, E. Ortega-Carrasco, J.-D. Marechal, J. Martinez-Costas, M. Eugenio Vazquez and M. V. Lopez, *Chem. Commun.*, 2014, **50**, 11097-11100.
 178. S. Bajusz, T. Janaky, V. J. Csernus, L. Bokser, M. Fekete, G. Srkalovic, T. W. Redding and A. V. Schally, *Proc. Natl. Acad. Sci. U. S. A.*, 1989, **86**, 6313-6317.
 179. B. L. Bray, *Nat. Rev. Drug. Discov.*, 2003, **2**, 587-593.
 180. C. Piguet, M. Borkovec, J. Hamacek and K. Zeckert, *Coord. Chem. Rev.*, 2005, **249**, 705-726.
 181. C. A. Schalley, A. Lützen and M. Albrecht, *Chem.-Eur. J.*, 2004, **10**, 1072-1080.
 182. M. J. Hannon and L. J. Childs, *Supramol. Chem.*, 2004, **16**, 7-22.
 183. M. Albrecht, *Chem.-Eur. J.*, 2000, **6**, 3485-3489.
 184. D. L. Caulder and K. N. Raymond, *Acc. Chem. Res.*, 1999, **32**, 975-982.
 185. E. C. Constable, *Tetrahedron*, 1992, **48**, 10013-10059.
 186. M. Elhabiri, R. Scopelliti, J.-C. G. Bünzli and C. Piguet, *J. Am. Chem. Soc.*, 1999, **121**, 10747-10762.
 187. J.-C. G. Bünzli, *Accounts Chem. Res.*, 2005, **39**, 53-61.
 188. J.-C. G. Bünzli, C. D. B. Vandevyver, A.-S. Chauvin, M. Gijs and A.-A. Lehr, *CHIMIA*, 2011, **65**, 361.
 189. J. Mason, *Magn. Reson. Chem.*, 1990, **28**, 737-738.
-

-
190. C. Piguet, J.-C. G. Bunzli, G. Bernardinelli, C. G. Bochet and P. Froidevaux, *Dalton Trans.*, 1995, 83-97.
191. A.-S. Chauvin, S. Comby, B. Song, C. D. B. Vandevyver, F. Thomas and J.-C. G. Bünzli, *Chem.-Eur. J.*, 2007, **13**, 9515-9526.
192. V. Alexander, *Chem. Rev.*, 1995, **95**, 273-342.
193. N. André, T. B. Jensen, R. Scopelliti, D. Imbert, M. Elhabiri, G. Hopfgartner, C. Piguet and J.-C. G. Bünzli, *Inorg. Chem.*, 2003, **43**, 515-529.
194. C. D. B. Vandevyver, A.-S. Chauvin, S. Comby and J.-C. G. Bünzli, *Chem. Commun.*, 2007, 1716-1718.
195. A. S. Chauvin, S. Comby, B. Song, C. D. B. Vandevyver, F. Thomas and J.-C. G. Bünzli, *Chem.-Eur. J.*, 2007, **13**, 9515-9526.
196. V. Fernandez-Moreira, B. Song, V. Sivagnanam, A.-S. Chauvin, C. D. B. Vandevyver, M. Gijs, I. Hemmila, H.-A. Lehr and J.-C. G. Bunzli, *Analyst*, 2010, **135**, 42-52.
197. M. Hannon, J. , C. Painting, L. , A. Jackson, J. Hamblin and W. Errington, *Chem. Commun.*, 1997, 1807-1808.
198. J. Malina, M. J. Hannon and V. Brabec, *Nucleic Acids Res.*, 2008, **36**, 3630-3638.
199. M. J. Hannon, V. Moreno, M. J. Prieto, E. Moldrheim, E. Sletten, I. Meistermann, C. J. Isaac, K. J. Sanders and A. Rodger, *Angew. Chem.-Int. Edit. Engl.*, 2001, **40**, 879-884.
200. A. D. Richards, A. Rodger, M. J. Hannon and A. Bolhuis, *Int. J. Antimicrob. Agents*, 2009, **33**, 469-472.
201. G. I. Pascu, A. C. G. Hotze, C. Sanchez-Cano, B. M. Kariuki and M. J. Hannon, *Angew. Chem.-Int. Edit. Engl.*, 2007, **46**, 4374-4378.
202. A. C. G. Hotze, N. J. Hodges, R. E. Hayden, C. Sanchez-Cano, C. Paines, N. Male, M.-K. Tse, C. M. Bunce, J. K. Chipman and M. J. Hannon, *Chem. Biol.*, 2008, **15**, 1258-1267.
203. H. Yu, X. Wang, M. Fu, J. Ren and X. Qu, *Nucleic Acids Res.*, 2008, **36**, 5695-5703.
204. H. Yu, C. Zhao, Y. Chen, M. Fu, J. Ren and X. Qu, *J. Med. Chem.*, 2009, **53**, 492-498.
205. C. Zhao, J. Geng, L. Feng, J. Ren and X. Qu, *Chem.-Eur. J.*, 2011, **17**, 8209-8215.
206. H. Yu, M. Li, G. Liu, J. Geng, J. Wang, J. Ren, C. Zhao and X. Qu, *Chem. Sci.*, 2012, **3**, 3145-3153.
207. M. J. Hannon, I. Meistermann, C. J. Isaac, C. Blomme, J. R. Aldrich-Wright and A. Rodger, *Chem. Commun.*, 2001, 1078-1079.
208. J. M. C. A. Kerckhoffs, J. C. Peberdy, I. Meistermann, L. J. Childs, C. J. Isaac, C. R. Pearmund, V. Reudegger, S. Khalid, N. W. Alcock, M. J. Hannon and A. Rodger, *Dalton Trans.*, 2007, 734-742.
209. L. Cardo and M. J. Hannon, *Inorg. Chim. Acta*, 2009, **362**, 784-792.
210. C. Uerpmann, J. Malina, M. Pascu, G. J. Clarkson, V. Moreno, A. Rodger, A. Grandas and M. J. Hannon, *Chem.-Eur. J.*, 2005, **11**, 1750-1756.
211. J. C. Peberdy, J. Malina, S. Khalid, M. J. Hannon and A. Rodger, *J. Inorg. Biochem.*, 2007, **101**, 1937-1945.
212. Y. Parajo, J. Malina, I. Meistermann, G. J. Clarkson, M. Pascu, A. Rodger, M. J. Hannon and P. Lincoln, *Dalton Trans.*, 2009, 4868-4874.
213. L. Cardo, V. Sadovnikova, S. Phongtongpasuk, N. J. Hodges and M. J. Hannon, *Chem. Commun.*, 2011, **47**, 6575-6577.
-

-
214. S. E. Howson, L. E. N. Allan, N. P. Chmel, G. J. Clarkson, R. van Gorkum and P. Scott, *Chem. Commun.*, 2009, 1727-1729.
 215. S. E. Howson, L. E. N. Allan, N. P. Chmel, G. J. Clarkson, R. J. Deeth, A. D. Faulkner, D. H. Simpson and P. Scott, *Dalton Trans.*, 2011, **40**, 10416-10433.
 216. A. D. Faulkner, R. A. Kaner, Q. M. A. Abdallah, G. Clarkson, D. J. Fox, P. Gurnani, S. E. Howson, R. M. Phillips, D. I. Roper, D. H. Simpson and P. Scott, *Nat. Chem.*, 2014, **6**, 797-803.

Chapter 2

Functionalised symmetrical flexicates

2.1 Introduction

In section 1.4.2 we described work from this laboratory on the synthesis of optically and diastereomerically pure (dr >200:1) helicate-like complexes referred to as flexicates.¹ In order to distinguish between flexicate architectures described, we refer to those linked *via* imine (**A**) *i.e.* $[M_2(\mathbf{BA-AB})_3]^{4+}$ as class Ia and the pyridine (**B**) *i.e.* $[M_2(\mathbf{AB-BA})_3]^{4+}$ as class Ib systems. Water soluble examples of such flexicates are remarkably stable over extended time periods in a variety of media (*vide infra*). Only the class Ia flexicates have been found to interact in a specific manner with DNA in a cell free environment² and exhibit antibiotic activity against MRSA (*Methicillin-resistant Staphylococcus aureus*) and *Escherichia coli*. Although, both class Ia and class Ib compounds have been found to have low toxicity towards the nematode worm *Caenorhabditis elegans*.¹

Since the self-assembly of flexicates is dictated by the formation of monometallic units at either end of the structure, it should be possible to use a range of linker classes and also to include a wider variety of functionality than which appears in traditional helicates. Flexicate architectures with differing functionalities incorporated into the ligand were proposed, with a focus on the class Ib systems. These have proved to be the most synthetically tractable and have shown some promising anticancer activity and selectivity.^{1, 2}

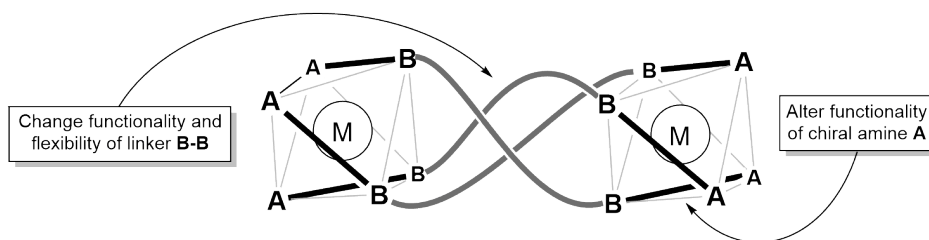


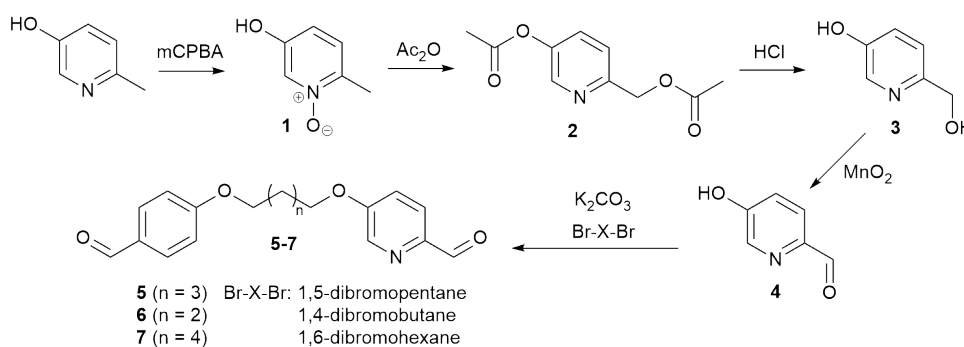
Figure 2.1 | Cartoon of the strategy to alter the flexicate ligand with a view to producing a library of architectures.

In this chapter we will begin to explore the extent to which the flexicate architecture $[M_2(AB-BA)_3]^{4+}$ can withstand inclusion of different functionalities, both at the chiral amine end group (A) and within the central dipyrrolyl linear linker (B-B) of the ligand. This would give us access to a previously unknown range of compounds. By including functional groups, the properties of the flexicate may be altered, for example to include different supramolecular interactions with key proteins, membranes or DNA. An investigation into the potential of these compounds as antimicrobial and anticancer agents is also detailed, along with several studies into their possible modes of action.

2.2 Synthesis of a range of functionalised flexicates

2.2.1 Synthesis of functionally diverse dialdehyde units

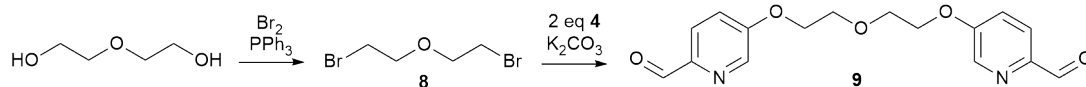
Dipyridyl units (**B-B**) with various lengths, hydrophilicity and rigidity were synthesised and characterised.



Scheme 2.1 | Synthesis of dipicolinaldehyde units **5-7** via 5-hydroxypicolinaldehyde (**4**).³

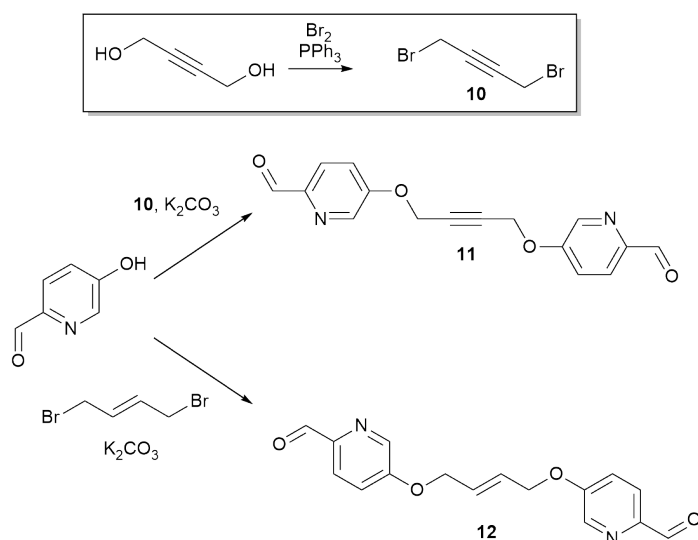
A key synthon for this work was 5-hydroxypicolinaldehyde **4**, which was prepared on a multigram scale several times using a modified literature method (scheme 2.1).³ First 25 g of 5-hydroxy-2-methylpyridine was treated with *m*-chloroperoxybenzoic acid (mCPBA) to give 5-hydroxy-2-methylpyridine-1-oxide (**1**). This was diacetylated to 6-[(acetyloxy)methyl]pyridine-3-yl acetate (**2**) and then hydrolysed in refluxing hydrochloric acid to 6-(hydroxymethyl)pyridine-3-ol (**3**). Oxidation with activated manganese dioxide gave 5.8 g of the target aldehyde **4** (23%).

Simple alkyl-bridged dipyridyls with C₄-C₆ units including the previously reported 5,5'-(pentane-1,5-diylbis(oxy))dipicolinaldehyde,⁴ (**5**) 5,5'-(butane-1,4-diylbis(oxy))dipicolinaldehyde (**6**), and 5,5'-(hexane-1,6-diylbis(oxy))-dipicolinaldehyde (**7**) were synthesised *via* Williamson etherification of **4** with the corresponding α,ω -dibromoalkane in the presence of potassium carbonate.⁴



Scheme 2.2 | Synthesis of 5,5'-(2,2'-oxybis(ethane-2,1-diyl)bis(oxy))dipicolinaldehyde (**9**) *via* 1-bromo-2-(2-bromoethoxy)ethane ⁵ (**8**).

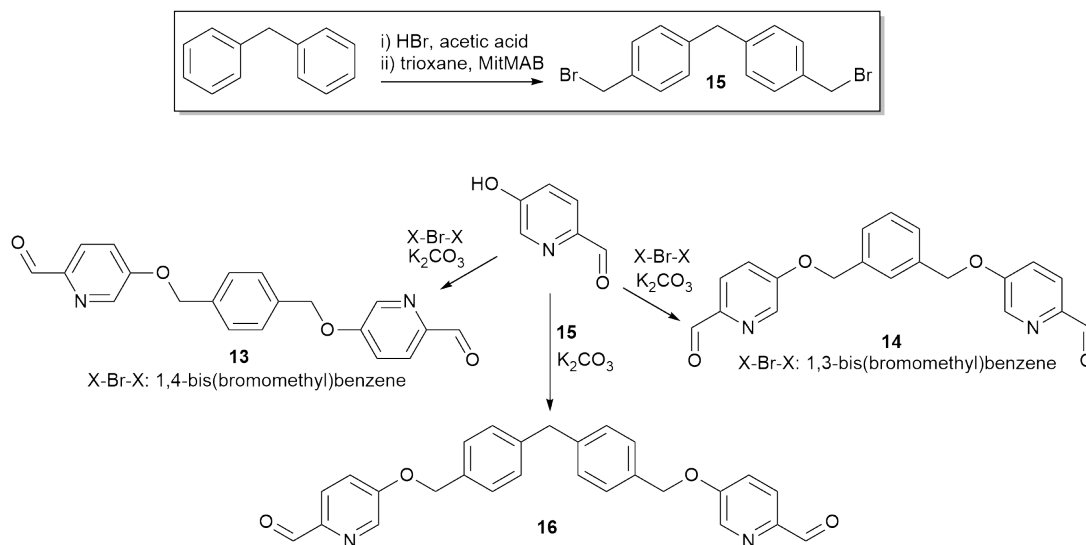
The inclusion of heteroatoms in the linker was also successful (scheme 2.2); 1-bromo-2-(2-bromoethoxy)ethane (**8**) was prepared by brominating diethylene glycol in the presence of triphenylphosphine, before etherification with **4** to 5,5'-(2,2'-oxybis(ethane-2,1-diyl)bis(oxy))dipicolinaldehyde (**9**).



Scheme 2.3 | Synthesis of 5,5'-(but-2-yne-1,4-diylbis(oxy))dipicolinaldehyde (**11**) *via* 1,4-dibromobut-2-yne (**10**) and (E)-5,5'-(but-2-ene-1,4-diylbis(oxy))dipicolinaldehyde (**12**)

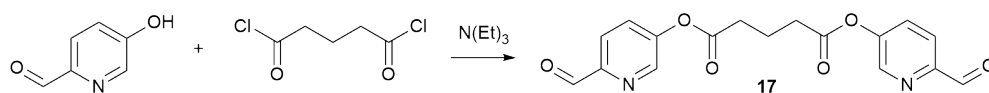
To increase the rigidity of the ligand a number of unsaturated and aromatic systems were synthesised (scheme 2.3). The alkyne 1,4-dibromobut-2-yne (**9**) was prepared *via* bromination of 2-butyne-1,4-diol.⁵ Subsequent etherification of this with 5-hydroxypicolinaldehyde in the presence of potassium carbonate gave 5,5'-(but-2-yne-1,4-diylbis(oxy))dipicolinaldehyde (**11**). The alkene (E)-5,5'-(but-2-ene-1,4-diylbis(oxy))dipicolinaldehyde (**12**) from 1,4-trans-dibromobut-2-ene.

The dialdehyde 5,5'-(1,4-phenylenebis(methylene))bis(oxy)dipicolinaldehyde (**13**), analogous to the aryl-bridged linker in a previously reported class Ia flexicate¹ was synthesised similarly from 1,4-bis(bromomethyl)benzene, and its isomer 5,5'-(1,3-phenylenebis(methylene))bis(oxy)dipicolinaldehyde (**14**) was also formed from 1,3-bis(bromomethyl)benzene (scheme 2.4).



Scheme 2.4 | Synthesis of 5,5'-(1,4-phenylenebis(methylene))bis(oxy)dipicolinaldehyde (**13**), 5,5'-(1,3-phenylenebis(methylene))bis(oxy)dipicolinaldehyde (**14**) and 5,5'-(4,4'-methylenebis(4,1-phenylene))bis(methylene))bis(oxy)dipicolinaldehyde (**16**) via bis(4-(bromomethyl)phenyl)methane (**15**)⁶.

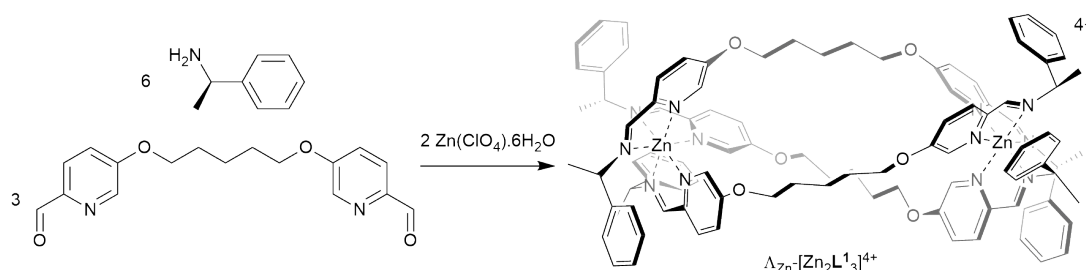
Bis(4-(bromomethyl)phenyl)methane (**15**) was synthesised *via* a literature method:⁶ the reaction of diphenylmethane, 1,3,5-trioxane and catalytic tetradecyltrimethyl ammonium bromide in hydrobromic and acetic acids (scheme 2.5). Following etherification with **4**, 5,5'-(4,4'-methylenebis(4,1-phenylene))bis(methylene))bis(oxy)dipicolinaldehyde (**16**) was successfully isolated.



Scheme 2.5 | Synthesis of bis(6-formylpyridin-3-yl) glutarate (**17**).⁷

An ester-linked dipicolinaldehyde unit was investigated (scheme 2.5); bis(6-formylpyridin-3-yl) glutarate (**17**) prepared *via* esterification⁷ of **4** and glutaryl chloride in dry tetrahydrofuran and triethyl amine and then was purified by column chromatography.

2.2.2 Synthesis of zinc(II) flexicates



Scheme 2.6 | Self-assembly of flexicate $\Lambda_{\text{Zn}}\text{-}[\text{Zn}_2\text{L}^1_3][\text{ClO}_4]_4$

The synthesis of all the class Ib flexicates followed the same method as the previously reported $\Lambda_{\text{Zn}}\text{-}[\text{Zn}_2\text{L}^1_3][\text{ClO}_4]_4$ (scheme 2.6).¹ (*R*)-1-phenylethan-1-amine (6 eq.) and the appropriate dialdehyde unit (3 eq.) were dissolved in acetonitrile. Zinc(II) perchlorate* hexahydrate (2 eq.) was added and the flexicate species self-assembled in solution at ambient temperature. The product that precipitated upon addition of ethyl acetate to the reaction mixture was collected and dried under reduced pressure. This self-assembly method typically gave the desired single species in 40% isolated yield, although NMR analysis indicated essentially complete conversion. The compounds were characterised by NMR spectroscopy, mass

* For perchlorate safety measures see section 5.1.1

spectrometry, infra-red spectroscopy and microanalysis. Typical data and features of interest in the data are discussed below.

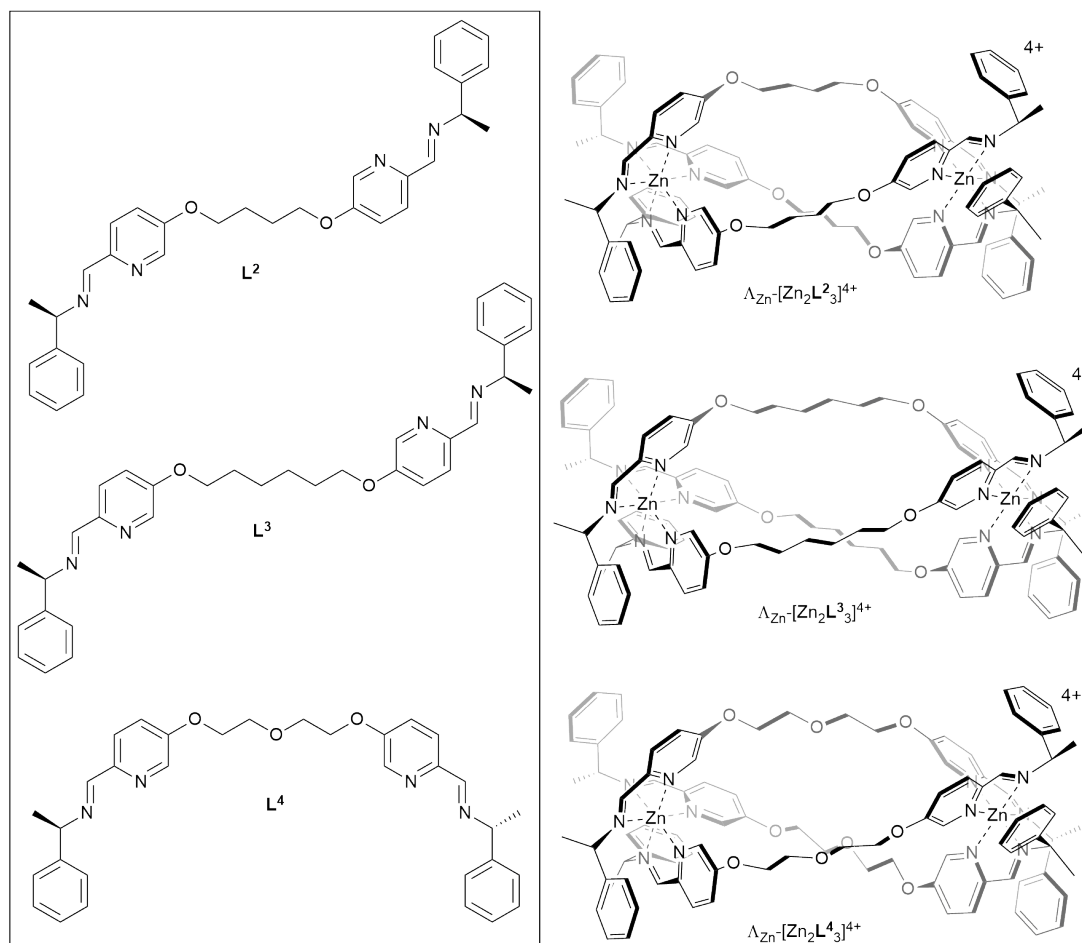


Figure 2.2 | Structure of L^2 - L^4 synthesised with flexible aliphatic linkers and structures of the assembled flexicates $\Lambda_{Zn}-[Zn_2L^x_3][ClO_4]_4$ ($x = 2-4$).

The range of aliphatic ether linked class 1b flexicates was extended successfully to include all the target compounds: $\Lambda_{Zn}-[Zn_2L^x_3][ClO_4]_4$ ($x = 1-4$). The first class 1b flexicates containing more rigid linkers were afforded; **11** and **12** gave $\Lambda_{Zn}-[Zn_2L^5_3][ClO_4]_4$ and $\Lambda_{Zn}-[Zn_2L^6_3][ClO_4]_4$ respectively. The 1H -NMR spectrum of $\Lambda_{Zn}-[Zn_2L^6_3][ClO_4]_4$ in d^3 -acetonitrile at 298 K indicates a high diastereomeric purity by the absence of additional peaks in the imine region (8-10 ppm). Indeed for each environment only one peak is seen (**a-e**, Fig 2.3ii).

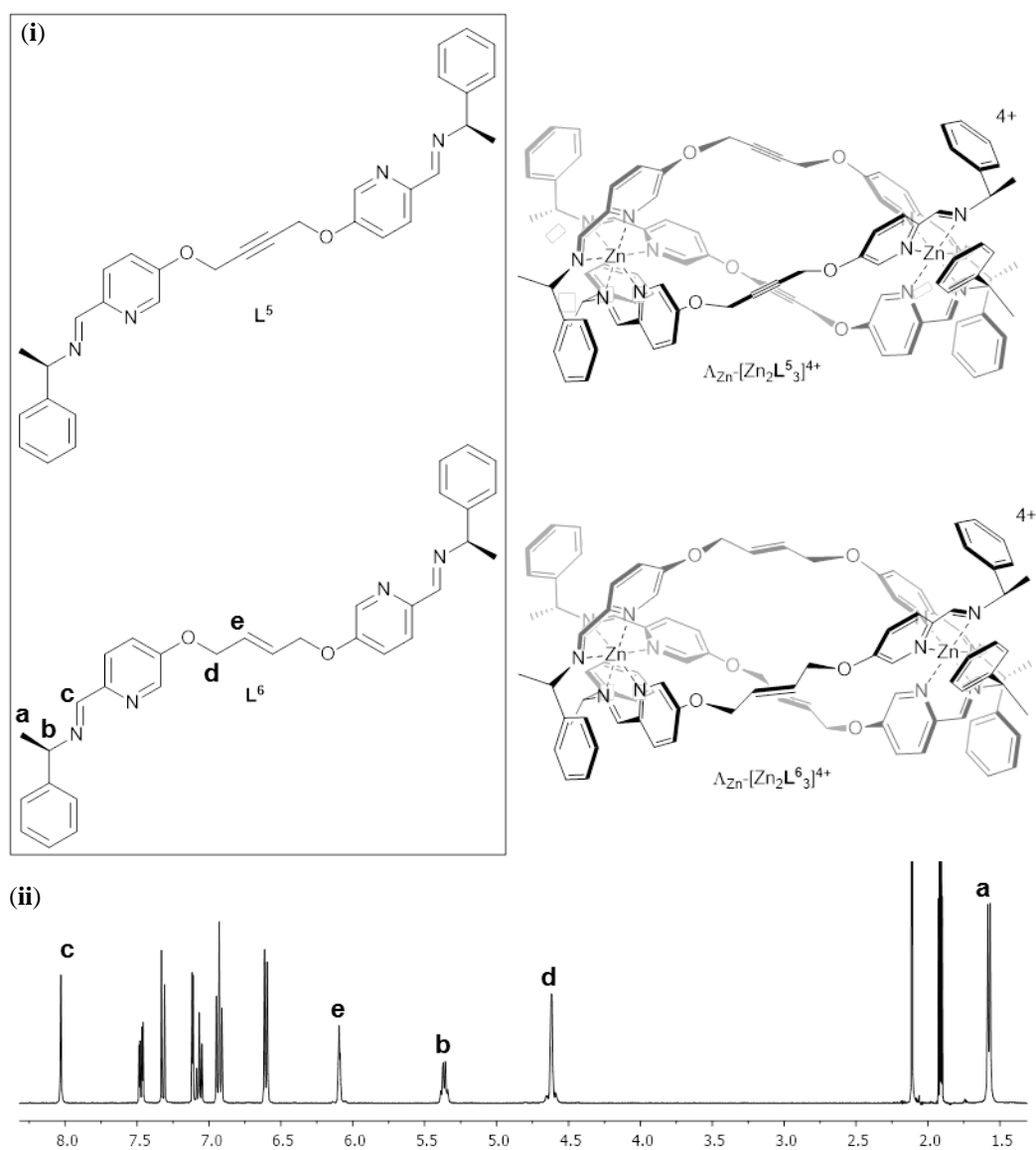


Figure 2.3 | (i) Structure of L^5 and L^6 and structures of the assembled flexicats $\Lambda_{Zn}-[Zn_2L^5_3][ClO_4]_4$ and $\Delta_{Zn}-[Zn_2L^6_3][ClO_4]_4$ (ii) 1H NMR spectrum of $\Lambda_{Zn}-[Zn_2L^6_3][ClO_4]_4$ at 298 K in d^3 -acetonitrile (δ_H 1.95, water present δ_H 2.19), recorded using 400 MHz spectrometer.

The 1,4-aryl-bridged system $\Lambda_{Zn}-[Zn_2L^7_3][ClO_4]_4$ was found to have reduced solubility compared to other architectures. However, the 1H -NMR spectrum in d^3 -acetonitrile at 298 K indicates that a highly symmetrical, diastereomerically pure species has formed (Fig. 2.4).

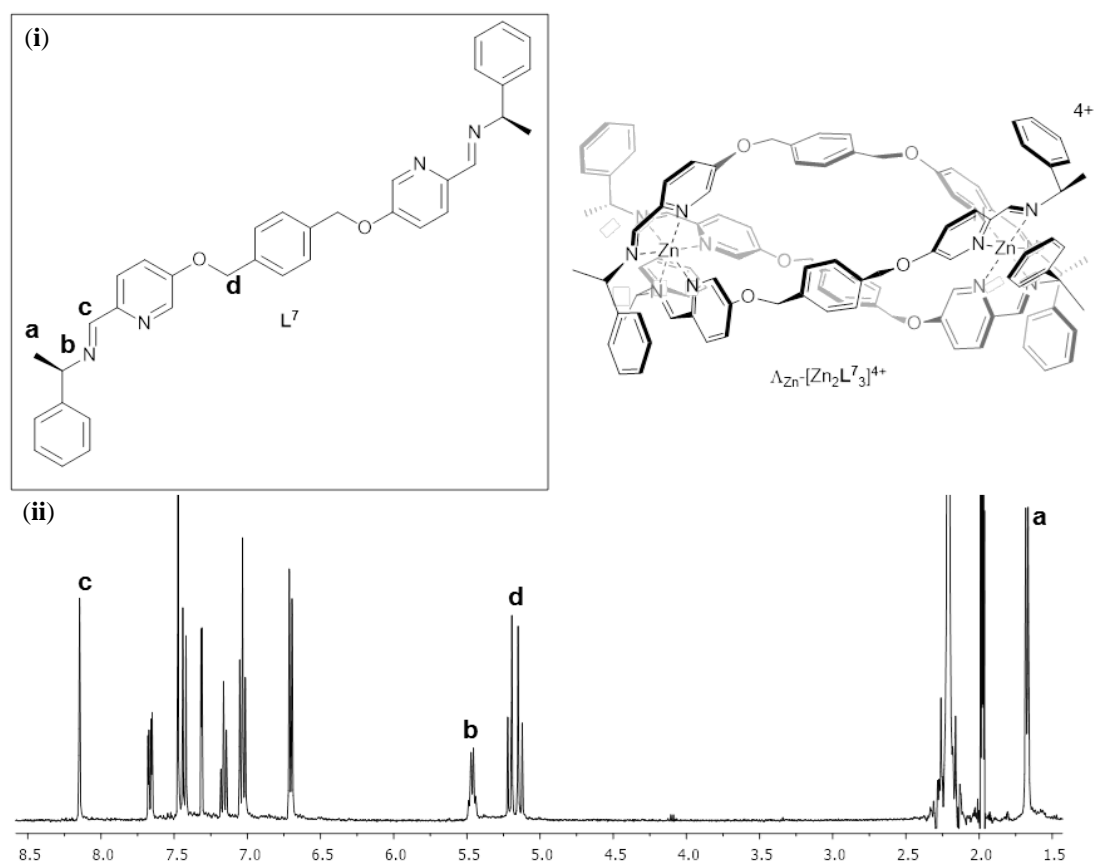


Figure 2.4 | (i) Structure of L^7 and structures of the assembled flexicates $\Lambda_{Zn}[\text{Zn}_2L^7_3][\text{ClO}_4]_4$ (ii) ^1H NMR spectrum of $\Lambda_{Zn}[\text{Zn}_2L^7_3][\text{ClO}_4]_4$ at 298 K in d^3 -acetonitrile (δ_{H} 1.95, water present δ_{H} 2.19), recorded using 400 MHz spectrometer at 298 K.

The complex containing the 1,3-phenylene bridge *i.e.* $\Lambda_{Zn}[\text{Zn}_2L^8_3][\text{ClO}_4]_4$ has a more complex ^1H -NMR spectrum, indicating the presence of more than one species (Fig 2.5). At 253 K the methyl group (a) doublet resonances at 1.4-1.7 ppm contain one large doublet and two broader resonances in the ratio *ca* 1.0:0.1:0.1. The proportion of the minor species increases with temperature and the resonances sharpen somewhat; such that by 313 K two of the smaller doublets corresponding to the minor species are relatively sharp and resolved while a third overlaps with the main resonance. By 353 K the minor peaks had broadened considerably and were observed to be in the ratio of 1.0:0.3:0.3 with the major peak. The imine region (8.5 – 7.6 ppm 1:0.1 at 253 K, 1:0.3 at 353 K) behaved in a corresponding manner.

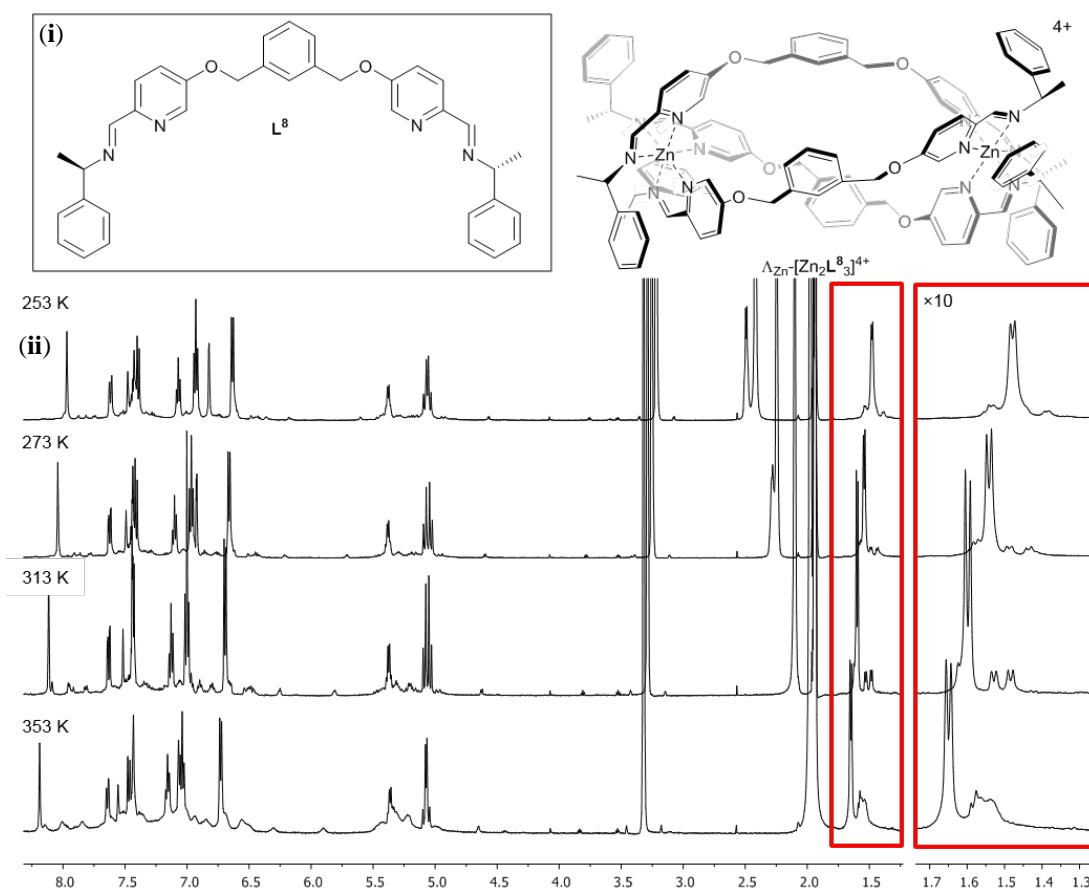


Figure 2.5 | (i) Structure of L^8 and structures of the assembled flexicate $\Lambda_{Zn}-[Zn_2L^8_3][ClO_4]_4$. (ii) 1H NMR spectra of $\Lambda_{Zn}-[Zn_2L^8_3][ClO_4]_4$ at 253 – 353 K in d^3 -acetonitrile (δ_H 1.95, water present δ_H 2.19), recorded using 400 MHz spectrometer at 298 K, with magnified area shown in red depicting increasing population of second asymmetric conformer.

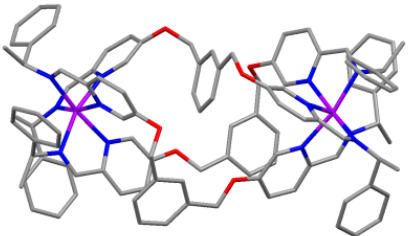
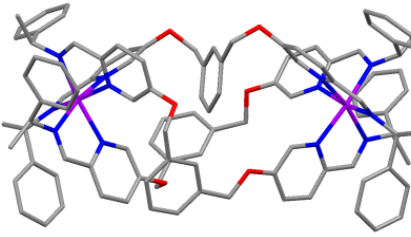
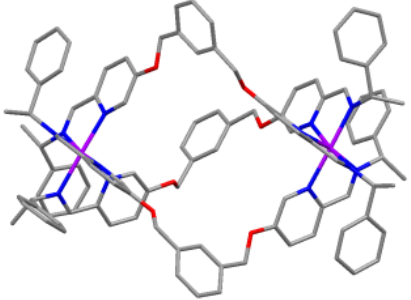
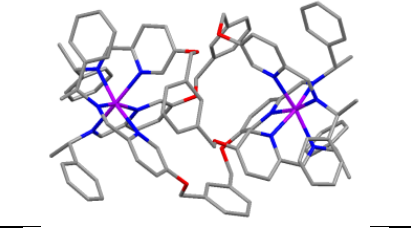
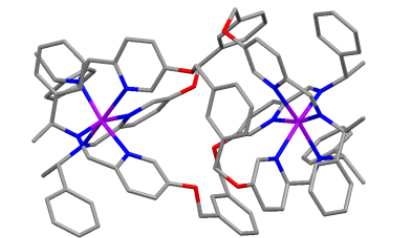
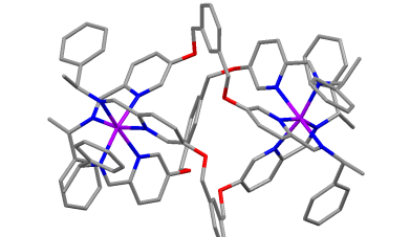
These observations are consistent with the presence of one high symmetry and one low symmetry species in thermodynamic equilibrium (ratio *ca* 1:0.3 at low temperature, increasing to 1:1 at high temperature). The processes leading to the observed variable temperature NMR behaviour may correspond to exchange between these conformers, or indeed between isostructural low symmetry species. While the spectra are not sufficiently well resolved to determine kinetic parameters, we sought to investigate this molecular system by computational means.

A number of possible conformers of $\Lambda_{\text{Zn}}\text{-}[\text{Zn}_2\text{L}_3][\text{ClO}_4]_4$ were constructed and optimised by Dr Alan Faulkner using the methods described in section 5.8. A range of candidate structures was constructed and annealed using DommiMOE at 500 K before cooling to 0 K. The output structures were then optimised using ORCA (DFT calculations) including a correction for solvent.

The six calculated conformers fell into two classes: those where the three *m*-xylenyl groups were oriented away from the central cavity *i.e.* *exo*, and those where one such group was oriented *endo*. No conformers were observed in which two or three *m*-xylenyl groups were oriented into the cavity. Presumably, this is due to such conformations being unstable for steric reasons and possibly having high strain about each octahedral metal subunit.

Structure *endo1* (Table 2.1) was found to be the lowest in energy, the next lowest being *endo2* (*ca* +5 kcal mol⁻¹) which differs only in the fold of one of the linkers. For these structures the Zn-Zn distances are *ca* 11.7 and 11.8 Å respectively. The structure *exo1* (+7 kcal mol⁻¹) has a large central cavity but a similar Zn-Zn distance (11.8 Å). The structure *exo2* (+8 kcal mol⁻¹) has a considerably shorter Zn-Zn distance at *ca* 9.5 Å with accompanying concertinaed fold. Furthermore, higher energy conformers *exo3* and *exo4* differed principally in how the *m*-xylenyl groups folded towards each metal centre. Both were found to have a short Zn-Zn distances of 9.4 and 9.5 Å respectively.

Table 2.1 | Calculated structures, relative energies (compared to *endo1*) and Zn-Zn distances of the six conformational isomers of $\Lambda_{\text{Zn}}\text{-}[\text{Zn}_2\text{L}_3][\text{ClO}_4]_4$.

Conformer		Relative energy /kcal mol ⁻¹	Zn-Zn distance /Å
	<i>endo1</i>	0	11.7
	<i>endo2</i>	5.4	11.8
	<i>exo1</i>	7.1	11.8
	<i>exo2</i>	7.9	9.5
	<i>exo3</i>	12.4	9.4
	<i>exo4</i>	24.8	9.5

Our expectation would be that the barrier to conversion between *exo* structures is low since it would involve a relatively simple concertina-type process; and we propose that the located *exo* species of Table 2.1 and perhaps other high symmetry conformations are responsible for the majority species in the NMR spectra (Fig. 2.5). The low symmetry *endo* species are proposed to give rise to the minority NMR spectrum described above. Conversion between *exo* and *endo* conformations requires the rotation of the *m*-xylenyl linker through a strained, high energy transition state. Given the total number of possible structures, the accompanying entropy becomes very difficult to take into account, so prediction of population from the above calculations is very challenging. Nevertheless, these calculations strongly support our proposal that the major symmetric isomer has the three 1,3-phenylene bridges in an *exo* conformation as shown in Fig 2.4(i), while an asymmetric species has one or more such groups in an *endo* conformation.

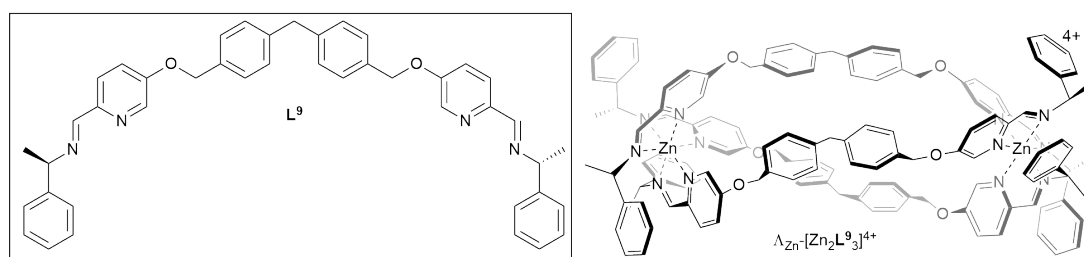


Figure 2.6 | Structure of L^9 and structure of the assembled flexicate $\Lambda_{Zn}-[Zn_2L^9_3][ClO_4]_4$.

In contrast to the above, the flexicate $\Lambda_{Zn}-[Zn_2L^9_3][ClO_4]_4$ incorporating the diphenylmethylene linker unit **16** gave a conventional 1H NMR spectrum; while the ligands L^8 and L^9 are topologically similar, steric effects preclude the possibility of *endo* conformers of the latter system.

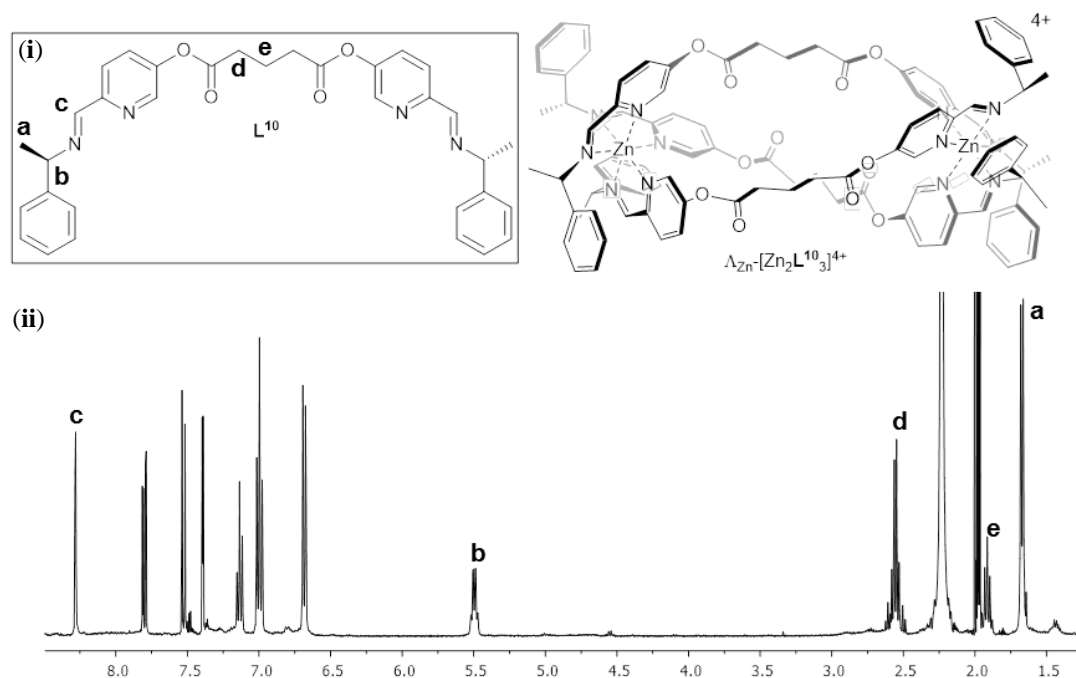


Figure 2.7 | (i) Structure of L^{10} and structure of the assembled flexicate $\Lambda_{Zn}-[Zn_2L^{10}_3][ClO_4]_4$ (ii) 1H NMR spectrum of $\Lambda_{Zn}-[Zn_2L^{10}_3][ClO_4]_4$ at 298 K in d^3 -acetonitrile (δ_H 1.95, water present δ_H 2.19), recorded using 400 MHz spectrometer at 298 K.

The ester-linked system $\Lambda_{Zn}-[Zn_2L^{10}_3][ClO_4]_4$ self-assembled to form a symmetric flexicate. In the 1H NMR spectrum, the diastereotopic CH_2 groups adjacent to the ester carbonyls appear as a second order system at 2.5 ppm (**d**) while the central CH_2 groups, being further away from the sources of chirality, give a simple quintet at 1.9 ppm (**e**).

2.2.3 Flexicates with functionalised amine units

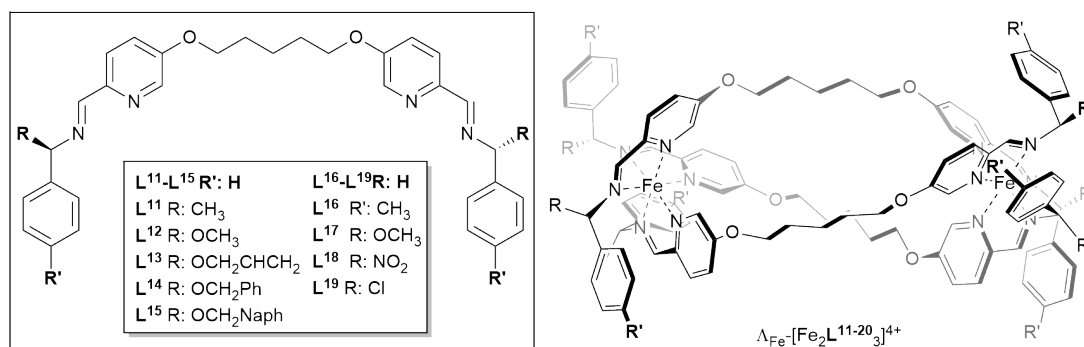
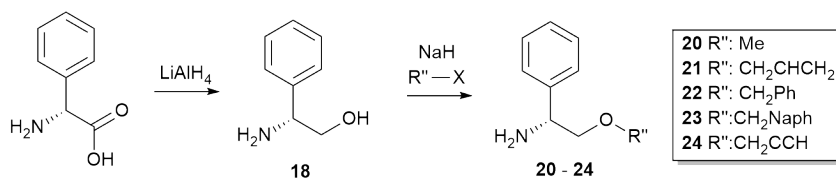


Figure 2.8 | Structure of L^{11-20} with differing functionality at position R and R' and structures of $\Lambda_{Fe}[\text{Fe}_2L^x_3][\text{ClO}_4]_4$ ($x = 11 - 20$).

It is possible to include functional groups on the chiral amine of the ligand, with a few examples having been demonstrated previously.^{1, 8} The inclusion of more functionality was explored here. In this study, iron(II) perchlorate was used as the metal source as it had been demonstrated to form the desired flexicate architecture with the previously known $[\text{Fe}_2L^S_3][\text{ClO}_4]_4$ and $[\text{Fe}_2L^1_3][\text{ClO}_4]_4$.¹

Reduction of optically pure D-phenylglycine with lithium aluminium hydride gave (*R*)-phenylglycinol (**18**).⁹ This alcohol was converted to a range of ethers (scheme 2.7) using a modified Williamson ether synthesis in the presence of sodium hydride (**20-25**).¹⁰



Scheme 2.7 | Reduction of (*R*)-phenylglycine to (*R*)-phenylglycinol and subsequent modified ether synthesis.^{9, 10}

The chiral amines (6 eq.) were dissolved in acetonitrile with dialdehyde **5**⁴ (3 eq.). Iron(II) perchlorate hexahydrate (2 eq.) was added, and after heating to reflux,

cooling and addition of ethyl acetate, the diastereomerically pure flexicate, a dark purple crystalline solid, was collected and dried. $[\text{Fe}_2\text{L}^{\mathbf{x}}_3][\text{ClO}_4]_4$ ($\mathbf{x} = \mathbf{11-15}$, Fig 2.8) formed in an analogous manner to the zinc(II) complexes described earlier (see chapter 5 for full analyses).

Single crystals of $\Delta_{\text{Fe}}\text{-}[\text{Fe}_2\text{L}^{\mathbf{14}}_3][\text{ClO}_4]_4$ were grown upon slow diffusion of a layer of water into a solution of the complex in acetonitrile. Diffraction data were recorded by Dr Guy Clarkson on an Xcalibur Gemini diffractometer, but the structure was only partially resolved because there was a high degree of disorder, particularly in the terminal alkene groups and the perchlorate counter ions (removed from Fig 2.9 for clarity). Each of the pentyl linkers takes a different path between the stereogenic octahedral iron(II) complexes at either end of the molecule and thus, as predicted, this diastereomerically pure class Ib flexicate is assembled without a contribution from mechanical coupling of the two metal centres. As in previous *monometallic* structures, the diastereoselection arises in part from hydrophobic inter-ligand π -stacking interactions.^{1, 11, 12} An acetonitrile molecule occupies the cavity between the two metal centres in the complex.

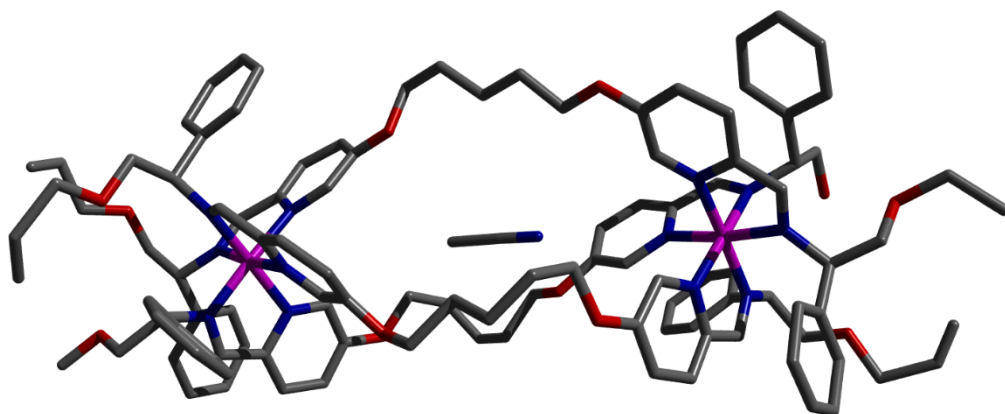


Figure 2.9 | Partially resolved crystal structure of $\Delta_{\text{Fe}}\text{-}[\text{Fe}_2\text{L}^{\mathbf{14}}_3][\text{ClO}_4]_4\cdot\text{MeCN}$ with acetonitrile molecule occupying the cavity.

In addition to the above phenylglycinol-derived examples, we exploited the availability of *p*-substituted phenylethylamines (Fig 2.8, **R'**), allowing us to further extend the range of functionality in class Ib flexicate architectures. The compounds $[\text{Fe}_2\text{L}^{\mathbf{x}}_3][\text{ClO}_4]_4$ (**x** = **16-19**, Fig 2.8) were synthesised by analogous methods to the above.

2.2.4 Synthesis of highly water soluble complexes

In order to prepare water-compatible systems for biological testing we turned to iron(II) chloride as the metal source. Four class Ib systems – $[\text{Fe}_2\text{L}^{\mathbf{x}}_3]\text{Cl}_4$ (**x** = **4, 5, 6** and **8**) – were selected to demonstrate these syntheses and to compliment the previously known class Ib ($[\text{Fe}_2\text{L}^{\mathbf{1}}_3]\text{Cl}_4$) and class Ia ($[\text{Fe}_2\text{L}^{\mathbf{S}}_3]\text{Cl}_4$) flexicates.^{2, 8} Unfortunately the *p*-xylenyl bridged $[\text{Fe}_2\text{L}^{\mathbf{7}}_3]\text{Cl}_4$ and diphenylmethylene-bridged $[\text{Fe}_2\text{L}^{\mathbf{9}}_3]\text{Cl}_4$ displayed poor solubility in aqueous media making them unsuitable for testing. The assembly of the ester linked $[\text{Fe}_2\text{L}^{\mathbf{10}}_3]\text{Cl}_4$ was unsuccessful, perhaps due to the ester carbonyl groups in the linker which may bind iron(II).

Pairs of water soluble flexicate enantiomers were synthesised in high yield by heating the appropriate dipicolinaldehyde linker (3 eq.) and either (*R*)- or (*S*)-1-phenylethan-1-amine (6 eq.), with iron(II) chloride (2 eq.) to reflux in methanol. The dark purple solutions were filtered through silica gel and evaporated carefully to dryness. The products were analysed by NMR spectroscopy, mass spectrometry, microanalysis, thermogravimetric analysis, infra-red, UV-vis absorption, and circular dichroism spectroscopies.

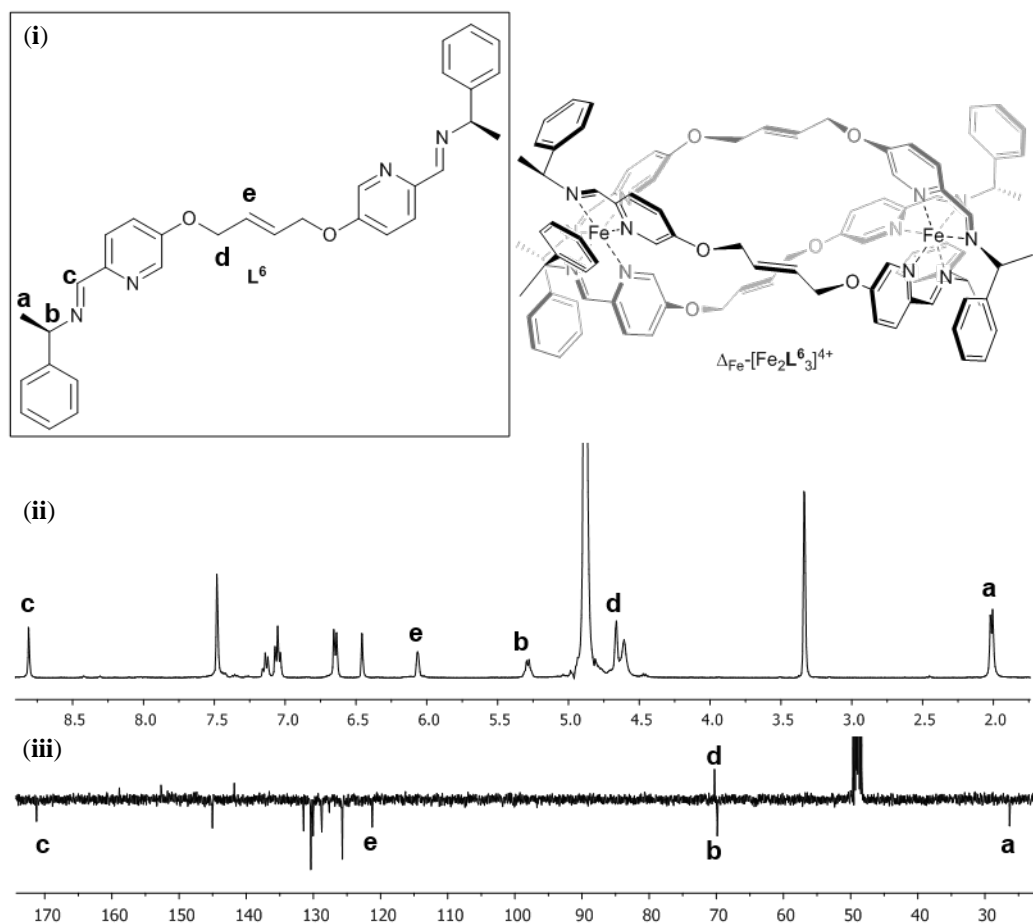


Figure 2.10 | (i) Structure of L^6 and structure of the assembled flexicate $\Delta_{Fe}[\text{Fe}_2L^6][\text{Cl}_4]$. (ii) ^1H -NMR spectrum (iii) $^{13}\text{C}\{^1\text{H}\}$ -NMR spectrum of $\Delta_{Fe}[\text{Fe}_2L^6]\text{Cl}_4$ 298 K in d^4 -methanol (δ_{H} 3.31, δ_{C} 49, water present δ_{H} 4.87), recorded using 400 MHz spectrometer at 298 K.

The complexes gave excellent electrospray mass spectrometry data with, for example $\Delta_{Fe}[\text{Fe}_2L^4]^{4+}$ giving a strong peak at m/z 420.17 Da for the tetracationic ion. The ^1H -NMR spectra were similar but typically broader than the analogous zinc(II) perchlorate complexes; the spectra of $\Delta_{Fe}[\text{Fe}_2L^6]\text{Cl}_4$ [Fig 2.10] are typical, and are consistent with the presence of single diastereomers. Circular dichroism spectra of each pair of enantiomers were recorded in water (0.03 mM). Each displayed equal and opposite spectra, indicating that the complexes were formed in non-racemic mixtures of opposite configurations. Spectra for other complexes are presented in chapter 5 and appendix A.

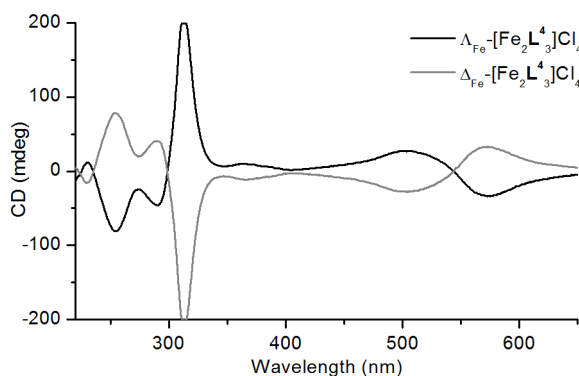


Figure 2.11 | CD spectra of $\Lambda_{\text{Fe}}\text{-[Fe}_2\text{L}_3\text{]Cl}_4$ and $\Delta_{\text{Fe}}\text{-[Fe}_2\text{L}_3\text{]Cl}_4$ (0.03 mM) in H_2O , showing each pair of enantiomers has equal and opposite spectra.

2.2.5 Water of crystallisation

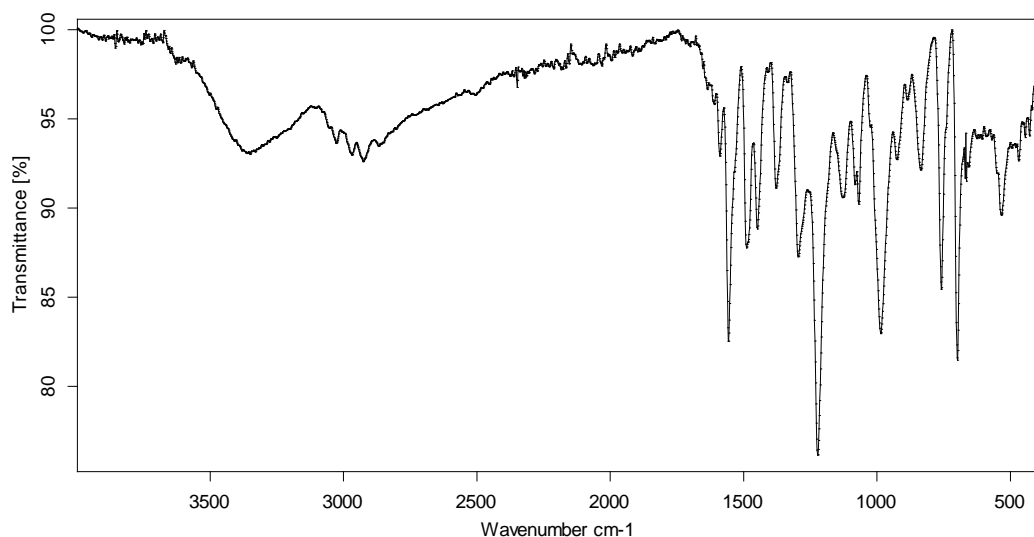


Figure 2.12 | Infra-red spectrum of $\Lambda_{\text{Fe}}\text{-[Fe}_2\text{L}_3\text{]Cl}_4\cdot 9\text{H}_2\text{O}$.

The formula weights of the panel of complexes, including the level of water of crystallisation were determined by combining data from a range of techniques. First, NMR spectroscopy showed that the samples contained only the complex and water; the latter was confirmed by IR spectroscopy (*e.g.* Fig 2.12) where the two broad and intense O-H stretching modes were observed in the region $3000\text{--}3500\text{ cm}^{-1}$.

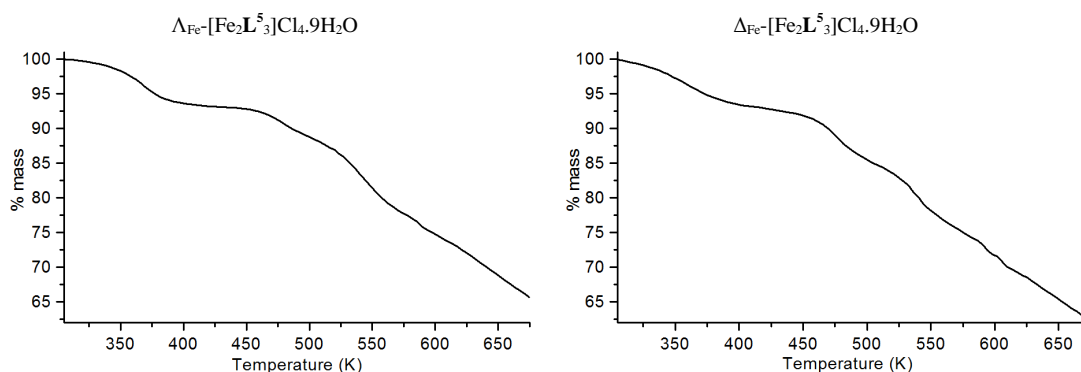


Figure 2.13 | Thermogravimetric spectra of $\Lambda_{\text{Fe}}\text{-}[\text{Fe}_2\text{L}^5_3]\text{Cl}_4\cdot 9\text{H}_2\text{O}$ and $\Delta_{\text{Fe}}\text{-}[\text{Fe}_2\text{L}^5_3]\text{Cl}_4\cdot 9\text{H}_2\text{O}$, indicating mass lost due to water of crystallisation and thermal decomposition.

Thermogravimetric analysis was performed (*e.g.* Fig 2.13) in all cases, showing a significant mass loss between 300 and 400 K, consistent with loss of water of crystallisation, before further mass loss at higher temperatures. In the case of enantiomers $\Lambda_{\text{Fe}}\text{-}[\text{Fe}_2\text{L}^5_3]\text{Cl}_4$ and $\Delta_{\text{Fe}}\text{-}[\text{Fe}_2\text{L}^5_3]\text{Cl}_4$ 8.5% ($\pm 0.5\%$) of the total mass was lost at the lower temperature, corresponding to nine equivalents of water per complex (for calculations, see appendix A). This result was typical for the complexes synthesised here. It was found that the thermogravimetric and microanalytical data (table 2.2) correlated well in all cases. Also, samples of enantiomers gave, within error limits, the same thermogravimetric and microanalytical results, thus adding further confidence to our interpretation of these measurements. Further data are presented in chapter 5 and appendix A.

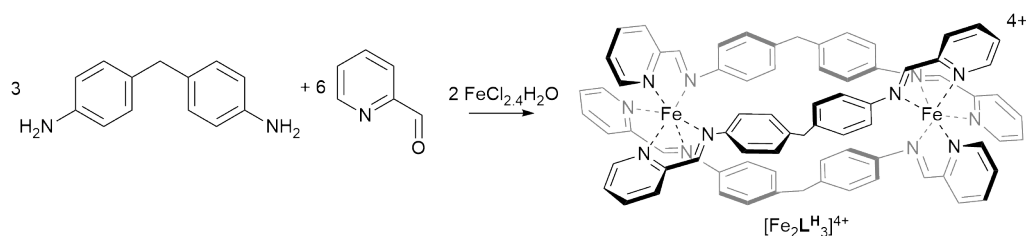
Table 2.2 | Recorded and theoretical elemental analysis of $\Lambda_{\text{Fe}}\text{-}[\text{Fe}_2\text{L}^5_3]\text{Cl}_4\cdot 9\text{H}_2\text{O}$ and $\Delta_{\text{Fe}}\text{-}[\text{Fe}_2\text{L}^5_3]\text{Cl}_4\cdot 9\text{H}_2\text{O}$.

Complex	% C	% H	% N
$\text{C}_{96}\text{H}_{90}\text{Cl}_4\text{Fe}_2\text{N}_{12}\text{O}_6\cdot 9\text{H}_2\text{O}$	60.0	5.7	8.7
$\Lambda_{\text{Fe}}\text{-}[\text{Fe}_2\text{L}^5_3]\text{Cl}_4\cdot 9\text{H}_2\text{O}$	59.6	5.5	8.6
$\Delta_{\text{Fe}}\text{-}[\text{Fe}_2\text{L}^5_3]\text{Cl}_4\cdot 9\text{H}_2\text{O}$	60.6	5.5	8.8

2.2.6 Synthesis of the Hannon helicate

We wished to include the water-soluble helicate from the Hannon group¹³ for comparison with our new complexes in biological studies, but while the synthesis of

this compound is described in outline,¹⁴ to our knowledge no detailed synthetic method or characterising data for this compound with chloride counter-ions have appeared.



Scheme 2.8 | Self-assembly of the known helicate, $[\text{Fe}_2\text{L}^{\text{H}}_3]\text{Cl}_4 \cdot 4\text{H}_2\text{O}$.

The synthesis of this helicate was investigated in detail by Pratik Gurnani. 4,4'-methylenedianiline and 2-pyridinecarboxaldehyde were heated to reflux with iron(II) chloride tetrahydrate in methanol. After careful evaporation of the solvent the crude product was shown to contain a number of impurities, but washing with dichloromethane and drying under reduced pressure gave clean samples which were thoroughly characterised. The material produced was consistently found, *via* thermogravimetric analysis and microanalysis as above, to contain four water molecules of crystallisation. To our knowledge this has not been noted in the literature. Attempts to separate this racemic helicate by chiral chromatography¹⁵ were not successful.

2.2.7 Complex stability in aqueous media

Sufficient stability in aqueous media is a vital attribute for any molecule which is intended to be tested for activity in the biological regime, unless its degradation is an integral part of any observed activity. To investigate how the water soluble class Ib flexicates behave in aqueous media over an extended period of time, their

absorbance spectra were recorded in various aqueous media. The Hannon helicate was included for comparison.

Little decomposition of the new flexicates occurred in neutral water over a reasonable timescale, but half-lives for decomposition could readily be recorded in acid. A 0.03 mM solution of each compound was made up in hydrochloric acid (0.2 M) and absorbance spectra in the range 350-650 nm were measured periodically. The absorbance at 540 nm, which corresponds to the MLCT band of the complex, was used to quantify the concentration of the complex since peaks for decomposition products are unlikely to appear in this region. The observed complex decay was best modelled by first order kinetics. The half-lives ($t_{1/2}$) were calculated using the following equations;

$$\ln[A] = -kt + \ln[A]_0 \quad t_{1/2} = \frac{\ln(2)}{k}$$

Equation 2.1

Equation 2.2

Table 2.3 | Solution half-life ($t_{1/2}$) of MLCT band (540 nm) for the iron (II)chloride flexicates, 0.03 mM in 0.2 M hydrochloric acid (pH 1.0) at 20°C.

Complex	pH 1, 20°C $t_{1/2}$ /hours (esd)
$[\text{Fe}_2\text{L}_3^{\text{H}}]\text{Cl}_4$	1.4 (9.5E-3)
$\Delta_{\text{Fe}}-[\text{Fe}_2\text{L}_3^{\text{I}}]\text{Cl}_4$	9.6 (0.3) (ref 1)
$\Lambda_{\text{Fe}}-[\text{Fe}_2\text{L}_3^{\text{II}}]\text{Cl}_4$	9.0 (0.5)
$\Delta_{\text{Fe}}-[\text{Fe}_2\text{L}_3^{\text{III}}]\text{Cl}_4$	9.0 (0.5)
$\Lambda_{\text{Fe}}-[\text{Fe}_2\text{L}_3^{\text{IV}}]\text{Cl}_4$	10.5 (0.5)
$\Delta_{\text{Fe}}-[\text{Fe}_2\text{L}_3^{\text{V}}]\text{Cl}_4$	11.0 (0.5)
$\Lambda_{\text{Fe}}-[\text{Fe}_2\text{L}_3^{\text{VI}}]\text{Cl}_4$	19.5 (0.9)
$\Delta_{\text{Fe}}-[\text{Fe}_2\text{L}_3^{\text{VII}}]\text{Cl}_4$	18.2 (0.5)
$\Lambda_{\text{Fe}}-[\text{Fe}_2\text{L}_3^{\text{VIII}}]\text{Cl}_4$	11.2 (1.1)
$\Delta_{\text{Fe}}-[\text{Fe}_2\text{L}_3^{\text{IX}}]\text{Cl}_4$	8.7 (0.9)

The range of recorded $t_{1/2}$ values indicates that the structure of the ligand affects stability. The most stable flexicate was the class Ia $[\text{Fe}_2\text{L}_3^{\text{S}}]\text{Cl}_4$ which had previously

been shown to not decay significantly in harsh acidic conditions even after 10 d.¹ Class Ib flexicate alkene-bridged $[\text{Fe}_2\text{L}^6_3]\text{Cl}_4$ was also found to be very stable with a half live of *ca* 19 h. Alkyne-bridged $[\text{Fe}_2\text{L}^5_3]\text{Cl}_4$, meta-arene bridged $[\text{Fe}_2\text{L}^8_3]\text{Cl}_4$, pentyl-bridged $[\text{Fe}_2\text{L}^1_3]\text{Cl}_4$ and glycol-bridged $[\text{Fe}_2\text{L}^4_3]\text{Cl}_4$ exhibited similar stability in these conditions, recording half-lives of around 10 h. In contrast, the Hannon system $[\text{Fe}_2\text{L}^H_3]\text{Cl}_4$ had a half-life under the same conditions of less than 2 h.

Screening of such compounds in antimicrobial, anticancer and other biological assays involves their dissolution and storage for long periods in complex growth media. We thus set out to assess the stability of the complexes in Roswell Park Memorial Institute (RPMI-1640) cell culture medium at 37°C. Preliminary studies indicated that the kinetics of decomposition did not follow simple rate laws and despite extensive efforts the data could not be modelled with a realistic number of parameters. Thus an estimate was made, based on repeat UV-vis storage experiments, of the amount of complex remaining after 96 h. $[\text{Fe}_2\text{L}^S_3]\text{Cl}_4$ was found to be extremely resistant to hydrolysis in these conditions with $90 \pm 5\%$ remaining., while for $[\text{Fe}_2\text{L}^1_3]\text{Cl}_4$ the integrity was $45 \pm 3\%$. Under the same conditions, $[\text{Fe}_2\text{L}^H_3]\text{Cl}_4$ gave rather inconsistent results but certainly decayed almost completely under these conditions.

Table 2.4 | % integrity in MLCT band (540 nm) after 96 h in RPMI-1640 cell culture medium at 37°C.

Complex	RPMI-1640 medium, 37°C 96h % integrity (esd)
$[\text{Fe}_2\text{L}^H_3]\text{Cl}_4$	12 (9)
$\Lambda_{\text{Fe}}-[\text{Fe}_2\text{L}^S_3]\text{Cl}_4$	90 (5)
$\Lambda_{\text{Fe}}-[\text{Fe}_2\text{L}^1_3]\text{Cl}_4$	45 (3)

The greater stability of all flexicates than the Hannon helicate, despite the fact that the latter contains an efficient helicand, is probably due to the presence of extensive π -stacking in the flexicates. Whatever the mechanism, these hydrophobic interactions must be disturbed in order to allow hydrolysis. The particularly high stability of the class Ia flexicate is probably due to the stereogenic amine unit being contained within the bridge rather than at the periphery of the complex. This will encumber rotation of the aryl ring out of the π -stacked arrangement.

2.3 Antimicrobial Activity

Minimum inhibitory concentration (MIC) is defined as the lowest concentration of an antimicrobial compound that will inhibit growth of a microorganism.¹⁶ Following the activity reported for class Ia $[\text{Fe}_2\text{L}^{\text{S}}_3]\text{Cl}_4$,¹ a range of class Ib flexicates $[\text{Fe}_2\text{L}^{\text{x}}_3]\text{Cl}_4$ ($x = 4, 5, 6$), and $[\text{Fe}_2\text{L}^{\text{I}}_3]\text{Cl}_4$,¹ were selected for screening, along with $[\text{Fe}_2\text{L}^{\text{H}}_3]\text{Cl}_4$ as synthesised by Pratik Gurnani, and the β -lactam ampicillin as a control.

Using a previously reported procedure,¹⁶ cultures of the Gram-positive bacterium *Methicillin-resistant Staphylococcus aureus*, USA300 (MRSA) and the Gram-negative *Escherichia coli*, TOP10 (*E. Coli*) were exposed to drug concentrations (2 – 128 $\mu\text{g/ml}$) in Mueller-Hinton broth over 20 h at 37°C by Daniel Simpson at the University of Warwick.

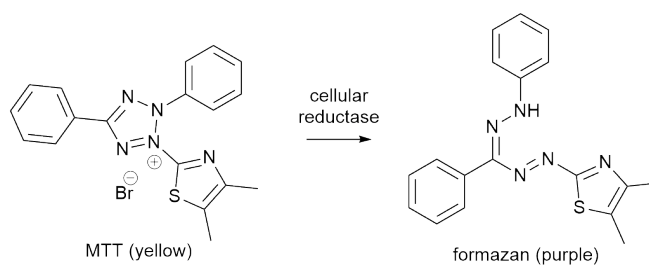
Table 2.5 | MIC values for ampicillin, class Ia ($\Lambda_{\text{Fe}}-[\text{Fe}_2\text{L}^{\text{S}}_3]\text{Cl}_4$) and class Ib ($\Lambda_{\text{Fe}}-[\text{Fe}_2\text{L}^{\text{x}}_3]\text{Cl}_4$, $x = 1, 4-6$) flexicates, and $[\text{Fe}_2\text{L}^{\text{H}}_3]\text{Cl}_4$ against *Staphylococcus aureus*, USA300 (MRSA) and *Escherichia coli*, TOP10 (*E. Coli*) over 20 h at 37°C in Mueller-Hinton broth.

Compound	MRSA MIC ($\mu\text{g ml}^{-1}$)	E. Coli MIC ($\mu\text{g ml}^{-1}$)
Ampicillin	<2	4
$\Lambda_{\text{Fe}}-[\text{Fe}_2\text{L}^{\text{S}}_3]\text{Cl}_4$	8	4
$\Lambda_{\text{Fe}}-[\text{Fe}_2\text{L}^{\text{I}}_3]\text{Cl}_4$	64	>128
$\Delta_{\text{Fe}}-[\text{Fe}_2\text{L}^{\text{I}}_3]\text{Cl}_4$	64	>128
$\Lambda_{\text{Fe}}-[\text{Fe}_2\text{L}^{\text{4}}_3]\text{Cl}_4$	128	>128
$\Lambda_{\text{Fe}}-[\text{Fe}_2\text{L}^{\text{5}}_3]\text{Cl}_4$	128	>128
$\Delta_{\text{Fe}}-[\text{Fe}_2\text{L}^{\text{6}}_3]\text{Cl}_4$	64	>128
$[\text{Fe}_2\text{L}^{\text{H}}_3]\text{Cl}_4$	>128	>128

While ampicillin behaved as expected,¹⁶ and our collaborator Bolhuis' results for the class Ia system and $\Lambda_{\text{Fe}}\text{-}[\text{Fe}_2\text{L}^1_3]\text{Cl}_4$ were reproduced, none of the class Ib flexicates were found to significantly inhibit cell growth or cause cell death at these concentrations. Notably, the Hannon system was also found to be inactive; we note however that the literature reports of antimicrobial activity for this complex refer to the use of a unique (Richards-Bolhuis) broth which was formulated specifically for this complex.¹³ Our expectation is that the discrepancy between our results here and those reported by Hannon and Bolhuis arise from the instability of that complex in conventional biological media.

2.4 Anticancer Activity

In cancer chemotherapeutic agent discovery, half maximal inhibitory concentration (IC_{50}) is defined as the concentration of a drug which permits 50% cell survival compared to an untreated control over a set time period. It is determined by constructing a dose response curve of drug concentration vs % cell survival. The specific method employed in this project is the MTT colorimetric assay.¹⁷ Live cells can reduce yellow, water-soluble 3-(4,5-dimethylthiazol-2-yl)-2,5-diphenyltetrazolium bromide (MTT) to purple insoluble formazan (scheme 2.9). The amount of MTT that is reduced to formazan can be used as a quantitative measurement of cell survival after drug treatment.



Scheme 2.9 | Cellular reduction of soluble yellow 3-(4,5-dimethylthiazol-2-yl)-2,5-diphenyltetrazolium bromide (MTT) to insoluble purple formazan.

Cells were seeded into 96 well plates (200 cells per well) and incubated for 24 h at 37°C in an atmosphere of 5% CO₂ prior to drug treatment. Drug dilutions (10 different dilutions 100 – 0.003 μ M) were added, leaving a row of drug-free reference wells. Following incubation for 96 h, MTT (20 μ l of 5 mg/ml per well) was added (Fig 2.14i) and after an incubation of 4 h all solutions were removed from the wells. Dimethyl sulfoxide was added to each well to dissolve the purple formazan crystals formed (Fig 2.14ii). The absorbance at 540 nm of each well was recorded as a quantitative measurement of the amount of formazan produced by the living cells

after drug treatment. This was plotted *vs* drug concentration to construct a dose response curve. The concentration at which absorbance was 50% of the untreated reference cells was determined to be the IC_{50} of that drug. These tests were conducted in triplicate.¹⁷

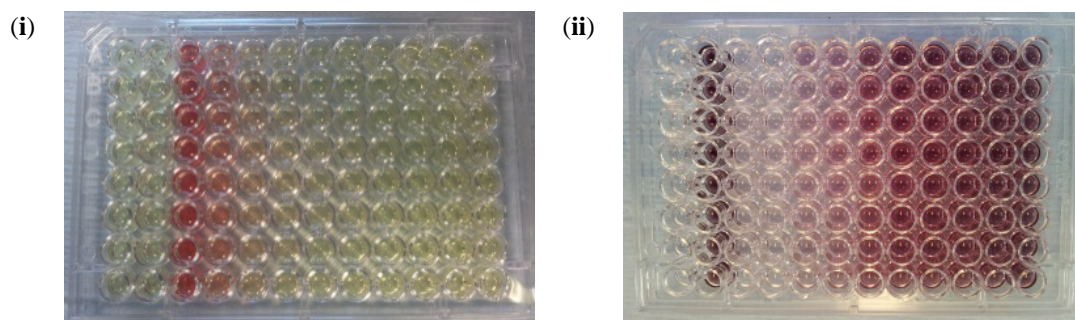


Figure 2.14 | (i) Photograph of a 96 well plate containing MDA-MB-468 cells after treatment with $\Delta_{Fe}-[Fe_2L^1_3]Cl_4$ and addition of MTT. (ii) Photograph of the same 96 well plate after incubation with MTT for 4 h and dissolution of the formazan produced in dimethyl sulfoxide.

2.4.1 Cytotoxicity in cancer cells

The activity of the water-soluble flexicates in several human tumour cell-lines was investigated. MDA-MB-468 (human epithelial breast adenocarcinoma) was chosen as it is a widely used cell line in chemosensitivity studies.¹⁸ Human colon carcinoma HCT116 with wild type p53 (+/+) was chosen because FK-16 (a fragment of human cathelicidin LL-37) is reported as active in this cell line (IC_{50} 40 μ M).¹⁹⁻²¹ A sister cell-line to HCT116 p53^{+/+} with mutated (-/-) p53²² was chosen, following the discovery of very encouraging activity in the wild type cells, to probe the involvement of p53 in the mechanism. Cisplatin was used as a control, principally because of the large number of studies made on this compound rather than because we have any expectation that flexicates act *via* an alkylator mechanism. We also included $[Fe_2L^H_3]Cl_4$ since, other than our own compounds,² this is the most extensively studied metalloheliix in the area and which has been shown to have

moderate activity in other human tumour cell lines.^{23, 24} All the complexes were found to be sufficiently soluble under assay conditions while in contrast, the component ligands were found to be insufficiently soluble for meaningful testing. Here the results are first discussed for each cell-line against the whole panel, and then highlighting important differences in potency (selectivity) against the various cell-lines for each compound.

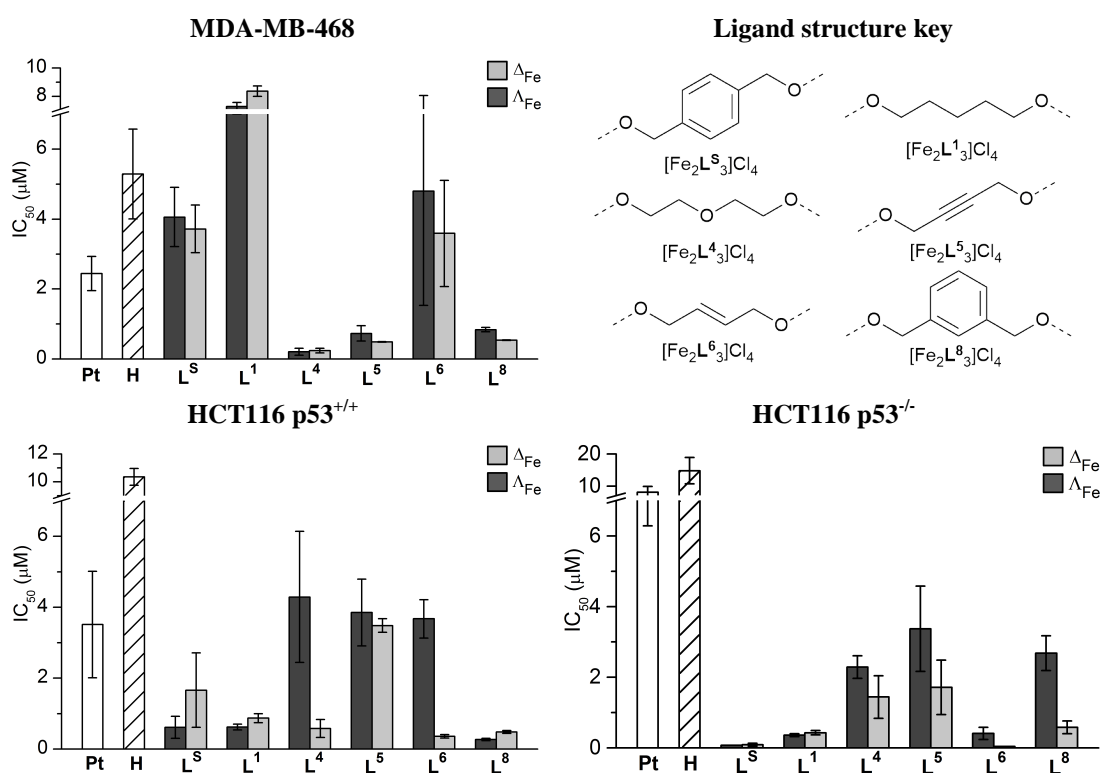


Figure 2.15 | IC_{50} values of cisplatin (Pt, white), $[Fe_2L^H]Cl_4$ (H, hashed) and flexicates $[Fe_2L^x]Cl_4$ ($x = S, 1, 4, 5, 6, 8$) (Δ_{Fe} - light grey, Δ_{Fe} - dark grey) against MDA-MB-468, HCT116 p53^{+/+} and HCT116 p53^{-/-} cells over 96 h and ligand structure key.

In MDA-MB-468 cells cisplatin displayed an IC_{50} of $2.5 \pm 0.5 \mu M$ while $[Fe_2L^H]Cl_4$ and the previously reported class Ia flexicate $[Fe_2L^S]Cl_4$ were slightly less active. The class Ib flexicates had a range of activities. Pairs of enantiomers had very similar effects on cells and may be considered equipotent. While the simple pentyl-bridged compound $[Fe_2L^1]Cl_4$ had the highest IC_{50} in this panel, the isostructural

glycol-bridged $[\text{Fe}_2\text{L}^4_3]\text{Cl}_4$ was extremely potent (IC_{50} 0.2 ± 0.1 μM) and an order of magnitude more toxic here than cisplatin. The alkyne-bridged $[\text{Fe}_2\text{L}^5_3]\text{Cl}_4$ and meta-xilylenyl $[\text{Fe}_2\text{L}^8_3]\text{Cl}_4$ also performed well while the alkene-bridged architecture $[\text{Fe}_2\text{L}^6_3]\text{Cl}_4$ had significantly lower activity.

At 3.5 ± 1.5 μM , cisplatin had a similar potency in HCT116 p53^{+/+} cells as in the breast cancer cell line, while the Hannon helicate at 10.4 ± 0.6 μM had significantly lower toxicity. The class Ia flexicate ($[\text{Fe}_2\text{L}^S_3]\text{Cl}_4$) was highly active, with IC_{50} as low as 0.6 ± 0.3 μM for the Λ_{Fe} enantiomer; the selectivity here – it being nearly an order of magnitude more active in HCT116 p53^{+/+} than in MDA-MB-468 – merits further study. Some of the class Ib compounds were even more potent, and in contrast to performance in the breast cancer cell line there were some significant enantiomeric differences; Δ_{Fe} enantiomers of glycol-bridged $[\text{Fe}_2\text{L}^4_3]\text{Cl}_4$ (IC_{50} 0.6 ± 0.3 μM) and alkene-bridged $[\text{Fe}_2\text{L}^6_3]\text{Cl}_4$ (IC_{50} 0.7 ± 0.1 μM) being up to an order of magnitude more potent than the Λ_{Fe} enantiomer. In contrast, both isomers of the alkyne-bridged $[\text{Fe}_2\text{L}^5_3]\text{Cl}_4$ had moderate activity – similar to cisplatin – while the meta-xylene compounds $[\text{Fe}_2\text{L}^8_3]\text{Cl}_4$ gave similar IC_{50} values of 0.4 ± 0.1 μM and 0.3 ± 0.03 μM respectively.

In HCT116 p53^{-/-} cells both cisplatin and the Hannon helicate showed modest activity. The class Ia flexicate $[\text{Fe}_2\text{L}^S_3]\text{Cl}_4$ was found to be extremely active, much more so than in the sister cell line, with an IC_{50} as low 70 ± 4 nM for the Λ_{Fe} enantiomer. For the class Ib compounds, the general trend is to higher potency (lower IC_{50}) in the p53 mutant, but the most striking improvements are for the alkene enantiomers $[\text{Fe}_2\text{L}^6_3]\text{Cl}_4$, with IC_{50} values falling by around an order of magnitude – in the case of the Δ_{Fe} -isomer to 40 ± 3 nM. In contrast, meta-xilylenyl Λ - $[\text{Fe}_2\text{L}^8_3]\text{Cl}_4$ is

the only compound showing substantially attenuated activity, an order of magnitude less potent at $2.7 \pm 0.5 \mu\text{M}$ than it was in the wild type at $0.3 \pm 0.03 \mu\text{M}$.

As the cell line with mutated p53 generally appeared to be more sensitive towards the panel of flexicates, this may indicate the mode of action involves a p53 pathway either in a direct or indirect manner.²⁵ This is extremely encouraging as many cancers have mutated p53,^{26, 27} which may lead to drug resistance if modes of action that involve a manipulation of only wild type p53 cannot activate.

2.4.2 Toxicity against non-cancerous human cells and selectivity

The selectivity of chemotherapeutic agents towards cancerous cells over healthy host cells in an organism is of paramount concern in respect to minimization of unwanted side effects caused by off-target interactions. To begin to elucidate this complex issue the toxicity of the most active flexicates in HCT116 p53^{-/-}, along with the control compounds, were investigated in human retinal pigment epithelial cells (ARPE19), which display normal growth behaviour in culture medium (Fig 2.16).²⁸

While cisplatin was found to be almost twice as toxic to this healthy cell line as it is to the cancer cell line HCT116 p53^{-/-} the flexicates tested showed very favourable selectivity. The most selective compounds were found to be $\Lambda_{\text{Fe}}\text{-}[\text{Fe}_2\text{L}^{\text{S}}_3]\text{Cl}_4$ and $\Delta_{\text{Fe}}\text{-}[\text{Fe}_2\text{L}^{\text{6}}_3]\text{Cl}_4$ which were up to 3 orders of magnitude more toxic to the cancer cell line than they were to the healthy one.

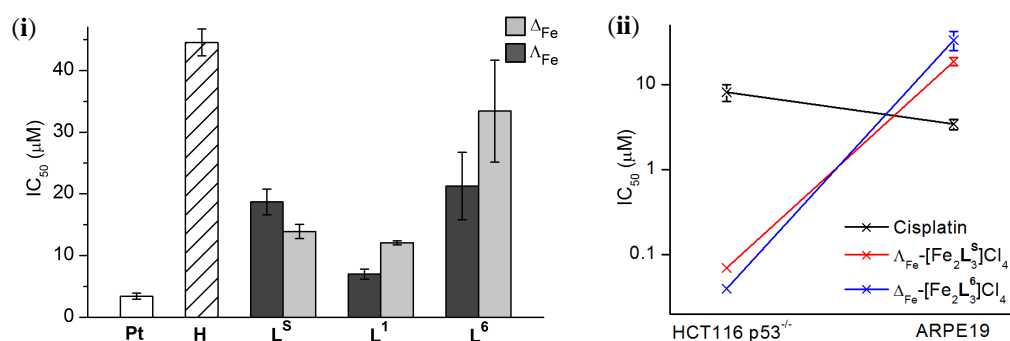


Figure 2.16 | (i) IC_{50} values of cisplatin (**Pt**, white), $[Fe_2L^H]Cl_4$ (**H**, hashed) and flexicates $[Fe_2L^x]Cl_4$ ($x = S, 1, 4$) (Δ_{Fe} - light grey, Λ_{Fe} - dark grey) against ARPE19 over 96 h (ii) comparison of activity of cisplatin (black), $\Lambda_{Fe}-[Fe_2L^S]Cl_4$ (red) and $\Delta_{Fe}-[Fe_2L^6]Cl_4$ (blue) in cancerous HCT116 p53^{-/-} and non-cancerous ARPE19 cells, on a logarithmic scale.

This result is encouraging evidence that these potential new anticancer compounds are acting in a highly selective and specific manner. They may well display reduced unwanted side effects, which can occur when a chemotherapy agent acts upon targets within healthy cells.

2.5 Mode of action

To better understand how flexicates cause the observed chemosensitivity in cancer cells several studies into their mode of action were undertaken: interactions with DNA in cell-free and *in vitro* systems, effect on the cell cycle and induction of apoptosis. Clinical cancer treatments often involve DNA binding and interactions, indeed cisplatin²⁹ and Hannon's tetracation^{30, 31} are both reported to affect cells in this way. $[\text{Fe}_2\text{L}_3]\text{Cl}_4$ is also reported to bind selectively and stabilise several moieties.²

2.5.1 Denaturation of ct-DNA

The denaturation temperature (T_m) of DNA is defined as the temperature at which half of the DNA strands have unwound from the double-helical to a random coil state.³² This can be measured by recording the absorbance of a buffered solution of ct-DNA at 260 nm as a function of temperature. ct-DNA (0.5 mg/ml) was mixed with each complex (7.5 μM) in buffered conditions (10 mM Tris, 1 mM EDTA at pH 7.0) to give 10 base: 1 complex and the absorbance at 260 nm between 25°C and 90°C was recorded (0.4 °C min⁻¹). T_m for each experiment was calculated from the first derivative of a Boltzmann sigmoidal fit of the plot of absorbance vs temperature.

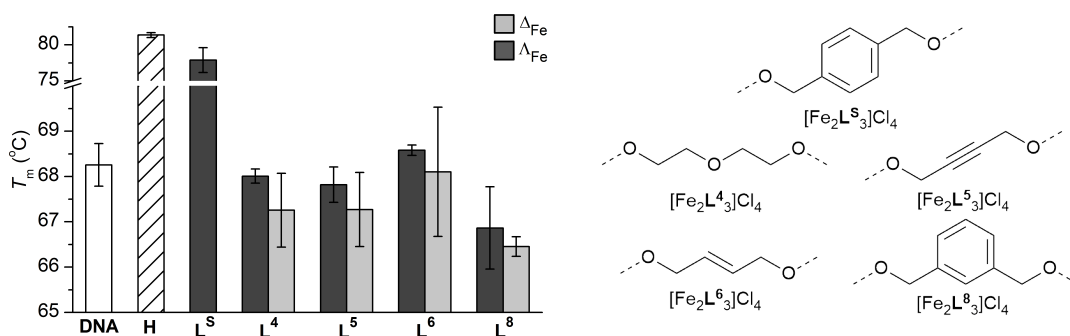


Figure 2.17 | Effect on T_m of linear ct-DNA (DNA, white) from interactions with $[\text{Fe}_2\text{L}^{\text{H}}_3]\text{Cl}_4$ (H, hashed) and flexicates $[\text{Fe}_2\text{L}^{\text{x}}_3]\text{Cl}_4$ (Δ_{Fe} - light grey, Λ_{Fe} - dark grey) in 1mM Trizma base (10:1 base pair to complex).

T_m of untreated ct-DNA (0.25 mg/ml in 10mM Tris, 1 mM EDTA at pH 7.0) was measured to be $68.3 \pm 0.5^\circ\text{C}$. The class Ia flexicate $[\text{Fe}_2\text{L}^{\text{S}}_3]\text{Cl}_4$ and $[\text{Fe}_2\text{L}^{\text{H}}_3]\text{Cl}_4$ have been previously reported to increase T_m ,^{1, 30} which we also observed ($\Delta > +10^\circ\text{C}$) – indicating that a specific constructive binding event occurred between these complexes and ct-DNA. The class Ib flexicate $[\text{Fe}_2\text{L}^{\text{1}}_3]\text{Cl}_4$ is reported to have no effect on T_m ($\Delta -0.1^\circ\text{C}$).¹ The functionalised class Ib flexicates were also observed to have no effect on the denaturation of ct-DNA which would indicate that no constructive or destructive binding event occurred.

2.5.2 Potency over 24 h in HCT116 p53^{+/+}

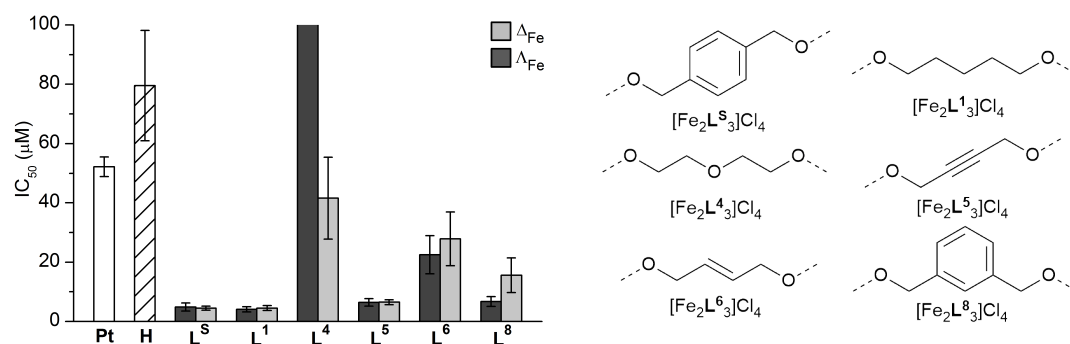


Figure 2.18 | IC_{50} values of cisplatin (Pt, white), $[\text{Fe}_2\text{L}^{\text{H}}_3]\text{Cl}_4$ (H, hashed) and flexicates (Δ_{Fe} - light grey, Λ_{Fe} - dark grey) against HCT116 p53^{+/+} over 24 h.

The timescale of drug treatment is an important factor when considering dose in mode of action studies. The potency of the flexicates over a shorter time period in HCT116 p53^{+/+} over 24 h was investigated. This was to determine the drug concentration that would be used (*i.e.* > IC₅₀) in mode of action studies with the most active compounds. The two most potent flexicates over this shorter timescale were found to be [Fe₂L^S₃]Cl₄ and [Fe₂L¹₃]Cl₄, both with IC₅₀ *ca* 4 μM. These were used in all further mode of action studies in this cell line.

2.5.3 Induction of DNA damage

DNA damage agents often bind in a chemically irreversible manner, causing lesions which can, in the absence of repair, lead to cell death.^{29, 33} In contrast to some helicates³⁴ cell free studies have shown that only the class Ia flexicate [Fe₂L^S₃]Cl₄ binds in a specific manner to DNA.² There is no evidence that any of the class Ib flexicates bind to DNA. While the metal ions here are intended to be structure-forming rather than reactive, the potential of [Fe₂L^S₃]Cl₄ and [Fe₂L¹₃]Cl₄ to induce DNA damage in cancer cells was investigated in collaboration with Dr Qasem Abdallah and Dr Roger Phillips at the Institute of Cancer Therapeutics. HCT116 p53^{+/+} cells were treated with each complex (20 μM) in RPMI-1640 medium for 24 h, fixed to slides and had their cell membranes lysed off. The treated cells were subjected to gel electrophoresis whereby any fragmented DNA would travel further than intact DNA across the potential gradient. The electrophoresed cells were then treated with SiBr-gold, which fluoresces when it intercalates DNA, immediately prior to fluorescence microscopy. The size of the ‘tail’ seen indicated the amount of DNA damage which has occurred through fragmentation.

When investigating the induction of single strand breaks (SSB), the larger the tail, the more fragmented the DNA has become compared to untreated cells

(considered 0% damage) hence SSB damage has been induced. For example, cells which have been treated with hydrogen peroxide after lysis can be considered to have 100% SSB DNA damage. As seen in Table 2.6(i), treating the cells with either flexicate did not induce any single strand breaks in the HCT116 p53^{+/+} cells compared to the untreated control (images of electrophoresed cells are shown in chapter 3, Fig 3.19).

Cisplatin is known to cause cross-linking between DNA strands.²⁹ This causes the tethered DNA to become heavier and so it will not travel as far as untethered DNA when subjected to electrophoresis. After lysis, drug treated cells are exposed to hydrogen peroxide to induce single strand breaks in the untethered DNA. The shorter the tail seen the more DNA cross-linking has occurred, with treatment with hydrogen peroxide alone being considered 0% DNA cross-linking. Table 2.6(ii) shows that treatment with either flexicate exhibits no DNA cross-linking.

Table 2.6 | (i) Mean tail moments of 50 HCT116 p53^{+/+} cells after treatment with 20 μ M flexicates for 24 h, with an untreated control (0% SSB) and H₂O₂ (100% SSB); (ii) Mean tail moments of 50 HCT116 p53^{+/+} cells after treatment with 20 μ M flexicates for 24 h and H₂O₂, with an untreated control and those treated with H₂O₂ only (0% X-link).

(i)	Complex		(ii)	Complex	
	Complex	SSB (esd)		Complex	X-link (esd)
	Untreated control	3.51 (1.30)		Untreated control	1.87 (0.39)
	H ₂ O ₂	36.04 (6.77)		H ₂ O ₂	36.44 (4.02)
	$\Lambda_{\text{Fe}}^-[\text{Fe}_2\text{L}_3^{\text{S}}]\text{Cl}_4$	3.77 (1.45)		$\Lambda_{\text{Fe}}^-[\text{Fe}_2\text{L}_3^{\text{S}}]\text{Cl}_4$	38.53 (1.68)
	$\Delta_{\text{Fe}}^-[\text{Fe}_2\text{L}_3^{\text{S}}]\text{Cl}_4$	4.35 (1.11)		$\Delta_{\text{Fe}}^-[\text{Fe}_2\text{L}_3^{\text{S}}]\text{Cl}_4$	41.90 (12.13)
	$\Lambda_{\text{Fe}}^-[\text{Fe}_2\text{L}_3^{\text{I}}]\text{Cl}_4$	4.87 (2.20)		$\Lambda_{\text{Fe}}^-[\text{Fe}_2\text{L}_3^{\text{I}}]\text{Cl}_4$	35.81 (1.93)
	$\Delta_{\text{Fe}}^-[\text{Fe}_2\text{L}_3^{\text{I}}]\text{Cl}_4$	3.81 (0.59)		$\Delta_{\text{Fe}}^-[\text{Fe}_2\text{L}_3^{\text{I}}]\text{Cl}_4$	41.04 (6.98)

γ -H₂AX is a histone which plays a key role in the repair of damaged DNA.³⁵⁻³⁸ It is expressed as a response to double strand breaks (DSB) which can be caused either directly or indirectly *via* SSB, cross links, intercalation, or the inhibition of certain key enzymes involved in the repair of DNA.³⁹ This therefore makes γ -H₂AX a

useful universal marker for DNA damage. The effect that the flexicates had on the γ -H₂AX expression in HCT116 p53^{+/+} cells has been studied.

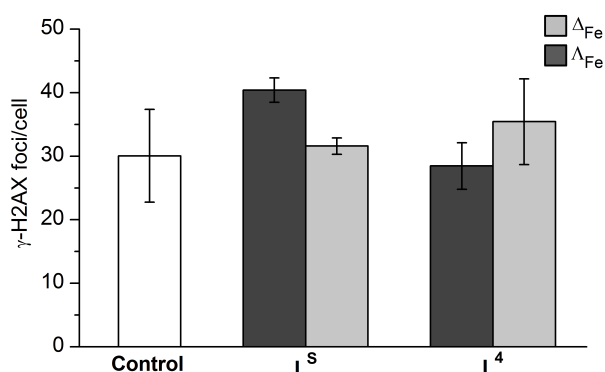


Figure 2.19 | Mean γ -H₂AX expression of HCT116 p53^{+/+} cells (untreated **control** – white) after treatment with flexicates (10 μ M, Δ_{Fe} - light grey, Λ_{Fe} - dark grey) for 24 h.

HCT116 p53^{+/+} cells (5×10^5 cells in 10 ml RPMI-1640 medium) were incubated with $[\text{Fe}_2\text{L}^S_3]\text{Cl}_4$ and $[\text{Fe}_2\text{L}^1_3]\text{Cl}_4$ (10 μ M) for 24 h, treated with primary rabbit anti-human phosphor Histone γ -H₂AX (Ser 139, 2 μ l) antibody (1:50), followed by AlexaFluor conjugated ant rabbit IgG secondary antibody (1:1000, 100 μ l). These, along with a control of untreated HCT116 p53^{+/+} cells were analysed using FACS. Neither of the flexicate architectures significantly altered the production of γ -H₂AX indicating that no DNA lesions or interruption of the γ -H₂AX pathway have occurred.

These results taken together give strong evidence that the chemosensitivity observed for flexicates does not involve the damage of DNA within the cell, despite some minor indications of DNA binding in a cell free environment.

2.5.4 Effects on the cell cycle

The cell division cycle is the process by which a cell prepares for and carries out self-replication. In cancerous cells this is often disrupted where mutations have occurred which switch off important regulatory processes.⁴⁰ Arresting cancerous

cells at a certain stage of this division cycle is an important indicator in the mode of action of an anticancer agent and can be used to give direction to further study of the effect of the compound on certain key biomolecules. The effect flexicates have on the cell cycle of HCT116 p53^{+/+} cells was assessed.

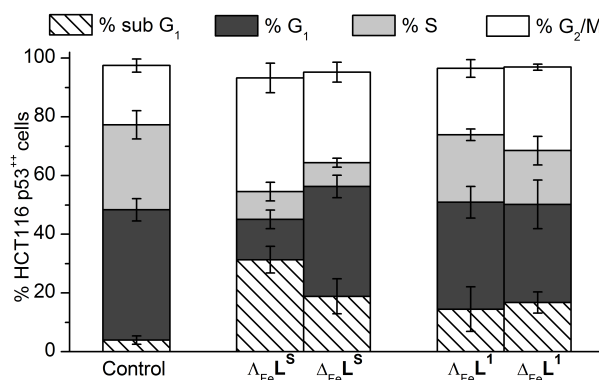


Figure 2.20 | % population of HCT116 p53^{+/+} cells in each of the phases of the cell cycle after treatment with flexicates (10 μM) for 24 h compared to a **control** of untreated cells.

HCT116 p53^{+/+} cells (5×10^5 cells in 1 ml RPMI-1640 medium) were incubated with each flexicate (10 μM) for 24 h and treated with the fluorescent dye propidium iodide (PI) which stains DNA quantitatively. The proportion of cells in the various phases of the cell cycle were determined by fluorescence *via* FACS analysis as a result of the differing amounts of DNA in the cells.⁴¹ [Fe₂L₃^S]Cl₄ flexicates show a dramatic increase in the proportion of cells in G₂/M phase compared to the control (from *ca* 20 to 40 % of cells); such arresting of cell growth at this phase is likely to be a significant factor in the mechanism of action. Interestingly [Fe₂L₁^S]Cl₄ flexicates did not show a significant increase in the G₂/M phase, indicating a different mechanism. There is a very pronounced increase in population of sub G₁ cells, from 4 % in the control to between 13 and 30 %, the latter result being, again, for [Fe₂L₃^S]Cl₄. Cells in the sub G₁ phase are considered apoptotic^{42, 43} and this

suggests that these compounds may well be inducing programmed cell death at a much higher rate than in an untreated cell over 24 h.

2.5.5 Induction of apoptosis

In the early stages of apoptosis cell membrane changes occur, without the loss of membrane integrity.⁴⁴⁻⁴⁶ These changes are recognised by Annexin-V-FLUOS (a fluorescent-conjugated calcium(II) dependant phospholipid binding protein).⁴⁷ As these cell membrane changes are also present in necrotic cells Annexin-V-FLOUS cannot differentiate between the two cell types. Propidium iodide (PI, a DNA stain) is thus introduced to distinguish between apoptotic and necrotic cells. PI will stain necrotic cells exclusively as the loss of membrane integrity membranes permits access to the intracellular environment. The induction of apoptosis and necrosis by flexicates was investigated by Dr Simon Allison, Bradford Institute of Cancer therapeutics.

HCT116 p53^{+/+} cells were seeded (5×10^5 cells per flask) and incubated for 24 h. Upon addition of fresh media containing no drug (control) or freshly dissolved drug (20 μ M) the cells were incubated for a further 72 h. Cells were then harvested by trypsinisation with non-adhered cells also collected, washed with PBS and stained with propidium iodide (100 μ l) and Annexin-V-FLUOS labelling solution (100 μ l). The proportion of live, early apoptotic and late apoptotic/necrotic cells were then quantitated by flow cytometry.⁴⁸

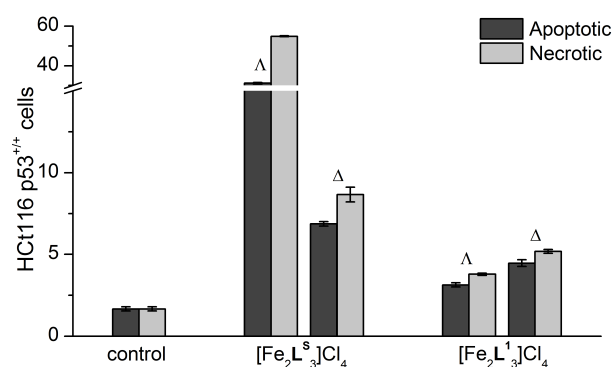


Figure 2.21 | Amount of early apoptotic (dark grey) and late apoptotic / necrotic (light grey) HCT116 p53^{+/+} cells after treatment with flexicates (20 μM) for 72 h, along with an untreated **control**.

Compared to the untreated control both class Ia and class Ib flexicates increased the number of both early apoptotic and necrotic cells significantly, with $\Lambda_{\text{Fe}}\text{-}[\text{Fe}_2\text{L}_3^{\text{S}}]\text{Cl}_4$ in particular having an extreme effect. This, with the cell cycle data, was a strong positive indication that these compounds are triggering early cell death as part of their mode of action.

2.6 Summary

At the beginning of this work we set out to make a library of functionalised flexicates by including different moieties in the structure of the ligand. This we have been able to achieve successfully and can now access the widest library of water-soluble complexes of this size and function available. Each complex of this library exists as a single diastereomerically pure species and is fully characterised by NMR spectroscopy, mass spectrometry, thermogravimetry, microanalysis and circular dichroism.

These novel compounds have also been found to be active and selective anticancer agents, particularly potent towards the human colon carcinoma cell lines, giving IC_{50} values in the nM range – substantially more toxic than cisplatin. For some flexicates the range of sensitivity in between human tumour and healthy cells is up to three orders of magnitude; very promising selectively. Enantiomers of class Ia $[Fe_2L^S_3]Cl_4$ have been shown previously to be selective DNA binders,^{1,2} however they, and the non-DNA binding class Ib flexicates, do not induce DNA damage as demonstrated by single gel electrophoresis and γ -H2AX expression analysis; the chemosensitivity is not caused by DNA damage. These compounds do, however, induce dramatic changes in cell-cycle population and a high level of apoptosis, which indicates that it is this promotion of programmed cell death that is crucial in their mode of action. Moving forwards in this project, further study into the mode of action is required. Whether an extrinsic or intrinsic apoptotic pathway is being triggered as well as interactions with key biomolecules, such as p53, are currently being investigated with our collaborators at the Institute of Cancer Therapeutics.

2.7 References

1. S. E. Howson, A. Bolhuis, V. Brabec, G. J. Clarkson, J. Malina, A. Rodger and P. Scott, *Nat. Chem.*, 2012, **4**, 31-36.
2. V. Brabec, S. E. Howson, R. A. Kaner, R. M. Lord, J. Malina, R. M. Phillips, Q. M. A. Abdallah, P. C. McGowan, A. Rodger and P. Scott, *Chem. Sci.*, 2013, **4**, 4407-4416.
3. M. Serebyuk, A. B. Gaspar, V. Ksenofontov, Y. Galyametdinov, J. Kusz and P. Gütllich, *J. Am. Chem. Soc.*, 2008, **130**, 1431-1439.
4. S. M. Bakunova, S. A. Bakunov, T. Wenzler, T. Barszcz, K. A. Werbovets, R. Brun and R. R. Tidwell, *J. Med. Chem.*, 2009, **52**, 4657-4667.
5. R. Machinek and W. LÜTke, *Synthesis*, 1975, **1975**, 255-256.
6. R. H. Mitchell and V. S. Iyer, *Synlett*, 1989, **1989**, 55-57.
7. J. S. Zakhari, I. Kinoyama, M. S. Hixon, A. Di Mola, D. Globisch and K. D. Janda, *Bioorgan. Med. Chem.*, 2011, **19**, 6203-6209.
8. S. E. Howson, *Ph.D. Thesis, University of Warwick*, 2011.
9. Y. Hsiao and L. S. Hegedus, *J. Org. Chem.*, 1997, **62**, 3586-3591.
10. R. N. Bream, S. V. Ley, B. McDermott and P. A. Procopiou, *J. Chem. Soc., Perkin Trans. 1*, 2002, 2237-2242.
11. S. E. Howson, L. E. N. Allan, N. P. Chmel, G. J. Clarkson, R. van Gorkum and P. Scott, *Chem. Commun.*, 2009, 1727-1729.
12. C. P. Sebli, S. E. Howson, G. J. Clarkson and P. Scott, *Dalton Trans.*, 2010, **39**, 4447-4454.
13. A. D. Richards, A. Rodger, M. J. Hannon and A. Bolhuis, *Int. J. Antimicrob. Agents*, 2009, **33**, 469-472.
14. M. Hannon, J. , C. Painting, L. , A. Jackson, J. Hamblin and W. Errington, *Chem. Commun.*, 1997, 1807-1808.
15. M. J. Hannon, I. Meistermann, C. J. Isaac, C. Blomme, J. R. Aldrich-Wright and A. Rodger, *Chem. Commun.*, 2001, 1078-1079.
16. J. M. Andrews, *J. Antimicrob. Chemother.*, 2001, **48 (suppl 1)**, 5-16.
17. T. Mosmann, *J. Immunol. Methods*, 1983, **65**, 55-63.
18. S. Pathak, M. J. Siciliano, R. Cailleau, C. L. Wiseman and T. C. Hsu, *J. Natl. Cancer Inst.*, 1979, **62**, 263-271.
19. W. K. K. Wu, G. Wang, S. B. Coffelt, A. M. Betancourt, C. W. Lee, D. Fan, K. Wu, J. Yu, J. J. Y. Sung and C. H. Cho, *Int. J. Cancer*, 2010, **127**, 1741-1747.
20. W. K. K. Wu, J. J. Y. Sung, K. F. To, L. Yu, H. T. Li, Z. J. Li, K. M. Chu, J. Yu and C. H. Cho, *J. Cell. Physiol.*, 2010, **223**, 178-186.
21. S. X. Ren, J. Shen, A. S. L. Cheng, L. Lu, R. L. Y. Chan, Z. J. Li, X. J. Wang, C. C. M. Wong, L. Zhang, S. S. M. Ng, F. L. Chan, F. K. L. Chan, J. Yu, J. J. Y. Sung, W. K. K. Wu and C. H. Cho, *PLoS One*, 2013, **8**, e63641.
22. M. D. Kaeser, S. Pebernard and R. D. Iggo, *J. Biol. Chem.*, 2004, **279**, 7598-7605.
23. A. C. G. Hotze, N. J. Hodges, R. E. Hayden, C. Sanchez-Cano, C. Paines, N. Male, M.-K. Tse, C. M. Bunce, J. K. Chipman and M. J. Hannon, *Chem. Biol.*, 2008, **15**, 1258-1267.
24. A. J. Pope, C. Bruce, B. Kysela and M. J. Hannon, *Dalton Trans.*, 2010, **39**, 2772-2774.
25. J. M. Brown and B. G. Wouters, *Cancer Res.*, 1999, **59**, 1391-1399.

26. M. Hollstein, D. Sidransky, B. Vogelstein and C. C. Harris, *Science*, 1991, **253**, 49-53.
27. S. J. Baker, E. R. Fearon, J. M. Nigro, S. R. Hamilton, A. C. Preisinger, J. M. Jessup, P. VanTuinen, D. H. Ledbetter, D. F. Barker, Y. Nakamura, R. White and B. Vogelstein, *Science*, 1989, **244**, 217-221.
28. K. C. Dunn, A. E. Aotaki-Keen, F. R. Putkey and L. M. Hjelmeland, *Exp. Eye Res.*, 1996, **62**, 155-170.
29. Z. H. Siddik, *Oncogene*, 2003, **22**, 7265-7279.
30. A. Rodger, K. J. Sanders, M. J. Hannon, I. Meistermann, A. Parkinson, D. S. Vidler and I. S. Haworth, *Chirality*, 2000, **12**, 221-236.
31. C. Ducani, A. Leczkowska, N. J. Hodges and M. J. Hannon, *Angew. Chem.-Int. Edit. Engl.*, 2010, **49**, 8942-8945.
32. J. SantaLucia, *Proc. Natl. Acad. Sci. USA*, 1998, **95**, 1460-1465.
33. D. Fu, J. A. Calvo and L. D. Samson, *Nat. Rev. Cancer*, 2012, **12**, 104-120.
34. M. J. Hannon, *Chem. Soc. Rev.*, 2007, **36**, 280-295.
35. J. Kobayashi, *J. Radiat. Res.*, 2004, **45**, 473-478.
36. T. L. DeWeese and M. Laiho, eds., *Molecular Determinants of Radiation Response*, Springer New York, New York, 2011.
37. W. M. Bonner, C. E. Redon, J. S. Dickey, A. J. Nakamura, O. A. Sedelnikova, S. Solier and Y. Pommier, *Nat. Rev. Cancer*, 2008, **8**, 957-967.
38. A. Celeste, S. Petersen, P. J. Romanienko, O. Fernandez-Capetillo, H. T. Chen, O. A. Sedelnikova, B. Reina-San-Martin, V. Coppola, E. Meffre, M. J. Difilippantonio, C. Redon, D. R. Pilch, A. Olaru, M. Eckhaus, R. D. Camerini-Otero, L. Tessarollo, F. Livak, K. Manova, W. M. Bonner, M. C. Nussenzweig and A. Nussenzweig, *Science*, 2002, **296**, 922-927.
39. L. J. Kou and L.-X. Yang, *In Vivo*, 2008, **22**, 305-309.
40. G. M. Cooper and R. E. Hausman, *The Cell: a molecular approach*, 6th edn., Sinauer Associates, Boston, 2013.
41. A. Krishan, *J. Cell Biol.*, 1975, **66**, 188-193.
42. I. Nicoletti, G. Migliorati, M. C. Pagliacci, F. Grignani and C. Riccardi, *J. Immunol. Methods*, 1991, **139**, 271-279.
43. M. Kajstura, H. D. Halicka, J. Pryjma and Z. Darzynkiewicz, *Cytometry Part A*, 2007, **71A**, 125-131.
44. H. A. Andree, C. P. Reutelingsperger, R. Hauptmann, H. C. Hemker, W. T. Hermens and G. M. Willems, *J. Biol. Chem.*, 1990, **265**, 4923-4928.
45. V. A. Fadok, D. R. Voelker, P. A. Campbell, J. J. Cohen, D. L. Bratton and P. M. Henson, *J. Immunol.*, 1992, **148**, 2207-2216.
46. C. E. Creutz, *Science*, 1992, **258**, 924-931.
47. G. Koopman, C. Reutelingsperger, G. Kuijten, R. Keehnen, S. Pals and M. van Oers, *Blood*, 1994, **84**, 1415-1420.
48. *Apoptosis, Cytotoxicity and Cell Proliferation*, 4th edn., Roche Diagnostics GmbH, Mannheim, Germany, 2008.

Chapter 3

Asymmetric triplex metallohelices with high and selective activity against cancer cells

3.1 Introduction

The chemistry and biology of the flexicate system explored in chapter 2 indicates significant potential of such molecules in the medicinal sphere. Nevertheless we consider that they fall short of addressing the criterion (e) of section 1.5 *i.e.* that metallo-helix platforms should allow the deliberate placement of functional groups. At present, flexicates and conventional helicates cannot at present provide us with anything approaching the exquisite functionality and topology present in natural α -helix systems. As a first step towards this, we considered the possibility of stereoselective synthesis of lower symmetry architectures.

3.1.1 Design of the triplex metallohelix

If directional ligands (**AB–CD**) are employed in helicate chemistry, Head-to-Head-to-Head [HHH, Fig 3.1(ii)] and Head-to-Head-to-Tail [HHT, Fig 3.1(iii)] constitutions of species $[M_2(\mathbf{AB-CD})_3]^{4+}$ may assemble. These two geometries can form either helical ($\Delta\Delta$ or $\Lambda\Lambda$) or mesocate-like ($\Delta\Lambda$ or $\Lambda\Delta$) structures with respect to the stereochemistry at the two metal centres. This leads to eight possible isomers overall; $\Delta_\alpha\Delta_\beta$ -HHH and $\Lambda_\alpha\Lambda_\beta$ -HHH, $\Delta_\alpha\Lambda_\beta$ -HHH and $\Lambda_\alpha\Delta_\beta$ -HHH, $\Delta_\alpha\Delta_\beta$ -HHT and $\Lambda_\alpha\Lambda_\beta$ -HHT, $\Delta_\alpha\Lambda_\beta$ -HHT and $\Lambda_\alpha\Delta_\beta$ -HHT. In the absence of any external effects these will exist in a statistical 3:1 HHT:HHH ratio, in much the same way as *fac* and *mer* configurations in monometallic systems. We have previously reported structures of the HHH type (ii) synthesised in a stepwise fashion (see appendix B).¹ Pioneering

work by Albrecht^{2, 3} and others⁴⁻⁹ led to observations of low symmetry HHT structures (iii) in single crystals, but these exist as mixture of stereo- and optical isomers in solution. Selective asymmetric self-assembly of only the homohelical HHT architecture presents a great challenge for (metallo)supramolecular chemistry.^{2,}

6

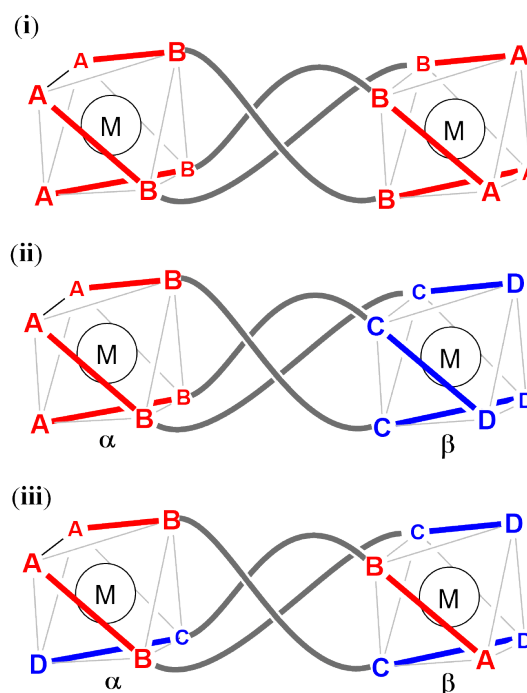


Figure 3.1 | Schematic diagrams of (i) the highly symmetrical Δ_M -[M₂(**AB-BA**)₃] configuration, (ii) the symmetric $\Delta_\alpha\Delta_\beta$ -Head-to-Head-to-Head [M₂(**AB-CD**)₃], and (iii) the asymmetric $\Delta_\alpha\Delta_\beta$ -Head-to-Head-to-Tail [M₂(**AB-CD**)₃] configurations.

Thus the use of a directional ditopic ligand design **AB-CD** was considered, where **AB-** is the stereogenic π -stacking α -phenyl iminopyridine unit derived from the monometallic and flexicate architectures previously described.^{1, 10-15} While the three ligands (**AB**) in the monometallic *fac*-[M(**AB**)₃]²⁺ case participate in a mutual π -stacking arrangement,¹⁰ the system is rather sterically congested. Substituting a smaller ligand **-CD** should lead to some relief of this. If, in addition, **-CD** is a planar, aryl bidentate ligand, then it may participate in interligand π -stacking with

the adjacent chiral iminopyridine **AB**-, but under normal circumstances may not form π -stacks with adjacent groups of its own kind. In the case of an HHT-[M(**AB**-**CD**)₃]⁴⁺ helicate system (Fig 3.1(iii)), the [M(**AB**)₂(**CD**)]²⁺ α -subunit can only adopt a *fac* configuration since it is tethered to the β -subunit. The [M(**AB**)(**CD**)₂]²⁺ β -subunit, contains only one carbon stereogenic centre so a relatively short or rigid tether to the α -subunit can link the two metal centres by helication.¹⁶ It has been reported that the π -stacking interaction between one aromatic ring with a fused or biaryl system is more favourable than that between two simple aromatic rings that can only be maximised in the HHT structures.^{17, 18} Therefore a combination of these effects could lead to a thermodynamic preference for the target homohelical asymmetric helicate system (HHT-[M₂(**AB**-**CD**)₃]⁴⁺).

Suitable **-CD** units for use in this strategy units include catechols,¹⁹ pyrrolylketones,²⁰ phenanthrolines,²¹ pyrazolyl-pyridines,²² or other diimines. We used 2,2'-bipyridine (bpy) in this preliminary study since its chemistry and use as a ligand are very well developed.²³

Two different directional ditopic ligands were designed, one where the bpy unit was attached to the pyridine side of the chiral unit (Fig 3.2, **L**²⁰) and the other where the bpy unit was attached to the imine side of the chiral unit (Fig 3.2, **L**^{F1}). The HHT-[M₂(**AB**-**CD**)₃] arrangement – which by analogy with the bi-directional motif of triplex DNA²⁴ we might refer to as a triplex metallohelix – is very appealing. Like the peptide α -helix, it is directional and, depending on the degree of helix twist, it could provide amphiphilic structures; note that in fig 3.1(iii) the **AB** units are on one side of the assembly.

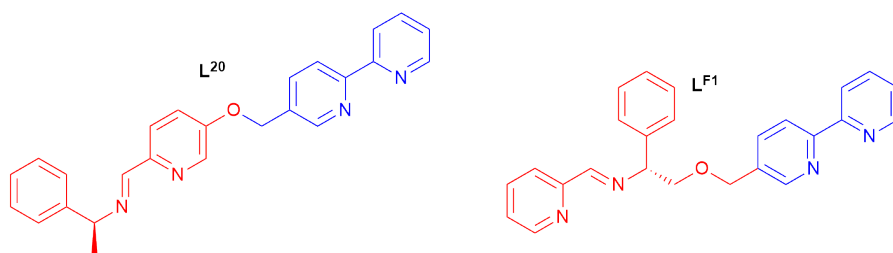


Figure 3.2 | Structure of L^{20} and L^{F1}

Following a brief description of computational prediction of structure and stereoselection, below we describe the synthesis of a range of new triplex metalloheliices of the general type $L^{20,*}$, study some biophysical properties, investigate their antimicrobial and anticancer activity, and obtain preliminary evidence as to mechanism of action in the latter disease area.

3.2 Assembly of triplex metalloheliices

3.2.1 Molecular modelling of $[M_2(AB-CD)_3]^{4+}$

The potential effects of helication and the thermodynamic preference of HHT vs HHH for bimetallic complexes $[M_2L^{20}_3]^{4+}$ ($M = \text{zinc(II)}$ or iron(II)) were investigated.²⁵ Each structure was optimised using ligand field molecular mechanics (LFMM)²⁶ as implemented in the DommiMOE program,²⁷ then annealing was implemented at 500 K for 1 ns, followed by cooling to 0 K and re-optimisation. Single point calculations were then performed at the B3LYP-D def2-TZVP level of theory on each structure.

In the case of L^{20} the increased stability for inter ligand π -stacking between phenyl and bpy over phenyl and pyridine is demonstrated by each HHT isomer being more stable than its corresponding HHH isomer.¹⁸ Each Δ_α metal centre is more

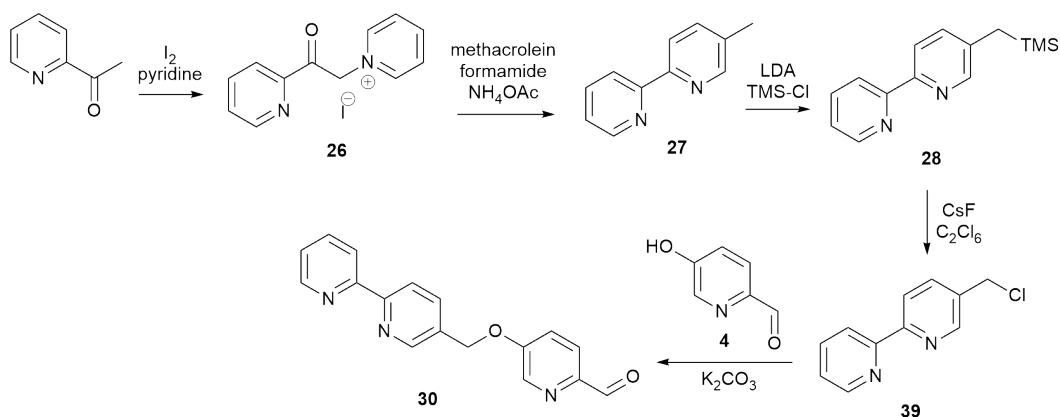
* The computational work in this chapter was conducted by Dr Alan Faulkner (Scott group, University of Warwick) as was the synthesis of complexes based on L^{F1} . The biological work for all systems was conducted by the author.

stable than its Λ_α enantiomer due to an observed reduction of the steric clashes¹⁰ between adjacent chiral iminopyridine groups in the latter case. Each monometallic subunit in the complex is found to be mechanically coupled to the other through the short $-\text{CH}_2\text{O}-$ bridge, causing the preference for Δ stereochemistry to be translated from the α - to the β -metal centre. Also, each HHT structure can be formed in three ligand permutations compared to only one for each HHH structure, and the corresponding entropy term favours the triplex architectures. These three effects lead to calculated Boltzmann populations with the $\Delta_\alpha\Delta_\beta$ -HHT isomer as the majority species. Calculations for the \mathbf{L}^{F1} system gave the same outcome.^{18, 25} Ultimately these studies appear to validate our proposed strategy to synthesise asymmetric triplex metallohelices.

Table 3.1 | Relative energies (compared to $\Delta_\alpha\Delta_\beta$ -HHT) of calculated structures of $(S)\text{-}[\text{M}_2\mathbf{L}^{\text{20}}_3]^{4+}$ ((M = Zn(II), Fe(II)) and predicted percentage Boltzmann population of each isomer at 298 K (calculated from the energy difference between each isomer and the lowest energy isomer, including a statistical correction term).²⁸

Complex	Isomer	Rel. energy kcal mol ⁻¹	Population/% (298 K)
$[\text{Zn}_2\mathbf{L}^{\text{20}}_3]^{4+}$	$\Delta_\alpha\Delta_\beta$ -HHT	0.00	93.8
	$\Delta_\alpha\Delta_\beta$ -HHH	+0.95	6.2
	$\Delta_\alpha\Lambda_\beta$ -HHT	+4.66	0.0
	$\Delta_\alpha\Lambda_\beta$ -HHH	+6.48	0.0
	$\Lambda_\alpha\Lambda_\beta$ -HHT	+8.07	0.0
	$\Lambda_\alpha\Lambda_\beta$ -HHH	+10.91	0.0
	$\Lambda_\alpha\Delta_\beta$ -HHT	+13.44	0.0
	$\Lambda_\alpha\Delta_\beta$ -HHH	+13.63	0.0
$[\text{Fe}_2\mathbf{L}^{\text{20}}_3]^{4+}$	$\Delta_\alpha\Delta_\beta$ -HHT	0.00	97.4
	$\Delta_\alpha\Delta_\beta$ -HHH	+1.51	2.6
	$\Delta_\alpha\Lambda_\beta$ -HHH	+7.62	0.0
	$\Delta_\alpha\Lambda_\beta$ -HHT	+8.82	0.0
	$\Lambda_\alpha\Lambda_\beta$ -HHT	+15.33	0.0
	$\Lambda_\alpha\Delta_\beta$ -HHT	+20.70	0.0
	$\Lambda_\alpha\Delta_\beta$ -HHH	+20.97	0.0
	$\Lambda_\alpha\Delta_\beta$ -HHH	+26.10	0.0

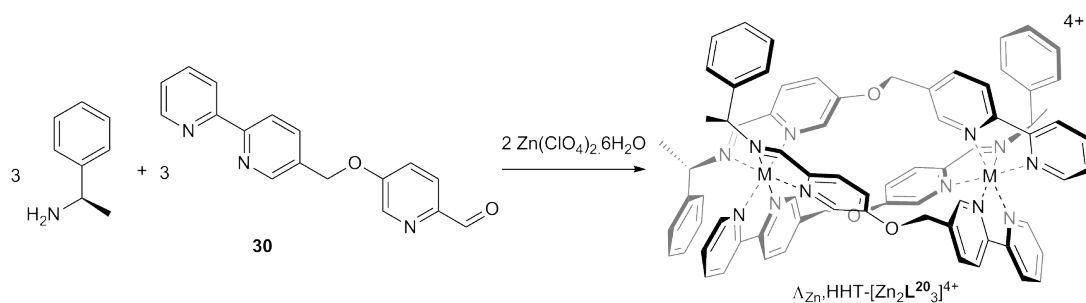
3.2.2 Synthesis of triplex metallohelices



Scheme 3.1 | Synthesis of 5-(2,2'-bipyridin-5-ylmethoxy)picolinaldehyde (**30**) via 5-(chloromethyl)-2,2'-bipyridine (**29**).^{29, 30}

In a Khronke pyridine synthesis (scheme 3.1), 27 g of 2-acetylpyridine was treated with iodine in pyridine to give the 1-(2-pyridylacetyl)pyridinium iodide salt (**26**).²⁹ This was then treated with ammonium acetate and freshly distilled methacrolein in formamide to give 5-methyl-2,2'-bipyridine (**27**); a clear oil. Chlorination was achieved *via* silylation to 5-((trimethylsilyl)methyl)-2,2'-bipyridine (**28**) with LDA and chlorotrimethylsilane, followed by treatment with hexachloroethane and caesium fluoride.³⁰ Recrystallisation from hot hexane yielded 10 g of the desired product as a yellow crystalline solid. This 5-(chloromethyl)-2,2'-bipyridine (**29**) was then etherified with 5-hydroxypicolinaldehyde in the presence of potassium carbonate to furnish 5-(2,2'-bipyridin-5-ylmethoxy)picolinaldehyde (**30**, 11 g).

In the **L**²⁰ series it is possible to develop analogues based on the pyridyl unit **30**. However, for this first study we considered that the amine unit provided the readiest entry to functionalised derivatives, similar to the flexicates of chapter 2. A range of (*R*)-phenylglycinol (**18**) derivatives and commercially-available phenylethylamines and used in the following self-assembly reactions.



Scheme 3.2 | Self-assembly of a triplex metallohelix $\Lambda_{\text{Zn,HHT}}\text{-}[\text{Zn}_2\text{L}^{20}_3][\text{ClO}_4]_4$.

(*R*)-1-Phenylethan-1-amine and 5-(2,2'-bipyridin-5-ylmethoxy)picolinaldehyde (**30**) were dissolved in acetonitrile. Zinc(II) perchlorate hexahydrate was added and after stirring at ambient temperature for a few minutes $\Lambda_{\text{Zn,HHT}}\text{-}[\text{Zn}_2\text{L}^{20}_3][\text{ClO}_4]_4$ was precipitated from the reaction solution by addition of ethyl acetate (scheme 3.2).

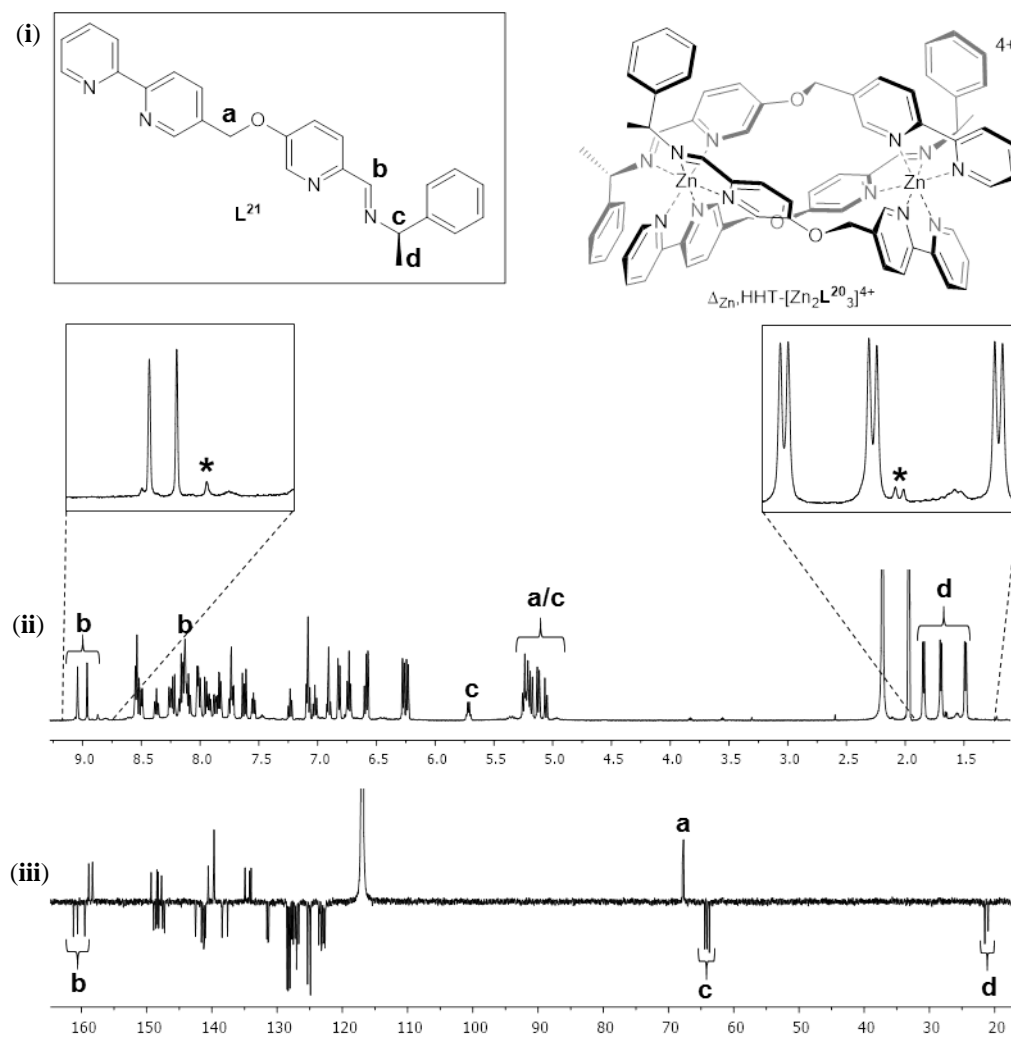


Figure 3.3 | (i) Structure of L^{20} and structure of the assembled triplex metallohelix $\Delta_{Zn,HHT}[\text{Zn}_2L^{20}]_3]^{4+}$ (ii) ^1H (500 MHz) and (iii) $^{13}\text{C}\{^1\text{H}\}$ (126 MHz) NMR spectra of $\Delta_{Zn,HHT}[\text{Zn}_2L^{20}]_3]^{4+}$ in d^3 -acetonitrile (δ_{H} 1.95, δ_{C} 117, water present δ_{H} 2.19) at 298 K, with some key assignments. * indicates the presence of the HHH-isomer, *ca* 3%.

Electrospray mass spectra were consistent with the formation of the proposed structure with a strong peak at m/z 324.15 Da for the tetracation. Figure 3.4 depicts the ^1H and ^{13}C NMR spectra (Fig 3.3) of $\Delta_{Zn,HHT}[\text{Zn}_2L^{20}]_3]^{4+}$ in d^3 -acetonitrile. These confirm the asymmetric self-assembly since each ligand is chemically inequivalent. Nevertheless, it is possible to assign the spectra, with the exception of the rather crowded aromatic regions. Three distinct doublets of the same intensity can be seen between 1.4 and 1.9 ppm; these arise from each methyl group of the three ligands

(d). Between 5.0 and 5.7 ppm each different CH (c) and CH₂ (a) group is identified, though there is significant overlap of individual peaks. Two of the three expected imine peaks can be seen clearly at around 9.0 ppm, the third, as assigned by HMQC coupling experiments, appears amongst the aromatic peaks (b). The ¹³C NMR spectrum can be assigned in a similar way with the key peaks being indicated in figure 3.4. Although some aromatic carbons seem to overlap, which is not unexpected given the high number in the complex, three distinct peaks representing each of the key groups can be identified. It is also possible to determine the diastereoselectivity of the assembly; two small peaks at 1.6 and 8.9 ppm respectively (Fig 3.3 *) in the ¹H NMR spectrum have been determined to arise from the presence of 3% $\Lambda_{\text{Zn},\text{HHH}}\text{-}[\text{Zn}_2\text{L}^{20}_3][\text{ClO}_4]_4$ isomer. This population was similar to – perhaps slightly better than – that predicted in the calculations of table 3.1.

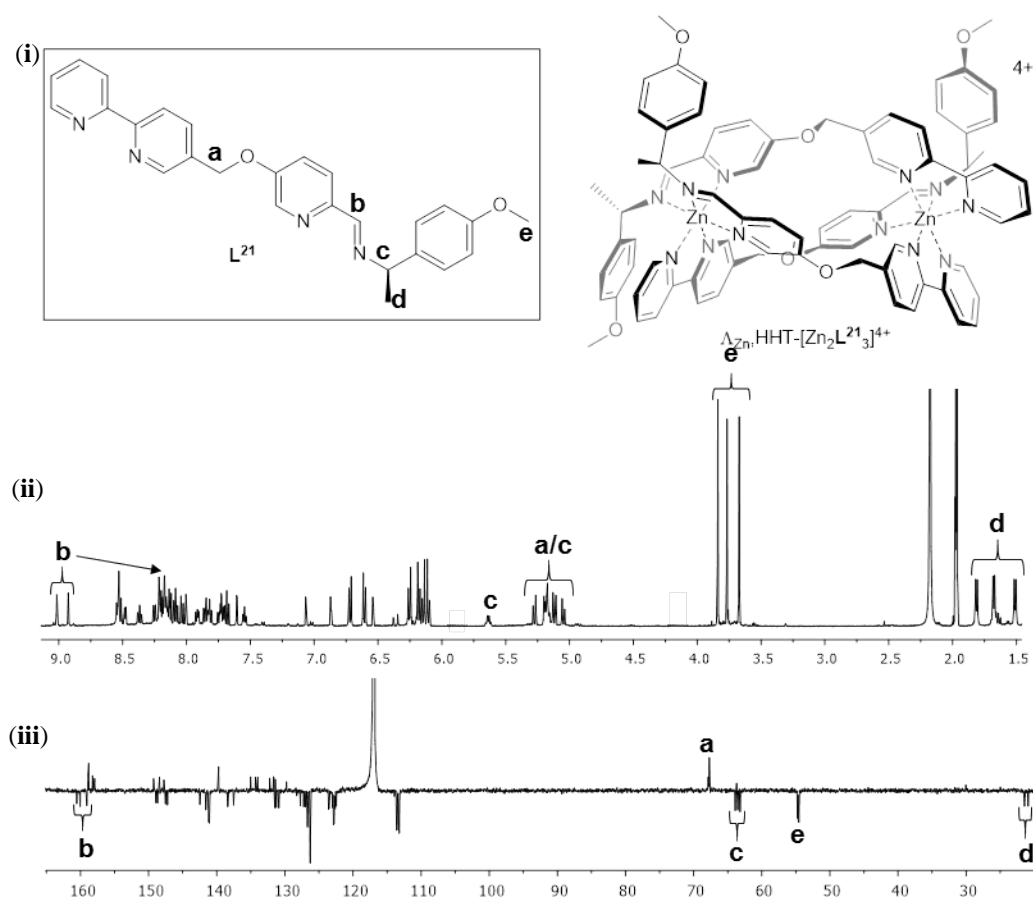


Figure 3.4 | (i) Structure of L^{21} and structure of the assembled triplex metallohelix $\Lambda_{Zn,HHT}-[Zn_2L^{21}_3][ClO_4]_4$ (ii) 1H (500 MHz) and (iii) $^{13}C\{^1H\}$ (126 MHz) NMR spectra of $\Lambda_{Zn,HHT}-[Zn_2L^{21}_3][ClO_4]_4$ in d^3 -acetonitrile (δ_H 1.95, δ_C 117, water present δ_H 2.19) at 298 K, with some key assignments.

$\Lambda_{Zn,HHT}-[Zn_2L^{21}_3][ClO_4]_4$ and $\Lambda_{Zn,HHT}-[Zn_2L^{22}_3][ClO_4]_4$ were successfully synthesised in a similar manner using the amines (*R*)-1-(4-methoxyphenyl)ethan-1-amine and (*R*)-1-(4-nitrophenyl)ethan-1-amine respectively. The NMR spectra were analogous to that of $\Lambda_{Zn,HHT}-[Zn_2L^{20}_3][ClO_4]_4$. In the case of $\Lambda_{Zn,HHT}-[Zn_2L^{21}_3][ClO_4]_4$ (fig 3.5) three methoxy peaks (e) were present between 3.7 and 3.9 ppm. 4% of the $\Lambda_{Zn}-HHH$ isomer observed, indicating a similar level of stereoselection to $\Lambda_{Zn,HHT}-[Zn_2L^{20}_3][ClO_4]_4$. Similarly $\Lambda_{Zn,HHT}-[Zn_2L^{22}_3][ClO_4]_4$ was observed to contain 6% of the $\Lambda_{Zn}-HHH$ isomer.

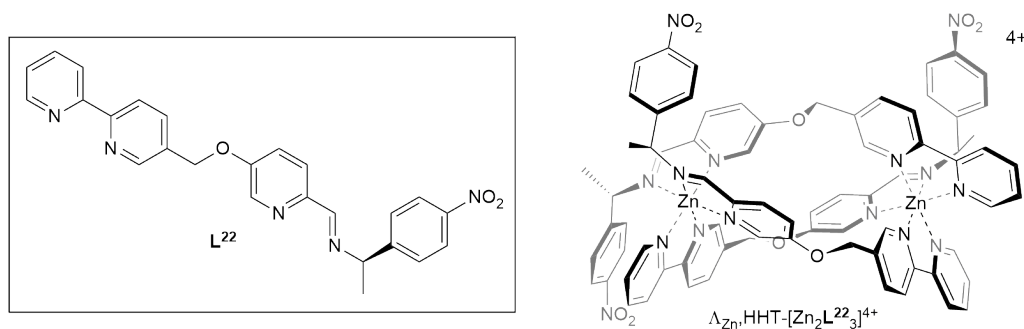


Figure 3.5 | Structure of **L**²² and structure of the assembled triplex metallohelix $\Lambda_{\text{Zn,HHT}}\text{-}[\text{Zn}_2\text{L}^{22}]^{4+}$.

A naphthyl group was successfully incorporated into the architecture in this position; $\Lambda_{\text{Zn,HHT}}\text{-}[\text{Zn}_2\text{L}^{23}][\text{ClO}_4]_4$ was formed with (*R*)-1-(naphthalen-1-yl)ethan-1-amine, 5-(2,2'-bipyridin-5-ylmethoxy)picolinaldehyde (**30**) and zinc(II) perchlorate hexahydrate in acetonitrile, although it had reduced solubility compared to other examples of triplex metallohelices.

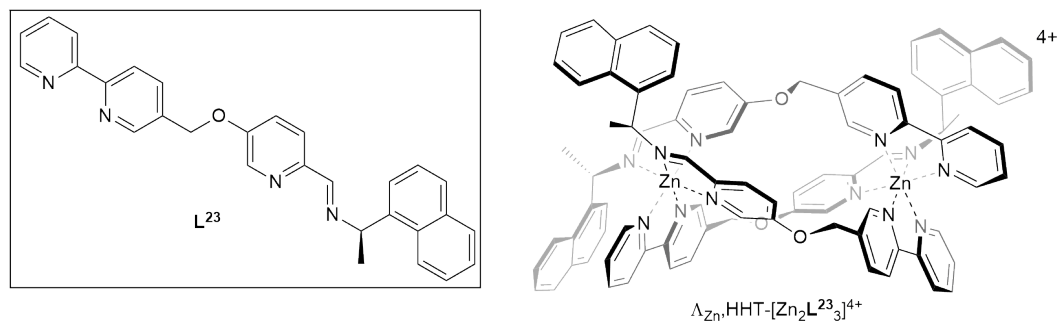


Figure 3.6 | Structure of **L**²³ and structure of the assembled triplex metallohelix $\Lambda_{\text{Zn,HHT}}\text{-}[\text{Zn}_2\text{L}^{23}]^{4+}$.

Substituting (*R*)-1-phenylethan-1-amine for optically pure (*R*)-phenylglycinol³¹ (**18**) gave $\Lambda_{\text{Zn,HHT}}\text{-}[\text{Zn}_2\text{L}^{24}][\text{ClO}_4]_4$ (Fig 3.8) with three external facing hydroxyl moieties on the complex with a similar stereoselectivity (3% $\Lambda_{\text{Zn}}\text{-HHH}$) to the previous examples. (*R*)-1-phenyl-2-(prop-2-yn-1-yloxy)ethan-1-amine (**25**) was formed in a modified Williamson ether synthesis of *R*-phenylglycinol in the presence

of sodium hydride.³² Subsequently $\Delta_{\text{Zn,HHT}}\text{-}[\text{Zn}_2\text{L}^{25}_3][\text{ClO}_4]_4$, with external facing propargyl functionality, formed successfully with amine **25** (5% $\Delta_{\text{Zn}}\text{-HHH}$). This complex was targeted in order to access functionalised systems *via* copper mediated azide-alkyne click reaction, in a similar manner to that previously reported in monometallic complexes by our research group.¹

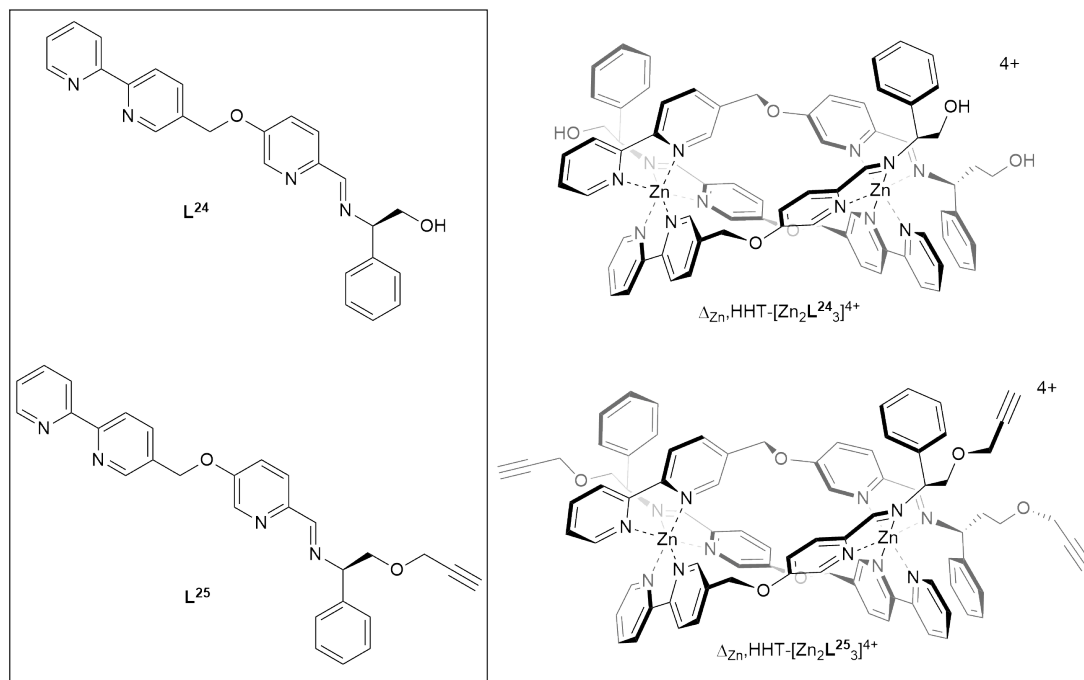


Figure 3.7 | Ligand structure of L^{24} and L^{25} and structures of the assembled triplex metallohelices



3.2.3 Synthesis of highly water soluble triplex metallohelices

Five systems – $[\text{Fe}_2\text{L}^x_3]\text{Cl}_4$ ($x = \mathbf{20-23}$ and **25**) – were synthesised and characterised for biological testing. Unfortunately the attempts to synthesise $[\text{Fe}_2\text{L}^{24}_3]\text{Cl}_4$ resulted in extremely broad ^1H NMR spectra and so these compounds were not considered suitable for testing. Five additional systems – $[\text{Fe}_2\text{L}^x_3]\text{Cl}_4$ ($x = \mathbf{F1-F5}$) – synthesised by Dr Alan Faulkner were chosen to compliment these compounds in biological tests.

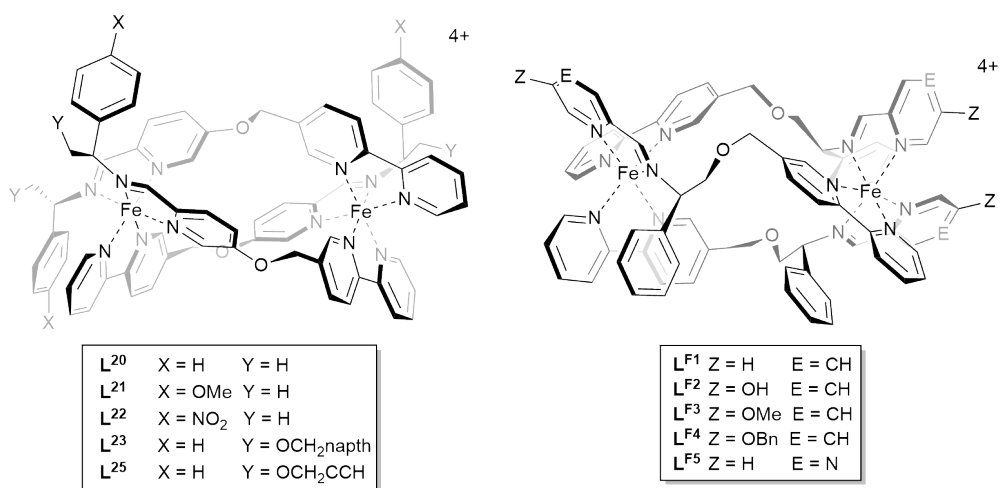


Figure 3.8 | Ligand functionality of water soluble iron(II) chloride triplex metallohelices.

Pairs of water soluble triplex metallohelix enantiomers were synthesised in high yield by heating **30** (3 eq.) and the appropriate chiral amine (3 eq.), with iron(II) chloride (2 eq.) to reflux in methanol. After being filtered through silica gel, the dark purple solutions were evaporated carefully to dryness. The products were analysed by NMR spectroscopy, mass spectrometry, microanalysis, thermogravimetric analysis, infra-red, UV-vis absorption, and circular dichroism spectroscopies.

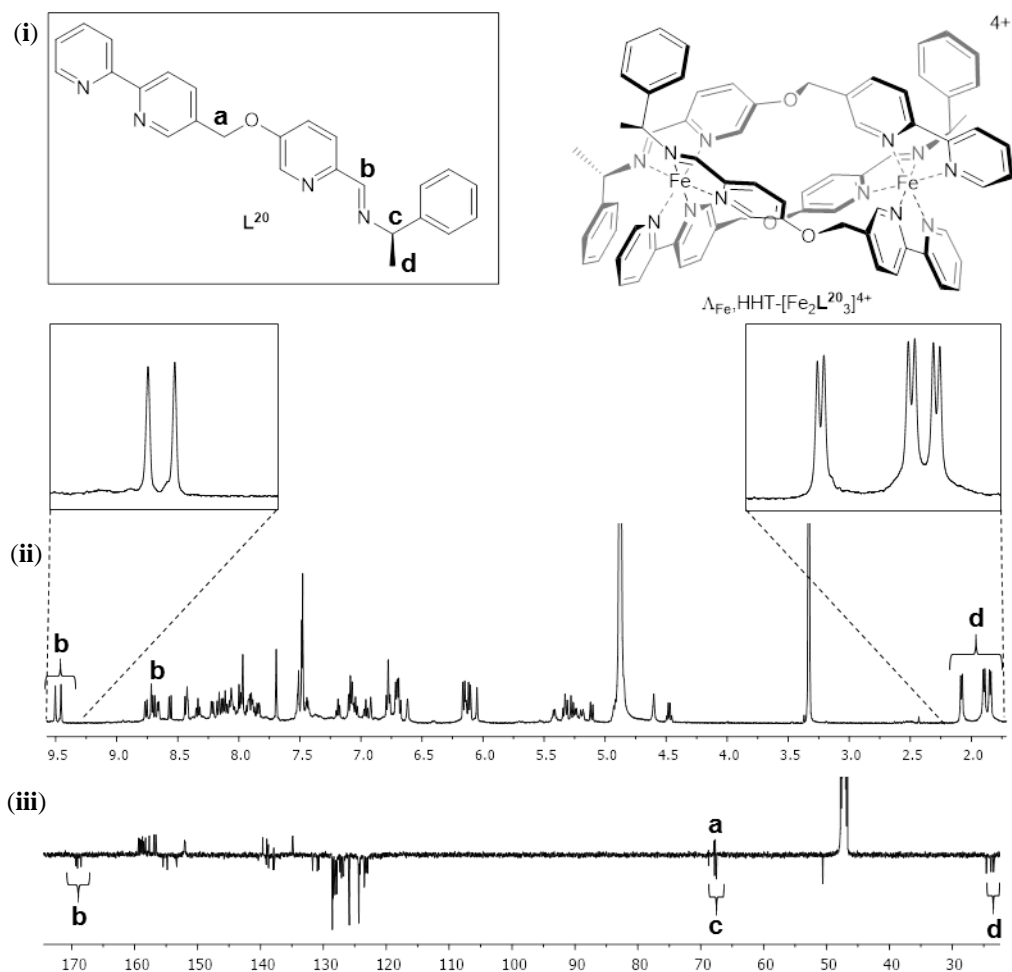


Figure 3.9 | (i) Structure of L^{20} and structure of the assembled triplex metallohelix $\Lambda_{Fe}-[Fe_2L^{20}_3]Cl_4$
(ii) 1H (500 MHz) and (iii) 1H (500 MHz) and $^{13}C\{^1H\}$ (126 MHz) NMR spectra of $\Lambda_{Fe,HHT}-[Fe_2L^{20}_3]Cl_4$ in d^4 -methanol (δ_H 3.31, δ_C 49, water present δ_H 4.87) at 298 K, with some key assignments.

The complexes gave excellent electrospray mass spectrometry data with, for example, $\Lambda_{Fe,HHT}-[Fe_2L^{20}_3]Cl_4$ giving a strong peak at m/z 323.19 Da for the tetracation, similar to the analogous zinc(II) perchlorate complex. 1H NMR spectra were broadened in comparison with the zinc(II) systems but partially resolved and fully assigned ^{13}C NMR spectra were obtained. Compared to the zinc(II) systems the iron(II) systems were more stereoselective towards the Λ_{Fe} -HHT isomer, in agreement with or with better stereoselectivity than the predicted Boltzmann populations in table 3.1. For example, the NMR spectra in figure 3.9 show that

$\Lambda_{\text{Fe,HHT}}\text{-}[\text{Fe}_2\text{L}^{20}_3]\text{Cl}_4$ has formed in a diastereomerically pure manner (>1% $\Lambda_{\text{Fe-HHH}}$). Circular dichroism spectra of each pair of enantiomers (0.03 mM in water) were found to be equal and opposite, indicating the complexes were formed of a non-racemic mixture of opposite configurations. This is in agreement with the previously described water soluble flexicates. Taken with the NMR spectra this showed that each of the pair of enantiomers has formed as a single thermodynamically stable species. Further data in chapter 5 and appendix A.

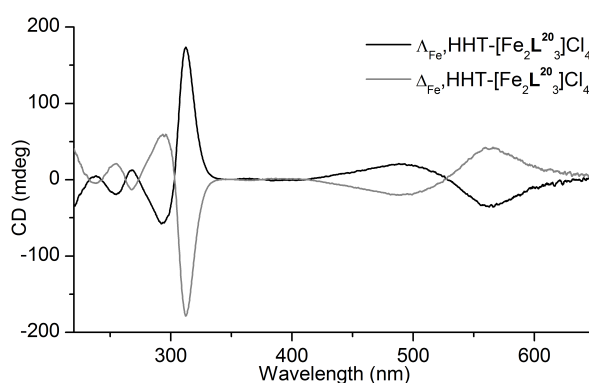


Figure 3.10 | CD spectra of $\text{HHT-}[\text{Fe}_2\text{L}^{20}_3]\text{Cl}_4$ (0.03 mM) in H_2O , each of the pair of enantiomers display an equal and opposite spectrum.

3.2.4 Water of crystallisation

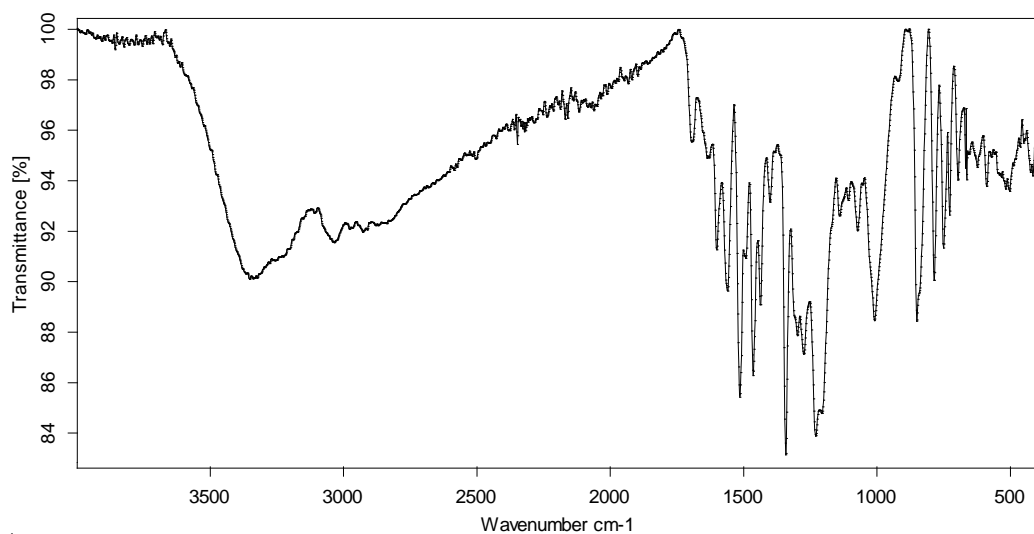


Figure 3.11 | Solid-state infra-red spectrum of $\Lambda_{\text{Fe,HHT}}\text{-}[\text{Fe}_2\text{L}^{22}_3]\text{Cl}_4$

NMR spectroscopies had showed that the samples contained only the complex and water. The latter was confirmed by solid-state IR spectroscopy (*e.g.* fig 3.11) where the two strong O-H stretching modes were observed in the region 3000-3500 cm^{-1} .

In thermogravimetric analyses, samples were heated from ambient temperature to 673 K at a rate of 10 K/min and the mass loss was recorded against temperature. As can be seen in figure 3.13 for $\Lambda_{\text{Fe,HHT}}\text{-}[\text{Fe}_2\text{L}^{20}_3]\text{Cl}_4$ and $\Delta_{\text{Fe,HHT}}\text{-}[\text{Fe}_2\text{L}^{20}_3]\text{Cl}_4$ there was a significant rate of mass loss up to *ca* 400 K, corresponding to 11.5% ($\pm 0.5\%$) of the total mass or 11 equivalents of water per complex. This was followed by a plateau of relative stability until degradative mass loss with an onset of *ca* 525 K.

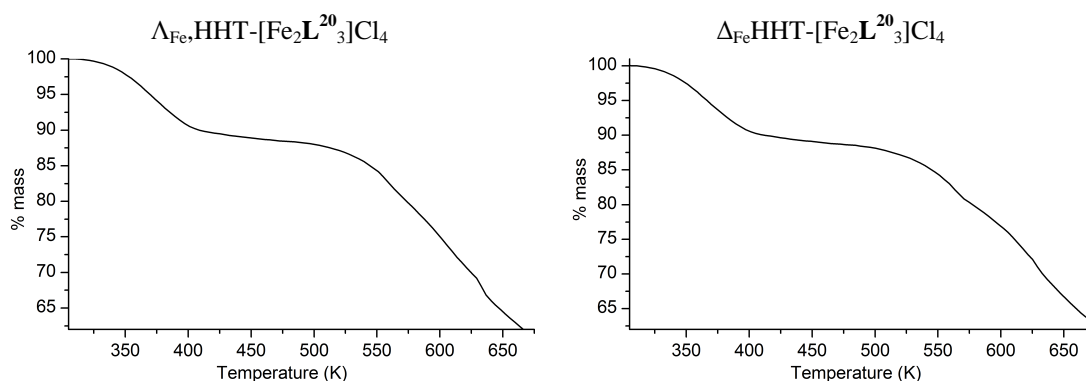
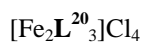


Figure 3.12 | Thermogravimetric spectra of $\Lambda_{\text{Fe,HHT}}\text{-}[\text{Fe}_2\text{L}^{20}_3]\text{Cl}_4$ and $\Delta_{\text{Fe,HHT}}\text{-}[\text{Fe}_2\text{L}^{20}_3]\text{Cl}_4$, indicating mass lost due to water of crystallisation and thermal decomposition.

It was found that the thermogravimetric and microanalytical data correlated well in all cases. Also, samples of enantiomers gave, within error limits, the same thermogravimetric and microanalytical results. Further data are presented in chapter 5 and appendix A. Each of the synthesised panel of complexes was observed to contain between eight and fourteen equivalents of water of crystallisation.

Table 3.2 | Recorded and theoretical elemental analysis of $\Lambda_{\text{Fe,HHT}}\text{-}[\text{Fe}_2\text{L}^{20}_3]\text{Cl}_4$ and $\Delta_{\text{Fe,HHT}}\text{-}[\text{Fe}_2\text{L}^{20}_3]\text{Cl}_4$ 

Complex	% C	% H	% N
Theory $[\text{Fe}_2\text{L}^{20}_3]\text{Cl}_4 \cdot 11\text{H}_2\text{O}$	55.1	5.4	10.3
Recorded $\Lambda_{\text{Fe}}\text{-}[\text{Fe}_2\text{L}^{20}_3]\text{Cl}_4 \cdot 11\text{H}_2\text{O}$	54.7	4.8	9.7
Recorded $\Delta_{\text{Fe}}\text{-}[\text{Fe}_2\text{L}^{20}_3]\text{Cl}_4 \cdot 11\text{H}_2\text{O}$	55.0	5.0	10.0

3.2.5 Complex stability in aqueous media

To investigate how the panel of triplex metallohelices behave in aqueous media over an extended period of time, their absorbance spectra were recorded periodically in different aqueous environments. The Hannon's racemic helicate ($[\text{Fe}_2\text{L}^{\text{H}}_3]\text{Cl}_4$), synthesised as described in chapter 2, was included for comparison. All of the complexes were found to be readily soluble in water, dilute acid (0.2 M HCl, pH 1.0) and RPMI-1640 cell culture medium.

Table 3.3 | Solution half-life ($t_{1/2}$) of MLCT band (540 nm) for triplex metallohelices and $[\text{Fe}_2\text{L}^{\text{H}}_3]\text{Cl}_4$ (0.03 mM) in water (pH 7.0) at 20°C, *a* Complete hydrolysis observed in 19 days.

Complex	pH 7, 20°C $t_{1/2}$ /days (esd)
$[\text{Fe}_2\text{L}^{\text{H}}_3]\text{Cl}_4$	<i>a</i>
$\Lambda_{\text{Fe,HHT}}\text{-}[\text{Fe}_2\text{L}^{20}_3]\text{Cl}_4$	61 (4)
$\Delta_{\text{Fe,HHT}}\text{-}[\text{Fe}_2\text{L}^{20}_3]\text{Cl}_4$	71 (7)
$\Lambda_{\text{Fe,HHT}}\text{-}[\text{Fe}_2\text{L}^{21}_3]\text{Cl}_4$	77 (10)
$\Delta_{\text{Fe,HHT}}\text{-}[\text{Fe}_2\text{L}^{21}_3]\text{Cl}_4$	78 (10)
$\Lambda_{\text{Fe,HHT}}\text{-}[\text{Fe}_2\text{L}^{22}_3]\text{Cl}_4$	52 (8)
$\Delta_{\text{Fe,HHT}}\text{-}[\text{Fe}_2\text{L}^{22}_3]\text{Cl}_4$	47 (8)

A 0.03 mM solution of each compound was made up in water and the absorbance of 200-800 nm light was recorded over 50 d. The reduction in absorbance at 540 nm, which corresponds to the MLCT band of the complex, was used as an indication of the presence of the complete complex. The complexes all appeared to decay *via* first order kinetics, with extrapolated $t_{1/2}$ of 60 – 80 days, except the complexes of nitroarene L^{22} which was significantly shorter at *ca* 50 d.

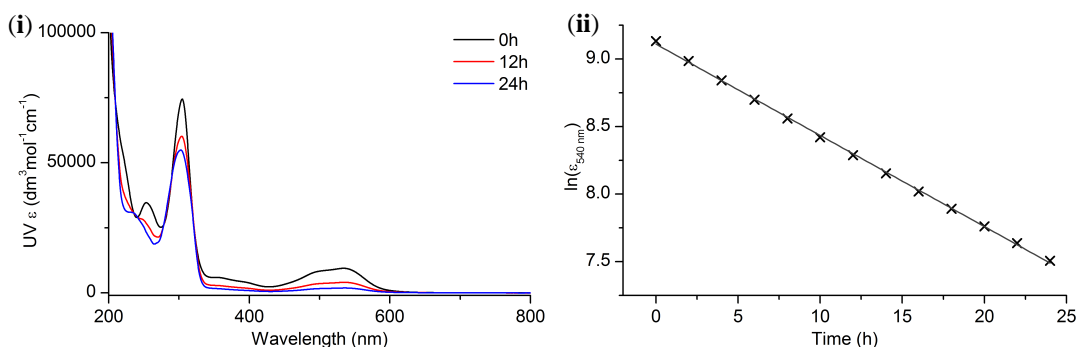


Figure 3.13 | (i) Absorbance spectra of $\Delta_{\text{Fe,HHT}}\text{-}[\text{Fe}_2\text{L}^{20}]_3\text{Cl}_4$ (0.03 mM in 0.2 M HCl at 20°C) at 0, 12 and 24 h. (ii) $\ln(\epsilon)$ at 540 nm (corresponding to MLCT band) of $\Delta_{\text{Fe,HHT}}\text{-}[\text{Fe}_2\text{L}^{20}]_3\text{Cl}_4$ (0.03 mM in 0.2 M HCl at 20°C).

In 0.2 M HCl (pH 1.0, 20°C) the complexes again appeared to decay by first order rate kinetics and with shorter half-lives. By far the most stable complexes were the HHT- $[\text{Fe}_2\text{L}^{\text{F1}}]_3\text{Cl}_4$ enantiomers which showed no signs of deterioration even over many days. The alkyne HHT- $[\text{Fe}_2\text{L}^{25}]_3\text{Cl}_4$ enantiomers were also extremely stable, with recorded half-lives of around 38 h. HHT- $[\text{Fe}_2\text{L}^{23}]_3\text{Cl}_4$ exhibited moderate stability with a recorded half-life of 15 h. The parent and methoxy derivatives $[\text{Fe}_2\text{L}^{\text{x}}]_3\text{Cl}_4$ ($\text{x} = \mathbf{20}, \mathbf{21}$) had similar recorded half-lives of around 10 h. HHT- $[\text{Fe}_2\text{L}^{22}]_3\text{Cl}_4$ was found to be much less stable to hydrolysis than the other triplex metallohelicenes with a recorded half-life similar to the known Hannon helicate of around 2 h.

Table 3.4 | Solution half-life ($t_{1/2}$) of MLCT band (540 nm) for triplex metallohelices and $[\text{Fe}_2\text{L}^{\text{H}}_3]\text{Cl}_4$ (0.03 mM), 0.2 M hydrochloric acid (pH 1.0) *a* No hydrolysis observed over a time period of the experiment (10 days).

Complex	pH 1, 20°C $t_{1/2}$ /hours (esd)
$[\text{Fe}_2\text{L}^{\text{H}}_3]\text{Cl}_4$	1.4 (0.01)
$\Lambda_{\text{Fe}}, \text{HHT}-[\text{Fe}_2\text{L}^{\text{F1}}_3]\text{Cl}_4$	<i>a</i>
$\Delta_{\text{Fe}}, \text{HHT}-[\text{Fe}_2\text{L}^{\text{F1}}_3]\text{Cl}_4$	<i>a</i>
$\Lambda_{\text{Fe}}, \text{HHT}-[\text{Fe}_2\text{L}^{20}_3]\text{Cl}_4$	10.3 (0.1)
$\Delta_{\text{Fe}}, \text{HHT}-[\text{Fe}_2\text{L}^{20}_3]\text{Cl}_4$	10.0 (0.04)
$\Lambda_{\text{Fe}}, \text{HHT}-[\text{Fe}_2\text{L}^{21}_3]\text{Cl}_4$	11.5 (0.1)
$\Delta_{\text{Fe}}, \text{HHT}-[\text{Fe}_2\text{L}^{21}_3]\text{Cl}_4$	11.3 (0.1)
$\Lambda_{\text{Fe}}, \text{HHT}-[\text{Fe}_2\text{L}^{22}_3]\text{Cl}_4$	2.0 (0.3)
$\Delta_{\text{Fe}}, \text{HHT}-[\text{Fe}_2\text{L}^{22}_3]\text{Cl}_4$	2.5 (0.4)
$\Lambda_{\text{Fe}}, \text{HHT}-[\text{Fe}_2\text{L}^{23}_3]\text{Cl}_4$	16.1 (0.8)
$\Delta_{\text{Fe}}, \text{HHT}-[\text{Fe}_2\text{L}^{23}_3]\text{Cl}_4$	15.5 (0.8)
$\Lambda_{\text{Fe}}, \text{HHT}-[\text{Fe}_2\text{L}^{25}_3]\text{Cl}_4$	38.5 (1.2)
$\Delta_{\text{Fe}}, \text{HHT}-[\text{Fe}_2\text{L}^{25}_3]\text{Cl}_4$	37.7 (1.1)

Preliminary studies in RPMI-1640 medium indicated that the kinetics of decomposition did not follow simple rate laws and the data could not be modelled in a realistic manner. Therefore an estimate of the amount of Λ_{Fe} complex (Δ_{Fe} assumed to be analogous) remaining after 96 h was recorded, based on the intensity of the MLCT band at 540 nm (table 3.5). HHT- $[\text{Fe}_2\text{L}^{20}_3]\text{Cl}_4$ was found to be the most stable complex with an integrity after 96 h of 72%.

Table 3.5 | % integrity in MLCT band (540 nm) of triplex metallohelices and $[\text{Fe}_2\text{L}^{\text{H}}_3]\text{Cl}_4$, (0.03 mM) after 96 h in RPMI-1640 cell culture medium at 37°C.

Complex	RPMI-1640 medium, 37°C 96h % integrity (esd)
$[\text{Fe}_2\text{L}^{\text{H}}_3]\text{Cl}_4$	12.0 (9.4)
$\Lambda_{\text{Fe}}, \text{HHT}-[\text{Fe}_2\text{L}^{20}_3]\text{Cl}_4$	71.6 (1.4)
$\Lambda_{\text{Fe}}, \text{HHT}-[\text{Fe}_2\text{L}^{22}_3]\text{Cl}_4$	12.6 (4.4)
$\Lambda_{\text{Fe}}, \text{HHT}-[\text{Fe}_2\text{L}^{23}_3]\text{Cl}_4$	10.1 (4.5)
$\Lambda_{\text{Fe}}, \text{HHT}-[\text{Fe}_2\text{L}^{25}_3]\text{Cl}_4$	38.6 (3.0)

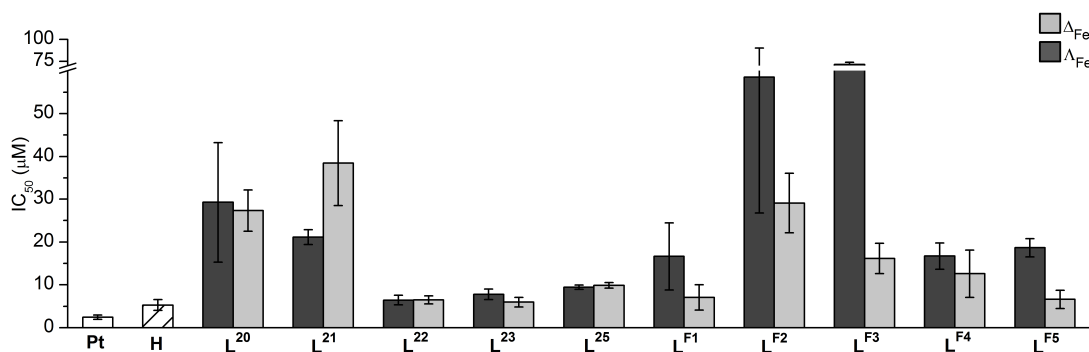
3.3 Antimicrobial activity

The class Ia flexicates have previously been found to be potent antimicrobial agents.¹⁵ The triplex metallohelices were tested against Gram-positive *Methicillin-resistant Staphylococcus aureus*, USA300 (MRSA) and Gram-negative *Escherichia coli*, TOP10 (E. Coli) by Daniel Simpson at University of Warwick. Each compound was tested over a range of concentrations (2 – 128 µg/ml) in Mueller-Hinton broth over 20 h at 37°C.³³ As can be seen in table 3.6 none of the tested triplex metallohelices inhibited cell growth even at the highest concentration of 128 µg ml⁻¹. It can therefore be deduced that the triplex metallohelices are not antimicrobial agents at clinically significant concentrations.

Table 3.6 | MIC values for triplex metallohelices, along with positive controls, $\Lambda_{\text{Fe}}\text{-}[\text{Fe}_2\text{L}^{\text{S}}_3]\text{Cl}_4$, the Helicate racemate and ampicillin against gram-positive *Staphylococcus aureus*, USA300 (MRSA) and gram-negative *Escherichia coli*, TOP10 (E. Coli) over 20 h at 37°C in Mueller-Hinton broth.

Compound	MRSA MIC (µg ml ⁻¹)	E. Coli MIC (µg ml ⁻¹)
$[\text{Fe}_2\text{L}^{\text{H}}_3]\text{Cl}_4$	>128	>128
Ampicillin	<2	4
$\Lambda_{\text{Fe}}\text{-}[\text{Fe}_2\text{L}^{\text{S}}_3]\text{Cl}_4$	8	4
$\Lambda_{\text{Fe},\text{HHT}}\text{-}[\text{Fe}_2\text{L}^{\text{20}}_3]\text{Cl}_4$	>128	>128
$\Delta_{\text{Fe},\text{HHT}}\text{-}[\text{Fe}_2\text{L}^{\text{20}}_3]\text{Cl}_4$	>128	>128
$\Lambda_{\text{Fe},\text{HHT}}\text{-}[\text{Fe}_2\text{L}^{\text{F1}}_3]\text{Cl}_4$	>128	>128
$\Delta_{\text{Fe},\text{HHT}}\text{-}[\text{Fe}_2\text{L}^{\text{F1}}_3]\text{Cl}_4$	>128	>128

3.4.1 MDA-MB-468



In MDA-MB-468 cells, none of the triplex metallohelices were more potent than cisplatin and showed only moderate toxicity (IC₅₀ 5-100 μM). HHT-[Fe₂L^x₃]Cl₄ (x = **20-23**, **25**) did not display an enantiomeric selectivity; the nitroarene, naphthyl and terminal alkyne compounds HHT-[Fe₂L^x₃]Cl₄ (x = **22**, **23**, **25**) were the most active

triplex metallohelices tested with a similar activity to $[\text{Fe}_2\text{L}^{\text{H}}_3]\text{Cl}_4$ in this cell line. Both the unfunctionalised and methoxy HHT- $[\text{Fe}_2\text{L}^{\text{x}}_3]\text{Cl}_4$ ($x = \mathbf{20}, \mathbf{21}$) compounds were substantially less active ($\text{IC}_{50} > 25 \mu\text{M}$).

All the Δ_{Fe} -HHT- $[\text{Fe}_2\text{L}^{\text{x}}_3]\text{Cl}_4$ ($x = \mathbf{F1-F5}$) complexes were found to be more active than their Λ_{Fe} enantiomers. Inclusion of hydroxyl or methoxy functionality HHT- $[\text{Fe}_2\text{L}^{\text{x}}_3]\text{Cl}_4$ ($x = \mathbf{F2}, \mathbf{F3}$) reduced the observed activity *ca* 4-fold compared with the unfunctionalised compound HHT- $[\text{Fe}_2\text{L}^{\text{F1}}_3]\text{Cl}_4$. Broadly it appeared that the more hydrophobic ligands led to a higher observed activity in this cell line.

3.4.2 HCT116 p53^{+/+}

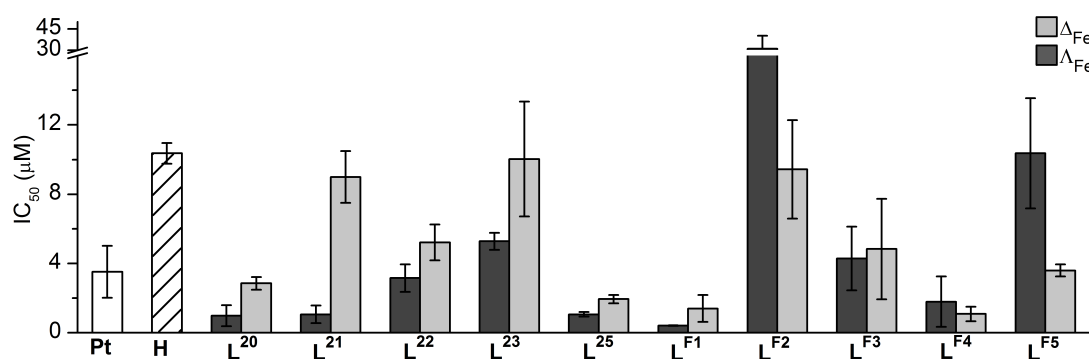


Figure 3.15 | IC_{50} values of cisplatin (**Pt**, white), $[\text{Fe}_2\text{L}^{\text{H}}_3]\text{Cl}_4$ (**H**, hashed) and the panel of triplex metallohelices (Δ_{Fe} - light grey, Λ_{Fe} - dark grey) against HCT116 p53^{+/+} over 96 h.

The triplex metallohelices showed substantially higher activity against HCT116 p53^{+/+} than MDA-MB-468 cells, with several examples exhibiting nanomolar potency. Λ_{Fe} -HHT- $[\text{Fe}_2\text{L}^{\text{x}}_3]\text{Cl}_4$ ($x = \mathbf{20-23}, \mathbf{25}$) compounds were more active than their Δ_{Fe} enantiomers. Λ_{Fe} -HHT- $[\text{Fe}_2\text{L}^{\text{x}}_3]\text{Cl}_4$ ($x = \mathbf{20}, \mathbf{21}, \mathbf{25}$) were all active in this cell line at IC_{50} *ca* 1 μM , but no coherent relationship between activity and ligand functionality is clear.

HHT-[Fe₂L^x₃]Cl₄ (x = **F1-F5**) compounds did not exhibit a consistent enantiomeric preference. Λ_{Fe} -HHT-[Fe₂L^{F1}₃]Cl₄ was the most active compound of this type, up to seven times more potent than cisplatin, while both enantiomers of hydroxyl HHT-[Fe₂L^{F2}₃]Cl₄ were much less so (IC₅₀ > 10 μ M). Again with this architecture of triplex metallohelix it appears that inclusion of hydrophilic functionality reduces the observed activity.

3.4.3 HCT116 p53^{-/-}

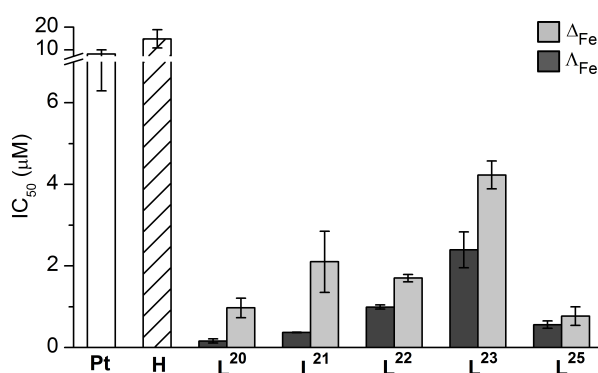


Figure 3.16 | IC₅₀ values of cisplatin (**Pt**, white), [Fe₂L^H₃]Cl₄ (**H**, hashed) and HHT-[Fe₂L^x₃]Cl₄ (x = **20-23**, **25**) (Δ Fe - light grey, Λ Fe - dark grey) against HCT116 p53^{-/-} over 96 h.

HHT-[Fe₂L^x₃]Cl₄ (x = **21-24**, **26**) were then investigated in HCT116 p53^{-/-} cells, which is genetically identical to HCT116 p53^{+/+} but with mutated p53. Although cisplatin and [Fe₂L^H₃]Cl₄ were less active in this than the sister cell line (IC₅₀ ca 12 μ M), all the tested triplex metallohelices were found to be substantially more active, with several examples exhibiting nanomolar IC₅₀ values, similar to the flexicates investigated in chapter 2. The Λ_{Fe} compounds were found to be up to five times more active than their Δ_{Fe} enantiomers and up to two orders of magnitude more active than cisplatin or [Fe₂L^H₃]Cl₄. Adding functionality to the para- position of the phenyl group of the ligand appeared to reduce the toxicity of the compound towards this cell line, possibly due to a disruption of a key interaction with a biomolecule.

3.4.4 Toxicity against non-cancerous human cells and selectivity

The toxicity of the most active of the triplex metallohelices was investigated in human retinal pigment epithelial cells (ARPE19), which display normal growth behaviour in culture medium.

The triplex metallohelices tested were found to be considerably less active in the healthy cell line than cisplatin, and much less active than they were in HCT116 p53^{-/-}, the most sensitive cancerous cell line. This indicated a high level of selectivity. In fact while cisplatin was almost twice as potent in the healthy cell line as the cancerous, $\Delta_{\text{Fe,HHT}}\text{-}[\text{Fe}_2\text{L}^{20}_3]\text{Cl}_4$ and $\Lambda_{\text{Fe,HHT}}\text{-}[\text{Fe}_2\text{L}^{25}_3]\text{Cl}_4$ were up to 200 times less active in the healthy cells than the cancerous cells.

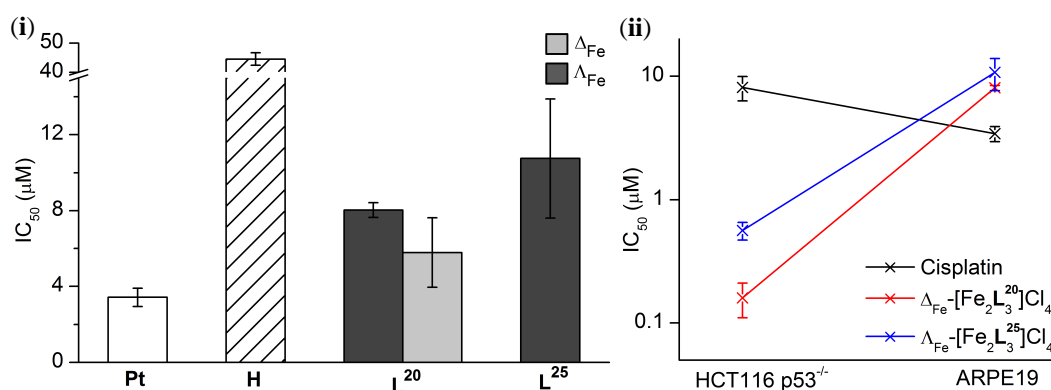


Figure 3.17 | (i) IC₅₀ values for the most active of the panel of complexes against ARPE19 cells over 96 h, presented on a logarithmic scale. (ii) Comparison of activity of Cisplatin, $\Delta_{\text{Fe,HHT}}\text{-}[\text{Fe}_2\text{L}^{20}_3]\text{Cl}_4$ and $\Lambda_{\text{Fe,HHT}}\text{-}[\text{Fe}_2\text{L}^{25}_3]\text{Cl}_4$ in HCT116 p53^{-/-} and ARPE19 cells.

The triplex metallohelices thus appear to be acting in a highly selective manner towards cancerous colon cells over both healthy cells and breast cancer cells. They may display reduced side effects compared to other chemotherapy agents acting on unwanted targets.

3.5 Mode of action

To further study how triplex metallohelices act on colon cancer cells their mode of action has been investigated. By studying their interactions with DNA in cell-free and *in vitro* systems, their effect on the cell cycle and their induction of apoptosis some indications of possible mode of action will become apparent.

3.5.1 Denaturation of ct-DNA

Following the procedure described in section 2.5.1, the triplex metallohelices effects on the denaturation temperature (T_m)³⁵ of linear ct-DNA (measured to be $68.3 \pm 0.5^\circ\text{C}$ when untreated) was investigated.

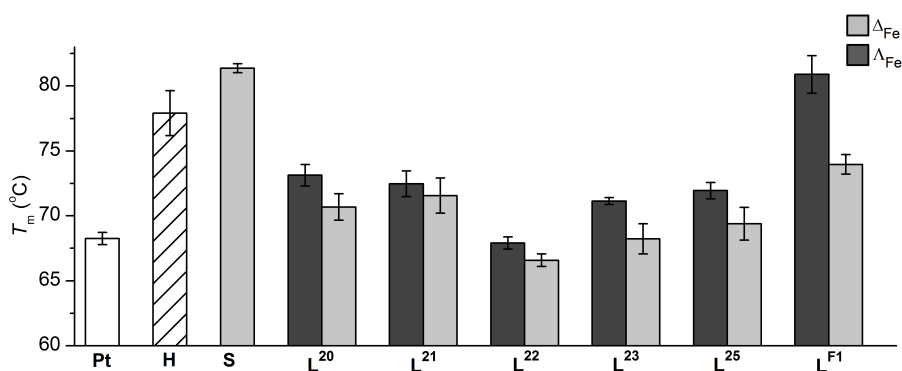


Figure 3.18 | Effect on T_m of linear ct-DNA (DNA, white) from interactions with $[\text{Fe}_2\text{L}^{\text{H}}_3]\text{Cl}_4$ (H, hashed) and triplex metallohelices in 1mM Trizma base (10:1 base pair to complex).

None of $\text{HHT-}[\text{Fe}_2\text{L}^{\text{x}}_3]\text{Cl}_4$ ($x = 20-23, 25$) had a significant effect on the denaturation temperature of ct-DNA. $\text{HHT-}[\text{Fe}_2\text{L}^{20}_3]\text{Cl}_4$ and $\text{HHT-}[\text{Fe}_2\text{L}^{21}_3]\text{Cl}_4$ both increased T_m ca 3°C possibly indicating a non-specific interaction between the DNA and complex, with the Λ_{Fe} enantiomer having a slightly stronger effect than Δ_{Fe} enantiomer. This would lead us to consider that any observable activity of $\text{HHT-}[\text{Fe}_2\text{L}^{\text{x}}_3]\text{Cl}_4$ ($x = 20-23, 26$) in biological systems is unlikely to involve DNA binding in the mode of action.

Conversely, $\Lambda_{\text{Fe,HHT}}\text{-}[\text{Fe}_2\text{L}^{\text{F1}}_3]\text{Cl}_4$ increased T_m *ca* 15°C, which is indicative of an electrostatic binding event occurring between the two molecules, similar to the known flexicate $\Lambda_{\text{Fe}}\text{-}[\text{Fe}_2\text{L}^{\text{S}}_3]\text{Cl}_4$.^{15, 36}

3.5.2 Induction of DNA damage

DNA breaking, binding or modifying is a common mode of action in anticancer drugs such as cisplatin³⁷ and cyclophosphamide.³⁸ The Hannon helicate is also reported to induce some DNA damage in cells.³⁹ As with the flexicates discussed in chapter 2, the metal ions in triplex metallohelices are intended to be merely a scaffold rather than providing a reaction centre. Nevertheless the ability of HHT- $[\text{Fe}_2\text{L}^{\text{x}}_3]\text{Cl}_4$ ($\text{x} = \mathbf{21-23}$) and HHT- $[\text{Fe}_2\text{L}^{\text{F1}}_3]\text{Cl}_4$ to induce DNA damage was studied by single cell gel electrophoresis, following the procedure described in section 2.5.3.

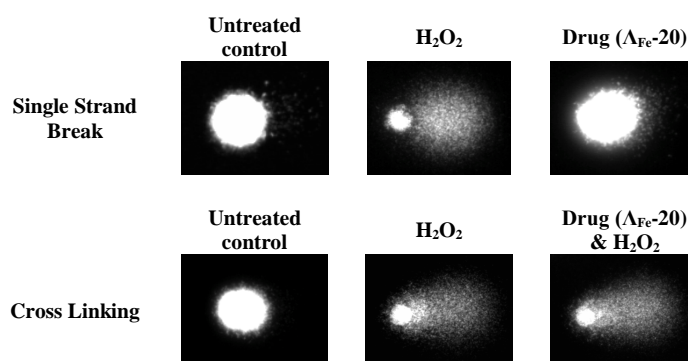


Figure 3.19 | Fluorescence microscopy images of single untreated control HCT116 p53^{+/+} cells, those exposed to $\Lambda_{\text{Fe,HHT}}\text{-}[\text{Fe}_2\text{L}^{\mathbf{20}}_3]\text{Cl}_4$ (20 μM) for 24 h, those exposed to H_2O_2 for 30 min and those exposed to both $\Lambda_{\text{Fe,HHT}}\text{-}[\text{Fe}_2\text{L}^{\mathbf{20}}_3]\text{Cl}_4$ and H_2O_2 .

As seen in figure 3.19 and table 3.7, treating the cells with triplex metallohelices did not induce any single strand breaks or cross linking³⁷ in the HCT116 p53^{+/+} cells compared to the untreated control.

Table 3.7 | (i) Mean tail moments of 50 HCT116 p53^{+/+} cells after treatment with 20 μ M triplex metallohelicies for 24 h, with an untreated control (0% SSB) and H₂O₂ (100% SSB); (ii) Mean tail moments of 50 HCT116 p53^{+/+} cells after treatment with 20 μ M triplex metallohelicies for 24 h and H₂O₂, with an untreated control and those treated with H₂O₂ only (0% X-link).

(i)	Complex	SSB (esd)	(ii)	Complex	X-link (esd)
	Untreated control	3.51 (1.30)		Untreated control	1.87 (0.39)
	H ₂ O ₂	36.04 (6.77)		H ₂ O ₂	36.44 (4.02)
	$\Delta_{\text{Fe}}, \text{HHT}-[\text{Fe}_2\text{L}^{\text{F1}}_3]\text{Cl}_4$	2.26 (0.42)		$\Delta_{\text{Fe}}, \text{HHT}-[\text{Fe}_2\text{L}^{\text{F1}}_3]\text{Cl}_4$	32.02 (0.76)
	$\Delta_{\text{Fe}}, \text{HHT}-[\text{Fe}_2\text{L}^{\text{F1}}_3]\text{Cl}_4$	1.38 (0.51)		$\Delta_{\text{Fe}}, \text{HHT}-[\text{Fe}_2\text{L}^{\text{F1}}_3]\text{Cl}_4$	-
	$\Delta_{\text{Fe}}, \text{HHT}-[\text{Fe}_2\text{L}^{\text{20}}_3]\text{Cl}_4$	2.44 (0.55)		$\Delta_{\text{Fe}}, \text{HHT}-[\text{Fe}_2\text{L}^{\text{20}}_3]\text{Cl}_4$	34.62 (5.45)
	$\Delta_{\text{Fe}}, \text{HHT}-[\text{Fe}_2\text{L}^{\text{20}}_3]\text{Cl}_4$	2.26 (1.50)		$\Delta_{\text{Fe}}, \text{HHT}-[\text{Fe}_2\text{L}^{\text{20}}_3]\text{Cl}_4$	-
	$\Delta_{\text{Fe}}, \text{HHT}-[\text{Fe}_2\text{L}^{\text{21}}_3]\text{Cl}_4$	2.16 (1.42)		$\Delta_{\text{Fe}}, \text{HHT}-[\text{Fe}_2\text{L}^{\text{21}}_3]\text{Cl}_4$	-
	$\Delta_{\text{Fe}}, \text{HHT}-[\text{Fe}_2\text{L}^{\text{22}}_3]\text{Cl}_4$	3.40 (2.21)		$\Delta_{\text{Fe}}, \text{HHT}-[\text{Fe}_2\text{L}^{\text{22}}_3]\text{Cl}_4$	-

γ -H₂AX – a DNA damage repair histone⁴⁰⁻⁴³ – is a useful universal marker for DNA damage. The effect HHT-[Fe₂L²⁰]₃Cl₄ and HHT-[Fe₂L^{F1}]₃Cl₄ had on the γ -H₂AX expression in HCT116 p53^{+/+} cells was studied following the procedure outlined in section 2.5.3. None of the tested triplex metallohelicies had a significant effect on the production of γ -H₂AX which would suggest these compounds did not cause DNA lesions or interruption of the γ -H₂AX pathway.

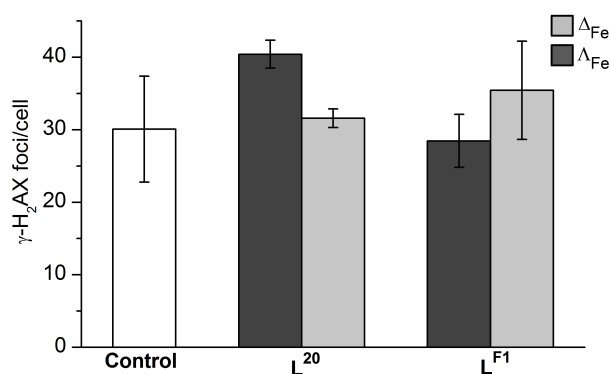


Figure 3.20 | Mean γ -H₂AX expression of HCT116 p53^{+/+} cells (untreated **control** – white) after treatment with HHT-[Fe₂L²⁰]₃Cl₄ or HHT-[Fe₂L^{F1}]₃Cl₄ (10 μ M, Δ_{Fe} - light grey, Λ_{Fe} - dark grey) for 24 h.

3.5.3 Effects on the cell division cycle

Investigating if an anticancer agent disrupts the cell cycle can indicate mode of action and give direction to further study.⁴⁴ Following the procedure in section 2.5.4⁴⁴ the tested complexes were found to cause a dramatic increase in the proportion of cells in the G₂/M phase, from *ca* 20 to 23-46% of cells. The compounds also reduced the percentage of cells found in the S (29% to 8-18%) and G₁ (44% to 4-43%) phases compared to the untreated cells. $\Delta_{\text{Fe,HHT}}\text{-}[\text{Fe}_2\text{L}^{\text{F1}}_3]\text{Cl}_4$ had the most pronounced effect on the populations of these phases, with $\Lambda_{\text{Fe,HHT}}\text{-}[\text{Fe}_2\text{L}^{20}_3]\text{Cl}_4$ having a similar but less extreme effect.

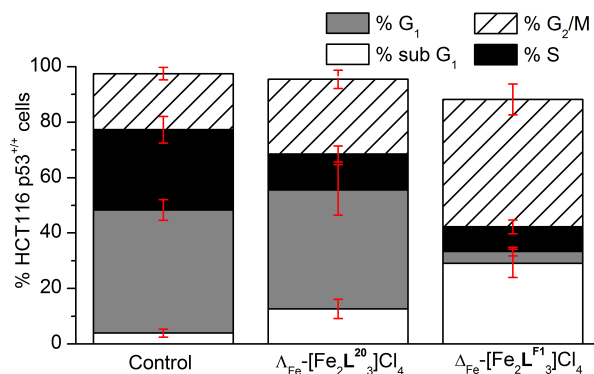


Figure 3.21 | Cell Cycle FACS Assay showing the % population of HCT116 p53^{+/+} cells when treated with $\Lambda_{\text{Fe,HHT}}\text{-}[\text{Fe}_2\text{L}^{20}_3]\text{Cl}_4$ and $\Delta_{\text{Fe,HHT}}\text{-}[\text{Fe}_2\text{L}^{\text{F1}}_3]\text{Cl}_4$ (10 μM) for 24 h and a **control** of untreated cells.

Upon treatment with the triplex metalloheliices there was a very pronounced change in the population of sub G₁ cells (*ca* 4% to 30%), which are considered apoptotic.^{70, 71} These data indicated that triplex metalloheliices induced programmed cell death in HCT116 p53^{+/+} colon carcinoma cells.

3.5.4 Induction of apoptosis

Due to the positive indication for induction of programmed cell death by triplex metalloheliices, further investigations were carried out by Dr Simon Allison,

Bradford Institute of Cancer therapeutics, following the same procedure as in section 2.5.5.⁴⁵

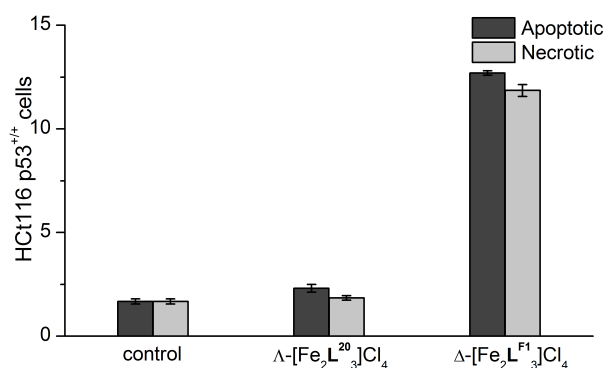


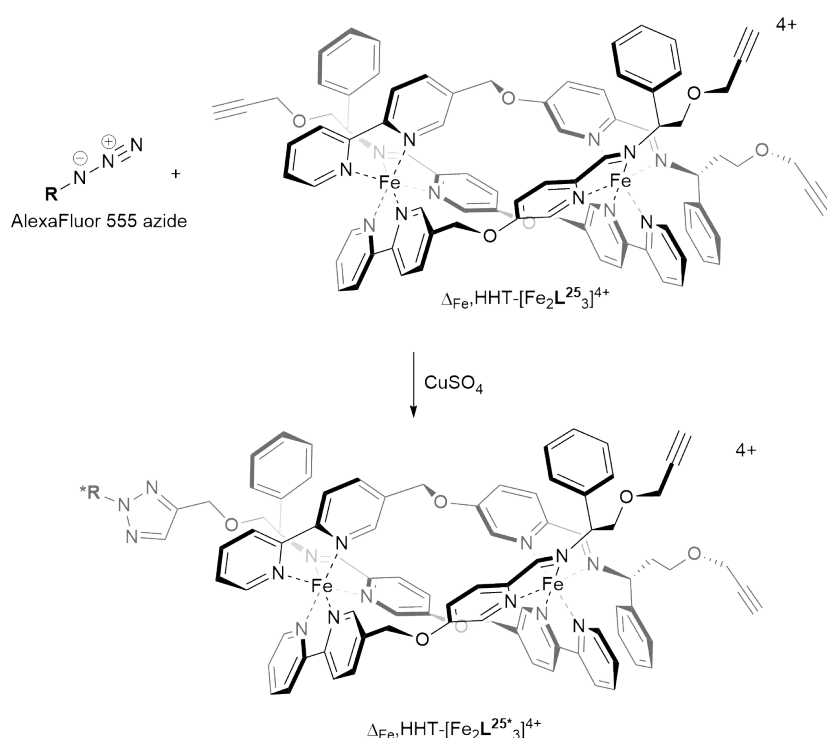
Figure 3.22 | Amount of early apoptotic (annexin-v positive, propidium iodide negative) and late apoptotic / necrotic (annexin-v positive, propidium iodide positive) HCT116 p53^{+/+} cells after incubation for 72 h with 20 μ M of each compound, compared to an untreated **control**.

Treatment with $\Delta_{\text{Fe,HHT}}\text{-[Fe}_2\text{L}^{\text{F1}}\text{]Cl}_4$ increased the number of both early and late apoptotic cells significantly compared to the untreated control. This was a solid indication that this compound was triggering early cell death as part of its mode of action. However, $\Delta_{\text{Fe,HHT}}\text{-[Fe}_2\text{L}^{\text{20}}\text{]Cl}_4$ appeared to only slightly increase the number of apoptotic cells over this time period. This could be due to several factors. In the cell cycle study described above $\Delta_{\text{Fe,HHT}}\text{-[Fe}_2\text{L}^{\text{20}}\text{]Cl}_4$ had a less pronounced effect on the cells than $\Delta_{\text{Fe,HHT}}\text{-[Fe}_2\text{L}^{\text{F1}}\text{]Cl}_4$ and so it is possible that it is acting in a similar but much less pronounced manner. However, as the two compounds were similarly cytotoxic in this cell line over 96 h it could be that $\Delta_{\text{Fe,HHT}}\text{-[Fe}_2\text{L}^{\text{20}}\text{]Cl}_4$ is not inducing apoptosis, but inhibiting cellular processes in another way. This could indicate a very subtle mode of action, which requires further study.

3.5.5 Cell localisation

The study of localisation of drug molecules in the cell during treatment can give valuable information concerning the mode of action. The terminal alkyne

functionality in $\Delta_{\text{Fe,HHT}}\text{-}[\text{Fe}_2\text{L}^{25}]_3\text{Cl}_4$ allowed us to attempt a whole-cell localisation experiment with the fluorescent tag AlexaFluor 555 azide *via* a copper(II) mediated alkyne-azide click reaction.^{46, 47} This dye is activated only on triazole formation, and thus gives no fluorescence in an alkyne free environment.^{48, 49} Preliminary examples of similar propargyl functionalised complexes being amenable to a conceptually similar copper(II) mediated alkyne-azide click reaction have been demonstrated in our research group.^{1, 18}



Scheme 3.3 | Copper(II) mediated click azide-alkyne reaction between $\Delta_{\text{Fe,HHT}}\text{-}[\text{Fe}_2\text{L}^{25}]_3\text{Cl}_4$ and AlexaFluor® 555 (structure not yet published by Invitrogen).

HCT116 p53^{+/+} cells were treated with $\Delta_{\text{Fe,HHT}}\text{-}[\text{Fe}_2\text{L}^{25}]_3\text{Cl}_4$ at a range of concentrations (1 – 30 μM) for 48 h. After washing, to remove any excess complex in the cell culture medium, they were permeabilised with Triton-X, and then treated with Click-iT® reaction buffer cocktail containing copper(II) sulphate (2 mM) and

AlexaFluor® 555 azide (5 μM) for 30 minutes in the absence of light. After washing with PBS the cells were analysed using confocal laser microscopy.⁵⁰

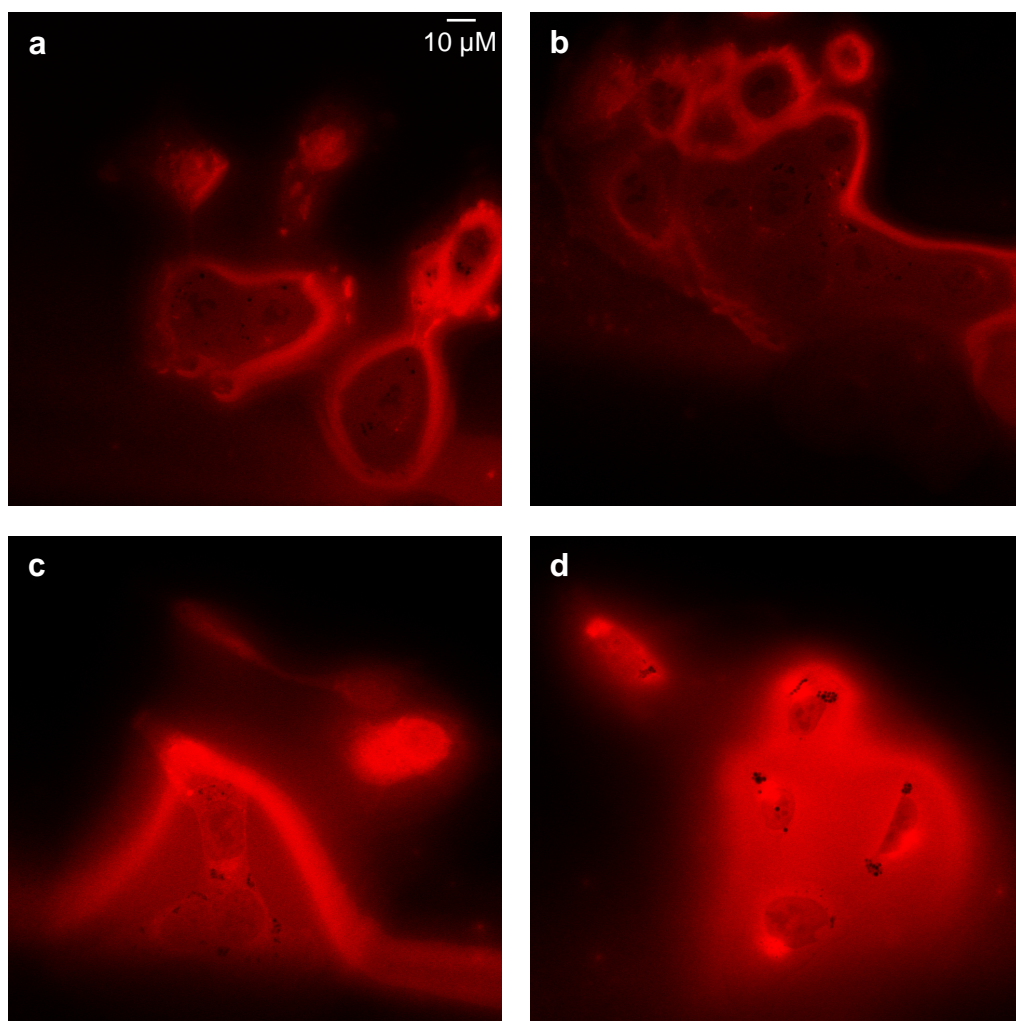


Figure 3.23 | Fluorescence microscopy images of HCT116 p53^{-/-} cells treated with different concentrations – (a) 1 μM , (b) 3 μM , (c) 10 μM , (d) 30 μM – of $\Delta_{\text{Fe,HHT}}\text{-}[\text{Fe}_2\text{L}^{25}]\text{Cl}_4$ for 48h and stained with AlexaFluor® 555 azide.

In this early study a wide range of drug concentrations (100 – 1 μM) were included to ensure the observation of the fluorescent species. As shown in fig 3.23, AlexaFluor® 555 azide and $\Delta_{\text{Fe,HHT}}\text{-}[\text{Fe}_2\text{L}^{25}]\text{Cl}_4$ successfully coupled in a copper(II) mediated alkyne-azide click reaction and the resulting red fluorescence was observed at least as low as 1 μM of the triplex metallohelix. At high drug

concentrations the increased amount of fluorescence seemed to obscure some of the finer details of the cellular environment, and the large amount of drug present may have necrotised the cells. In general it appeared that $\Delta_{\text{Fe,HHT}}\text{-[Fe}_2\text{L}^{25}_3\text{]Cl}_4$ had congregated principally in the region of the cell membrane of HCT116 p53^{+/+} cells at the observed IC₅₀ (*ca* 1.5 μM) although some may have accessed parts of the intracellular environment (dark and light spots seen in fig 3.23).

This first localisation study could indicate that $\Delta_{\text{Fe,HHT}}\text{-[Fe}_2\text{L}^{25}_3\text{]Cl}_4$ may act on cells in a similar manner to innate peptidic α -helices,⁵¹ and the complex may be affecting key processes of biomolecules found on the cell membrane.

3.6 Summary

A strategy for the selective formation of anti-parallel triplex metallohelices has been successfully established through both molecular modelling, synthetic and structural studies. Ultimately, while absolute configuration at the metal centres was achieved by conventional diastereoselection, the far greater challenge of selectivity for the target asymmetric HHT structure was achieved by maximisation of the relatively strong phenyl-bipyridine inter ligand π -stacks which were present only in the triplex architectures. These secondary interactions also contribute to chemical stability such that the rates of hydrolysis in biologically-relevant media were found to be exceptionally low. In addition, the modular self-assembly has allowed for the production of a large and diverse library of metallohelices. We believe that this represents a significant step towards α -helix-peptide-like candidates for biochemical targets and phenotypic screens.

To this end, and as with the peptidic α -helices they are designed to emulate, triplex metallohelices have been shown to display potent, selective and structure-dependent toxicity to certain cancer cell-lines. They also exhibit no measured toxicity to example Gram-positive and Gram-negative bacteria, alongside a low potency in non-cancerous human epithelial cells. Thus, a subtle biomimetic mechanism rather than broad-spectrum cytotoxicity is indicated. This is corroborated by the observation of major changes to the cell cycle, indications of programmed apoptosis and by localisation on the extracellular cell membrane, without detected DNA damage.

3.7 References

1. S. E. Howson, G. J. Clarkson, A. D. Faulkner, R. A. Kaner, M. J. Whitmore and P. Scott, *Dalton Trans.*, 2013, **42**, 14967-14981.
2. M. Albrecht and R. Fröhlich, *J. Am. Chem. Soc.*, 1997, **119**, 1656-1661.
3. M. Albrecht, M. Napp, M. Schneider, P. Weis and R. Fröhlich, *Chem. Commun.*, 2001, 409-410.
4. M. J. Hannon, S. Bunce, A. J. Clarke and N. W. Alcock, *Angew. Chem.-Int. Edit. Engl.*, 1999, **38**, 1277-1278.
5. E. C. Constable, F. R. Heitzler, M. Neuburger and M. Zehnder, *Supramol. Chem.*, 1995, **5**, 197-200.
6. C. R. Rice, C. J. Baylies, J. C. Jeffery, R. L. Paul and M. D. Ward, *Inorg. Chim. Acta*, 2001, **324**, 331-335.
7. S. Torelli, S. Delahaye, A. Hauser, G. Bernardinelli and C. Piguet, *Chem.-Eur. J.*, 2004, **10**, 3503-3516.
8. F. E. Hahn, C. Schulze Isfort and T. Pape, *Angew. Chem. Int. Edit.*, 2004, **43**, 4807-4810.
9. C. Schulze Isfort, T. Krickmann, T. Pape, R. Fröhlich and F. E. Hahn, *Chemistry*, 2007, **13**, 2344-2357.
10. S. E. Howson, L. E. N. Allan, N. P. Chmel, G. J. Clarkson, R. van Gorkum and P. Scott, *Chem. Commun.*, 2009, **2009**, 1727-1729.
11. C. P. Sebli, S. E. Howson, G. J. Clarkson and P. Scott, *Dalton Trans.*, 2010, **39**, 4447-4454.
12. S. E. Howson, L. E. N. Allan, N. P. Chmel, G. J. Clarkson, R. J. Deeth, A. D. Faulkner, D. H. Simpson and P. Scott, *Dalton Trans.*, 2011, **40**, 10416-10433.
13. S. E. Howson and P. Scott, *Dalton Trans.*, 2011, **40**, 10268-10277.
14. S. E. Howson, *Ph.D. Thesis, University of Warwick*, 2011.
15. S. E. Howson, A. Bolhuis, V. Brabec, G. J. Clarkson, J. Malina, A. Rodger and P. Scott, *Nat. Chem.*, 2012, **4**, 31-36.
16. J.-M. Lehn, A. Rigault, J. Siegel, J. Harrowfield, B. Chevrier and D. Moras, *Proc. Natl Acad. Sci. USA*, 1987, **84**, 2565-2569.
17. S. Grimme, *Angew. Chem. Int. Edit.*, 2008, **47**, 3430-3434.
18. A. D. Faulkner, *University of Warwick*, 2014.
19. T. J. McMurtry, K. N. Raymond and P. H. Smith, *Science*, 1989, **244**, 938-943.
20. S. Rubino, S. Petruso, R. Pierattelli, G. Bruno, G. C. Stocco, L. Steardo, M. Motta, M. Passerotto, E. D. Giudice and G. Gulì, *J. Inorg. Biochem.*, 2004, **98**, 2071-2079.
21. J. K. Barton, A. T. Danishefsky and J. M. Goldberg, *J. Am. Chem. Soc.*, 1984, **106**, 2172-2176.
22. M. D. Ward, J. A. McCleverty and J. C. Jeffery, *Coord. Chem. Rev.*, 2001, **222**, 251-272.
23. C. Kaes, A. Katz and M. W. Hosseini, *Chem. Rev.*, 2000, **100**, 3553-3590.
24. M. D. Frankkamenetskii and S. M. Mirkin, *Annu. Rev. Biochem.*, 1995, **64**, 65-95.
25. A. D. Faulkner, R. A. Kaner, Q. M. A. Abdallah, G. Clarkson, D. J. Fox, P. Gurnani, S. E. Howson, R. M. Phillips, D. I. Roper, D. H. Simpson and P. Scott, *Nat. Chem.*, 2014, **6**, 797-803.

-
26. R. J. Deeth, A. Anastasi, C. Diedrich and K. Randell, *Coord. Chem. Rev.*, 2009, **253**, 795-816.
 27. R. J. Deeth, N. Fey and B. Williams–Hubbard, *J. Comput. Chem.*, 2005, **26**, 123-130.
 28. P. Comba, *Molecular Modelling of Inorganic Compounds*, Wiley-VCH, Weinheim, Germany, 2009.
 29. P. Das, A. Ghosh, M. K. Kesharwani, V. Ramu, B. Ganguly and A. Das, *Eur. J. Inorg. Chem.*, 2011, **2011**, 3050-3058.
 30. C. Dallaire, I. Kolber and M. Gingras, *Org. Synth.*, 2002, **78**, 42.
 31. Y. Hsiao and L. S. Hegedus, *J. Org. Chem.*, 1997, **62**, 3586-3591.
 32. R. N. Bream, S. V. Ley, B. McDermott and P. A. Procopiu, *J. Chem. Soc., Perkin Trans. 1*, 2002, 2237-2242.
 33. J. M. Andrews, *J. Antimicrob. Chemother.*, 2001, **48 (suppl 1)**, 5-16.
 34. T. Mosmann, *J. Immunol. Methods*, 1983, **65**, 55-63.
 35. J. SantaLucia, *Proc. Natl. Acad. Sci. USA*, 1998, **95**, 1460-1465.
 36. A. Rodger, K. J. Sanders, M. J. Hannon, I. Meistermann, A. Parkinson, D. S. Vidler and I. S. Haworth, *Chirality*, 2000, **12**, 221-236.
 37. Z. H. Siddik, *Oncogene*, 2003, **22**, 7265-7279.
 38. A. R. Ahmed and S. M. Hombal, *J. Am. Acad. Dermatol.*, 1984, **11**, 1115-1126.
 39. M. J. Hannon, *Chem. Soc. Rev.*, 2007, **36**, 280-295.
 40. J. Kobayashi, *J. Radiat. Res.*, 2004, **45**, 473-478.
 41. T. L. DeWeese and M. Laiho, eds., *Molecular Determinants of Radiation Response*, Springer New York, New York, 2011.
 42. W. M. Bonner, C. E. Redon, J. S. Dickey, A. J. Nakamura, O. A. Sedelnikova, S. Solier and Y. Pommier, *Nat. Rev. Cancer*, 2008, **8**, 957-967.
 43. A. Celeste, S. Petersen, P. J. Romanienko, O. Fernandez-Capetillo, H. T. Chen, O. A. Sedelnikova, B. Reina-San-Martin, V. Coppola, E. Meffre, M. J. Difilippantonio, C. Redon, D. R. Pilch, A. Oлару, M. Eckhaus, R. D. Camerini-Otero, L. Tessarollo, F. Livak, K. Manova, W. M. Bonner, M. C. Nussenzweig and A. Nussenzweig, *Science*, 2002, **296**, 922-927.
 44. A. Krishan, *J. Cell Biol.*, 1975, **66**, 188-193.
 45. *Apoptosis, Cytotoxicity and Cell Proliferation*, 4th edn., Roche Diagnostics GmbH, Mannheim, Germany, 2008.
 46. H. C. Kolb, M. G. Finn and K. B. Sharpless, *Angew. Chem.-Int. Edit. Engl.*, 2001, **40**, 2004-2021.
 47. V. V. Rostovtsev, L. G. Green, V. V. Fokin and K. B. Sharpless, *Angew. Chem.Int. Edit.*, 2002, **41**, 2596-2599.
 48. R. Breinbauer and M. Köhn, *Chem. Bio. Chem.*, 2003, **4**, 1147-1149.
 49. Q. Wang, T. R. Chan, R. Hilgraf, V. V. Fokin, K. B. Sharpless and M. G. Finn, *J. Am. Chem. Soc.*, 2003, **125**, 3192-3193.
 50. *The Molecular Probes Handbook*, 11th edn., Life Technologies, London, 2010.
 51. F. Schweizer, *Eur. J. Pharmacol.*, 2009, **625**, 190-194.
-

Chapter 4

Progress towards α -helix mimetic metallohelices

Scott and Howson reported several criteria that metallohelix systems should satisfy in order to be relevant in the biomedical domain.¹ They must be optically pure and non-racemising, soluble and resistant to deterioration in aqueous solutions, available from scalable and functionally flexible syntheses, and display relevant potent and selective biology. In chapter 1 we extended these criteria, stating that to be able to act as functional mimics of natural α -helices, an ideal system should present a low symmetry architecture in order to approach acute placement of functionality.

The work detailed in this thesis makes significant progress towards these goals. This brief chapter summarises our progress, describes some remaining targets, and proposes how this research might be progressed and refined to deliver more sophisticated α -helix mimetics.

4.1 Progress through this research project

We have developed a new range of compounds which have very selective and potent anticancer activity. Following Scott and Howson's conception of the flexicate architecture,² work reported in chapter 2 extended this area of research through the synthesis of a range of modified class Ib flexicates. We have demonstrated that this architecture allows for the inclusion of varied functionality, although there are still many possible ligand designs to investigate.

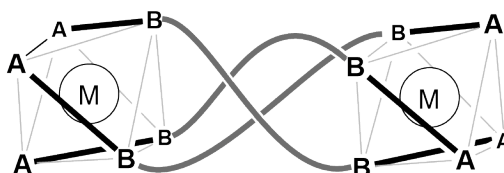


Figure 4.1 | Schematic diagram of a symmetrical flexicate metallohelix.

Water soluble examples of flexicates act by inducing cell cycle arrest and apoptosis, without causing DNA damage in cancer cells. They show high activity in habitually resistant cell lines A2780cis³ (cisplatin resistant ovarian carcinoma) and HCT116 p53^{-/-} (colon carcinoma with mutated p53).

With respect to the supposition that we are creating amphipathic α -helix mimetics, the flexicate design is unable to satisfy our extended criteria. Such assemblies are unable to present the asymmetric topologies we were aiming to imitate. Therefore it would be unrealistic to posit that flexicates are actually mimicking α -helix behaviour. Further, we do not fully understand how these compounds act on cells; it could be that they are merely soluble delivery systems of one or more ligand components.

In chapter 3 we demonstrated that we were able to access lower symmetry architectures. Using directional ligands evolved from the flexicate design, we synthesised asymmetric HHT constitutions which we named triplex metallohelices.⁴ This new system makes a significant step towards satisfying our stated criteria for α -helix mimetics from metal scaffolded self-assembly. Albrecht recently commented favourably on our approach.⁵

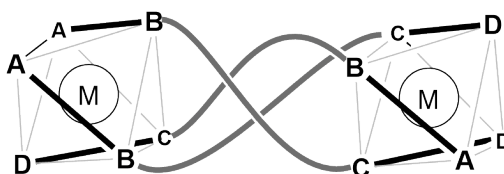


Figure 4.2 | Schematic diagram of an asymmetric HHT triplex metallohelix.

Water soluble and stable examples of triplex metallohelices were found to be similarly active and selective in cancer to the flexicate system. Preliminary studies into possible mechanisms of action show these compounds do not induce DNA damage, but do promote early apoptosis, cause significant changes to the cell cycle and congregate on the membrane. This is a positive indication towards a similar mode of action to innate host-defence peptides and gives us confidence that we have achieved the aim of accessing a range of low symmetry functional α -helix mimetics.

4.2 Potential future developments

An in depth study into the pharmacokinetics and mode of action of lead flexicates needs to be undertaken to further progress the discovery of high anticancer activity. This is with a view to developing this system as a chemotherapeutic panel.

Triplex metallohelices represent a promising new area of chemistry and pharmacology that is in its infancy, and there is still much to discover. To further this work a more detailed investigation into how these new low symmetry architectures act on cells should be conducted. These should include: interactions with membranes, pathways to the observed activation of apoptosis and refinement of the visualisation experiments. Although several lead examples have been identified as being of particular interest, additional screening of new compounds should be continued.

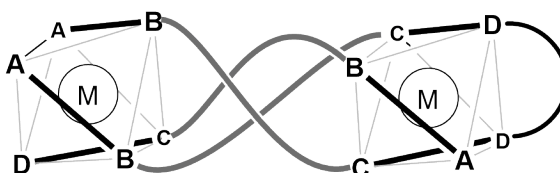


Figure 4.3 | Schematic diagram of a hairpin-tethered HHT metallohelix.

We must also consider how to further refine the structures we can produce with a view to acutely controlling the placement of individual functional groups. Key concepts from the literature could be combined with our asymmetric triplex metallohelix system to create a new generation of low symmetry compounds. For example, linking two of the directional ligands with a variety of hairpin tethers could afford a novel class of compounds. They may have increased stability and would provide unique sites on the architecture – different **D** groups (Fig. 4.3) – for the inclusion of functionality. Adding peptide or carbohydrate groups may also tune the

properties of the complex and could be used to build recognition motifs into such low symmetry architectures.

If triplex and future metallohelix systems are indeed to be considered as α -helix mimetics, then many other applications in medicinal chemistry need to be addressed, such as the research of their activity in other disease areas. These investigations should particularly be in relation to the design, discovery and exploitation of interactions with proteins.

4.3 References

1. S. E. Howson and P. Scott, *Dalton Trans.*, 2011, **40**, 10268-10277.
2. S. E. Howson, A. Bolhuis, V. Brabec, G. J. Clarkson, J. Malina, A. Rodger and P. Scott, *Nat. Chem.*, 2012, **4**, 31-36.
3. V. Brabec, S. E. Howson, R. A. Kaner, R. M. Lord, J. Malina, R. M. Phillips, Q. M. A. Abdallah, P. C. McGowan, A. Rodger and P. Scott, *Chem. Sci.*, 2013, **4**, 4407-4416.
4. A. D. Faulkner, R. A. Kaner, Q. M. A. Abdallah, G. Clarkson, D. J. Fox, P. Gurnani, S. E. Howson, R. M. Phillips, D. I. Roper, D. H. Simpson and P. Scott, *Nat. Chem.*, 2014, **6**, 797-803.
5. M. Albrecht, *Nat. Chem.*, 2014, **6**, 761-762.

Chapter 5

Experimental details

5.1.1 Solvents and chemicals

All solvents and chemicals purchased from commercial sources (Sigma-Aldrich, Acros, Fisher Scientific, Alfa Aesar or Invitrogen) were used without further purification unless otherwise stated. Sodium hydride dispersions in mineral oil were placed in a Schlenk vessel under an inert atmosphere and washed three times with diethyl ether to remove the oil, then dried and stored under argon in an MBraun dry box. Necessary solvents were dried by heating to reflux for 3 d under dinitrogen over the appropriate drying agents (potassium for tetrahydrofuran, sodium/potassium alloy for diethyl ether, and calcium hydride for acetonitrile and pyridine) and degassed before use. Tetrahydrofuran and diethyl ether were additionally pre-dried over sodium wire. Dried solvents were stored in glass ampoules under argon. Deuterated solvents were purchased from Sigma-Aldrich or Cambridge Isotope Laboratories and pre-dried over molecular sieves (3A for methanol, dimethyl sulfoxide and acetonitrile; 4A for chloroform), for 24 h prior to use. Zinc(II) and iron(II) perchlorate hexahydrate pose a risk of explosion and were therefore used only on a small scale.

5.1.2 Equipment and instrumentation

Where appropriate, reactions were carried out under argon using a dual manifold argon/vacuum line and standard Schlenk techniques or an MBraun dry box. All glassware and cannulae for these techniques were stored in an oven at > 375 K.

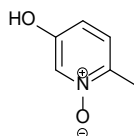
NMR spectra were recorded on Bruker Spectrospin DPX-300/400 and Bruker AV II DRX-500 spectrometers. Routine NMR assignments were confirmed by ^1H - ^1H (COSY) and ^{13}C - ^1H (HMQC) correlation experiments where necessary. The spectra were internally referenced using the residual protio solvent (CDCl_3 , CD_3CN etc.) resonance relative to tetramethylsilane ($\delta = 0$ ppm). ESI mass spectra were recorded in a methanol-water mix (80:20 v/v) on either an Agilent Technologies 1260 Infinity spectrometer or a Bruker Daltonics MicroTOF spectrometer. Infra-red spectra were measured using a Bruker Alpha-P FTIR spectrometer. Elemental analyses were performed by Medac Ltd. Chobham, Surrey GU24, 8JB, UK or Warwick Analytical Service, Coventry, CV4 7EZ. Optical rotation measurements were performed on a Perkin Elmer Polarimeter 341 by Warwick Analytical Services, Coventry, UK. In all cases the following parameters were used: solvent methanol, temperature 20°C , pathlength 100 mm, wavelength 589 nm.

Suitable single crystals for X-ray diffraction were mounted on a glass fibre with Fomblin oil on a Bruker-Nonius FR591 rotating anode diffractometer with a Bruker APEX II CCD camera on a kappa goniostat. The crystals were kept at 120 ± 2 K during data collection. Using Olex2,¹ the structure was solved with the ShelXS² structure solution program using Direct Methods and refined with the ShelXL² refinement package using Least Squares minimisation.

5.2 5-hydroxypicolinaldehyde

5-hydroxypicolinaldehyde was synthesised using a modified literature procedure.³

5-hydroxy-2-methylpyridine-1-oxide (1)



5-hydroxy-2-methylpyridine (25.0 g, 0.23 mol) and *m*-chloroperoxybenzoic acid (43.0 g, 0.23 mol) were suspended in chloroform (250 ml) and heated at reflux (75°C) for 1.5 h before being cooled to ambient temperature and stirring for a further 18 h. The solvent was removed under reduced pressure yielding a yellow solid which was dried *in vacuo* at 30°C. This was washed with hot ethyl acetate (200 ml) and the pale yellow solid was isolated by filtration.

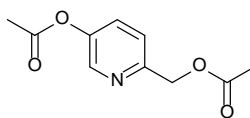
Yield 16.17 g, 56%.

¹H NMR (300MHz, 298 K, DMSO) δ_{H} 10.24 (1H, br s, OH), 7.81 (1H, d, $^4J_{\text{HH}} = 2.0\text{Hz}$), 7.26 (1H, d, $^3J_{\text{HH}} = 8.5\text{ Hz}$), 6.78 (1H, dd, $^3J_{\text{HH}} = 8.5\text{ Hz}$, $^4J_{\text{HH}} = 2.0\text{ Hz}$, Py), 2.22 (3H, s, CH₃).

¹³C{¹H} NMR (101 MHz, 298 K, DMSO) δ_{C} 154.3, 138.9, 127.4, 125.9, 113.7 (Py), 16.3 (CH₃).

MS (ESI) *m/z* 109 [M-O]⁺, 126 [M+H]⁺, 148 [M+Na]⁺

IR $\nu\text{ cm}^{-1}$ 2359 m, 1619 w, 1570 w, 1527 m, 1457 m, 1308 m, 1225 w, 1160 m, 1115 m, 999 w, 962 W, 861 s, 824 m, 774 w, 739 s, 690 w.

6-[(acetyloxy)methyl]pyridine-3-yl acetate (2)

1 (16.0 g, 0.12 mol) was suspended in acetic anhydride (200 ml) and heated at reflux (150°C) for 3 h, causing a colour change from yellow to dark brown. The solvent was removed under reduced pressure and the resulting dark brown liquid was dried *in vacuo* at 50°C.

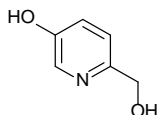
Yield 29.01 g, 99%.

^1H NMR (400 MHz, 298 K, CDCl_3) δ_{H} 8.40 (1H, d, $^4J_{\text{HH}} = 2.5$ Hz), 7.52 (1H, dd, $^3J_{\text{HH}} = 8.0$ Hz, $^4J_{\text{HH}} = 2.5$ Hz), 7.41 (1H, d, $^3J_{\text{HH}} = 8.5$ Hz, Py), 5.21 (2H, s, CH_2), 2.32 (3H, s), 2.17 (3H, s, CH_3).

$^{13}\text{C}\{^1\text{H}\}$ NMR (100 MHz, 298K, DMSO) δ_{C} 170.0, 169.0 (CO), 152.9, 146.4, 142.7, 130.3, 122.4 (Py), 65.6 (CH_2), 20.7, 20.6 (CH_3).

MS (ESI) m/z 210 $[\text{M}+\text{H}]^+$, 232 $[\text{M}+\text{Na}]^+$

IR ν cm^{-1} 2946 w, 1765 m, 1738 s, 1581 w, 1485 m, 1436 w, 1370 m, 1182 s, 1024 s, 925 m, 898 m, 856 m, 722 w, 670 w.

6-(hydroxymethyl)pyridine-3-ol (3)

2 (29.0 g, 0.12 mol) was dissolved in concentrated hydrochloric acid (36%, 100 ml) and stirred at reflux (110°C) for 24 h. The volatiles were removed under reduced

pressure to 20 ml and the solution was neutralised with sodium hydroxide solution (2 M, 50 ml) to pH 7.0. The solvent was removed under reduced pressure yielding a brown solid which was dried *in vacuo* at 50°C. This solid was heated to reflux in acetonitrile (200 ml), filtered hot and the solvent was removed giving a pale yellow solid, which was dissolved in hot acetonitrile (20 ml) and allowed to cool to ambient temperature and the product was collected upon filtration.

Yield 4.55 g, 30%.

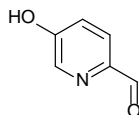
^1H NMR (300 MHz, 298 K, DMSO) δ_{H} 9.72 (1H, br s, PyOH), 8.02 (1H, d, $^4J_{\text{HH}} = 2.5$ Hz), 7.24 (1H, d, $^3J_{\text{HH}} = 8.0$ Hz), 7.13 (1H, dd, $^3J_{\text{HH}} = 8.0$ Hz, $^4J_{\text{HH}} = 2.5$ Hz), 5.21 (2H, br s, CH_2OH), 4.43 (1H, s, CH_2).

$^{13}\text{C}\{^1\text{H}\}$ NMR (100 MHz, 298K, DMSO) δ_{C} 152.2, 152.0, 136.3, 122.5, 121.0 (Py), 63.9 (CH_2).

MS (ESI) m/z 124 $[\text{M}-\text{H}]^-$

IR ν cm^{-1} 3439 w, 2407 w, 1765 w, 1570 m, 1483 m, 1461 m, 1445 m, 1335 m, 1270 s, 1209 s, 1127 m, 1117 m, 1072 s, 1027 m, 893 m, 858 m, 830 s, 760 m, 714 m, 656 s.

5-hydroxypicolinaldehyde (4)



3 (4.50 g, 36 mmol) was dissolved in isopropanol (200 ml). Activated manganese dioxide (4.75 g, 90 mmol) was added and the reaction was heated at reflux (100°C) for 4 h, allowed to cool to ambient temperature and stirred for a further 18 h. The

reaction mixture was filtered through celite and the solvent was removed under reduced pressure. The resulting brown solid was dissolved in hot water (50 ml) and precipitated by cooling to 5°C, before being collected by filtration.

Yield 1.02 g, 23%.

^1H NMR (300 MHz, 298 K, DMSO) δ_{H} 11.11 (1H, br s, OH), 9.82 (1H, s, CHO), 8.31 (1H, d, $^4J_{\text{HH}} = 2.5$ Hz), 7.83 (1H, d, $3J_{\text{HH}} = 8.5$ Hz), 7.33 (1H, dd, $^3J_{\text{HH}} = 8.5$ Hz, $^4J_{\text{HH}} = 2.5$ Hz, Py), 3.37 (1H, br s, PyOH).

$^{13}\text{C}\{^1\text{H}\}$ NMR (105 MHz, 298 K, DMSO) δ_{C} 191.8 (CHO), 157.9, 144.7, 138.7, 123.6, 122.3 (Py).

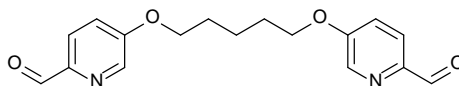
MS (ESI) m/z 124 $[\text{M}-\text{H}]^-$, 159 $[\text{M}+\text{Cl}]^-$

IR ν cm^{-1} 2506 w, 1694 m, 1597 w, 1567 s, 1471 w, 1311 m, 1273 m, 1209 s, 1115 s, 1024 m, 911 m, 871 m, 847 s, 790 s, 730 m, 660 s.

Elemental analysis found (calculated for $\text{C}_6\text{H}_5\text{NO}_2$) % C 58.59 (58.54), H 3.93 (4.09), N 11.30 (11.37).

5.3 Dipicolinaldehyde units

5,5'-(pentane-1,5-diylbis(oxy))dipicolinaldehyde⁴ (5)



4 (0.54 g, 4.4 mol) was dissolved in acetonitrile (50 ml). Potassium carbonate (0.64 g, 4.6 mol) followed by 1,5-dibromopentane (0.62 g, 2.7 mol) were added and the solution was stirred at reflux (80°C) for 16 h. The reaction mixture was filtered through a silica plug and the solvent was removed under reduced pressure. The crude product was dissolved in dichloromethane (50 ml), dried over sodium sulphate, filtered and the solvent was removed under reduced pressure to give a pale brown solid.

Yield 0.486 g, 71%.

¹H NMR (300 MHz, 298 K, CD₃CN) δ_H 9.88 (2H, s, CHO), 8.49 (2H, d, ⁴J_{HH} = 2.5 Hz), 7.91 (2H, d, ³J_{HH} = 8.0 Hz), 7.60 (2H, dd, ³J_{HH} = 8.5 Hz, ⁴J_{HH} = 2.5 Hz, Py), 4.21 (4H, t, ³J_{HH} = 6.5 Hz), 1.85 (4H, m), 1.61 (2H, m, CH₂).

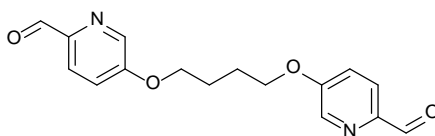
¹³C{¹H} NMR (75 MHz, 298 K, CD₃CN) δ_C 193.00 (CHO), 159.6, 145.3, 139.8, 124.1, 121.6 (Py), 69.6, 29.2, 21.1 (CH₂).

MS (ESI) m/z 315 [M+H]⁺, 337 [M+Na]⁺

IR ν cm⁻¹ 2950 w, 2839 w, 1694 s, 1572 s, 1496 m, 1469 s, 1395 m, 1370 w, 1311 s, 1256 s, 1209 s, 1132 s, 1109 m, 1067 m, 1030 s, 1013 m, 979 m, 925 m, 869 w, 829 s, 790 s, 758 m, 735 m, 663 m.

Elemental analysis found (calculated for $C_{17}H_{18}N_2O_4$) % C 64.48 (64.96), H 5.59 (5.77), N 8.91 (8.91).

5,5'-(butane-1,4-diylbis(oxy))dipicolinaldehyde (6)



6 was synthesised using the procedure described for **5**, substituting 1,5-dibromopentane for 1,4-dibromobutane.

Yield 0.512 g, 84%.

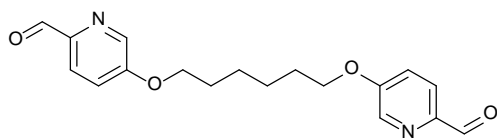
^1H NMR (300 MHz, 298 K, CDCl_3) δ_{H} 9.93 (2H, s, CHO), 8.37 (2H, d, $^3J_{\text{HH}} = 2.5$ Hz), 7.89 (2H, d, $^3J_{\text{HH}} = 9.0$ Hz), 7.26 (2H, dd, $^3J_{\text{HH}} = 9.0$ Hz, $^4J_{\text{HH}} = 2.5$ Hz, Ar), 4.15 (2H, m), 2.03 (4H, m, CH_2).

$^{13}\text{C}\{^1\text{H}\}$ NMR (75 MHz, 298 K, CDCl_3) δ_{C} 192.1 (CHO), 158.4, 146.4, 138.8, 123.53, 120.6 (Ar), 68.3, 25.8 (CH_2).

MS (ESI) m/z 301 $[\text{M}+\text{H}]^+$, 323 $[\text{M}+\text{Na}]^+$

IR ν cm^{-1} 2824 w, 1700 m, 1568 m, 1306 m, 1205 s, 964 m, 831 m, 604 s.

Elemental analysis found (calculated for $C_{16}H_{16}N_2O_4$) % C 62.48 (63.99), H 5.59 (5.37), N 8.99 (9.32) – incomplete combustion.

5,5'-(hexane-1,6-diylbis(oxy))dipicolinaldehyde (7)

7 was synthesised using the procedure described for **5**, substituting 1,5-dibromopentane for 1,6-dibromohexane.

Yield 0.406 g, 61%.

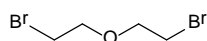
^1H NMR (300 MHz, 298 K, CDCl_3) δ_{H} 9.98 (2H, s, CHO), 8.41 (2H, d, $^3J_{\text{HH}} = 2.5$ Hz), 7.93 (2H, d, $^3J_{\text{HH}} = 8.0$ Hz), 7.26 (2H, dd, $^3J_{\text{HH}} = 9.0$ Hz, $^4J_{\text{HH}} = 2.5$ Hz, Py), 4.12 (4H, t, $^3J_{\text{HH}} = 6.0$ Hz), 1.90 (4H, m), 1.58 (4H, m, CH_2).

$^{13}\text{C}\{^1\text{H}\}$ NMR (75 MHz, 298 K, CDCl_3) δ_{C} 192.2 (CHO), 158.6, 146.4, 138.9, 123.54, 120.6 (Ar), 68.7, 29.0, 25.8 (CH_2).

MS (ESI) m/z 329 $[\text{M}+\text{H}]^+$, 351 $[\text{M}+\text{Na}]^+$

IR ν cm^{-1} 2951 w, 1700 m, 1567 s, 1315 s, 1208 m, 1011 m, 851 m, 656 s.

Elemental analysis found (calculated for $\text{C}_{18}\text{H}_{20}\text{N}_2\text{O}_4$) % C 64.72 (65.84), H 6.39 (6.14), N 8.46 (8.53) – incomplete combustion.

1-bromo-2-(2-bromoethoxy)ethane⁵ (8)

Triphenylphosphine (25 g, 94 mmol) was suspended in dry acetonitrile (20 ml) and cooled to 0°C using an ice-water bath. Bromine (5 ml, 94 mmol) was added dropwise followed by diethylene glycol (5 ml, 47 mmol). The reaction was stirred at reflux (80°C) for 18 h under argon. The solvent was removed under

reduced pressure and the residue was taken up in diethyl ether (150 ml). The solution was then filtered and the solvent was removed under reduced pressure to give the crude product as a yellow liquid. This was purified by Kugelrohr distillation to give a clear liquid (b.p. 95°C under high vacuum).

Yield 8.21 g, 76%.

^1H NMR (400 MHz, 298 K, CDCl_3) δ_{H} 3.83 (4H, t, $^3J_{\text{HH}} = 6.0$ Hz, 3.48 (4H, t, $^3J_{\text{HH}} = 6.0$ Hz, CH_2).

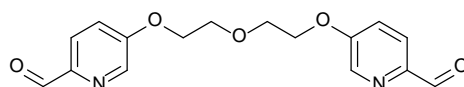
^{13}C -NMR (101 MHz, CDCl_3): δ 71.0, 30.2 (CH_2).

MS (ESI) m/z 233 $[\text{M}+\text{H}]^+$

IR ν cm^{-1} : 2966 w, 2856 w, 1739 m, 1438 w, 1421 m, 1361 w, 1279 m, 1226 w, 1111 s, 1030 m, 1005 m, 948 m, 726 m, 691 m, 663 m.

Elemental analysis found (calculated for $\text{C}_4\text{H}_8\text{Br}_2\text{O}$) % C 20.78 (20.72), H 3.49 (3.48).

5,5'-(2,2'-oxybis(ethane-2,1-diyl)bis(oxy))dipicolinaldehyde (**9**)



9 was synthesised using the procedure described for **5**, substituting 1,5-dibromopentane for **8**.

Yield 1.02 g, 75%.

^1H NMR (400 MHz, 298 K, CD_3CN): δ 9.99 (2H, s, CHO), 8.45 (2H, d, $^3J_{\text{HH}} = 2.5$ Hz), 7.96 (2H, d, $^3J_{\text{HH}} = 8.5$), 7.33 (2H, dd, $^3J_{\text{HH}} = 8.5$ Hz, $^4J_{\text{HH}} = 2.5$ Hz, Py), 4.30 (4H, t, $^3J_{\text{HH}} = 4.5$ Hz), 4.00 (4H, t, $^3J_{\text{HH}} = 4.5$ Hz, CH_2).

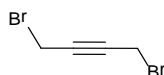
$^{13}\text{C}\{^1\text{H}\}$ NMR (75 MHz, 298 K, CD_3CN) δ 193.0 (CHO), 165.6, 163.6, 139.9, 124.1, 121.9 (Py), 70.1, 69.3 (CH_2).

MS (ESI) m/z 339 $[\text{M}+\text{Na}]^+$

IR ν cm^{-1} 3650 w, 2963 m, 1695 m, 1573 m, 1491 m, 1456 w, 1278 m, 1258 s, 1221 m, 1093 s, 1045 s, 1010 s, 947 m, 923 m, 842 m, 795 s, 765 m, 720 m, 696 m, 663 s.

Elemental analysis found (calculated for $\text{C}_{16}\text{H}_{16}\text{N}_2\text{O}_5$) % C 60.47 (60.76), H 5.05 (5.10), N 9.14 (8.85).

1,4-dibromobut-2-yne⁵ (10)



Triphenylphosphine was crystallised from hot toluene (250 ml) and dried *in vacuo*. at ambient temperature for 18 h. Triphenylphosphine (25 g, 95 mmol) was suspended in dry acetonitrile (20 ml) and cooled to 0°C using an ice-water bath. Bromine (5 ml, 93 mmol) was added dropwise followed by 2-butyne-1,4-diol (3.6 g, 46 mmol) in dry acetonitrile (10 ml). The reaction was stirred at ambient temperature for 18 h under argon. The solvent was removed under reduced pressure and the residue was taken up in diethyl ether (150 ml). The solution was then filtered and the solvent was removed under reduced pressure to give the crude product as a yellow liquid. This was purified by Kugelrohr distillation to give a clear liquid (b.p. 95°C under high vacuum).

Yield 1.04 g, 42%.

^1H NMR (300 MHz, 298 K, CDCl_3) δ_{H} 3.95 (4H, s, CH_2).

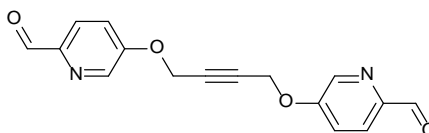
$^{13}\text{C}\{^1\text{H}\}$ NMR (75 MHz, 298 K, CDCl_3) δ_{C} 81.7, 14.0 (CH_2).

MS (ESI) m/z 212 $[\text{M}+\text{H}]^+$

IR ν cm^{-1} 2899 w, 1704 m, 1311 m, 1281 m, 998 m, 724 m, 601 s.

Elemental analysis found (calculated for $\text{C}_4\text{H}_4\text{Br}_2$) % C 85.22 (85.26), H 8.08 (8.11), N 6.64 (6.63).

5,5'-(but-2-yne-1,4-diylbis(oxy))dipicolinaldehyde (**11**)



11 was synthesised using the procedure described for **5**, substituting 1,5-dibromopentane for **10**.

Yield 0.208 g, 60 %.

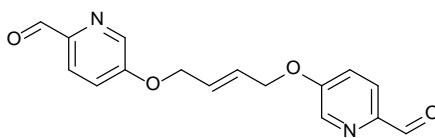
^1H NMR (400 MHz, 298 K, CD_3CN) δ_{H} 9.88 (2H, s, CHO), 8.40 (2H, d, $^3J_{\text{HH}} = 3.0$ Hz), 7.80 (2H, d, $^3J_{\text{HH}} = 8.5$ Hz), 7.40 (2H, dd, 1H, $^3J_{\text{HH}} = 8.5$ Hz, $^4J_{\text{HH}} = 3.0$ Hz, Py), 4.94 (4H, s, CH_2).

$^{13}\text{C}\{^1\text{H}\}$ NMR (101 MHz, 298 K, CD_3CN) δ_{C} 192.8 (CHO), 160.1, 139.8, 134.5, 123.6, 122.2 (Py), 69.4, 57.1 (CH_2).

MS (ESI) m/z 297 $[\text{M}+\text{H}]^+$, 319 $[\text{M}+\text{Na}]^+$

IR ν cm^{-1} 2854 w, 1699 m, 1568 s, 1307 m, 1199 s, 998 m, 824 m, 611 s.

Elemental analysis found (calculated for $\text{C}_{16}\text{H}_{12}\text{N}_2\text{O}_4$) % C 62.85 (64.86), H 3.95 (4.08), N 9.11 (9.45) – incomplete combustion.

(E)-5,5'-(but-2-ene-1,4-diylbis(oxy))dipicolinaldehyde (12)

12 was synthesised using the procedure described for **5**, substituting 1,5-dibromopentane for 1,4-trans-dibromobut-2-ene.

Yield 0.323 g, 53%.

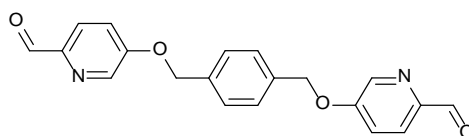
^1H NMR (300 MHz, 298 K, CD_3CN) δ_{C} 9.93 (2H, s, CHO), 8.46 (2H, d, $^3J_{\text{HH}} = 2.5$ Hz), 7.91 (2H, d, $^3J_{\text{HH}} = 8.0$ Hz), 7.47 (2H, dd, $^3J_{\text{HH}} = 8.0$ Hz, $^4J_{\text{HH}} = 2.5$ Hz, Py), 6.16 (2H, m CH), 4.80 (4H, m, CH_2).

$^{13}\text{C}\{^1\text{H}\}$ NMR (75 MHz, 298 K, CD_3CN) δ_{C} 193.0 (CHO), 165.4, 142.3, 140.0, 129.2, 124.1, 122.1 (Py), 69.1 (CH_2).

MS (ESI) m/z 321 $[\text{M}+\text{Na}]^+$

IR $\nu\text{ cm}^{-1}$ 2844 w, 1710 m, 1566 m, 1273 s, 1121 s, 803 m, 609 m.

Elemental analysis found (calculated for $\text{C}_{16}\text{H}_{14}\text{N}_2\text{O}_4$) % C 62.85 (64.42), H 4.59 (4.73), N 9.11 (9.39) – incomplete combustion.

5,5'-(1,4-phenylenebis(methylene))bis(oxy)dipicolinaldehyde (13)

13 was synthesised using the procedure described for **5**, substituting 1,5-dibromopentane for 1,4-bis(bromomethyl)benzene.

Yield 0.636 g, 90%.

^1H NMR (400 MHz, 298 K, CDCl_3) δ_{H} 9.76 (2H, s, CHO), 8.27 (2H, d, $^3J_{\text{HH}} = 3.0$ Hz), 7.72 (2H, d, $^3J_{\text{HH}} = 9.0$ Hz), 7.26 (2H, s), 7.14 (2H, dd, $^3J_{\text{HH}} = 8.5$ Hz, $^4J_{\text{HH}} = 2.5$ Hz), 7.03 (2H, s, Ar), 4.99 (4H, s, CH_2).

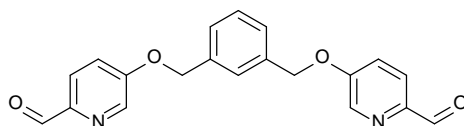
$^{13}\text{C}\{^1\text{H}\}$ NMR (101 MHz, 298 K, CDCl_3) δ_{C} 192.0 (CHO), 158.1, 146.6, 139.0, 135.7, 128.0, 123.3, 121.1 (Ar), 70.2 (OCH_2).

MS (ESI) m/z 371 $[\text{M}+\text{Na}]^+$

IR ν cm^{-1} 2821 w, 1698 m, 1569 s, 1312 m, 1206 s, 1010 m, 848 m, 602 m.

Elemental analysis found (calculated for $\text{C}_{20}\text{H}_{16}\text{N}_2\text{O}_4$) % C 67.85 (68.96), H, 4.67 (4.63), N 8.41 (8.04) – incomplete combustion.

5,5'-(1,3-phenylenebis(methylene))bis(oxy)dipicolinaldehyde (14)



^1H NMR (300 MHz, 298 K, CD_3CN) δ_{H} 9.69 (2H, s, CHO), 8.27 (2H, d, $^3J_{\text{HH}} = 2.5$ Hz), 7.68 (d, 2H, $^3J_{\text{HH}} = 8.5$ Hz), 7.38 (2H, s), 7.24 (4H, m, Ar), 5.05 (4H, s, CH_2).

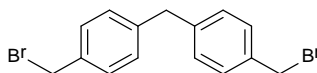
$^{13}\text{C}\{^1\text{H}\}$ NMR (75 MHz, 298 K, CD_3CN) δ_{C} 193.0 (CHO), 159.2, 142.6, 140.1, 137.6, 130.1, 128.9, 128.2, 124.1, 122.2 (Ar), 71.2 (OCH_2).

MS (ESI) m/z 347 $[\text{M}-\text{H}]^-$, 349 $[\text{M}+\text{H}]^+$, 371 $[\text{M}+\text{Na}]^+$, 383 $[\text{M}+\text{Cl}]^-$

IR ν cm^{-1} 3049 w, 2820 w, 1700 s, 1570 s, 1210 s, 1156 s, 1012 m, 838 m, 795 m, 616 m.

Elemental analysis found (calculated for $\text{C}_{20}\text{H}_{16}\text{N}_2\text{O}_4$) % C 68.45 (68.96), H 4.40 (4.63), N 8.23 (8.04).

bis(4-(bromomethyl)phenyl)methane⁶ (15)



Diphenylmethane (5.0 g, 30 mmol) was added to a solution of hydrobromic acid (40%, 80 ml) and acetic acid (20 ml) followed by 1,3,5-trioxane (5.0 g, 60 mmol) and tetradecyltrimethylammonium bromide (0.2 g, 0.48 mmol). The solution was stirred at reflux (125°C) for 16 h. After cooling to 0 °C in an ice bath a yellow precipitate formed which was collected and washed with water (50 ml). This was dissolved in dichloromethane (100 ml), washed with water (100 ml), dried over sodium sulphate and the solvent removed under reduced pressure. The desired product was collected upon crystallisation from hot dichloromethane.

Yield 1.48 g, 14%.

^1H NMR (400 MHz, 298 K, CDCl_3) δ_{H} 7.23 (4H, d, $^3J_{\text{HH}} = 7.5$ Hz), 7.09 4H, d, $^3J_{\text{HH}} = 7.5$ Hz, Ph), 4.41 (4H, s), 3.89 (2H, s, CH_2).

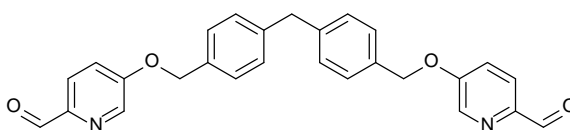
$^{13}\text{C}\{^1\text{H}\}$ NMR (101 MHz, 298 K, CDCl_3) δ_{C} 141.2, 135.9, 129.5, 129.4 (Ph), 41.5, 33.6 (CH_2).

MS (ESI) m/z 275 $[\text{M}-\text{Br}+\text{H}]^+$

IR ν cm^{-1} 2922 w, 1700 w, 1509 w, 1223 m, 734 m, 714 m, 692 m, 595 s.

Elemental analysis found (calculated for $\text{C}_{15}\text{H}_{14}\text{Br}_2$) % C 51.54 (50.88), H 3.96 (3.99).

5,5'-(4,4'-methylenebis(4,1-phenylene))bis(methylene))bis(oxy)dipicolinaldehyde (16)



16 was synthesised using the procedure described for **5**, substituting 1,5-dibromopentane for **15**.

Yield 0.510 g, 28%.

^1H NMR (400 MHz, 298 K, CD_3CN) δ_{H} 9.88 (2H, s, CHO), 8.45 (2H, d, $^3J_{\text{HH}} = 2.5$ Hz), 7.87 (2H, d, 2H, $^3J_{\text{HH}} = 8.0$ Hz), 7.46 (2H, dd, $^3J_{\text{HH}} = 9.0$ Hz, $^4J_{\text{HH}} = 3.5$ Hz), 7.36 (4H, d, $^3J_{\text{HH}} = 7.5$ Hz), 7.27 (4H, d, $^3J_{\text{HH}} = 7.5$ Hz, Ar), 5.18 (4H, s, CH_2O), 3.98 (2H, s, CH_2).

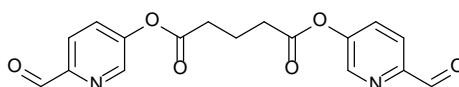
$^{13}\text{C}\{^1\text{H}\}$ NMR (75 MHz, 298 K, CD_3CN) δ_{C} 193.3 (CHO), 164.2, 159.7, 143.0, 140.4, 135.1, 130.3, 129.6, 124.4, 122.4 (Ar), 71.5 (OCH_2), 42.0 (CH_2).

MS (ESI) m/z 440 $[M+H]^+$, 463 $[M+Na]^+$.

IR ν cm^{-1} 2924 w, 2820 w, 1720 w, 1578 s, 1521 w, 1222 m, 795 m, 730 m, 713 m, 697 m.

Elemental analysis found (calculated for $\text{C}_{27}\text{H}_{22}\text{N}_2\text{O}_4$) % C 73.22 (73.96), H 4.90 (5.06), N 5.94 (6.39).

bis(6-formylpyridin-3-yl) glutarate (17)



Following a related literature method,⁷ **4** (1.0 g, 8.1 mmol) was dissolved in dry tetrahydrofuran (25 ml) under argon and cooled to 0 °C in an ice bath. Triethylamine (1.71 ml, 12.2 mmol) was added slowly, followed by glutaroyl chloride (0.52 ml, 0.69 g, 4.1 mmol). After warming to ambient temperature this was stirred for 3 h, diluted with ethyl acetate (20 ml) and quenched with saturated ammonium chloride solution (30 ml). The product was extracted into ethyl acetate (50 ml), washed with distilled water (100 ml) and brine (100 ml), dried over sodium sulfate and the solvent was removed under reduced pressure. The product was purified *via* column chromatography (hexane: ethyl acetate, 1:2) and the solvent was removed to yield the desired product; a yellow solid.

Yield 0.154 g, 6%.

^1H NMR (400 MHz, 298 K, CD_3CN) δ_{H} 9.80 (2H, s, CHO), 8.42 (2H, d, $^3J_{\text{HH}} = 2.5$ Hz), 7.80 (2H, d, $^3J_{\text{HH}} = 8.5$ Hz), 7.58 (2H, dd, $^3J_{\text{HH}} = 8.5$ Hz, $^4J_{\text{HH}} = 2.0$ Hz, Py), 2.62 (4H, t, $^3J_{\text{HH}} = 6.5$ Hz), 1.75 (2H, quin, $^3J_{\text{HH}} = 2.5$ Hz, CH_2).

$^{13}\text{C}\{^1\text{H}\}$ NMR (101 MHz, 298 K, CD_3CN) δ_{C} 192.9 (CHO), 171.7, 151.1, 144.8, 131.1, 123.1 (Ar), 117.9, (CO), 33.15, 19.86 (CH_2).

MS (ESI) m/z 365 $[\text{M}+\text{Na}]^+$

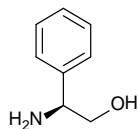
IR $\nu \text{ cm}^{-1}$ 2961 w, 1702 s, 1572 s, 1483 m, 1475 s, 1395 m, 1311 s, 1256 s, 1067 m, 1030 s, 925 m, 869 w, 735 m, 610 m.

Elemental analysis found (calculated for $\text{C}_{17}\text{H}_{14}\text{N}_2\text{O}_6$) % C 58.90 (59.65) H 4.77 (4.12) N 8.04 (8.18).

5.4 Phenylglycinol and derived ethers

5.4.1 Phenylglycinol⁸

(S)-phenylglycinol (18)



L-phenylglycine (20.0 g, 0.13 mol) was suspended in dry tetrahydrofuran (100 ml) under argon and added drop-wise to a stirred solution of lithium aluminium hydride (10.0 g, 0.26 mol) in dry tetrahydrofuran (100 ml) at 0°C. The suspension was allowed to warm to ambient temperature and then heated at reflux (70°C) for 16 h. After cooling to 0°C the reaction mixture was quenched by adding saturated potassium carbonate solution (250 ml) drop-wise. The solid was filtered off to give a yellow solution. The solvent was removed under reduced pressure to give a yellow solid, which upon recrystallisation from hot toluene gave a white crystalline solid.

Yield 9.09 g, 50%.

¹H NMR (400 MHz, 298 K, CDCl₃) δ_H 7.28 (5H, m, Ph), 3.95 (1H, dd, ³J_{HH} = 8.0 Hz, ⁴J_{HH} = 4.0 Hz, CH), 3.68 (1H, dd, ³J_{HH} = 10.5 Hz, ⁴J_{HH} = 4.0 Hz), 3.50 (1H, dd, ³J_{HH} = 10.5 Hz, ⁴J_{HH} = 8.0 Hz, CH₂), 2.09 (2H, s, NH₂).

¹³C{¹H} NMR (101 MHz, 298 K, CDCl₃) δ_C 142.8, 128.8, 127.6, 126.6 (Ph), 68.1 (CH₂), 57.5 (CH).

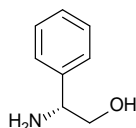
MS (ESI) m/z 120 [M-OH]⁺

IR ν cm⁻¹ 3327 w, 2831 s, 1598 m, 1250 m, 1062 m, 932 m, 750 m, 702 s, 554 m, 402 m.

Elemental analysis found (calculated for $C_8H_{11}NO$) % C 69.88 (70.04), H 8.12 (8.08), N 10.18 (10.21).

Optical Rotation $+24.99^\circ$ (6.652 g/100 ml MeOH).

(R)-phenylglycinol (19)



19 was synthesised using the procedure described for **18**, substituting L-phenylglycine for D-phenylglycine.

Yield 8.55 g, 47%.

1H NMR (300 MHz, 298 K, $CDCl_3$) δ_H 7.28 (5H, m, Ph), 3.97 (1H, dd, $^3J_{HH} = 8.0$ Hz, $^4J_{HH} = 4.5$ Hz, CH), 3.65 (1H, dd, $^3J_{HH} = 10.5$ Hz, $^4J_{HH} = 4.5$ Hz), 3.51 (1H, dd, $^3J_{HH} = 10.5$ Hz, $^4J_{HH} = 8.0$ Hz, CH_2).

$^{13}C\{^1H\}$ NMR (75 MHz, 298 K, $CDCl_3$) δ_C 142.5, 128.7, 127.6, 126.6 (Ph), 67.9 (CH_2), 57.5 (CH).

MS (ESI) m/z 120 $[M-OH]^+$

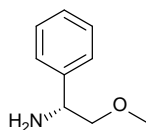
IR ν cm^{-1} 2835 m, 1604 m, 1497 m, 1453 m, 1361 w, 1197 w, 1077 m, 1047 m, 978 m, 882 m, 755 s, 700 s.

Elemental analysis found (calculated for $C_8H_{11}NO$) % C 69.65 (70.04), H 8.60 (8.06), N 10.14 (10.21).

Optical Rotation -25.99° (6.619 g/100 ml MeOH) [Lit. -25.8° (6.60 g/100 ml)]⁹

5.4.2 Phenylglycinol derived ethers

(*R*)-2-methoxy-1-phenylethanamine¹⁰ (**20**)



Following a literature method,¹⁰ **19** (2.0 g, 14.6 mmol) was dissolved in dry tetrahydrofuran under argon and added drop-wise to a suspension of sodium hydride (0.32 g, 16.0 mmol) in dry tetrahydrofuran, which was then stirred at ambient temperature for 1 h under reduced pressure. Iodomethane (2.1 g, 14.6 mmol) was added drop-wise and the solution was heated at reflux (65°C) under partial vacuum for 18 h. Brine (20 ml) was added after the solution had been cooled to ambient temperature. The product was extracted into dichloromethane (3 × 100 ml), dried over sodium sulphate and the solvent was removed under reduced pressure, taken up in diethyl ether (50 ml), filtered and the solvent was removed to give a yellow or brown oil, which was purified *via* Kügelrohr distillation at 70°C to give a clear oil.

Yield 1.38 g, 63%.

¹H NMR (300 MHz, 298 K, CDCl₃) δ_H 7.20 (5H, m, Ph), 4.12 (1H, dd, ³J_{HH} = 4.0 Hz, 9.0 Hz, CH), 3.43 (1H, dd, ²J_{HH} = 8.5 Hz, ³J_{HH} = 4.0 Hz, CH₂), 3.32-3.26 (4H, m, CH₂, CH₃), 1.67 (2H, s, NH₂).

¹³C{¹H} NMR (75 MHz, 298 K, CDCl₃) δ_C 142.6, 128.4, 127.4, 126.8 (Ph), 79.0 (CH₂), 58.9 (CH₃), 55.4 (CH).

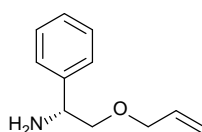
MS (ESI) *m/z* 135 [M-NH₂]⁺

IR ν cm^{-1} 3028 w, 2888 m, 1603 w, 1493 m, 1453 m, 1355 w, 1194 m, 1111 s, 968 m, 844 m, 758/700 s.

Elemental analysis found (calculated for $\text{C}_9\text{H}_{13}\text{NO}$) % C 70.98 (71.49), H 9.00 (8.67), N 9.39 (9.26).

Optical rotation -69.25° (3.03 g/ 100ml) [Lit. -34.04° (5.963 g/100 ml)]¹¹

(*R*)-2-(allyloxy)-1-phenylethanamine (21)



21 was synthesised using the procedure described for **20**, substituting iodomethane for 3-bromoprop-1-ene. Distilled under high vacuum at 110°C .

Yield 1.33 g, 52%.

^1H NMR (300 MHz, 298 K, CDCl_3) δ_{H} 7.21 (5H, m, Ph), 5.79 (1H, m, $\text{HC}=\text{C}$), 5.19 (1H, dd, $^3J_{\text{HH}} = 17.0$ Hz, $^4J_{\text{HH}} = 1.5$ Hz), 5.08 (1H, dd, $^3J_{\text{HH}} = 10.5$ Hz, $^3J_{\text{HH}} = 1.5$ Hz, $\text{H}_2\text{C}=\text{C}$), 4.08 (1H, dd, $^3J_{\text{HH}} = 9.5$ Hz, $^3J_{\text{HH}} = 3.0$ Hz, CH), 3.89 (2H, d, $^3J_{\text{HH}} = 5.5$ Hz), 3.44 (1H, dd, $^3J_{\text{HH}} = 9.5$ Hz, $^3J_{\text{HH}} = 3.5$ Hz, CH_2), 3.28 (1H, t, $^3J_{\text{HH}} = 9.5$ Hz, CH_2), 1.74 (2H, s, NH_2).

$^{13}\text{C}\{^1\text{H}\}$ NMR (101 MHz, 298 K, CDCl_3) δ_{C} 145.5, 137.0 (Ar), 134.7 (CH), 128.6, 127.9, 127.7, 127.0 (Ar), 117.3 (CH_2), 78.2, 75.5, (CH_2), 55.7 (CH).

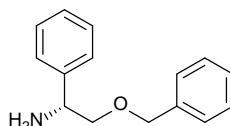
MS (ESI) m/z 178 $[\text{M}+\text{H}]^+$ 200 $[\text{M}+\text{Na}]^+$

IR ν cm^{-1} 3028 w, 2854 w, 1667 m, 1603 w, 1493 m, 1453 m, 1353 w, 1257 w, 1085 s, 1027 w, 991 m, 9212 m, 842 w, 758 s, 699 s.

Elemental analysis found (calculated for $C_{11}H_{15}NO$) % C 75.89 (74.54), H 8.83 (8.53), N 6.89 (7.90) – incomplete combustion.

Optical rotation -94.25 (4.733 g/100 ml)

(*R*)-2-(benzyloxy)-1-phenylethanamine¹² (22)



22 was synthesised using the procedure described for **20**, substituting iodomethane for (bromomethyl)benzene. Distilled under high vacuum 135 °C.

Yield 1.50 g, 47%.

1H NMR (300 MHz, 298 K, $CDCl_3$) δ_H 7.30 (10H, m, Ph), 4.49 (2H, s, CH_2), 4.16 (1H, dd, $^3J_{HH} = 9.5$ Hz, $^4J_{HH} = 4.0$ Hz, CH), 3.53 (1H, dd, $^3J_{HH} = 9.0$ Hz, $^4J_{HH} = 3.5$ Hz), 3.39 (1H, t, $^3J_{HH} = 8.0$ Hz, CH_2), 1.73 (2H, s, NH_2).

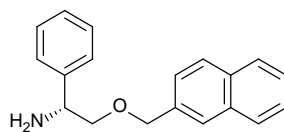
$^{13}C\{^1H\}$ NMR (75 MHz, 298, $CDCl_3$) δ_C 142.1, 137.8, 128.1, 127.4, 127.4, 127.1, 126.5 (Ar), 77.2, 73.0 (CH_2), 55.3 (CH).

MS (ESI) m/z 228 $[M+H]^+$, 250 $[M+Na]^+$

IR ν cm^{-1} 3028 w, 2856 w, 1603 w, 1494 m, 1452 m, 1356 w, 1205 w, 1090 s, 1075 s, 1027 m, 845 w, 735 m, 695 s.

Elemental analysis found (calculated for $C_{15}H_{17}NO$) % C 79.02 (79.26), H 7.65 (7.54), N 5.93 (6.16).

Optical rotation -55.09 (3.015 g/ 100ml) [Lit. -18.87° (3.02 g/100 ml)]¹¹

(R)-2-(naphthalen-2-ylmethoxy)-1-phenylethanamine (23)

23 was synthesised using the procedure described for **20**, substituting iodomethane for 2-(bromomethyl)naphthalene. Distilled under high vacuum at 140 °C.

Yield 0.209 g, 5.1%.

^1H NMR (300 MHz, 298 K, CDCl_3) δ_{H} 7.74 (4H, m), 7.40 (3H, m), 7.31 (5H, m, Ph), 4.65 (2H, s, OCH_2), 4.19 (1H, dd, $^3J_{\text{HH}} = 8.5$ Hz, $^4J_{\text{HH}} = 3.5$ Hz, Ch), 3.57 (1H, dd, $^3J_{\text{HH}} = 9.5$ Hz, $^4J_{\text{HH}} = 3.5$ Hz), 3.43 (1H, t, $^3J_{\text{HH}} = 8.5$ Hz, CH_2), 1.72 (2H, s, NH_2).

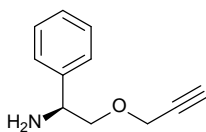
$^{13}\text{C}\{^1\text{H}\}$ NMR (101 MHz, 298 K, CDCl_3) δ_{C} 138.5, 133.5, 133.1, 128.8, 128.4, 128.0, 127.8, 127.7, 126.6, 126.3, 126.0, 125.5, 125.3 (Ar), 68.1, 65.5 (CH_2), 57.4 (CH).

MS (ESI) m/z 278 $[\text{M}+\text{H}]^+$, 300 $[\text{M}+\text{Na}]^+$

IR ν cm^{-1} 3056 w, 2856 w, 1682 w, 1634 w, 1601 m, 1508 w, 1493 w, 1452 m, 1352 m, 1269 w, 1170 w, 1123 m, 1085 s, 1026 m, 951 w, 891 w, 854 m, 814 m, 747 s, 698 s.

Elemental analysis found (calculated for $\text{C}_{19}\text{H}_{19}\text{NO}$) % C 78.67 (82.28), H 6.98 (6.90), N 5.05 (2.92) – incomplete combustion.

Optical rotation -22.24 (1/.194 g/ 100ml)

(S)-1-phenyl-2-(prop-2-ynyloxy)ethanamine¹¹ (24)

24 was synthesised using the procedure described for **20**, substituting iodomethane for 3-bromoprop-1-yne (80% in toluene) and (*R*)-phenylglycinol for (*S*)-phenylglycinol. Distilled under high vacuum at 110 °C.

Yield 1.03 g, 81%.

¹H NMR (400 MHz, 298 K, CDCl₃) δ_H 7.45-7.20 (5H, m, Ph), 4.26-4.16 (3H, m, CH, CH₂), 3.68 (1H, dd, ³J_{HH} = 9.0 Hz, ⁴J_{HH} = 4.0 Hz), 3.47 (1H, t, ³J_{HH} = 9.0 Hz, CH₂), 2.43 (1H, t, ⁴J_{HH} = 2.5 Hz, CH), 1.70 (2H, s, NH₂).

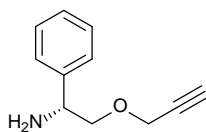
¹³C{¹H} NMR (101 MHz, 298 K, CDCl₃) δ_C 142.1, 128.3, 127.3, 126.7 (Ph), 79.4 (C), 74.4 (CH), 60.2, 58.3 (CH₂), 55.2 (CH).

MS (ESI) m/z 159 [M-NH₂]⁺, 176 [M+H]⁺

IR ν cm⁻¹ 3286 w, 2855 w, 1087 s, 861 m, 759 s, 699 s.

Elemental analysis found (calculated for C₁₁H₁₃NO) % C 74.92 (75.40), H 7.56 (7.48), N 7.92 (7.99).

Optical rotation +65.74° (3.10 g/ 100ml)

(R)-1-phenyl-2-(prop-2-ynyloxy)ethanamine (25)

25 was synthesised using the procedure described for **20**, substituting iodomethane for 3-bromoprop-1-yne (80% in toluene). Distilled under high vacuum at 110 °C.

Yield 0.37 g, 28%.

^1H NMR (400 MHz, 298 K, CDCl_3) δ_{H} 7.43-7.22 (5H, m, Ph), 4.25-4.17 (3H, m, CH, CH_2), 3.68 (1H, dd, $^3J_{\text{HH}} = 9.0$ Hz, $^4J_{\text{HH}} = 4.0$ Hz), 3.47 (1H, t, $^3J_{\text{HH}} = 9.0$ Hz, CH_2), 2.43 (1H, t, $^4J_{\text{HH}} = 2.5$ Hz, CH), 1.68 (2H, s, NH_2).

$^{13}\text{C}\{^1\text{H}\}$ NMR (101 MHz, 298 K, CDCl_3) δ_{C} 142.7, 128.5, 127.5, 126.8 (Ph), 79.6 (C), 74.6 (CH), 60.4, 58.4 (CH_2), 55.4 (CH).

MS (ESI) m/z 159 $[\text{M}-\text{NH}_2]^+$, 176 $[\text{M}+\text{H}]^+$

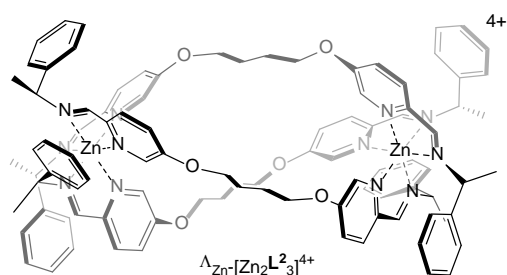
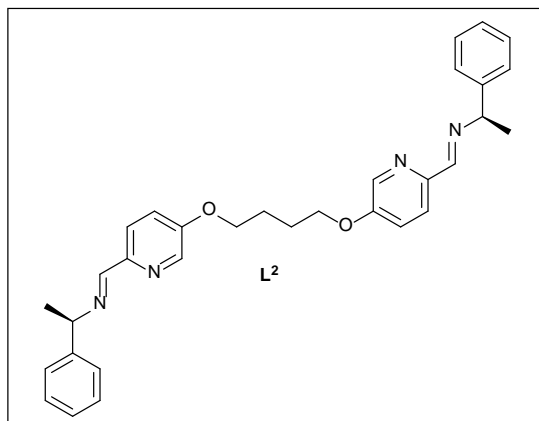
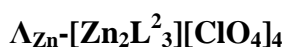
IR ν cm^{-1} 3285 w, 2855 w, 1088 s, 859 m, 759 s, 699 s.

Elemental analysis found (calculated for $\text{C}_{11}\text{H}_{13}\text{NO}$) % C 74.82 (75.40), H 7.60 (7.48), N 7.81 (7.99).

Optical rotation -81.60° (3.12 g/ 100ml) [Lit. -32.11° (6.08 g/100 ml)]¹¹

5.5 Functionalised flexicates

5.5.1 $[\text{Zn}_2\text{L}^{2-10}_3][\text{ClO}_4]_4$



6 (0.13 g, 0.44 mmol) and (*R*)-1-phenylethan-1-amine (0.11 g, 0.88 mmol) were stirred in acetonitrile (10 ml) for 1 h. Zinc (II) perchlorate hexahydrate (0.11 g, 0.29 mmol) was added and the solution was stirred at ambient temperature for 20 h ethyl acetate was added drop-wise to cause precipitation of a white crystalline solid.

Yield 0.192 g, 64%.

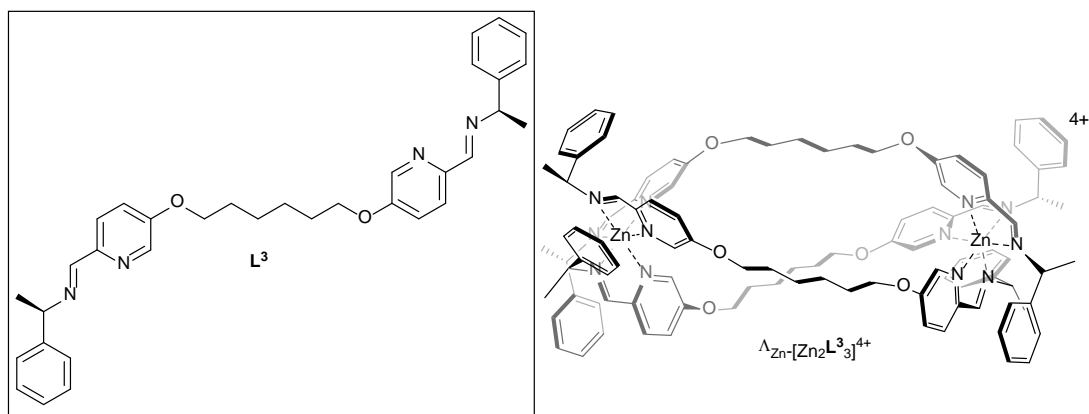
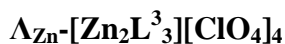
^1H NMR (400 MHz, 298 K, CD_3CN) δ_{H} 8.09 (6H, s, CHN), 7.51 (6H, dd, $^3J_{\text{HH}} = 8.5$ Hz, $^4J_{\text{HH}} = 3.0$ Hz), 7.39 (6H, d, $^3J_{\text{HH}} = 8.5$ Hz), 7.09 (12H, m), 6.98 (12H, t, $^3J_{\text{HH}} = 8.0$ Hz), 6.67 (12H, d, $^3J_{\text{HH}} = 7.0$ Hz, Ar), 5.40 (6H, q, $^3J_{\text{HH}} = 6.5$ Hz, CH), 4.17 (6H, m), 4.09 (6H, m), 1.90 (12H, m, CH_2), 1.62 (18H, d, $^3J_{\text{HH}} = 5.5$ Hz, CH_3).

$^{13}\text{C}\{^1\text{H}\}$ NMR (101 MHz, 298 K, CD_3CN) δ_{C} 161.8 (CHN), 160.2, 156.1, 142.0, 139.6, 139.6, 132.4, 129.7, 128.5, 126.4, 122.5 (Ar), 69.9 (CH_2), 64.7 (CH), 26.1 (CH_2), 23.6 (CH_3).

MS (ESI) m/z 413 $[\text{Zn}_2\text{L}_3]^{4+}$, 507 $[\text{L}+\text{H}]^+$, 529 $[\text{L}+\text{Na}]^+$

IR ν cm^{-1} 2936 w, 1641 m, 1262 m, 1081 s, 702 m, 621 s.

Elemental analysis found (calculated for $\text{C}_{96}\text{H}_{102}\text{Cl}_4\text{N}_{12}\text{O}_{22}\text{Zn}_2$) % C 54.02 (54.38), H 4.79 (5.23), N 7.81 (7.93).



$\Lambda_{\text{Zn}}\text{-}[\text{Zn}_2\text{L}^3][\text{ClO}_4]_4$ was synthesised using the procedure described for $\Lambda_{\text{Zn}}\text{-}[\text{Zn}_2\text{L}^2][\text{ClO}_4]_4$, substituting **6** for **7**.

Yield 0.145 g, 41%.

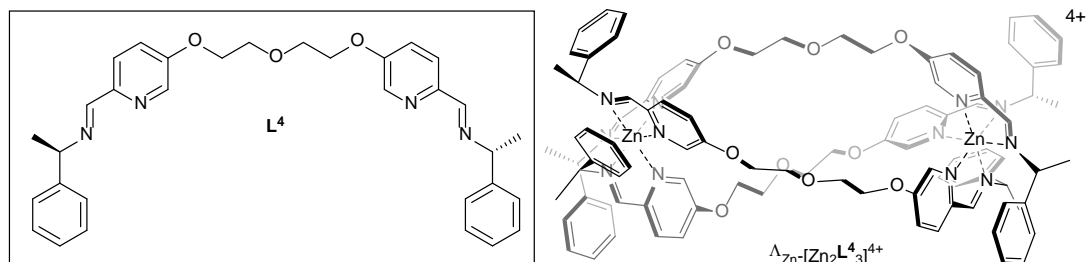
^1H NMR (300 MHz, CD_3CN) δ 8.09 (6H, s, CHN), 7.50 (6H, dd, $^3J_{\text{HH}} = 8.5$ Hz, $^4J_{\text{HH}} = 2.5$ Hz), 7.38 (6H, d, $^3J_{\text{HH}} = 8.5$ Hz), 7.17-7.06 (12H, m), 6.97 (12H, t, $^3J_{\text{HH}} = 7.5$ Hz), 6.67 (12H, d, $^3J_{\text{HH}} = 7.5$ Hz, Ar), 5.41 (6H, q, $^3J_{\text{HH}} = 6.5$ Hz, CH), 4.20-3.96 (12H, m), 1.68 (12H, m, CH_2), 1.61 (18H, d, $^3J_{\text{HH}} = 6.5$ Hz), 1.53-1.39 (12H, m, CH_2).

$^{13}\text{C}\{^1\text{H}\}$ NMR (75 MHz, CD_3CN) δ_{C} 165.43 (CHN), 165.4, 161.8, 139.6, 139.5, 132.4, 132.2, 129.6, 128.5, 126.4, 122.7 (Ar), 74.2, 70.3 (CH_2), 64.7 (CH), 45.4 (CH_2), 30.9 (CH_3).

MS (ESI) m/z 432 $[\text{Zn}_2\text{L}_3]^{4+}$, 535 $[\text{L}+\text{H}]^+$, 557 $[\text{L}+\text{Na}]^+$

IR cm^{-1} 2936 w, 1591 w, 1227 w, 1082 m, 702 w, 621 w.

Elemental analysis found (calculated for $\text{C}_{102}\text{H}_{114}\text{Cl}_4\text{N}_{12}\text{O}_{22}\text{Zn}_2$) % C 55.22 (55.57), H 5.13 (5.58), N 7.49 (7.62).



$\Lambda_{\text{Zn}}\text{-}[\text{Zn}_2\text{L}^4][\text{ClO}_4]_4$ was synthesised using the procedure described for $\Lambda_{\text{Zn}}\text{-}[\text{Zn}_2\text{L}^2][\text{ClO}_4]_4$, substituting **6** for **9**.

Yield 0.390 g, 75%.

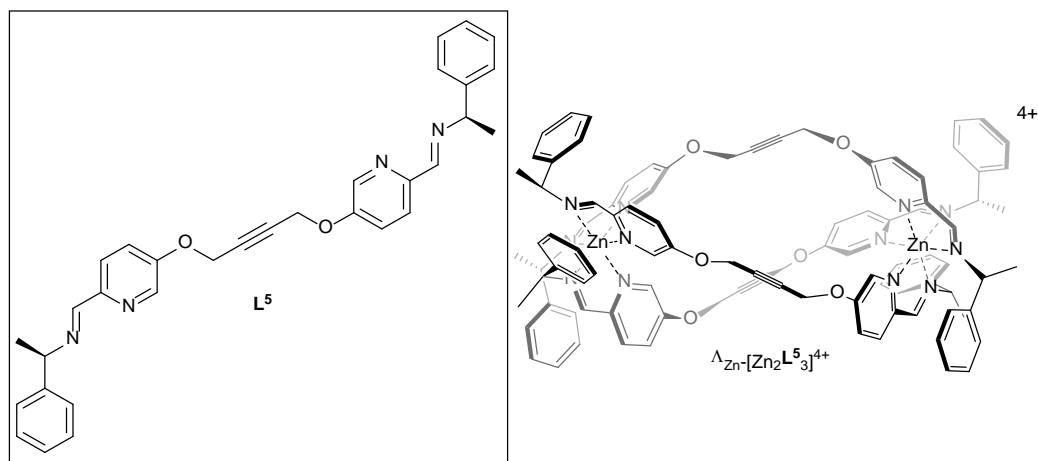
^1H NMR (400 MHz, 298 K, CD_3CN) δ_{H} 8.09 (6H, s, CHN), 7.49 (6H, dd, $^3J_{\text{HH}} = 8.5$ Hz, $^4J_{\text{HH}} = 2.5$ Hz), 7.41 (6H, d, $^3J_{\text{HH}} = 8.5$ Hz), 7.06 (6H, t, $^3J_{\text{HH}} = 7.5$ Hz), 6.96 (12H, t, $^3J_{\text{HH}} = 7.5$ Hz), 6.91 (6H, d, $^4J_{\text{HH}} = 2.5$ Hz), 6.67 (12H, d, $^3J_{\text{HH}} = 7.5$ Hz, Ar), 5.35 (6H, q, $^3J_{\text{HH}} = 6.5$ Hz, CH), 4.11-4.01 (12H, m), 3.85-3.74 (12H, m, OCH_2), 1.57 (18H, d, $^3J_{\text{HH}} = 6.5$ Hz, CH_3).

$^{13}\text{C}\{^1\text{H}\}$ NMR (101 MHz, 298 K, CD_3CN) δ_{C} 161.6 (CHN), 156.0, 157.8, 154.2, 143.9, 138.2, 132.1, 129.6, 128.6, 126.6, 124.5 (Ar), 70.1, 70.0 (CH_2), 64.8 (CH), 23.7 (CH_3).

MS (ESI) m/z 523 $[\text{L}+\text{H}]^+$, 545 $[\text{L}+\text{Na}]^+$

IR v cm^{-1} 2935 w, 1570 m, 1267 m, 1082 s, 651 w, 622 m.

Elemental analysis found (calculated for $C_{106}H_{102}Cl_4N_{12}O_{25}Zn_2 \cdot 6H_2O$) % C (51.54), H 4.74 (5.21), N 7.33 (7.62).



$\Lambda_{Zn}-[Zn_2L^5_3][ClO_4]_4$ was synthesised using the procedure described for $\Lambda_{Zn}-[Zn_2L^2_3][ClO_4]_4$, substituting **6** for **11**.

Yield 0.152 g, 35%.

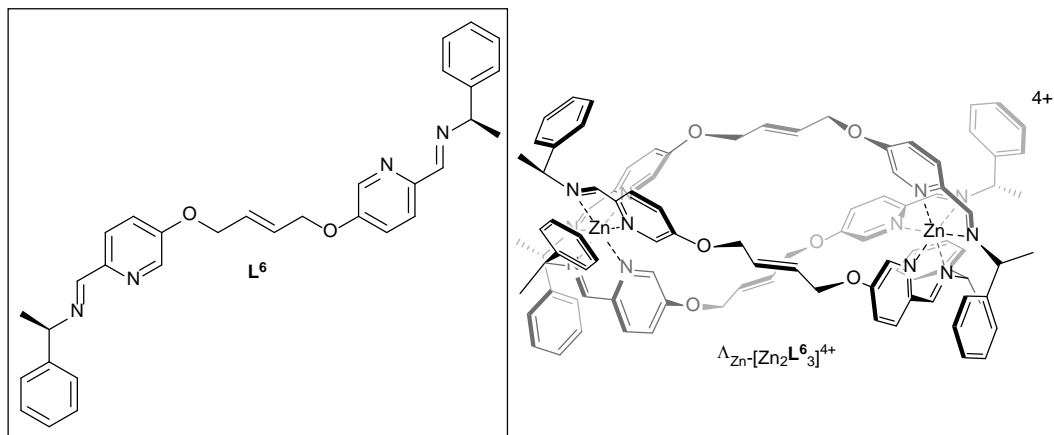
1H NMR (400 MHz, 298 K, CD_3CN) δ_H 8.05 (6H, s, CHN), 7.48 (6H, dd, $^3J_{HH} = 8.0$ Hz, $^4J_{HH} = 2.5$ Hz), 7.40 (6H, dd, $^3J_{HH} = 8.0$ Hz, $^4J_{HH} = 2.5$ Hz), 7.08 (6H, t, $^3J_{HH} = 7.0$ Hz), 7.04 (6H, d, $^3J_{HH} = 2.5$ Hz), 6.94 (12H, t, $^3J_{HH} = 8.0$ Hz), 6.65 (12H, d, $^3J_{HH} = 7.0$ Hz, Ar), 5.39 (6H, q, $^3J_{HH} = 6.0$ Hz, CH), 4.88 (12H, s, CH_2), 1.58 (18H, d, $^3J_{HH} = 6.0$ Hz, CH_3).

$^{13}C\{^1H\}$ NMR (101 MHz, 298 K, CD_3CN) δ_C 161.7 (CHN), 142.0, 140.4, 140.1, 139.7, 132.3, 129.7, 128.6, 126.6, 123.1 (Ar), 82.7 (C) 64.9 (CH), 58.5 (CH_2), 23.6 (CH_3).

MS (ESI) m/z 410 $[Zn_2L_3]^{4+}$.

IR ν cm^{-1} 2971 m, 1567 w, 1225 m, 1076 s, 621 m.

Elemental analysis found (calculated for $C_{96}H_{90}Cl_4N_{12}O_{22}Zn_2 \cdot 6H_2O$) % C 53.56 (53.77), H 4.28 (4.79), N 7.72 (7.84).



$\Lambda_{Zn}-[Zn_2L^6_3][ClO_4]_4$ was synthesised using the procedure described for $\Lambda_{Zn}-[Zn_2L^2_3][ClO_4]_4$, substituting **6** for **12**.

Yield 0.214 g, 57%.

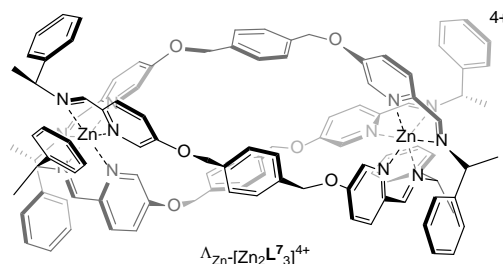
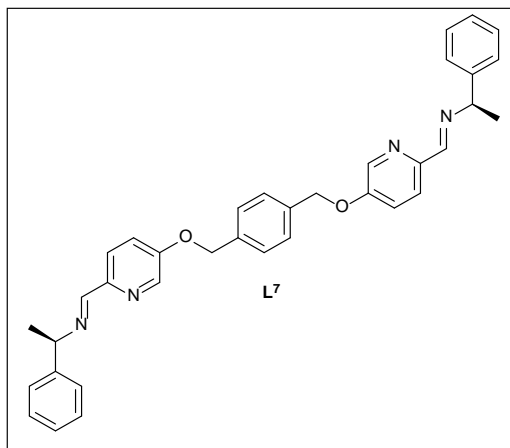
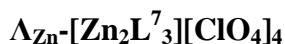
1H NMR (400 MHz, 298 K, CD_3CN) δ_H 8.06 (6H, s, CHN), 7.49 (6H, dd, $^3J_{HH} = 8.5$ Hz, $^4J_{HH} = 3.5$ Hz), 7.36 (6H, d, $^3J_{HH} = 8.5$ Hz), 7.14 (6H, d, $^3J_{HH} = 3.5$ Hz), 7.09 (6H, t, $^3J_{HH} = 8.0$ Hz), 6.95 (12H, t, $^3J_{HH} = 7.5$ Hz), 6.64 (12H, d, $^3J_{HH} = 7.0$ Hz, Ar), 6.12 (6H, m), 5.38 (6H, q, $^3J_{HH} = 6.5$ Hz, CH), 4.64 (12H, s, CH_2), 1.61 (18H, d, $^3J_{HH} = 6.5$ Hz).

$^{13}C\{^1H\}$ NMR (101 MHz, 298 K, CD_3CN) δ_C 161.8 (CHN), 159.6, 142.0, 139.9, 139.4, 132.3 (Ar), 129.7 (CH), 129.4, 128.5, 126.4, 122.7 (Ar), 69.7 (CH_2), 64.7 (CH), 23.6 (CH_3).

MS (ESI) m/z 411 $[Zn_2L_3]^{4+}$.

IR ν cm^{-1} 2976 w, 1570 m, 1316 m, 1225 m, 1082 s, 762 w, 703 m, 653 m.

Elemental analysis found (calculated for $\text{C}_{96}\text{H}_{96}\text{Cl}_4\text{N}_{12}\text{O}_{22}\text{Zn}_2 \cdot 10\text{H}_2\text{O}$) % C 51.08 (51.88), H 4.82 (5.26), N 7.38 (7.56).



$\Lambda_{\text{Zn}}\text{-}[\text{Zn}_2\text{L}^7_3][\text{ClO}_4]_4$ was synthesised using the procedure described for $\Lambda_{\text{Zn}}\text{-}[\text{Zn}_2\text{L}^2_3][\text{ClO}_4]_4$, substituting **6** for **13**.

Yield 0.051 g, 24%.

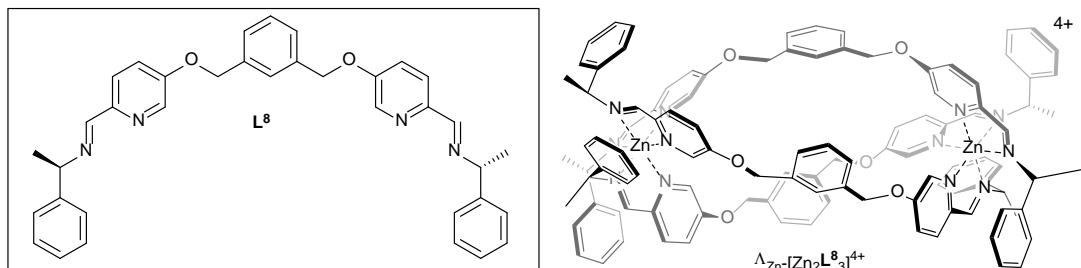
^1H NMR (400 MHz, , 298 K, CD_3CN) δ_{H} 8.15 (6H, s, CHN), 7.65 (6H, dd, $^3J_{\text{HH}} = 8.5$ Hz, $^4J_{\text{HH}} = 3.0$ Hz), 7.47 (24H, s), 7.44 (6H, d, $^3J_{\text{HH}} = 8.5$ Hz), 7.31 (6H, d, $^3J_{\text{HH}} = 2.5$ Hz), 7.16 (6H, t, $^3J_{\text{HH}} = 2.5$ Hz), 7.03 (12H, t, $^3J_{\text{HH}} = 7.5$ Hz), 6.71 (12H, d, $^3J_{\text{HH}} = 8.0$ Hz, Ar), 5.46 (6H, q, $^3J_{\text{HH}} = 6.5$ Hz, CH), 1.67 (18H, d, $^3J_{\text{HH}} = 7.0$ Hz, CH_3).

$^{13}\text{C}\{^1\text{H}\}$ NMR (101 MHz, 298 K, CD_3CN) δ_{C} 162.0 (CHN), 160.6, 142.5, 140.5, 138.5, 137.0, 132.5, 130.9, 129.6, 129.0, 128.5, 126.3, 125.3 (Ar), 72.9 (CH_2), 65.3 (CH_3), 24.8 (CH).

MS (ESI) m/z 502 $[\text{L}+\text{H}]^+$, 409 $[\text{Zn}_2\text{L}_3]^{4+}$.

IR ν cm^{-1} 2974 w, 1569 m, 1224 m, 1083 s, 702 m, 651 m.

Elemental analysis found (calculated for $C_{108}H_{102}Cl_4N_{12}O_{22}Zn_2 \cdot 4H_2O$) % C 56.79 (57.28), H 4.30 (4.90), N 7.30 (7.40).



$\Lambda_{Zn}-[Zn_2L^8_3][ClO_4]_4$ was synthesised using the procedure described for $\Lambda_{Zn}-[Zn_2L^2_3][ClO_4]_4$, substituting **6** for **14**.

Yield 0.220 g, 53%.

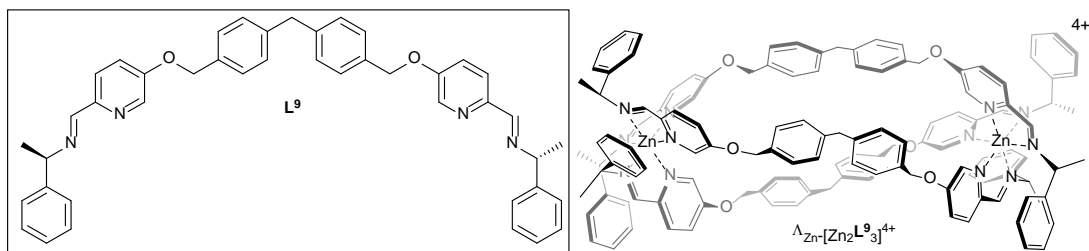
1H NMR (400 MHz, 298 K, CD_3CN) δ_H 8.13 (6H, s, CHN), 7.65 (6H, dd, $^3J_{HH} = 9.0$ Hz, $^4J_{HH} = 3.0$ Hz), 7.54 (6H, s), 7.48 (18H, m), 7.16 (6H, t, $^3J_{HH} = 7.0$ Hz), 7.02 (12H, m), 6.73 (12H, d, $^3J_{HH} = 7.0$ Hz, Ar), 5.41 (6H, q, $^3J_{HH} = 7.0$ Hz, CH), 5.23 (6H, m), 5.09 (6H, m, CH_2), 1.62 (18H, d, $^3J_{HH} = 7.0$ Hz, CH_3).

$^{13}C\{^1H\}$ NMR (101 MHz, 298 K, CD_3CN) δ_c 161.8 (CHN), 160.3, 142.25, 140.4, 138.3, 137.0, 132.5, 130.9, 129.9, 129.8, 128.8, 126.8, 125.0 (Ar), 72.0 (CH_2), 65.1 (CH_3), 24.0 (CH).

MS (ESI) m/z 502 $[L+H]^+$, 409 $[Zn_2L_3]^{4+}$.

IR ν cm^{-1} 2972 w, 1569 m, 1225 m, 1083 s, 702 m, 622 m.

Elemental analysis found (calculated for $C_{108}H_{102}Cl_4N_{12}O_{22}Zn_2 \cdot 4H_2O$) % C 56.77 (57.28), H 4.41 (4.90), N 7.32 (7.40).



$\Lambda_{\text{Zn}}\text{-}[\text{Zn}_2\text{L}^9][\text{ClO}_4]_4$ was synthesised using the procedure described for $\Lambda_{\text{Zn}}\text{-}[\text{Zn}_2\text{L}^2][\text{ClO}_4]_4$, substituting **6** for **16**.

Yield 0.124 g, 27%.

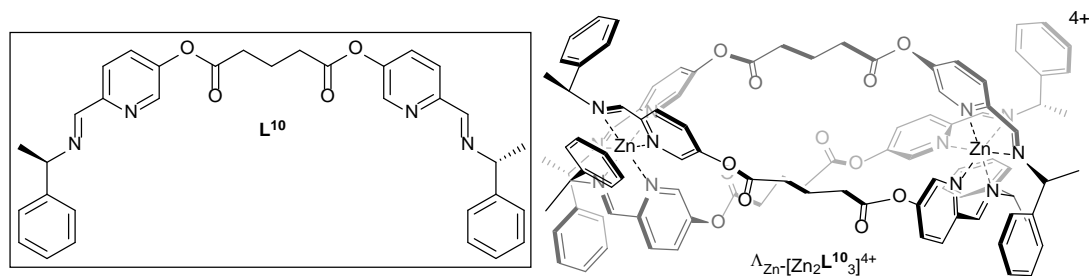
^1H NMR (400 MHz, 298 K, CD_3CN) δ_{H} 8.12 (6H, s, CHN), 7.58 (6H, dd, $^3J_{\text{HH}} = 8.5$ Hz, $^4J_{\text{HH}} = 3.0$ Hz), 7.45 (12H, d, $^3J_{\text{HH}} = 9.0$ Hz), 7.26 (18H, d, $^3J_{\text{HH}} = 8.5$ Hz), 7.14 (30H, m), 7.01 (24H, t, $^3J_{\text{HH}} = 8.5$ Hz), 6.70 (12H, d, $^3J_{\text{HH}} = 8.0$ Hz, Ar), 5.39 (6H, q, $^3J_{\text{HH}} = 6.0$ Hz, CH), 5.01 (6H, d, $^3J_{\text{HH}} = 8.5$ Hz), 4.96 (6H, d, $^3J_{\text{HH}} = 8.5$ Hz), 3.96 (6H, s, CH_2), 1.53 (18H, t, $^3J_{\text{HH}} = 8.5$ Hz, CH_3).

$^{13}\text{C}\{^1\text{H}\}$ NMR (101 MHz, 298 K, CD_3CN) δ_{C} 161.6 (CHN), 159.7, 141.8, 139.8, 138.8, 133.7, 132.1, 129.9, 129.6, 129.5, 128.4, 126.4, 124.0, 118.1 (Ar), 71.8, 64.7 (CH_2), 23.3 (CH), 1.3 (CH_3).

MS (ESI) m/z 517 $[\text{ZnL}_3]^{4+}$

IR ν cm^{-1} 2974 m, 1569 m, 1226 m, 1084 s, 702 m, 622 m.

Elemental analysis found (calculated for $\text{C}_{129}\text{H}_{120}\text{Cl}_4\text{N}_{12}\text{O}_{22}\text{Zn}_2 \cdot 13\text{H}_2\text{O}$) % C 57.12 (57.44), H 5.44 (5.46), N 6.31 (6.23).



$\Lambda_{\text{Zn}}\text{-}[\text{Zn}_2\text{L}^{10}_3][\text{ClO}_4]_4$ was synthesised using the procedure described for $\Lambda_{\text{Zn}}\text{-}[\text{Zn}_2\text{L}^2_3][\text{ClO}_4]_4$, substituting **6** for **17**.

Yield 0.13 g, 64%.

^1H NMR (400 MHz, 298 K, CD_3CN) δ_{H} 8.28 (6H, s, CHN), 7.79 (6H, dd, $^3J_{\text{HH}} = 8.0$ Hz, $^4J_{\text{HH}} = 2.5$ Hz), 7.54 (6H, d, $^3J_{\text{HH}} = 9.0$ Hz), 7.39 (6H, d, $^3J_{\text{HH}} = 2.5$ Hz), 7.14 (6H, t, $^3J_{\text{HH}} = 7.5$ Hz), 7.00 (12H, t, $^3J_{\text{HH}} = 8.0$ Hz), 6.69 (12H, d, $^3J_{\text{HH}} = 7.5$ Hz, Ar), 5.49 (6H, q, $^3J_{\text{HH}} = 6.5$ Hz, CH), 2.55 (12H, m), 1.91 (6H, m, CH_2), 1.66 (18H, d, $^3J_{\text{HH}} = 6.0$ Hz, CH_3).

$^{13}\text{C}\{^1\text{H}\}$ NMR (101 MHz, 298 K, CD_3CN) δ_{C} 160.9 (CHN), 156.0, 155.8, 154.2 (Ar), 140.4 (CO), 138.7, 132.1, 120.2, 128.7, 126.9, 121.4 (Ar), 70.5, 70.8 (CH_2), 64.1 (CH), 25.0 (CH_3).

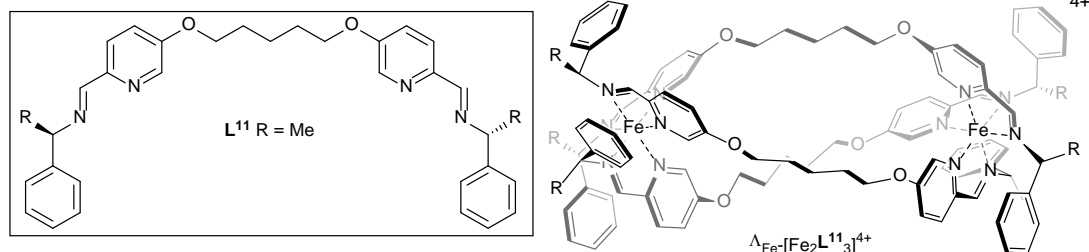
MS (ESI) m/z 444 $[\text{Zn}_2\text{L}_3]^{4+}$

IR ν cm^{-1} 2980 m, 1748 s, 1566 m, 1384 m, 1005 s, 811 m, 645 m.

Elemental analysis found (calculated for $\text{C}_{99}\text{H}_{96}\text{Cl}_4\text{N}_{12}\text{O}_{28}\text{Zn}_2\cdot 4\text{H}_2\text{O}$) % C 52.12 (52.93), H 5.01 (4.67), N 7.73 (7.48).

5.5.2 $[\text{Fe}_2\text{L}^{11-20}_3][\text{ClO}_4]_4^{13}$

$\Lambda_{\text{Fe}^-}[\text{Fe}_2\text{L}^{11}_3][\text{ClO}_4]_4 \cdot 4\text{H}_2\text{O}$



5 (0.10 g, 0.32 mmol) and (*R*)-1-phenylpropan-1-amine (0.09 g, 0.64 mmol) were dissolved in acetonitrile (10 ml). Iron (II) perchlorate hexahydrate (0.08 g, 0.21 mmol) was added and an immediate colour change to deep magenta was seen. The solution was heated at reflux (80°C) for 20 h and after cooling to ambient temperature ethyl acetate was added drop-wise to cause precipitation of a dark purple crystalline solid.

Yield 0.116 g, 49%.

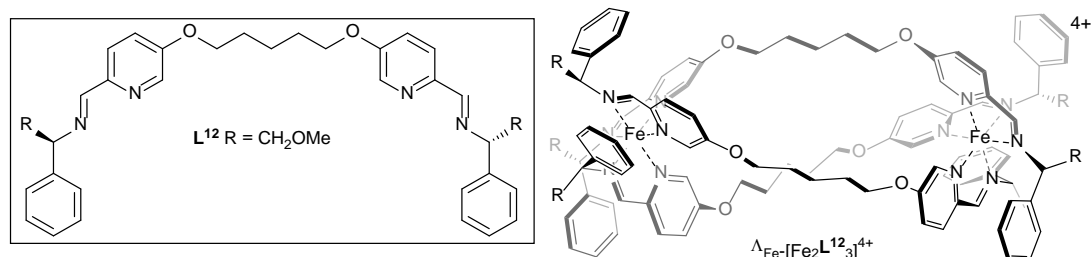
^1H NMR (300 MHz, 298 K, CD_3CN) δ_{H} 8.68 (6H, s, CHN), 7.40 (6H, d, $^3J_{\text{HH}} = 8.5$ Hz), 7.18 (6H, dd, $^3J_{\text{HH}} = 8.5$ Hz, $^4J_{\text{HH}} = 3.0$ Hz), 7.11 (6H, t, $^3J_{\text{HH}} = 7.0$ Hz), 7.02 (12H, t, $^3J_{\text{HH}} = 7.0$ Hz), 6.67 (12H, d, $^3J_{\text{HH}} = 7.0$ Hz), 6.03 (6H, d, $^4J_{\text{HH}} = 3.0$ Hz, Ar), 4.63 (6H, d, $^3J_{\text{HH}} = 11.5$ Hz), 3.88 (6H, m, CH), 3.71 (6H, m, CH_2), 1.65 (12H, m), 1.30 (6H, m), 0.92 (18H, t, $^3J_{\text{HH}} = 7.0$ Hz, CH_2), 0.83 (12H, t, $^3J_{\text{HH}} = 8.0$ Hz, CH_3).

$^{13}\text{C}\{^1\text{H}\}$ NMR (75 MHz, 298 K, CD_3CN) δ_{C} 170.4 (CHN), 156.3, 150.6, 143.7, 135.2, 130.3, 128.7, 127.1, 126.0, 121.2 (Ar), 72.0, 71.7 (CH_2), 69.6 (CH), 56.11 (CH_3), 26.31, 22.91 (CH_2).

MS (ESI) m/z 439.5 $[\text{Fe}_2\text{L}_3]^{4+}$

IR ν cm^{-1} 2969 m, 1559 m, 1496 w, 1240 m, 1081 s, 703 m, 622 m.

Elemental analysis found (calculated for $C_{105}H_{120}Cl_4Fe_2N_{12}O_{22} \cdot 4H_2O$) % C 45.35 (56.61), H 4.49 (5.79), N 5.85 (7.55) incomplete combustion.



$\Delta_{Fe}-[Fe_2L^{12}_3][ClO_4]_4$ was synthesised using the procedure described for $\Lambda_{Fe}-[Fe_2L^{11}_3][ClO_4]_4$, substituting (*R*)-1-phenylpropan-1-amine for **20**.

Yield 0.258 g, 70%.

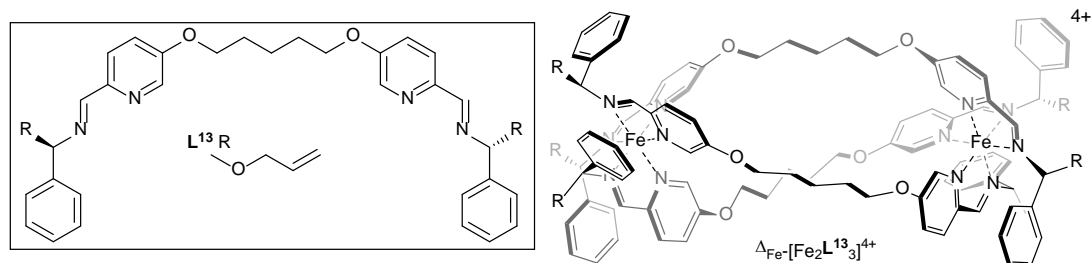
1H NMR (400 MHz, 298 K, CD_3CN) δ_H 8.75 (6H, s, CHN), 7.30 (6H, d, $^3J_{HH} = 8.0$ Hz), 7.07 (12H, d, $^3J_{HH} = 8.0$ Hz), 6.99 (12H, t, $^3J_{HH} = 7.0$ Hz), 6.73 (12H, d, $^3J_{HH} = 8.0$ Hz), 6.18 (6H, d, $^3J_{HH} = 2.5$ Hz Ar), 5.61 (6H, dd, $^3J_{HH} = 10.5$ Hz, $^4J_{HH} = 3.0$ Hz, CH_2), 4.16 (6H, t, $^3J_{HH} = 12.0$ Hz, CH), 3.83 (6H, m), 3.71 (6H, m), 3.46 (6H, dd, $^3J_{HH} = 11.0$ Hz, $^4J_{HH} = 3.0$ Hz, CH_2), 3.26 (12H, s, CH_3), 1.70 (12H, m), 1.31 (6H, m, CH_2).

$^{13}C\{^1H\}$ NMR (105 MHz, 298 K, CD_3CN) δ_C 169.8 (CHN), 159.6, 158.9, 152.2, 143.4, 133.0, 130.7, 126.8, 122.0, 115.2 (Ar), 70.6 (CH_2), 58.6, 56.1 (CH_3), 29.4, 26.3, 22.91 (CH_2).

MS (ESI) m/z 603 $[L+Na]^+$, 735 $[Fe_2L_2(ClO_4)_2]^{2+}/[FeL(ClO_4)]^+$

IR ν cm^{-1} 2939 w, 2169 w, 1592 w, 1558 m, 1495 m, 1453 m, 1374 w, 1308 m, 1280 w, 1236 m, 1195 w, 1079 s, 974 w, 841 w, 750 m, 700 m.

Elemental analysis found (calculated for $C_{105}H_{120}Cl_4Fe_2N_{12}O_{28}.4H_2O$) % C 54.45 (54.27), H 5.25 (5.55), N 7.22 (7.23).



$\Delta_{Fe}-[Fe_2L^{13}_3][ClO_4]_4$ was synthesised using the procedure described for $\Lambda_{Fe}-[Fe_2L^{11}_3][ClO_4]_4$, substituting (*R*)-1-phenylpropan-1-amine for **21**.

Yield 0.08g, 77%

1H NMR (300 MHz, 298 K, CD_3CN) δ_H 8.85 (6H, s, CHN), 7.36 (6H, d, $^3J_{HH} = 8.0$ Hz), 7.11 (12H, m), 7.03 (12H, t, $^3J_{HH} = 7.5$ Hz), 6.82 (12H, d, $^3J_{HH} = 7.5$ Hz), 6.20 (6H, d, $^3J_{HH} = 2.5$ Hz, Ar), 6.11 (6H, m), 5.74 (6H, d, $^3J_{HH} = 9.0$ Hz, CH), 5.50 (6H, d, $^3J_{HH} = 16.0$ Hz), 5.33 (6H, d, $^3J_{HH} = 9.5$ Hz), 4.32 (12H, m), 3.87 (6H, m), 3.76 (6H, m), 3.51 (6H, d, $^3J_{HH} = 10.5$ Hz), 1.66 (6H, m), 1.35 (6H, m, CH_2).

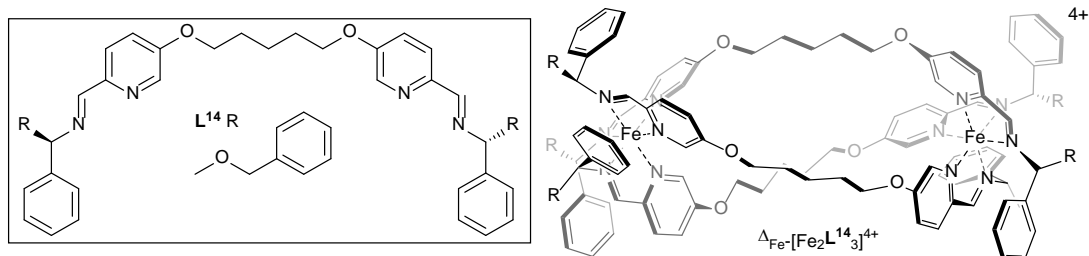
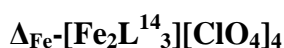
$^{13}C\{^1H\}$ NMR (75 MHz, 298 K, CD_3CN) δ_C 169.2 (CHN), 157.2, 151.0, 141.7, 135.2 (Ar), 134.0 (C=C), 129.6, 128.4, 127.8, 125.6, 121.3 (Ar), 117.0 (C=C), 71.7, 71.5 (CH_2), 69.8 (CH), 68.6, 28.0, 21.5 (CH_2).

MS (ESI) m/z : 655 $[L+Na]^+$, 1675 $[Fe_2L_2.3ClO_4]^+$

IR $\nu\text{ cm}^{-1}$ 2159 m, 2018 w, 1557 m, 1495 w, 1236 m, 1077 s, 760 m, 700 s.

Elemental analysis found (calculated for $C_{117}H_{132}Cl_4Fe_2N_{12}O_{28}.4H_2O$) % C 56.19 (56.67), 5.10 (5.69), 6.77 (6.78).

Crystal data for $C_{126.5}H_{149}Cl_4Fe_2N_{17.5}O_{29.5}$ ($M = 2640.12$ g/mol): orthorhombic, space group $P2_12_12_1$ (no. 19), $a = 12.362(3)$ Å, $b = 21.345(4)$ Å, $c = 49.687(10)$ Å, $V = 13110(5)$ Å³, $Z = 4$, $T = 120(2)$ K, $\mu(\text{MoK}\alpha) = 0.383$ mm⁻¹, $D_{\text{calc}} = 1.338$ g/cm³, 33155 reflections measured ($5.922^\circ \leq 2\theta \leq 54.968^\circ$), 14840 unique ($R_{\text{int}} = 0.0524$, $R_{\text{sigma}} = 0.0646$) which were used in all calculations. The final R_1 was 0.1453 ($I > 2\sigma(I)$) and wR_2 was 0.3278 (all data).



$\Delta_{\text{Fe}}\text{-}[\text{Fe}_2\text{L}^{14}]_3[\text{ClO}_4]_4$ was synthesised using the procedure described for $\Lambda_{\text{Fe}}\text{-}[\text{Fe}_2\text{L}^{11}]_3[\text{ClO}_4]_4$, substituting (*R*)-1-phenylpropan-1-amine for **22**.

Yield 0.14 g, 39%.

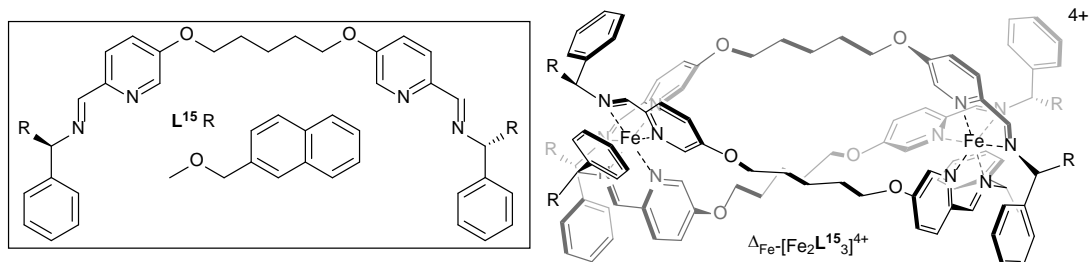
^1H NMR (400 MHz, 298 K, CD_3CN) δ_{H} 8.76 (6H, s, CHN), 7.56 (12H, d, $^3J_{\text{HH}} = 7.0$ Hz), 7.34 (24H, m), 7.02 (12H, m), 6.89 (12H, t, $^3J_{\text{HH}} = 7.5$ Hz), 6.57 (12H d, $^3J_{\text{HH}} = 7.5$ Hz), 6.12 (6H, s, Ar), 5.53 (6H, d, $^3J_{\text{HH}} = 10.0$ Hz, CH), 4.72 (12H, s, 12H), 4.07 (6H, t, $^3J_{\text{HH}} = 10.0$ Hz, CH_2), 3.81 (6H, m), 3.70 (6H, m, OCH_2), 3.23 (6H, d, $^3J_{\text{HH}} = 10.0$ Hz), 1.61 (12H, m), 1.29 (6H, m, CH_2).

$^{13}\text{C}\{^1\text{H}\}$ NMR (105 MHz, 298 K, CD_3CN) δ_{C} 170.5 (CHN), 158.4, 152.4, 142.9, 138.4, 136.3, 130.7, 129.5, 129.4, 129.3, 129.1, 129.0, 128.9, 126.8, 126.0, 122.5, 122.3, 118.1 (Ar), 74.4 (CH_2), 73.0, 70.9 (OCH_2), 69.8 (CH), 28.3, 21.8 (CH_2).

MS (ESI) m/z 1254 $[\text{Fe}_2\text{L}_3(\text{ClO}_4)_2]^{2+}$

IR ν cm^{-1} 2864 w, 2159 w, 2030 w, 1591 m, 1557 m, 1495 m, 1453 m, 1362 s, 1307 m, 1280 m, 1236 m, 1075 s, 999 s, 841 m, 739 m, 697 s.

Elemental analysis found (calculated for $\text{C}_{141}\text{H}_{144}\text{Cl}_4\text{Fe}_2\text{N}_{12}\text{O}_{28}$) % C 61.31 (61.79), H 5.23 (5.47), N 6.08 (6.41).



$\Delta_{\text{Fe}}\text{-}[\text{Fe}_2\text{L}^{15}]_3[\text{ClO}_4]_4$ was synthesised using the procedure described for $\Lambda_{\text{Fe}}\text{-}[\text{Fe}_2\text{L}^{11}]_3[\text{ClO}_4]_4$, substituting (*R*)-1-phenylpropan-1-amine for **23**.

Yield 0.053 g, 21%.

^1H NMR (300 MHz, 298 K, CD_3CN) δ_{H} 8.76 (6H, s, CHN), 7.91 (6H, s), 7.82 (18H, s), 7.71 (6H, d, $^3J_{\text{HH}} = 8.5$ Hz), 7.47 (12H, m), 7.31 (6H, d, $^3J_{\text{HH}} = 8.5$ Hz), 7.07 (6H, d, $^3J_{\text{HH}} = 7.5$ Hz), 6.97 (6H, t, $^3J_{\text{HH}} = 7.5$ Hz), 6.83 (12H, t, $^3J_{\text{HH}} = 7.5$ Hz), 6.57 (12H, d, $^3J_{\text{HH}} = 7.5$ Hz), 6.10 (6H, s, Ar), 5.53 (6H, d, $^3J_{\text{HH}} = 8.5$ Hz, CH), 4.75 (6H, s), 4.02 (6H, t, $^3J_{\text{HH}} = 10.0$ Hz), 3.80 (6H, m), 3.67 (6H, m), 3.26 (6H, d, $^3J_{\text{HH}} = 9.5$ Hz), 1.59 (12H, m), 1.27 (6H, m, CH_2).

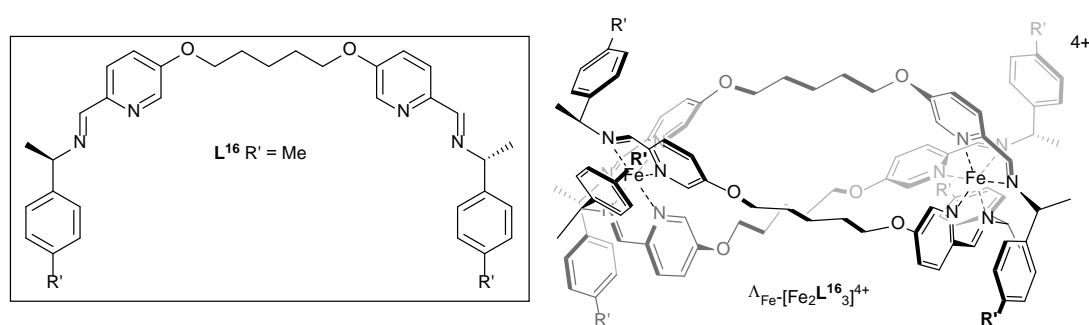
$^{13}\text{C}\{^1\text{H}\}$ NMR (101 MHz, 298 K, CD_3CN) δ_{C} 170.7 (CHN), 158.4, 152.1, 142.9, 136.2, 135.9, 134.0, 133.9, 130.8, 129.3, 129.2, 128.9, 128.6, 128.5, 128.4, 127.4, 127.3, 127.2, 127.2, 126.8, 122.3, 118.2 (Ar), 74.4, 73.0 (CH_2), 70.8 (CH), 69.7, 29.02, 22.6 (CH_2).

MS (ESI) m/z 855 $[L+Na]^+$, 1405 $[Fe_2L_3(ClO_4)_2]^{2+}$

IR ν cm^{-1} : 2863 w, 2159 w, 2028 w, 1592 w, 1558 m, 1495 w, 1307 m, 1280 m, 1237 m, 1081 s, 820 m, 753 m, 700 m.

Elemental analysis found (calculated for $C_{165}H_{156}Cl_4Fe_2N_{12}O_{28} \cdot 8H_2O$) % C 62.43 (62.86), H 4.99 (5.50), N 5.40 (5.33).

$\Lambda_{Fe}-[Fe_2L^{16}_3][ClO_4]_4 \cdot 4H_2O$



$\Lambda_{Fe}-[Fe_2L^{16}_3][ClO_4]_4$ was synthesised using the procedure described for $\Lambda_{Fe}-[Fe_2L^{11}_3][ClO_4]_4$, substituting (*R*)-1-phenylpropan-1-amine for (*R*)-1-(*p*-tolyl)ethan-1-amine.

Yield 0.097 g, 45%.

1H NMR (300 MHz, 298 K, CD_3CN) δ_H 8.55 (6H, s, CHN), 7.36 (12H, m), 6.77 (12H, d, 2H, $^3J_{HH} = 8.0$ Hz), 6.48 (12H, d, $^3J_{HH} = 8.0$ Hz), 6.15 (6H, d, $^3J_{HH} = 2.5$ Hz, Ar), 5.10 (6H, q, $^3J_{HH} = 6.5$ Hz, CH), 3.95 (6H, m), 3.81 (6H, m, CH_2), 2.26 (18H, m), 1.89 (18H, d, $^3J_{HH} = 6.0$, CH_3), 1.70 (12H, m, 2H), 1.39 (6H, m, 1H, CH_2).

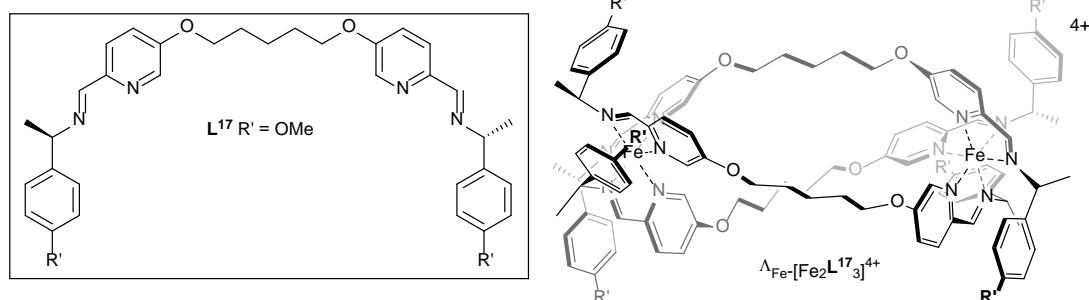
$^{13}C\{^1H\}$ NMR (75 MHz, 298 K, CD_3CN) δ_C 169.9 (CHN), 159.0, 152.1, 143.3, 138.2, 130.8, 130.4, 125.5, 121.8 (Ar), 70.0 (CH_2), 69.0 (CH), 29.4 (CH_2), 26.2 (CH_3), 23.1 (CH_2), 20.9 (CH_3), 2.1 (CH_2).

MS (ESI) m/z 439.5 $[\text{Fe}_2\text{L}_3]^{4+}$

IR ν cm^{-1} 2901 m, 1557 w, 1509 w, 1236 m, 1071 s, 828 m, 671 m.

Elemental analysis found (calculated for $\text{C}_{105}\text{H}_{120}\text{Cl}_4\text{Fe}_2\text{N}_{12}\text{O}_{22} \cdot 4\text{H}_2\text{O}$) % C 54.56 (56.61), H 5.24 (5.79), N 7.22 (7.55) – incomplete combustion.

$\Lambda_{\text{Fe}}\text{-}[\text{Fe}_2\text{L}^{17}]_3[\text{ClO}_4]_4 \cdot 4\text{H}_2\text{O}$



$\Lambda_{\text{Fe}}\text{-}[\text{Fe}_2\text{L}^{17}]_3[\text{ClO}_4]_4$ was synthesised using the procedure described for $\Lambda_{\text{Fe}}\text{-}[\text{Fe}_2\text{L}^{11}]_3[\text{ClO}_4]_4$, substituting (*R*)-1-phenylpropan-1-amine for (*R*)-1-(4-methoxyphenyl) ethan-1-amine.

Yield 0.322 g, 83%.

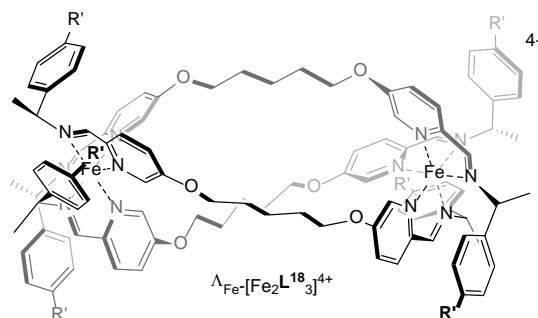
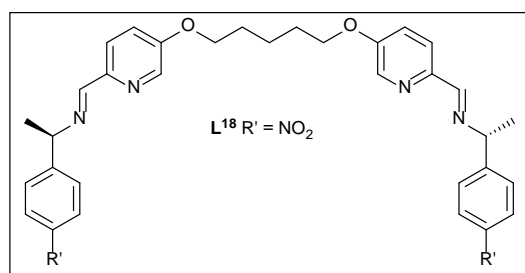
^1H NMR (300 MHz, 298 K, CD_3CN) δ_{H} 8.57 (6H, s, CHN), 7.43 (6H, d, 6H, $^3J_{\text{HH}} = 8.5$ Hz), 7.30 (6H, dd, $^3J_{\text{HH}} = 8.5$ Hz, $^4J_{\text{HH}} = 2.5$ Hz), 6.49 (24H, s), 6.13 (6H, d, $^3J_{\text{HH}} = 3.0$ Hz, Ar), 5.05 (6H, q, $^3J_{\text{HH}} = 7.0$ Hz, CH), 3.90 (6H, m), 3.79 (6H, m, CH_2), 3.73 (18H, s), 1.86 (18H, d, $^3J_{\text{HH}} = 5.0$ Hz, CH_3), 1.70 (12H, m), 1.37 (6H, m, CH_2).

$^{13}\text{C}\{^1\text{H}\}$ NMR (75 MHz, 298 K, CD_3CN) δ_{C} 169.8 (CHN), 159.6, 158.9, 152.2, 143.4, 133.0, 130.7, 126.8, 122.0, 115.2 (Ar), 70.1 (CH_2), 68.7, 56.1 (CH_3), 29.4, 26.3, 22.91 (CH_2).

MS (ESI) m/z 463 $[\text{Fe}_2\text{L}_3]^{4+}$

IR ν cm^{-1} 2901 m, 1557 w, 1509 w, 1236 m, 1071 s, 828 m, 671 m.

Elemental analysis found (calculated for $\text{C}_{105}\text{H}_{120}\text{Cl}_4\text{Fe}_2\text{N}_{12}\text{O}_{28}\cdot 4\text{H}_2\text{O}$) % C 53.49 (54.27), H 5.13 (5.55), N 6.97 (7.23).



$\Lambda_{\text{Fe}}\text{-}[\text{Fe}_2\text{L}^{18}]_3[\text{ClO}_4]_4$ was synthesised using the procedure described for $\Lambda_{\text{Fe}}\text{-}[\text{Fe}_2\text{L}^{11}]_3[\text{ClO}_4]_4$, substituting (*R*)-1-phenylpropan-1-amine for (*R*)-1-(4-nitrophenyl)ethan-1-amine.

Yield 0.211 g, 70%.

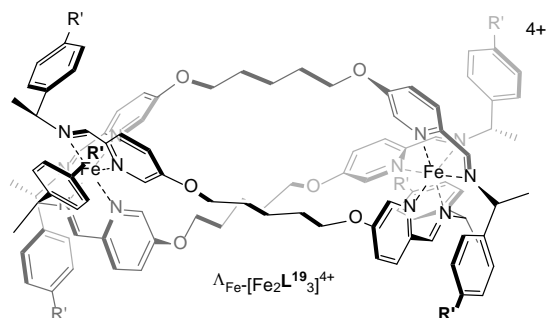
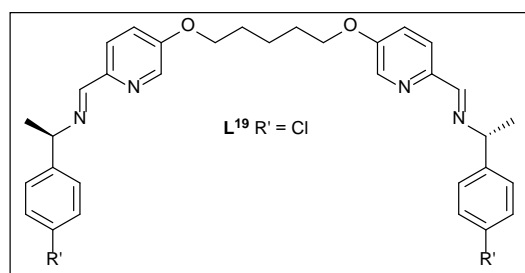
^1H NMR (400 MHz, 298 K, CD_3CN) δ_{H} 8.65 (6H, s, CHN), 7.80 (12H, d, $^3J_{\text{HH}} = 8.5$ Hz), 7.46 (6H, d, $^3J_{\text{HH}} = 9.0$ Hz), 7.31 (6H, dd, $^3J_{\text{HH}} = 8.5$ Hz, $^4J_{\text{HH}} = 3.0$ Hz), 6.86 (12H, d, $^3J_{\text{HH}} = 8.5$ Hz), 6.20 (6H, d, $^3J_{\text{HH}} = 2.5$ Hz, Ar), 5.27 (6H, q, $^3J_{\text{HH}} = 6.5$ Hz, CH), 3.95 (6H, m), 3.88 (6H, m, CH_2), 1.92 (18H, m, CH_3) 1.79 (6H, m), 1.71 (6H, m), 1.40 (6H, m, CH_2).

$^{13}\text{C}\{^1\text{H}\}$ NMR (101 MHz, 298 K, CD_3CN) δ_{C} 171.6 (CHN), 159.6, 151.5, 148.1, 147.8, 144.6, 143.9, 136.0, 131.6, 126.9, 124.9, 122.4 (Ar), 70.3 (CH), 68.7, 29.1 (CH_2), 25.9 (CH_3), 22.7 (CH_2).

MS (ESI) m/z 486 $[\text{Fe}_2\text{L}_3]^{4+}$

IR ν cm^{-1} 3453 w, 2970 w, 1544 w, 1386 w, 1359 w, 1042 m, 627 m.

Elemental analysis found (calculated for $\text{C}_{99}\text{H}_{102}\text{Cl}_4\text{Fe}_2\text{N}_{18}\text{O}_{34}\cdot 4\text{H}_2\text{O}$) % C 48.93 (49.27), H 4.58 (4.59), N 10.31 (10.45).



$\Lambda_{\text{Fe}}\text{-}[\text{Fe}_2\text{L}^{19}]_3[\text{ClO}_4]_4$ was synthesised using the procedure described for $\Lambda_{\text{Fe}}\text{-}[\text{Fe}_2\text{L}^{11}]_3[\text{ClO}_4]_4$, substituting (*R*)-1-phenylpropan-1-amine for (*R*)-1-(4-chlorophenyl)ethan-1-amine.

Yield 0.174 g, 58%.

^1H NMR (400 MHz, 298 K, CD_3CN) δ_{H} 8.60 (6H, s, CHN), 7.48 (6H, d, $^3J_{\text{HH}} = 8.0$ Hz), 7.36 (6H, dd, $^3J_{\text{HH}} = 9.0$ Hz, $^4J_{\text{HH}} = 2.5$ Hz), 6.97 (12H, d, $^3J_{\text{HH}} = 8.0$ Hz), 6.59 (12H, d, $^3J_{\text{HH}} = 8.0$ Hz), 6.16 (6H, d, $^3J_{\text{HH}} = 2.5$, Hz Ar), 5.08 (6H, q, $^3J_{\text{HH}} = 6.0$ Hz, CH), 3.95 (6H, m), 3.82 (6H, m, CH_2), 1.86 (18H, d, $^3J_{\text{HH}} = 7.0$ Hz, CH_3), 1.77 (6H, m), 1.67 (6H, m), 1.38 (6H, m, CH_2).

$^{13}\text{C}\{^1\text{H}\}$ NMR (101 MHz, 298 K, CD_3CN) δ_{C} 170.8 (CHN), 159.4, 152.0, 143.7, 139.7, 133.8, 131.2, 129.9, 127.4, 122.0 (Ar), 70.2 (CH_2), 68.7 (CH_3), 26.2 (CH_2), 22.8 (CH), 1.5 (CH_2).

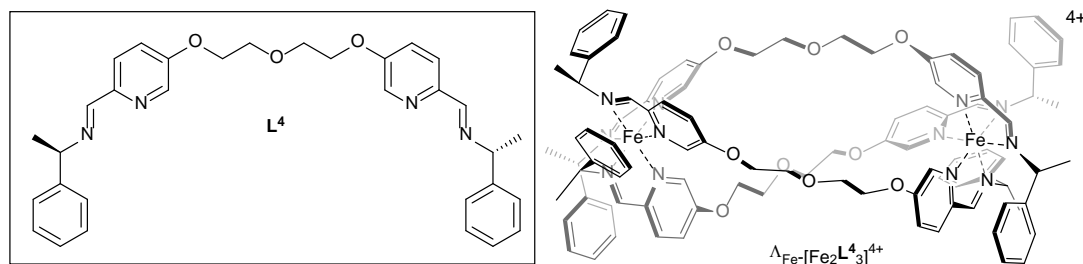
MS (ESI) m/z 470 $[\text{Fe}_2\text{L}_3]^{4+}$

IR ν cm^{-1} 2971 m, 1558 w, 1236 w, 1074 s, 827 m, 621 m.

Elemental analysis found (calculated for $C_{99}H_{102}Cl_{10}Fe_2N_{12}O_{22} \cdot 4H_2O$) % C 50.04 (50.59), 4.34 (4.72), 6.95 (7.15).

5.5.3 $[Fe_2L_3]Cl_4^{13}$

$\Lambda_{Fe}-[Fe_2L_3]Cl_4 \cdot 13H_2O$



9 (0.1 g, 0.32 mmol) and (*R*)-1-phenylethan-1-amine (0.08 g, 0.63 mmol) were dissolved in methanol. Iron (II) chloride (0.03 g, 0.21 mol) was added and an immediate colour change to deep purple was seen. The solution was heated to reflux (75°C) for 48 h. The solvent was removed under reduced pressure to yield a dark purple solid.

Yield 0.235 g, 78%.

1H NMR (400 MHz, 298 K, MeOD) δ_H 8.80 (6H, s, CHN), 7.47 (6H, br s), 7.13 (6H, t, $^3J_{HH} = 7.5$ Hz), 7.04 (12H, t, $^3J_{HH} = 7.5$ Hz), 6.64 (12H, d, $^3J_{HH} = 7.5$ Hz), 6.47 (6H, s), 6.05 (6H, s, Ar), 5.26 (6H, q, $^3J_{HH} = 6.5$ Hz, CH), 4.65 (12H, br s), 4.59 (12H, br s, CH_2), 1.99 (18H, d, $^3J_{HH} = 6.5$ Hz, CH_3).

$^{13}C\{^1H\}$ NMR (101 MHz, 298 K, MeOD) δ_C 171.2 (CHN), 159.0, 152.4, 145.0, 141.7, 131.4, 130.3, 130.0, 128.7, 125.7, 121.2 (Ar), 70.3 (CH_3), 69.8, 26.3 (CH_2).

MS (ESI) m/z 420 $[Fe_2L_3]^{4+}$, 522 $[L+H]$.

IR ν cm^{-1} 3373 br s, 2927 s, 1557 s, 1491 m, 1450 m, 1300 m, 1231 s, 1122 m, 1038 s, 921 w, 841 w, 760 m, 660 m.

Elemental analysis found (calculated for $\text{C}_9\text{H}_{102}\text{Cl}_4\text{Fe}_2\text{N}_{12}\text{O}_9 \cdot 13\text{H}_2\text{O}$) % C 55.03 (56.09), H 5.81 (6.28), N 7.74 (8.18).

$\Delta_{\text{Fe}}\text{-}[\text{Fe}_2\text{L}_3]\text{Cl}_4 \cdot 13\text{H}_2\text{O}$

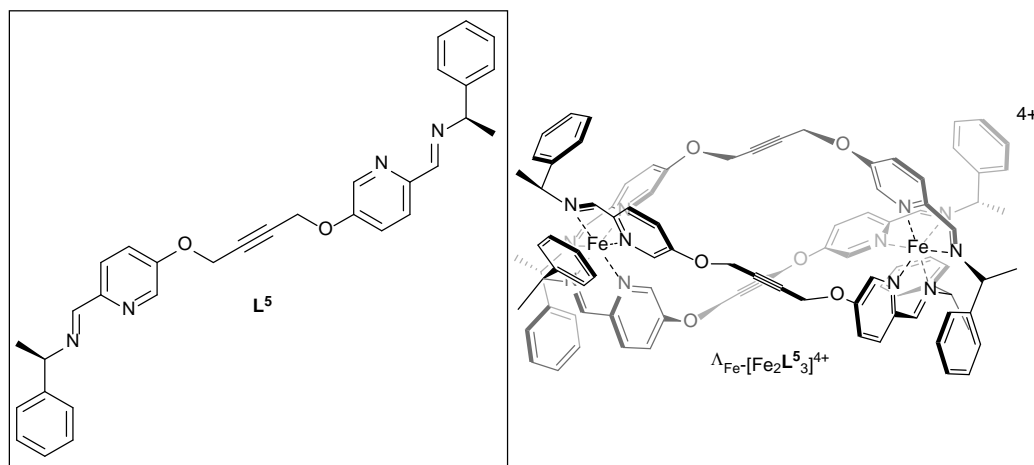
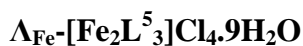
$\Delta_{\text{Fe}}\text{-}[\text{Fe}_2\text{L}_3]\text{Cl}_4$ was synthesised using the procedure described for $\Lambda_{\text{Fe}}\text{-}[\text{Fe}_2\text{L}_3]\text{Cl}_4$, substituting (*R*)-1-phenylethan-1-amine for (*S*)-1-phenylethan-1-amine.

Yield 0.271g, 90%.

MS (ESI) m/z 420 $[\text{Fe}_2\text{L}_3]^{4+}$, 522 $[\text{L}+\text{H}]$.

IR ν cm^{-1} : 3366 br s, 2987 m, 1556 s, 1486 m, 1450 m, 1382 w, 1231 s, 1121 m, 1039 m, 924 w, 842 w, 761 m, 700 m, 543 m.

Elemental analysis found (calculated for $\text{C}_9\text{H}_{102}\text{Cl}_4\text{Fe}_2\text{N}_{12}\text{O}_9 \cdot 13\text{H}_2\text{O}$) % C 56.26 (56.09), H 5.95 (6.28), 7.89 (8.18).



$\Lambda_{\text{Fe}}\text{-}[\text{Fe}_2\text{L}^5_3]\text{Cl}_4$ was synthesised using the procedure described for $\Lambda_{\text{Fe}}\text{-}[\text{Fe}_2\text{L}^4_3]\text{Cl}_4$, substituting **11** for **9**.

Yield 0.301 g, 86%.

^1H NMR (400 MHz, 298 K, MeOD) δ_{H} 8.83 (6H, s, CHN), 7.57 (6H, t, $^4J_{\text{HH}} = 2.5$ Hz), 7.47 (6H, d, $^3J_{\text{HH}} = 4.5$ Hz), 7.12 (6H, t, $^3J_{\text{HH}} = 7.0$ Hz), 7.01 (12H, t, $^3J_{\text{HH}} = 7.0$ Hz), 6.66 (12H, d, $^3J_{\text{HH}} = 7.0$ Hz), 6.27 (6H, d, $^4J_{\text{HH}} = 2.5$ Hz, Ar), 5.34 (6H, q, $^3J_{\text{HH}} = 6.5$ Hz, CH), 4.90 (12H, s, CH_2), 2.01 (18H, d, $^3J_{\text{HH}} = 6.5$ Hz).

$^{13}\text{C}\{^1\text{H}\}$ NMR (101 MHz, 298 K, MeOD) δ_{C} 157.7 (Ar), 153.2 (CHN), 145.3, 141.7, 131.2, 130.3, 128.8, 127.6, 125.8, 122.2 (Ar), 83.4 ($\text{C}\equiv\text{C}$), 70.2 (CH), 57.5 (CH_2), 26.3 (CH_3).

MS (ESI) m/z 405 $[\text{Fe}_2\text{L}_3]^{4+}$, 503 $[\text{L}+\text{H}]$.

IR ν cm^{-1} 3350 br, s, 2926 m, 1557 m, 1490 m, 1223 s, 987 s, 836 w, 780 m, 699 m, 535 w.

Elemental analysis found (calculated for $C_{96}H_{90}Cl_4Fe_2N_{12}O_6 \cdot 9H_2O$) % C 59.62 (59.95), H 5.45 (5.66), N 8.56 (8.74).

$\Delta_{Fe}-[Fe_2L^5]Cl_4 \cdot 9H_2O$

$\Delta_{Fe}-[Fe_2L^5]Cl_4$ was synthesised using the procedure described for $\Lambda_{Fe}-[Fe_2L^5]Cl_4$, substituting (*R*)-1-phenylethan-1-amine for (*S*)-1-phenylethan-1-amine.

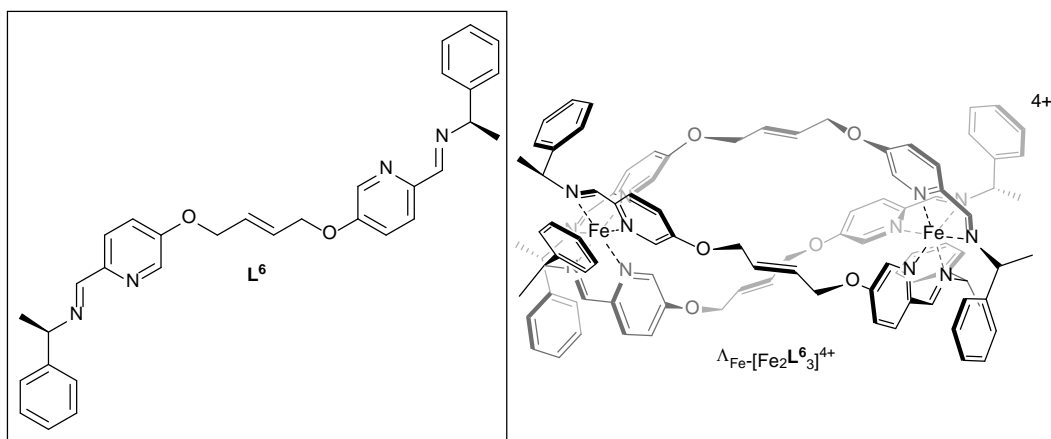
Yield 0.319 g, 91%.

MS (ESI) m/z 405 $[Fe_2L_3]^{4+}$, 503 $[L+H]$.

IR ν cm^{-1} 3362 br s, 2928 br s, 1557 m, 1488 w, 1449 w, 1298 m, 1224 s, 988 m, 759 m, 699 s, 533 w, 467 w.

Elemental analysis found (calculated for $C_{96}H_{90}Cl_4Fe_2N_{12}O_6 \cdot 9H_2O$) % C 60.64 (59.95), H 5.49 (5.66), N 8.82 (8.74).

$\Lambda_{Fe}-[Fe_2L^6]Cl_4 \cdot 9H_2O$



$\Lambda_{Fe}-[Fe_2L^6]Cl_4$ was synthesised using the procedure described for $\Lambda_{Fe}-[Fe_2L^4]Cl_4$, substituting **12** for **9**.

Yield 0.388 g, 97%.

^1H NMR (400 MHz, 298 K, MeOD) δ_{H} 8.80 (6H, s, CHN), 7.47 (6H, s), 7.13 (6H, t, $^3J_{\text{HH}} = 7.0$ Hz), 7.04 (12H, t, $^3J_{\text{HH}} = 7.0$ Hz), 6.64 (12H, d, $^3J_{\text{HH}} = 7.0$ Hz), 6.44 (6H, s), 6.05 (6H, s, Ar), 5.26 (6H, q, $^3J_{\text{HH}} = 6.0$ Hz, CH), 4.65 (12H, s, CH_2), 4.59 (6H, br s, CH), 1.99 (18H, d, $^3J_{\text{HH}} = 6.0$ Hz, CH_3).

$^{13}\text{C}\{^1\text{H}\}$ NMR (101 MHz, 298 K, MeOD) δ_{C} 171.0 (CHN), 158.8, 152.5, 144.8, 141.7, 131.2, 130.1, 129.8, 128.5, 125.5 (Ar), 121.0 (CH), 70.0 (CH_2), 69.6 (CH), 26.1 (CH_3).

MS (ESI) m/z 406 $[\text{Fe}_2\text{L}_3]^{4+}$, 505 $[\text{L}+\text{H}]$.

IR ν cm^{-1} 3352 br s, 2970 br s, 1589 s, 1557 w, 1488 w, 1381 m, 1299 s, 1067 m, 1028 m, 760 m, 699 s, 562 w.

Elemental analysis found (calculated for $\text{C}_{96}\text{H}_{96}\text{Cl}_4\text{Fe}_2\text{N}_{12}\text{O}_6 \cdot 9\text{H}_2\text{O}$) % C 59.92 (59.76), H 5.84 (5.96), N 8.63 (8.71).

$\Delta_{\text{Fe}}\text{-}[\text{Fe}_2\text{L}^6_3]\text{Cl}_4 \cdot 9\text{H}_2\text{O}$

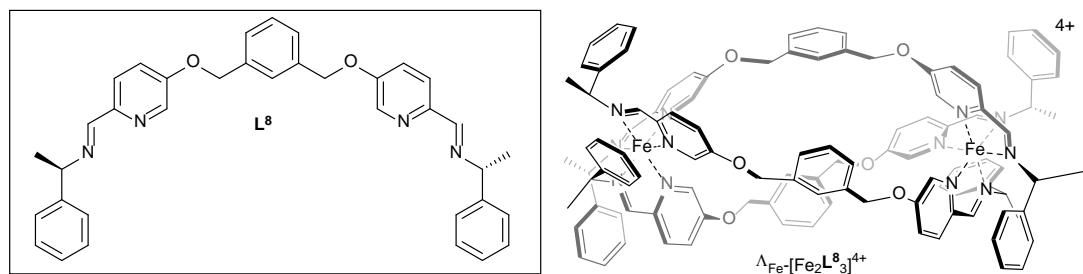
$\Delta_{\text{Fe}}\text{-}[\text{Fe}_2\text{L}^6_3]\text{Cl}_4$ was synthesised using the procedure described for $\Lambda_{\text{Fe}}\text{-}[\text{Fe}_2\text{L}^6_3]\text{Cl}_4$, substituting (*R*)-1-phenylethan-1-amine for (*S*)-1-phenylethan-1-amine.

Yield 0.340 g, 89%.

MS (ESI) m/z 406 $[\text{Fe}_2\text{L}_3]^{4+}$, 505 $[\text{L}+\text{H}]$.

IR ν cm^{-1} 3360 br s, 2928 m, 1589 w, 1557 s, 1485 m, 1451 m, 1381 w, 1299 m, 1230 s, 1135 w, 1069 m, 976 s, 836 w, 760 m, 699 m, 545 m.

Elemental analysis found (calculated for $\text{C}_{96}\text{H}_{96}\text{Cl}_4\text{Fe}_2\text{N}_{12}\text{O}_6 \cdot 9\text{H}_2\text{O}$) % C 59.34 (59.76), H 5.93 (5.96), N 8.54 (8.71).

$\Lambda_{\text{Fe}}\text{-}[\text{Fe}_2\text{L}^8_3]\text{Cl}_4\cdot 6\text{H}_2\text{O}$ 

$\Lambda_{\text{Fe}}\text{-}[\text{Fe}_2\text{L}^8_3]\text{Cl}_4$ was synthesised using the procedure described for $\Lambda_{\text{Fe}}\text{-}[\text{Fe}_2\text{L}^4_3]\text{Cl}_4$, substituting **14** for **9**.

Yield 0.228 g, 76%.

^1H NMR (400 MHz, 298 K, MeOD) δ_{H} 8.83 (6H, s, CHN), 7.52 (6H, dd, $^3J_{\text{HH}} = 9.0$ Hz, $^4J_{\text{HH}} = 3.0$ Hz), 7.46 (6H, s), 7.32 (18H, m), 7.08 (6H, t, $^3J_{\text{HH}} = 7.0$ Hz), 6.95 (18H, m), 6.69 (12H, d, $^3J_{\text{HH}} = 7.0$ Hz, Ar), 5.25 (6H, q, $^3J_{\text{HH}} = 7.0$ Hz, CH), 5.12 (6H, m), 5.03 (6H, m, CH_2), 1.62 (18H, d, CH_3).

$^{13}\text{C}\{^1\text{H}\}$ NMR (101 MHz, 298 K, MeOD) δ_{C} 171.2 (CHN), 141.7, 131.2, 140.4, 130.3, 130.1, 129.8, 129.3, 128.5, 127.6, 127.4, 125.5 (Ar), 71.83 (CH_2), 52.13 (CH_3), 26.20 (CH).

MS (ESI) m/z 444 $[\text{Fe}_2\text{L}_3]^{4+}$

IR ν cm^{-1} 3352 br s, 3026 br s, 1556 m, 1491 m, 1299 m, 1230 s, 1069 w, 997 m, 759 m, 698 s, 532 w.

Elemental analysis found (calculated for $\text{C}_{108}\text{H}_{102}\text{Cl}_4\text{Fe}_2\text{N}_{12}\text{O}_6\cdot 6\text{H}_2\text{O}$) % C 63.62 (64.04), H 5.73 (5.67), N 7.96 (8.30).

 $\Delta_{\text{Fe}}\text{-}[\text{Fe}_2\text{L}^8_3]\text{Cl}_4\cdot 4\text{H}_2\text{O}$

$\Delta_{\text{Fe}}\text{-}[\text{Fe}_2\text{L}^8_3]\text{Cl}_4$ was synthesised using the procedure described for $\Lambda_{\text{Fe}}\text{-}[\text{Fe}_2\text{L}^8_3]\text{Cl}_4$, substituting (*R*)-1-phenylethan-1-amine for (*S*)-1-phenylethan-1-amine.

Yield 0.198 g, 66%.

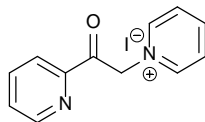
MS (ESI) m/z 444 $[\text{Fe}_2\text{L}_3]^{4+}$

IR ν cm^{-1} 3366 br s, 2970 br s, 1557 m, 1491 w, 1226 s, 1082 w, 1010 m, 759 m, 698 s, 531 w.

Elemental analysis found (calculated for $\text{C}_{108}\text{H}_{102}\text{Cl}_4\text{Fe}_2\text{N}_{12}\text{O}_6\cdot 4\text{H}_2\text{O}$) % C 65.99 (65.20), H 5.67 (5.57), N 8.53 (8.45).

5.6 5-(2,2'-bipyridin-5-ylmethoxy)picolinaldehyde

1-(2-oxo-2-(pyridin-2-yl)ethyl)pyridinium iodide¹⁴ (26)



2-Acetylpyridine (27.0 g, 25 ml, 0.22 mol) was added to a suspension of iodine (56.5 g, 0.22 mol) in dry pyridine (225 ml) under argon, then stirred at reflux (130°C) for 2h. Diethyl ether (100 ml) was added and the solution was cooled to 0°C. The resulting black precipitate was filtered off, washed with diethyl ether (3 × 100 ml), and dried in air. The solid was then dissolved in hot methanol (250 ml) with activated charcoal (30 g) and stirred at reflux (70°C) for 30 min. The solution was filtered through celite in a fritted funnel, washed with hot methanol (3 × 50 ml) and the solvent was removed under reduced pressure to leave the crude product. Recrystallisation from hot methanol (300 ml) resulted in light green crystals which were filtered, washed with cold methanol (50 ml), and dried *in vacuo*.

Yield 40.1 g, 55%.

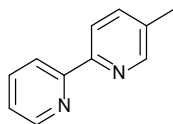
¹H NMR (400 MHz, 298 K, DMSO) δ_{H} 8.70 (2H, dd, $^3J_{\text{HH}} = 7.0$ Hz, $^4J_{\text{HH}} = 1.5$ Hz), 8.58 (1H, dt, $^3J_{\text{HH}} = 4.5$ Hz, $^4J_{\text{HH}} = 1.5$ Hz), 8.44 (1H, tt, $^3J_{\text{HH}} = 8.0$ Hz, $^4J_{\text{HH}} = 1.5$ Hz), 7.97 (2H, t, $^3J_{\text{HH}} = 7.5$ Hz) 7.86 (1H, td $^3J_{\text{HH}} = 8.0$ Hz, $^4J_{\text{HH}} = 4.5$ Hz), 7.79 (1H, dt, $^3J_{\text{HH}} = 8.0$ Hz, $^4J_{\text{HH}} = 1.5$ Hz), 7.54 (1H, m, Py), 6.22 (2H, s, CH₂).

¹³C{¹H} NMR (75 MHz, 298 K, DMSO) δ_{C} 192.0 (CO), 150.9, 150.1, 146.8, 146.4, 138.7, 129.7, 128.2, 122.6 (Py), 67.2 (CH₂).

MS (ESI) m/z 199 [M]⁺

IR ν cm^{-1} 3039 w, 1704 m, 1478 m, 993 m, 788 m, 761 m, 692 m, 672 m, 570 m.

5-methyl-2,2'-bipyridine¹⁴ (27)



Methacrolein was degassed then vacuum transferred to remove the initiator, then stored under argon before use. Formamide was degassed and stored under argon before use. **26** (40 g, 0.12 mol) and ammonium acetate (22.0 g, 0.29 mol) were dissolved in dry formamide (100 ml), followed by dry, distilled methacrolein (10 ml, 0.13 mol) and stirred at reflux (80°C) for 6 h. After cooling to ambient temperature water (80 ml) was added and the reaction mixture was extracted into dichloromethane (3 × 200 ml), washed with saturated brine (100 ml), dried over sodium sulphate and the solvent was removed under reduced pressure to leave the crude product as a brown liquid. This was distilled under high vacuum at 100-110°C to give a clear liquid.

Yield 11.3 g, 55 %.

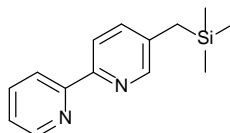
¹H NMR (400 MHz, 298 K, CDCl₃) δ_{H} 8.66 (1H, d, ³J_{HH} = 4.5 Hz), 8.51 (1H, d, ³J_{HH} = 2.0 Hz), 8.35 (1H, d, ³J_{HH} = 8.0 Hz), 8.29 (1H, d, ³J_{HH} = 8.5 Hz), 7.80 (1H, td, ³J_{HH} = 8.0 Hz, ⁴J_{HH} = 2.0 Hz), 7.62 (1H, dd, ³J_{HH} = 8.0 Hz, ⁴J_{HH} = 2.0 Hz), 7.28 (1H, m, Py), 2.39 (3H, s, CH₃).

¹³C{¹H} NMR (101 MHz, 298 K, CDCl₃) δ_{C} 156.3, 153.7, 149.7, 149.1, 137.5, 136.9, 133.4, 123.4, 120.8, 120.6 (Py), 18.4 (CH₃).

MS (ESI) m/z 171 [M+H]⁺, 193 [M+Na]⁺

IR ν cm^{-1} 3002 w, 1458 s, 1431 s, 1379 m, 787 s, 740 s.

5-((trimethylsilyl)methyl)-2,2'-bipyridine¹⁵ (28)



A schlenk vessel was charged with dry tetrahydrofuran (100 ml) and diisopropylamine (9.8 ml, 0.07 mol) and cooled to -78°C , then n-butyllithium (23.2 ml, 2.5 M, 0.06 mol) was added and the solution was stirred for 10 min warmed to 0°C for 10 mins, then cooled to -78°C . **27** (8.2 g, 0.05 mol) in dry tetrahydrofuran (50 ml) was then added drop wise and the solution was stirred for at -78°C for 1h. Chlorotrimethylsilane (7.9 ml, 0.056 mol) was then added rapidly to the solution and after 1 min the reaction was quenched by the rapid addition of absolute ethanol (200 ml) and the solution was warmed to ambient temperature. Saturated NaHCO_3 (150 ml), was added and the solution was extracted into dichloromethane (3×75 ml), dried over sodium sulphate, filtered and the solvent was removed under reduced pressure to give a white solid.

Yield 10.5 g, 66 %.

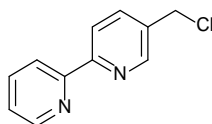
^1H NMR (400 MHz, 298 K, CDCl_3) δ_{H} 8.69 (1H, dq, $^3J_{\text{HH}} = 4.5$ Hz, $^4J_{\text{HH}} = 1.0$ Hz), 8.42-8.40 (2H, m), 8.33 (1H, d, $^3J_{\text{HH}} = 8.5$ Hz), 7.78 (1H, td, $^3J_{\text{HH}} = 8.0$ Hz, $^4J_{\text{HH}} = 2.0$ Hz), 7.46 (1H, dd, $^3J_{\text{HH}} = 8.0$ Hz, $^4J_{\text{HH}} = 2.5$ Hz), 7.25 (1H, ddd, $^3J_{\text{HH}} = 7.5$ Hz, $^3J_{\text{HH}} = 4.5$ Hz, $^4J_{\text{HH}} = 1.0$ Hz, Py), 2.14 (2H, s, CH_2), 0.05 (9H, s, CH_3).

$^{13}\text{C}\{^1\text{H}\}$ NMR (100 MHz, 298 K, CDCl_3) δ_{C} 156.2, 152.2, 148.9, 148.4, 136.7, 136.2, 135.8, 122.9, 120.5, 120.4 (Py), 23.9 (CH_2), 2.2 (CH_3).

MS (ESI) m/z 243 $[M+H]^+$

IR ν cm^{-1} 3050 w, 1589 m, 1258 s, 1432 s, 1269 w, 1145 w, 874 m.

5-(chloromethyl)-2,2'-bipyridine¹⁵ (29)



28 (12 g, 0.1 mol), hexachloroethane (40 g, 0.2 mol) and caesium fluoride (20 g, 0.2 mol) were suspended in dry acetonitrile (200 ml) at 60°C for 4 h. After cooling to ambient temperature water (100 ml) was added and extracted into ethyl acetate (3 × 150 ml), washed with brine, dried over sodium sulphate, filtered and the solvent was removed under reduced pressure and the resulting brown solid was extracted into hot hexane and the solvent was removed under reduced pressure. Recrystallisation from hot hexane gave a pale yellow crystalline solid.

Yield 10.5 g, 50%.

¹H NMR (400 MHz, 298 K, CDCl₃) δ_{H} 8.67 (2H, s), 8.41 (2H, t, ³J_{HH} = 6.5 Hz), 7.93-7.77 (2H, m), 7.31 (1H, t, ³J_{HH} = 6.5 Hz, Py), 4.65 (2H, s, CH₂).

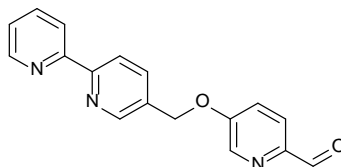
¹³C{¹H} NMR (101 MHz, 298 K, CDCl₃) δ_{C} 149.7, 149.5, 142.9, 137.6, 137.4, 133.6, 128.6, 124.4, 121.7, 121.4 (Py), 43.6 (CH₂).

MS (ESI) m/z 205 $[M+H]^+$, 227 $[M+Na]^+$, 242 $[M+K]^+$

IR ν cm^{-1} 2969 w, 1492 m, 1437 m, 1391 m, 1261 m, 1250 m, 746 m, 731 s, 674 s, 647 m.

Elemental analysis found (calculated for $C_{11}H_9ClN_2$) % C 64.28 (64.56), 4.11 (4.43), 13.60 (13.68).

5-(2,2'-bipyridin-5-ylmethoxy)picolinaldehyde (30**)**



4 (2.0 g, 0.016 mol) was dissolved in acetonitrile (50 ml). Potassium carbonate (2.65 g, 0.019 mol) followed by **29** (3.32 g, 0.016 g) were added and the solution was stirred at reflux (80°C) for 16 h. The reaction mixture was filtered through a silica plug and the solvent was removed under reduced pressure. The crude product was taken up in dichloromethane (50 ml), filtered and the solvent was removed under reduced pressure to give the desired **30**, a pale brown solid.

Yield 3.67 g, 79%.

^1H NMR (400 MHz, 298 K, CDCl_3) δ_{H} 9.94 (1H, s, CHO), 8.69 (1H, d, $^3J_{\text{HH}} = 2.0$ Hz), 8.62 (1H, d, $^3J_{\text{HH}} = 4.5$ Hz), 8.47 (1H, d, $^3J_{\text{HH}} = 2.5$ Hz), 8.40 (1H, $^3J_{\text{HH}} = 8.0$ Hz), 8.34 (1H, d, $^3J_{\text{HH}} = 8.0$ Hz), 7.91 (1H, d, $^3J_{\text{HH}} = 8.5$ Hz), 7.84 (1H, dd, $^3J_{\text{HH}} = 8.5$ Hz, $^4J_{\text{HH}} = 2.5$ Hz), 7.77 (1H, td, $^3J_{\text{HH}} = 8.0$ Hz, $^4J_{\text{HH}} = 2.0$ Hz), 7.34 (1H, dd, $^3J_{\text{HH}} = 8.0$ Hz, $^4J_{\text{HH}} = 3.0$ Hz), 7.27 (1H, m, Py), 5.21 (2H, s, CH_2).

$^{13}\text{C}\{^1\text{H}\}$ NMR (75 MHz, 298 K, CDCl_3) δ_{C} 192.1 (CHO), 149.4, 148.6, 139.0, 138.1, 137.2, 136.6, 136.6, 131.9, 130.9, 124.3, 124.2, 123.5, 122.7, 121.4, 121.2 (Py), 68.3 (CH_2).

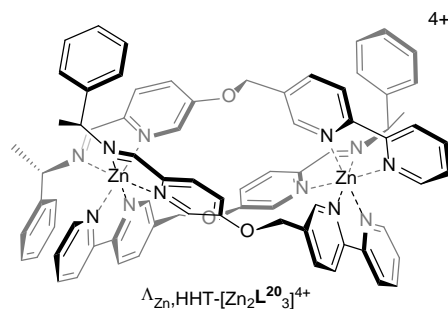
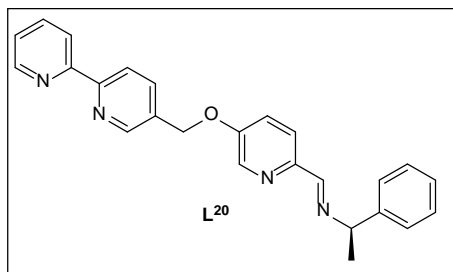
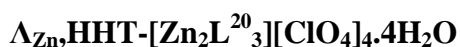
MS (ESI) m/z 292 $[\text{M}+\text{H}]^+$, 314 $[\text{M}+\text{Na}]^+$

IR ν cm^{-1} 2811 w, 1701 s, 1567 s, 1455 m, 1204 s, 788 s, 736 s, 590 s.

Elemental analysis found (calculated for $\text{C}_{17}\text{H}_{13}\text{N}_3\text{O}_2$) % C 69.28 (70.09), H 4.52 (4.50), N 14.08 (14.52).

5.7 Triplex metallohelices

5.7.1 $[\text{Zn}_2\text{L}^{20-26}_3][\text{ClO}_4]_4$



30 (0.10 g, 0.46 mmol) and (*R*)-1-phenylethan-1-amine (0.06 g, 0.46 mmol) were dissolved in acetonitrile (10 ml). Zinc (II) perchlorate hexahydrate (0.11 g, 0.30 mmol) was added and the solution was stirred at ambient temperature for 20 h then ethyl acetate was added drop-wise to cause precipitation of a crystalline solid.

Yield 0.11 g, 41%.

^1H NMR (400 MHz, 298 K, CD_3CN) δ_{H} 8.99 (1H, s), 8.91 (1H, s, CHN), 8.51-8.44 (4H, m), 8.33 (1H, t, $^3J_{\text{HH}} = 7.0$ Hz) 8.22-8.19 (2H, m, Ar), 8.16-8.03 (7H, CHN / Ar), 7.97 (2H, d, $^3J_{\text{HH}} = 9.0$ Hz), 7.91-7.86 (2H, m), 7.84-7.76 (3H, m), 7.71-7.67 (3H, m), 7.60-7.55 (3H, m), 7.50 (1H, t, $^3J_{\text{HH}} = 6.0$ Hz), 7.20 (1H, t, $^3J_{\text{HH}} = 7.0$ Hz), 7.06 (3H, t, $^3J_{\text{HH}} = 7.5$ Hz), 6.97 (1H, t, $^3J_{\text{HH}} = 7.5$ Hz), 6.87 (2H, t, $^3J_{\text{HH}} = 6.0$ Hz), 6.78 (2H, d, $^3J_{\text{HH}} = 7.5$ Hz), 6.69 (2H, t, $^3J_{\text{HH}} = 7.5$ Hz), 6.57-6.53 (3H, m), 6.20 (4H, q, $^3J_{\text{HH}} = 7.5$ Hz, Ar), 5.68 (1H, q, $^3J_{\text{HH}} = 7.5$ Hz, CH), 5.19-5.06 (7H, m, CH / CH_2), 5.01 (1H, d, $^3J_{\text{HH}} = 9.5$ Hz, CH_2), 1.81 (3H, d, $^3J_{\text{HH}} = 6.5$ Hz), 1.65 (3H, d, $^3J_{\text{HH}} = 6.5$ Hz), 1.45 (3H, d, $^3J_{\text{HH}} = 6.5$ Hz, CH_3).

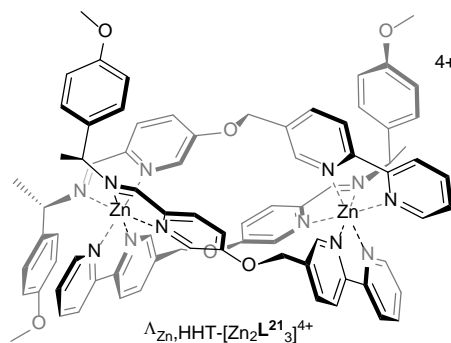
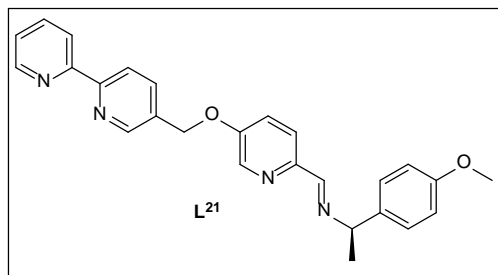
$^{13}\text{C}\{^1\text{H}\}$ NMR (126 MHz, 298 K, CD_3CN) δ_{C} 162.0, 161.3, 160.2 (NCH), 159.6, 159.6, 159.0, 150.1, 149.7, 149.3, 149.2, 149.1, 149.1, 149.0, 149.0, 148.9, 148.5, 148.3, 148.0, 143.3, 142.3, 142.0, 142.0, 141.9, 141.8, 141.3, 140.6, 140.5, 140.4, 140.4, 139.2, 139.1, 138.3, 135.7, 135.0, 134.7, 132.3, 132.1, 132.0, 129.2, 129.0, 128.8, 8.7, 128.5, 128.3, 128.0, 127.8, 127.4, 126.1, 125.7, 125.6, 124.4, 124.3, 124.0, 123.9, 123.9, 123.7, 123.6, 123.4 (Ar), 68.6, 68.5, 68.5 (CH), 65.2, 64.8, 64.5 (CH_2), 22.3, 22.3, 21.7 (CH_3).

MS (ESI) m/z 324 $[\text{Zn}_2\text{L}_3]^{4+}$

IR $\nu\text{ cm}^{-1}$ 3120 w, 1571 m, 1224 w, 1083 s, 791 w, 702 w, 621 m, 412 w.

Elemental analysis found (calculated for $\text{C}_{75}\text{H}_{66}\text{Cl}_4\text{N}_{12}\text{O}_{19}\text{Zn}_2\cdot 4\text{H}_2\text{O}$) % C 49.39 (50.49), H 3.64 (4.18), N 9.18 (9.42).

$\Lambda_{\text{Zn,HHT}}\text{-}[\text{Zn}_2\text{L}^{21}_3][\text{ClO}_4]_4\cdot 4\text{H}_2\text{O}$



$\Lambda_{\text{Zn,HHT}}\text{-}[\text{Zn}_2\text{L}^{21}_3][\text{ClO}_4]_4$ was synthesised using the procedure described for $\Lambda_{\text{Zn,HHT}}\text{-}[\text{Zn}_2\text{L}^{20}_3][\text{ClO}_4]_4$, substituting (*R*)-1-phenylethan-1-amine for (*R*)-1-(4-methoxyphenyl)ethan-1-amine.

Yield: 0.09 g, 40%.

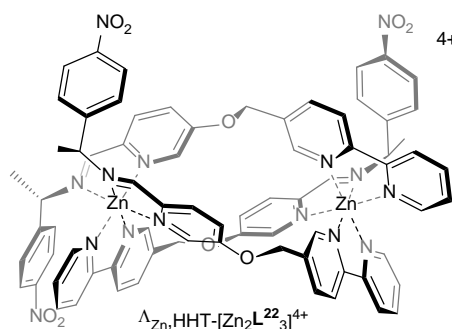
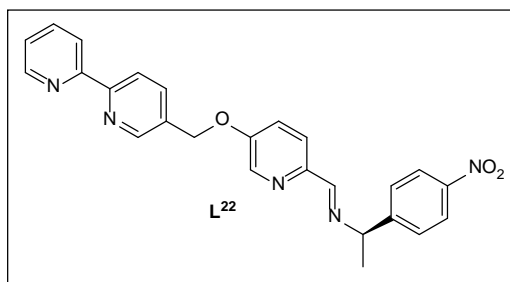
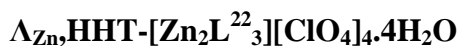
^1H NMR (400 MHz, 298 K, CD_3CN) δ_{H} 9.01 (1H, s), 8.92 (1H, s, CHN), 8.53 3H, t, $^3J_{\text{HH}} = 8.5$ Hz), 8.47 (1H, d, $^3J_{\text{HH}} = 5.0$ Hz), 8.37 (1H, t, $^3J_{\text{HH}} = 8.5$ Hz), 8.26 (1H, d, $^3J_{\text{HH}} = 7.5$ Hz, Ar), 8.22-8.00 (12H, m, Ar/CHN), 7.92 (1H, m), 7.87-7.80 (6H, m), 7.76-7.67 (4H, m), 7.60 (1H, s), 7.55 (1H, m), 7.34 (1H, d, $^3J_{\text{HH}} = 7.5$ Hz), 7.06 (1H, d, $^4J_{\text{HH}} = 3.5$ Hz), 6.98 (1H, d, $^3J_{\text{HH}} = 7.5$ Hz), 6.87 (1H, d, $^4J_{\text{HH}} = 3.5$ Hz), 6.71 (2H, d, $^3J_{\text{HH}} = 7.5$ Hz), 6.62 (1H, d, $^3J_{\text{HH}} = 8.5$ Hz), 6.54 (1H, d, $^4J_{\text{HH}} = 3.5$ Hz), 6.27-6.25 (2H, m), 6.20-6.10 (5H, m, Ar), 5.63 (1H, q, $^3J_{\text{HH}} = 6.5$ Hz, CH), 5.26 (1H, d, $^3J_{\text{HH}} = 10.0$ Hz, CH_2), 5.19-5.16 (4H, m, CH_2/CH), 5.11 (2H, d, $^3J_{\text{HH}} = 10.0$ Hz), 5.06 (1H, d, $^3J_{\text{HH}} = 10.0$ Hz, CH_2), 3.85 (3H, s), 3.77 (3H, s), 3.68 (3H, s), 1.81 (3H, d, $^3J_{\text{HH}} = 6.5$ Hz), 1.69 (3H, d, $^3J_{\text{HH}} = 6.5$ Hz), 1.51 (3H, d, $^3J_{\text{HH}} = 6.5$ Hz, CH_3).

$^{13}\text{C}\{^1\text{H}\}$ NMR (126 MHz, 298 K, CD_3CN) δ 162.1, 161.57, 160.6 (CHN), 160.3, 159.8, 159.7, 159.4, 150.8, 150.4, 150.2, 150.0, 149.9, 149.3, 149.1, 148.8, 144.0, 143.1, 142.7, 142.6, 141.3, 141.3, 139.9, 139.9, 139.0, 136.6, 135.9, 135.5, 133.8, 133.2, 133.0, 132.9, 132.8, 132.4, 131.3, 129.8, 129.7, 129.3, 128.8, 128.5, 128.2, 127.8, 125.1, 125.0, 124.6, 124.4, 124.3, 124.1, 124.0, 118.5, 115.5, 115.1, 115.0, 114.7 (Ar), 69.4, 69.2 (CH_2), 65.4 (CH), 65.2 (CH_2), 65.1, 64.7 (CH), 56.3, 56.1, 56.1 (OCH_3), 23.0, 23.0, 22.4 (CH_3).

MS (ESI) m/z 425 $[\text{L}+\text{H}]^+$, 501 $[\text{Zn}_2\text{L}_3][\text{ClO}_4]^{3+}$, 801 $[\text{Zn}_2\text{L}_3][\text{ClO}_4]_2^{2+}$

IR ν cm^{-1} 2900.7 br, w, 1573 w, 1513 m, 1316 w, 1249 w, 1091 s, 835 w, 622 m, 416 w.

Elemental analysis found (calculated for $\text{C}_{78}\text{H}_{72}\text{Cl}_4\text{N}_{12}\text{O}_{22}\text{Zn}_2 \cdot 4\text{H}_2\text{O}$) % C 49.23 (49.99), H 3.73 (4.03) N 8.36 (8.97).



$\Lambda_{\text{Zn,HHT}}\text{-}[\text{Zn}_2\text{L}^{22}]_3[\text{ClO}_4]_4$ was synthesised using the procedure described for $\Lambda_{\text{Zn,HHT}}\text{-}[\text{Zn}_2\text{L}^{20}]_3[\text{ClO}_4]_4$, substituting (*R*)-1-phenylethan-1-amine for (*R*)-1-(4-nitrophenyl)ethan-1-amine.

Yield 0.13 g, 47%.

^1H NMR (500 MHz, 298 K, CD_3CN) δ_{H} 9.07 (1H, s), 8.98 (1H, s, CHN), 8.53-8.47 (3H, m), 8.35 (1H, t, $^3J_{\text{HH}} = 6.5$ Hz), 8.22 (3H, d, $^3J_{\text{HH}} = 8.0$ Hz), 8.16 (3H, t, $^3J_{\text{HH}} = 8.5$ Hz), 8.12 (2H, t, $^3J_{\text{HH}} = 7.5$ Hz), 8.06 (2H, d, $^3J_{\text{HH}} = 8.0$ Hz), 7.98-7.96 (3H, m), 7.92-7.89 (4H, m), 7.86-7.76 (5H, m), 7.70 (1H, d, $^3J_{\text{HH}} = 5.5$ Hz), 7.66 (2H, d, $^3J_{\text{HH}} = 9.0$ Hz), 7.55-7.51 (4H, m), 7.37 (2H, d, $^3J_{\text{HH}} = 8.5$ Hz), 7.07-7.03 (2H, m), 6.90 (1H, s), 6.58 (1H, s), 6.52 (4H, dd, $^3J_{\text{HH}} = 8.0$ Hz, $^4J_{\text{HH}} = 4.0$ Hz, Ar), 5.85 (1H, q, $^3J_{\text{HH}} = 6.0$ Hz, CH), 5.39-5.34 (2H, m), 5.30-5.25 (2H, m, CH_2), 5.20 (1H, d, $^3J_{\text{HH}} = 9.0$ Hz, CH), 5.11 (2H, t, $^3J_{\text{HH}} = 10.0$ Hz, CH_2), 5.04 (1H, d, $^3J_{\text{HH}} = 9.0$ Hz), 1.87 (3H, t, $^3J_{\text{HH}} = 6.5$ Hz), 1.73 (3H, t, $^3J_{\text{HH}} = 6.5$ Hz), 1.47 (3H, t, $^3J_{\text{HH}} = 6.5$ Hz, CH_3).

$^{13}\text{C}\{^1\text{H}\}$ NMR (126 MHz, 298 K, CD_3CN) δ_{C} 164.1, 163.3, 162.4 (CHN), 160.8, 160.4, 159.9, 150.7, 150.5, 150.3, 150.1, 149.7, 149.4, 149.3, 149.2, 149.2, 149.0, 148.8, 148.5, 148.5, 148.4, 147.9, 147.7, 144.0, 143.0, 142.9, 142.7, 140.9, 140.8, 140.7, 140.0, 139.5, 136.8, 136.2, 135.3, 133.4, 133.3, 132.8, 129.2, 128.7, 127.9,

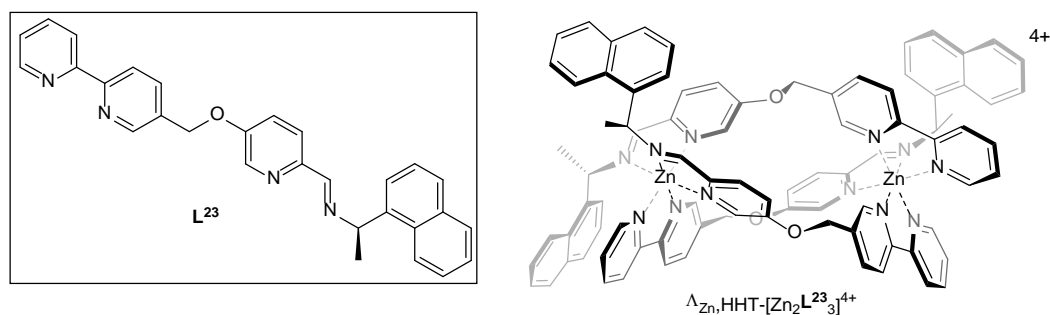
127.7, 127.6, 125.0, 125.0, 124.9, 124.5, 124.3, 124.2, 124.1, 124.1, 124.0, 118.3 (Ar), 69.3, 69.2, 69.1 (CH), 65.1, 64.6, 64.5 (CH₂), 22.6, 22.5, 21.9 (CH₃).

MS (ESI) m/z 361 [Zn₂L₃]⁴⁺

IR ν cm⁻¹ 3450 (br, w), 2986 (w), 1571 (w), 1349 (w), 1316 (w), 1082 (m), 622 (m).

Elemental analysis found (calculated for C₇₅H₆₃Cl₄N₁₅O₂₅Zn₂·4H₂O) % C 46.02 (46.94), H 3.22 (3.73), 10.55 (10.95).

$\Lambda_{\text{Zn,HHT}}\text{-[Zn}_2\text{L}^{23}\text{]}\text{[ClO}_4\text{]}_4\cdot 4\text{H}_2\text{O}$



$\Lambda_{\text{Zn,HHT}}\text{-[Zn}_2\text{L}^{23}\text{]}\text{[ClO}_4\text{]}_4$ was synthesised using the procedure described for $\Lambda_{\text{Zn,HHT}}\text{-[Zn}_2\text{L}^{20}\text{]}\text{[ClO}_4\text{]}_4$, substituting (*R*)-1-phenylethan-1-amine for (*R*)-1-(naphthalen-1-yl)ethan-1-amine.

Yield 0.068 g, 33%.

¹H NMR (500 MHz, 298 K, CD₃CN) δ_{H} 9.16 (1H, s), 8.98 (1H, s, CHN), 8.70 (2H, d, ³J_{HH} = 5.0 Hz), 8.53-8.50 (2H, m, Ar), 8.40-8.35 (3H, m, CHN / Ar), 8.25 (1H, d, ³J_{HH} = 8.0 Hz), 8.20 (2H, d, ³J_{HH} = 8.0 Hz), 8.13 (3H, t, ³J_{HH} = 9.0 Hz), 8.09 (1H, d, ³J_{HH} = 8.0 Hz), 7.99-7.75 (12H, m), 7.72-7.55 (8H, m), 7.46-7.36 (9H, m), 7.26 (2H, q, ³J_{HH} = 8.0 Hz), 7.16 (1H, br s), 7.10 (1H, s), 6.89 (1H, t, ³J_{HH} = 8.0 Hz), 6.63 (1H, t, ³J_{HH} = 8.0 Hz), 6.50 (1H, q, ³J_{HH} = 6.5 Hz), 6.34-6.28 (2H, m, Ar), 6.19 (1H, br s), 5.97 (1H, d, ³J_{HH} = 6.5 Hz, CH₂), 5.53 (1H, br s, CH), 5.39-5.27 (2H, m), 5.16 (2H,

q, $^3J_{\text{HH}} = 11.0$ Hz, CH₂), 5.07 (1H, d, $^3J_{\text{HH}} = 9.5$ Hz), 4.98 (1H, d, $^3J_{\text{HH}} = 9.5$ Hz, CH), 2.00 (3H, d, $^3J_{\text{HH}} = 6.5$ Hz), 1.83 (3H, br s), 0.49 (3H, br s, CH₃).

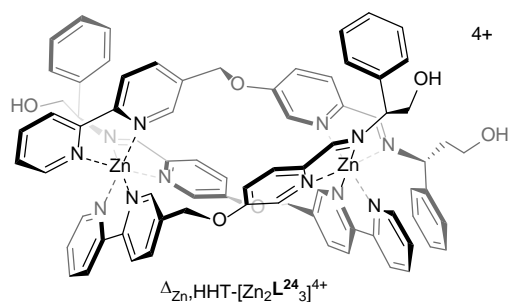
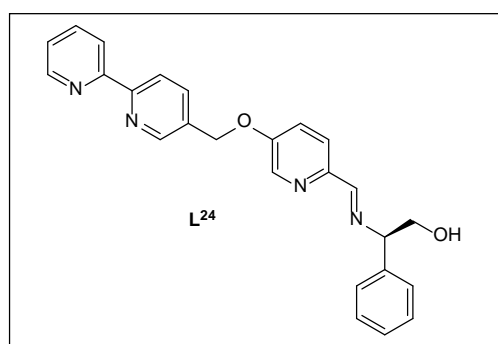
$^{13}\text{C}\{^1\text{H}\}$ NMR (126 MHz, CD₃CN) δ_{C} 163.8, 162.8, 160.8 (CHN), 160.5, 160.4, 159.9, 150.9, 150.5, 150.1, 149.9, 148.9, 148.7, 148.4, 148.0, 147.9, 144.1, 143.1, 142.9, 141.8, 141.4, 141.3, 140.8, 140.0, 139.9, 139.4, 137.9, 137.0, 136.4, 135.7, 135.4, 135.2, 134.7, 134.6, 133.1, 133.1, 131.4, 131.0, 130.7, 129.8, 129.8, 129.4, 129.1, 128.9, 128.8, 128.6, 128.0, 127.7, 127.1, 127.0, 126.6, 126.5, 125.9, 125.1, 124.7, 124.4, 124.3, 124.2, 123.7, 123.4, 123.3, 123.1 (Ar), 69.4, 69.3, 69.2, (CH₂) 65.3, 62.3, 60.5 (CH), 21.7, 20.8, 20.0 (CH₃).

MS (ESI) m/z 366 $[\text{Zn}_2\text{L}_3]^{4+}$

IR ν cm⁻¹ 3502 w, 3004 w, 1571 w, 1987 m, 780 w, 622 m.

Elemental analysis found (calculated for C₈₇H₇₂Cl₄N₁₂O₁₉Zn₂·4H₂O) % C 54.12 (54.02), H 3.85 (4.17), 8.70 (8.69).

$\Delta_{\text{Zn},\text{HHT}}\text{-}[\text{Zn}_2\text{L}^{24}]_3[\text{ClO}_4]_4\cdot 6\text{H}_2\text{O}$



$\Delta_{\text{Zn},\text{HHT}}\text{-}[\text{Zn}_2\text{L}^{24}]_3[\text{ClO}_4]_4$ was synthesised using the procedure described for $\Lambda_{\text{Zn},\text{HHT}}\text{-}[\text{Zn}_2\text{L}^{20}]_3[\text{ClO}_4]_4$, substituting (*R*)-1-phenylethan-1-amine for (*R*)-phenylglycinol.

Yield 0.102 g, 50%.

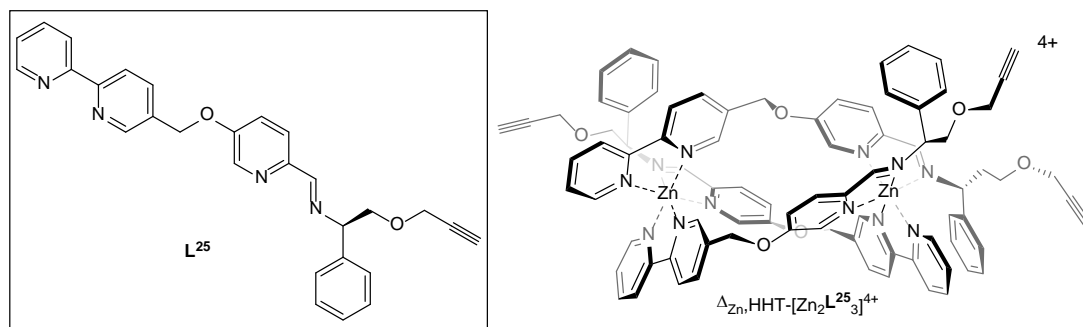
^1H NMR (400 MHz, 298 K, CD_3CN) δ_{H} 9.09 (1H, s), 9.01 (1H, s, CHN), 8.89 (1H, t, $^3J_{\text{HH}} = 4.5$ Hz), 8.51 (2H, q, $^3J_{\text{HH}} = 4.5$ Hz, Ar), 8.46 (1H, s, CHN), 8.34 (2H, t, $^3J_{\text{HH}} = 7.5$ Hz), 8.26-8.19 (3H, m), 8.16-8.03 (3H, m), 7.98 (2H, t, $^3J_{\text{HH}} = 7.0$ Hz), 7.90-7.66 (9H, m), 7.62 (1H, dd, $^3J_{\text{HH}} = 9.0$ Hz, $^4J_{\text{HH}} = 3.0$ Hz), 7.55-7.50 (4H, m), 7.19 (1H, t, $^3J_{\text{HH}} = 7.5$ Hz), 7.11-7.04 (3H, m), 6.94-6.86 (3H, m), 6.76 (3H, t, $^3J_{\text{HH}} = 7.5$ Hz), 6.65-6.59 (2H, m), 6.25-6.23 (3H, m, Ar), 5.62 (1H, q, $^3J_{\text{HH}} = 9.5$ Hz, $^4J_{\text{HH}} = 4.0$ Hz, CH), 5.21-5.01 (8H, m, CH / CH_2), 3.95-3.81 (3H, m), 3.79 (1H, t, $^3J_{\text{HH}} = 5.5$ Hz), 3.67 (1H, t, $^3J_{\text{HH}} = 5.5$ Hz), 3.35 (1H, t, $^3J_{\text{HH}} = 5.5$ Hz, CH_2).

$^{13}\text{C}\{^1\text{H}\}$ NMR (126 MHz, 298 K, CD_3CN) δ_{C} 163.4, 163.0, 162.7 (CHN), 160.3, 160.1, 159.8, 150.7, 150.5, 150.0, 149.9, 149.8, 149.8, 149.5, 149.4, 149.2, 148.7, 144.0, 142.9, 142.6, 142.6, 142.4, 142.4, 141.0, 141.0, 139.9, 139.9, 139.2, 136.5, 136.4, 136.3, 136.0, 135.7, 135.4, 133.1, 132.9, 132.5, 130.0, 129.5, 129.5, 129.3, 129.1, 129.0, 129.0, 128.6, 128.5, 128.4, 128.2, 127.8, 127.7, 127.3, 124.9, 124.9, 124.5, 124.4, 124.3, 124.2, 124.1, 124.1, 123.9 (Ar), 71.2, 71.0, 70.8 (CH), 69.3, 69.1, 69.0, 64.3, 64.0, 63.7 (CH_2).

MS (ESI) m/z 344 $[\text{Zn}_2\text{L}_3]^{4+}$

IR ν cm^{-1} 2973 w, 1571 m, 1316 w, 1223 w, 1082 s, 702 m, 654 m.

Elemental analysis found (calculated for $\text{C}_{75}\text{H}_{66}\text{Cl}_4\text{N}_{12}\text{O}_{25}\text{Zn}_2 \cdot 6\text{H}_2\text{O}$) % C 46.22 (48.22), H 3.75 (4.21), N 8.48 (9.00).

$\Delta_{\text{Zn,HHT}}\text{-}[\text{Zn}_2\text{L}^{25}]_3[\text{ClO}_4]_4\cdot 7\text{H}_2\text{O}$ 

$\Delta_{\text{Zn,HHT}}\text{-}[\text{Zn}_2\text{L}^{25}]_3[\text{ClO}_4]_4$ was synthesised using the procedure described for $\Delta_{\text{Zn,HHT}}\text{-}[\text{Zn}_2\text{L}^{20}]_3[\text{ClO}_4]_4$, substituting (*R*)-1-phenylethan-1-amine for **25**.

Yield 0.088 g, 42%.

^1H NMR (500 MHz, 298 K, CD_3CN) δ_{H} 9.01 (1H, s), 8.96 (1H, s, CHN), 8.86 (2H, s), 8.53 (1H, dd, $^3J_{\text{HH}} = 8.5$ Hz, $^4J_{\text{HH}} = 2.5$ Hz, Ar), 8.42 (1H, s, CHN), 8.33 (2H, t, $^3J_{\text{HH}} = 7.5$ Hz), 8.25 (2H, dd, $^3J_{\text{HH}} = 8.0$ Hz, $^4J_{\text{HH}} = 2.0$ Hz), 8.20 (2H, d, $^3J_{\text{HH}} = 8.5$ Hz), 8.16-7.97 (10H, m), 7.89-7.68 (8H), 7.59 (1H, dd, $^3J_{\text{HH}} = 8.5$ Hz, $^4J_{\text{HH}} = 3.0$ Hz), 7.53 (2H, t, $^3J_{\text{HH}} = 7.0$ Hz), 7.50 (1H, d, $^3J_{\text{HH}} = 8.5$ Hz), 7.45 (1H, s), 7.20 (1H, t, $^3J_{\text{HH}} = 7.5$ Hz), 7.13-7.05 (3H, m), 6.93 (1H, t, $^3J_{\text{HH}} = 7.5$ Hz), 6.90-6.86 (2H, m), 6.79 (1H, t, $^3J_{\text{HH}} = 8.0$ Hz), 6.65 (1H, d, $^4J_{\text{HH}} = 2.5$ Hz), 6.61 (1H, t, $^3J_{\text{HH}} = 8.0$ Hz), 6.27 (3H, dd, $^3J_{\text{HH}} = 8.0$ Hz, $^4J_{\text{HH}} = 3.0$ Hz, Ar), 5.65 (1H, dd, $^3J_{\text{HH}} = 11.0$ Hz, $^4J_{\text{HH}} = 3.5$ Hz, CH_2), 5.21 (3H, t, $^3J_{\text{HH}} = 10.0$ Hz, CH), 5.12 (3H, dd, $^3J_{\text{HH}} = 10.0$ Hz, $^4J_{\text{HH}} = 6.0$ Hz), 5.02 (1H, d, $^3J_{\text{HH}} = 10.0$ Hz), 4.39 (2H, d, $^4J_{\text{HH}} = 2.0$ Hz), 4.33 (2H, t, $^4J_{\text{HH}} = 2.0$ Hz), 4.28 (2H, d, $^4J_{\text{HH}} = 2.0$ Hz, CH_2), 4.19 (1H, t, $^3J_{\text{HH}} = 11.0$ Hz, CH), 4.10-4.03 (2H, m), 3.96 (1H, dd, $^3J_{\text{HH}} = 11.0$ Hz, $^4J_{\text{HH}} = 3.5$ Hz, CH_2), 3.90 (1H, t, $^3J_{\text{HH}} = 10.0$ Hz, CH), 3.74 (2H, br s, CH_2), 2.93 (1H, t, $^4J_{\text{HH}} = 2.0$ Hz), 2.91 (1H, t, $^4J_{\text{HH}} = 2.0$ Hz), 2.90 (1H, t, $^4J_{\text{HH}} = 2.0$ Hz, CCH).

Yield 0.31 g, 96%.

$^{13}\text{C}\{^1\text{H}\}$ NMR (126 MHz, 298 K, MeOH) δ_{C} 171.1, 170.8, 170.3 (CHN), 161.1, 160.9, 160.8, 160.5, 160.3, 160.0, 159.4, 158.7, 158.4, 157.2, 156.6, 155.1, 153.9, 153.8, 153.7, 142.1, 141.4, 140.8, 140.7, 140.5, 140.5, 139.7, 139.75, 139.6, 136.7, 136.6, 136.6, 133.5, 132.7, 132.5, 130.3, 130.2, 130.2, 129.9, 129.8, 129.6, 129.1, 128.9, 128.7, 128.6, 128.5, 127.6, 126.1, 126.0, 125.3, 125.0, 124.9, 124.7 (Ar), 70.5, 70.5, 69.6, 69.6, 69.5, 69.3 (CH/CH₂), 26.4, 25.6, 25.2 (CH₃).

MS (ESI) m/z 323 $[\text{Fe}_2\text{L}_3]^{4+}$

IR ν cm⁻¹ 3358 (br, s), 3001 (w), 1555 (m), 1467 (w), 1233 (m), 759 (w), 701 (m).

Elemental analysis found (calculated for C₇₅H₆₆Cl₄Fe₂N₁₂O₃·11H₂O) % C 54.70 (55.09), H 4.76 (5.42), N 9.67 (10.28).

$\Delta_{\text{Fe},\text{HHT}}\text{-}[\text{Fe}_2\text{L}^{20}_3]\text{Cl}_4\cdot 11\text{H}_2\text{O}$

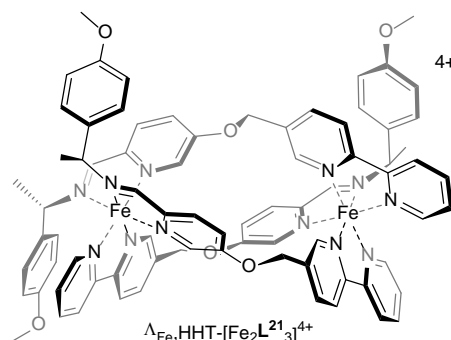
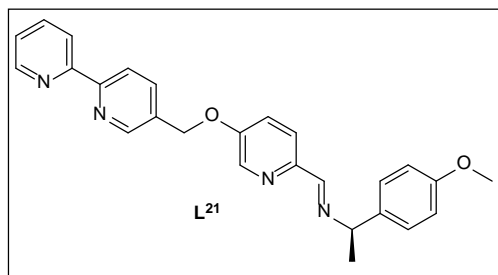
$\Delta_{\text{Fe},\text{HHT}}\text{-}[\text{Fe}_2\text{L}^{20}_3]\text{Cl}_4$ was synthesised using the procedure described for $\Lambda_{\text{Fe},\text{HHT}}\text{-}[\text{Fe}_2\text{L}^{20}_3]\text{Cl}_4$, substituting (*R*)-1-phenylethan-1-amine for (*S*)-1-phenylethan-1-amine.

Yield 0.32 g, 96%.

MS (ESI) m/z 323 $[\text{Fe}_2\text{L}_3]^{4+}$

IR ν cm⁻¹ 3348 (br, s), 2986 (m), 1555 (w), 1301 (w), 1233 (m), 759 (w), 701 (w).

Elemental analysis found (calculated for C₇₅H₆₆Cl₄Fe₂N₁₂O₃·11H₂O) % C 55.02 (55.09), H 4.99 (5.42), N 10.04 (10.28).

$\Lambda_{\text{Fe,HHT}}\text{-[Fe}_2\text{L}^{21}\text{]}_3\text{Cl}_4\cdot 14\text{H}_2\text{O}$ 

$\Lambda_{\text{Fe,HHT}}\text{-[Fe}_2\text{L}^{21}\text{]}_3\text{Cl}_4$ was synthesised using the procedure described for $\Lambda_{\text{Fe,HHT}}\text{-[Fe}_2\text{L}^{20}\text{]}_3\text{Cl}_4$, substituting (*R*)-1-phenylethan-1-amine for (*R*)-1-(4-methoxyphenyl)ethan-1-amine.

Yield 0.33 g, 94%.

$^{13}\text{C}\{^1\text{H}\}$ NMR (126 MHz, 298 K, MeOH) δ_{C} 170.6, 170.9, 169.7 (CHN), 161.8, 161.1, 161.0, 160.9, 160.6, 160.5, 160.4, 160.2, 160.0, 159.4, 158.6, 158.3, 157.2, 156.6, 155.0, 154.0, 153.9, 153.8, 140.5, 139.7, 139.6, 136.7, 136.6, 133.3, 133.1, 132.6, 132.5, 131.3, 129.8, 129.1, 129.0, 128.5, 127.4, 127.4, 125.9, 125.3, 125.0, 124.9, 124.5, 115.6, 115.4, 115.2, 114.9 (Ar), 70.5, 70.0, 69.6, 69.5, 69.0, 68.7 (CH/CH₂), 56.0, 55.9, 55.9, (OCH₃), 26.3, 25.5, 25.1 (CH₃).

MS (ESI) m/z 346 $[\text{Fe}_2\text{L}_3]^{4+}$

IR ν cm⁻¹ 3359 br s, 2968 m, 1607 w, 1510 m, 1301 m, 1235 s, 1023 m, 834 m.

Elemental analysis found (calculated for C₇₈H₇₂Cl₄Fe₂N₁₂O₆·14H₂O) % C 51.97 (52.65), H 5.33 (5.67), N 9.29 (9.45).

$\Delta_{\text{Fe,HHT}}\text{-[Fe}_2\text{L}^{21}\text{]}_3\text{Cl}_4\cdot 14\text{H}_2\text{O}$

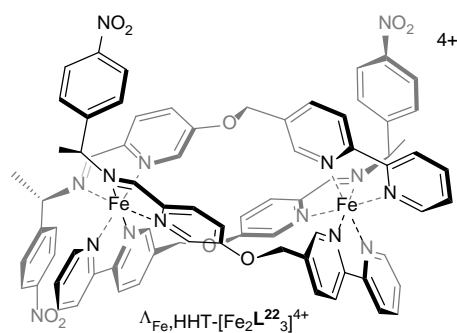
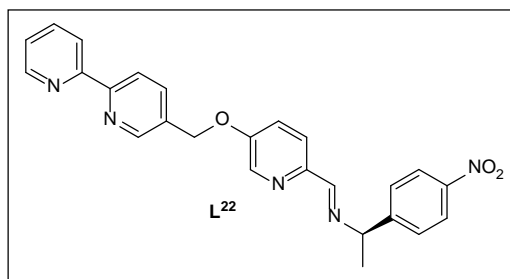
$\Delta_{\text{Fe,HHT}}\text{-[Fe}_2\text{L}^{21}\text{]}_3\text{Cl}_4$ was synthesised using the procedure described for $\Delta_{\text{Fe,HHT}}\text{-[Fe}_2\text{L}^{21}\text{]}_3\text{Cl}_4$, substituting (*R*)-1-phenylethan-1-amine for (*S*)-1-phenylethan-1-amine.

Yield 0.32 g, 96%.

MS (ESI) m/z 346 $[\text{Fe}_2\text{L}_3]^{4+}$

IR ν cm^{-1} 3350 br s, 2968 m, 1697 w, 1510 m, 1302 m, 1236 s, 1178 m, 1012 m, 834 m, 544 w.

Elemental analysis found (calculated for $\text{C}_{78}\text{H}_{72}\text{Cl}_4\text{Fe}_2\text{N}_{12}\text{O}_6\cdot 14\text{H}_2\text{O}$) % C 52.83 (52.65), H 5.48 (5.67), N 9.43 (9.45).

 $\Delta_{\text{Fe,HHT}}\text{-[Fe}_2\text{L}^{22}\text{]}_3\text{Cl}_4\cdot 13\text{H}_2\text{O}$ 

$\Delta_{\text{Fe,HHT}}\text{-[Fe}_2\text{L}^{22}\text{]}_3\text{Cl}_4$ was synthesised using the procedure described for $\Delta_{\text{Fe,HHT}}\text{-[Fe}_2\text{L}^{20}\text{]}_3\text{Cl}_4$, substituting (*R*)-1-phenylethan-1-amine for (*R*)-1-(4-nitrophenyl)ethan-1-amine.

Yield 0.36 g, 99%.

MS (ESI) m/z 357 $[\text{Fe}_2\text{L}_3]^{4+}$

IR ν cm^{-1} 3352 br s, 3035 m, 1602 m, 1561 m, 1216 m, 1344 s, 1232 s, 1011 m, 853 m, 788 w, 753 w.

Elemental analysis found (calculated for $\text{C}_{75}\text{H}_{63}\text{Cl}_4\text{Fe}_2\text{N}_{15}\text{O}_9 \cdot 13\text{H}_2\text{O}$) % C 48.88 (49.88), H 4.31 (4.97), N 10.65 (11.63).

$\Delta_{\text{Fe},\text{HHT}}\text{-}[\text{Fe}_2\text{L}^{22}_3]\text{Cl}_4 \cdot 13\text{H}_2\text{O}$

$\Delta_{\text{Fe},\text{HHT}}\text{-}[\text{Fe}_2\text{L}^{22}_3]\text{Cl}_4$ was synthesised using the procedure described for $\Delta_{\text{Fe},\text{HHT}}\text{-}[\text{Fe}_2\text{L}^{22}_3]\text{Cl}_4$, substituting (*R*)-1-phenylethan-1-amine for (*S*)-1-phenylethan-1-amine.

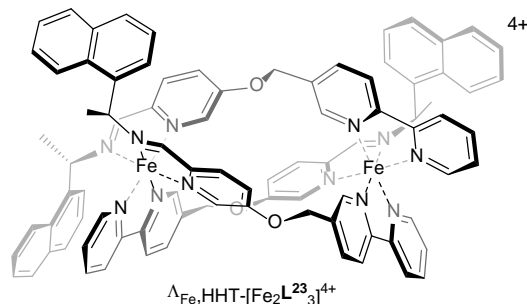
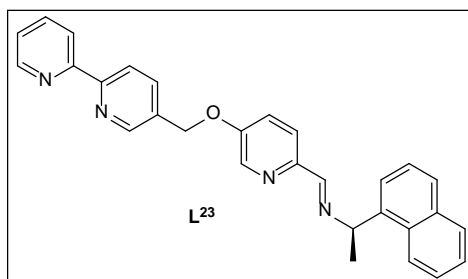
Yield 0.33 g, 90%.

MS (ESI) m/z 357 $[\text{Fe}_2\text{L}_3]^{4+}$

IR ν cm^{-1} 3351 br s, 3036 m, 1602 m, 1562 m, 1513 s, 1501 s, 1343 s, 1301 m, 1232 s, 1205 s, 1009 m, 853 m, 787 m, 670 m.

Elemental analysis found (calculated for $\text{C}_{75}\text{H}_{63}\text{Cl}_4\text{Fe}_2\text{N}_{15}\text{O}_9 \cdot 13\text{H}_2\text{O}$) % C 50.15 (49.88), H 4.35 (4.97), N 10.89 (11.63).

$\Delta_{\text{Fe},\text{HHT}}\text{-}[\text{Fe}_2\text{L}^{23}_3]\text{Cl}_4$



$\Delta_{\text{Fe},\text{HHT}}\text{-}[\text{Fe}_2\text{L}^{23}_3]\text{Cl}_4$ was synthesised using the procedure described for $\Delta_{\text{Fe},\text{HHT}}\text{-}[\text{Fe}_2\text{L}^{20}_3]\text{Cl}_4$, substituting (*R*)-1-phenylethan-1-amine for (*R*)-1-(naphthalen-1-yl)ethan-1-amine.

Yield 0.267 g, 89%.

$^{13}\text{C}\{^1\text{H}\}$ NMR (126 MHz, 298 K, MeOH) δ_{C} 172.7, 172.2, 171.7 (CHN), 161.1, 161.9, 160.5, 160.4, 160.0, 159.7, 158.9, 157.7, 156.5, 155.4, 153.6, 153.4, 151.8, 149.5, 148.6, 148.5, 148.4, 148.3, 147.9, 147.4, 144.7, 142.8, 142.3, 141.2, 141.0, 140.6, 140.2, 140.0, 137.2, 137.1, 136.9, 136.6, 134.0, 133.4, 132.9, 130.6, 129.9, 129.6, 129.0, 128.9, 127.6, 127.5, 126.9, 125.2, 125.1, 125.1, 124.9, 124.8, 124.7, 124.4, 123.3, 122.8, 122.4 (Ar), 70.5 (CH_2), 69.8 (CH), 69.6, 69.5 (CH_2), 68.8, 68.7 (CH), 27.1, 25.9, 25.0 (CH_3).

MS (ESI) m/z 467 $[\text{L}+\text{Na}]^+$, 493 $[\text{Fe}_2\text{L}_3][\text{Cl}]^{3+}$

IR ν cm^{-1} 3364 br s, 2973 m, 1568 w, 1510 w, 1228 m, 1074 m, 702 w, 621 w.

$\Delta_{\text{Fe},\text{HHT}}\text{-}[\text{Fe}_2\text{L}^{23}_3]\text{Cl}_4$

$\Delta_{\text{Fe},\text{HHT}}\text{-}[\text{Fe}_2\text{L}^{23}_3]\text{Cl}_4$ was synthesised using the procedure described for $\Lambda_{\text{Fe},\text{HHT}}\text{-}[\text{Fe}_2\text{L}^{23}_3]\text{Cl}_4$, substituting (*R*)-1-phenylethan-1-amine for (*S*)-1-phenylethan-1-amine.

Yield 0.211 g, 77%.

MS (ESI) m/z 467 $[\text{L}+\text{Na}]^+$, 493 $[\text{Fe}_2\text{L}_3][\text{Cl}]^{3+}$

IR ν cm^{-1} 3356 br s, 2975 m, 1567 w, 1531 m, 1229 m, 1074 m, 702 w, 621 w.

 $\Delta_{\text{Fe,HHT}}\text{-}[\text{Fe}_2\text{L}^{25}_3]\text{Cl}_4\cdot 9\text{H}_2\text{O}$

$\Delta_{\text{Fe,HHT}}\text{-}[\text{Fe}_2\text{L}^{25}_3]\text{Cl}_4$ was synthesised using the procedure described for $\Delta_{\text{Fe,HHT}}\text{-}[\text{Fe}_2\text{L}^{25}_3]\text{Cl}_4$, substituting **25** for **24**.

Yield 0.222 g, 74%.

MS (ESI) m/z 364 $[\text{Fe}_2\text{L}_3]^{4+}$, 449 $[\text{L}+\text{H}]^+$.

IR ν cm^{-1} 3355 br s, 3027 m, 1556 w, 1486 w, 1233 m, 1082 m, 700 m.

Elemental analysis found (calculated for $\text{C}_{84}\text{H}_{72}\text{Cl}_4\text{Fe}_2\text{N}_{12}\text{O}_6\cdot 9\text{H}_2\text{O}$) % C 56.68 (57.29), H 4.85 (5.15), N 9.29 (9.54).

5.8 Molecular modelling

Conducted by Dr Alan Faulkner, University of Warwick.

Starting points for geometry optimisations were taken from crystallographic data that was available, and where unavailable, starting structures were created from existing crystallographic fragments. Monometallic structures were first optimised using the B3LYP-D3(BJ)¹⁶ functional and the 6-31g* basis set, with convergence criteria of 0.0001 a.u. as implemented in the Firefly quantum chemistry package,¹⁷ which is partially based on the GAMESS(US) source code.¹⁸ Bimetallic systems were optimised using ligand field molecular mechanics (LFMM)¹⁹ as implemented in the DommiMOE program,²⁰ before being annealed at 500 K for 1 ns prior to re-optimisation. Single point energy calculations of all structures were performed using the B3LYP-D3(BJ)¹⁶ functional and the def2-TZVP basis set with energy convergence criteria of 0.0001 a.u. as implemented in the Firefly quantum chemistry package.¹⁷

Where indicated these calculations were conducted by employing the RIJCOSX approximation with SCF convergence criteria set to ‘tight’, both of which are defined internally as part of the ORCA DFT quantum chemistry package.²¹ Where relevant, acetonitrile solvate correction was performed using the conductor-like screening model (COSMO)²² as implemented in ORCA.²¹

5.9 Biophysical analysis

5.9.1 Circular dichroism

Each compound was dissolved in water to 0.03 mM and spectra were measured on a Jasco J-815 spectrometer, calibrated conventionally using a 0.060% ACS holmium filter. Measurements were collected using a 1 cm path-length quartz cuvette. The parameters used were; bandwidth 1 nm, response time 1 sec, wavelength scan range 200 – 750 nm, data pitch 0.2 nm, scanning speed 100 nm/min and accumulation 4.

5.9.2 Thermogravimetric analysis

To determine the amount of water of crystallisation present in the chloride salts of iron (II) triplex helicates thermogravimetric analysis was performed using a DSC1-1600 scanning calorimeter. An accurately weighed 40 μ l aluminium crucible was heated from 25 to 400°C at 10 °C/min under dinitrogen. The mass lost was plotted against temperature and the % mass loss from ambient temperature to 200°C (loss of water) was calculated; a worked example is shown in Appendix A.

5.9.3 Absorbance spectroscopy and stability

Visible absorbance spectra for stability studies were recorded using a Carey IE spectrometer. Measurements were collected in a 1 cm path-length polystyrene cuvette and the standard parameters used were bandwidth 1 nm, response time 1 sec, wavelength scan range 350 – 800 nm, data pitch 0.2 nm, scanning speed 200 nm/min and accumulation 1. A 0.03 mM solution of each compound was measured in water (20°C, every 7 d for 50 d) RPMI-1640 cell culture medium (37°C, every 6 h for 96 h) and 0.2 M hydrochloric acid (20°C, every 2 h for 24 h) was measured.

5.9.4 Denaturation of ct-DNA

ct-DNA (0.5 mg/ml, 7.5×10^{-5} per base, as determined by absorbance at 200 nm) was mixed with each complex (7.5 μ M) in buffered conditions (10mM Tris, 1 mM EDTA at pH 7.0) to give 10 base: 1 complex. The absorbance at 260 nm as a function of temperature (every 1°C, 25-90°C) was measured in a 1 cm masked quartz cuvette at a rate of 0.4°C min⁻¹ and run in triplicate. T_m was calculated from the first derivative of a Boltzmann sigmoidal fit of the plot of absorbance at 260 nm against temperature for each complex.

5.10 Antimicrobial Activity

Conducted by Daniel Simpson, University of Warwick.

Verified stocks of MRSA [USA300] and *E. coli* [TOP10] were grown to 10^8 cfu/ml (cfu = colony forming units) respectively in sterile Luria-Bertani (LB) medium, as measured by OD₆₀₀ (optical density measured at wavelength: 600 nm) and confirmed by hemocytometer measurement. These were used to dilute to 10^6 cfu/ml in sterile Mueller-Hinton (MH) broth (15% w/v glycerol) and flash-frozen in liquid N₂ to store before use.

Minimum inhibitory concentrations (MICs)²³ were established using the standardised macrobroth dilution method in cation-adjusted MH broth. 200 µl aliquots (128 µg/ml of each complex in sterilized MH broth, diluted 2^n µg/ml \times 5) were added to 96-well plates in duplicate. This was inoculated with each bacterial strain (bacterial density of 10^3 cfu/ml, ~200 cells per well) and sealed. After mixing at 720 strokes/min for 10 seconds, growth was monitored over 20 h at 37 °C by recording OD₆₀₀ every 10 mins with an iEMS 96-well plate reader. The lowest concentration to inhibit growth across each repeat is classified as the MIC. Positive (medium and untreated bacteria) and negative (medium only) controls were run with each plate. The antimicrobial properties of our recently reported flexicate systems¹³ were reproduced as a positive control alongside ampicillin.

5.11 Pharmacology

Conducted in collaboration with Dr Roger Phillips and Dr Qasem Abdallah, Institute of Cancer Therapeutics.

Complete cell media containing either – for cancerous cells – RPMI-1640, supplemented with 10% foetal calf serum, sodium pyruvate (1 mM) and L-glutamine (2 mM), or – for normal cells – DMEM/F12 (1:1), supplemented with 10% foetal calf serum and L-glutamine (2 mM), was used to prepare the desired cell concentration and reference wells.

Stocks of MDA-MB-468 (human breast adenocarcinoma), HCT116 p53^{+/+} (human colon carcinoma, wild type p53), HCT116 p53^{-/-} (human colon carcinoma, mutated p53) and ARPE19 (human retinal pigment epithelium) were maintained in T75 flasks in complete cell medium. At 80% confluence cells were passaged and seeded into new flasks or used in the following experiments.

5.11.1 MTT assay

Cells were incubated in 96-well plates at a cell concentration of 2.0×10^4 cells/ml for 24 h at 37°C in an atmosphere of 5% CO₂, prior to drug exposure. All compounds were dissolved in sterilized deionised water to give an initial concentration of 100 mM and diluted further with complete cell media to obtain concentrations ranging from 100 µM – 5 nM. Cell media (200 µl) was added to the reference cells and differing concentrations of drug solution (200 µl) were added to the remaining wells. The plates were incubated for a further 96 h at 37°C in an atmosphere of 5% CO₂. 3-(4,5-Dimethylthiazol-1-yl)-2,5-diphenyltetrazolium bromide (MTT) solution (0.5 mg/ml, 20 µl per well) was added to each well and incubated for a further 4 h at 37°C in an atmosphere of 5% CO₂. Upon completion

all solutions were removed from the wells and dimethyl sulfoxide (150 μ l) was added to each well to dissolve the purple formazan crystals. A Thermo Scientific Multiskan EX microplate photometer was used to measure the absorbance at 540 nm. Lanes containing 100% cell media and untreated cells were used as a blank and 100% cell survival respectively. Cell survival was determined as the absorbance of treated cells minus the blank cell media, divided by the absorbance of the untreated control; this value was expressed as a percentage. The IC₅₀ values were determined from a plot of percentage cell survival against drug concentration (μ M). All assays were conducted in triplicate and the mean IC₅₀ \pm standard deviation was determined.

5.11.2 Single cell gel electrophoresis (comet assay)

Conducted in collaboration with Dr Roger Phillips and Dr Qasem Abdallah, Institute of Cancer Therapeutics.

The induction of single strand breaks (SSB) and cross linking in HCT116 p53^{+/+} cells was determined *via* single cell gel electrophoresis. Cells were seeded at 3×10^5 cells in 6 well plates in complete RPMI-1640 medium and incubated for 18 h at 37°C in an atmosphere of 5% CO₂. Following treatment with each compound (10 μ M in complete RPMI-1640 medium for 24 h) the cells were washed twice with Hanks balanced salt solution (HBSS), harvested by trypsinisation and embedded in 0.5% low-melting point agarose and transferred to agarose coated glass slides. These slides were immersed in freshly prepared ice-cold lysis buffer (2.5 M NaCl, 100 mM Na₂EDTA, 10 mM Tris base, 1% sodium hydroxide, pH 10.0) 1% Triton X-100 and 10% dimethyl sulfoxide. The slides were then submerged in electrophoresis buffer (300 mM sodium hydroxide, 1 mM Na₂EDTA, pH > 13.0) for 30 min in a horizontal gel electrophoresis, and then subjected to electrophoresis at 0.6 V cm⁻¹ for 25 min. Following electrophoresis, the slides were neutralised (3 \times drop wise

addition of 0.4 M Trisma buffer, pH 7.5) rinsed with water and fixed with 100% ice-cold ethanol and dried in air for 18 h. To detect cross-links drug treated cells were further treated with 100 μ M of hydrogen peroxide for 20 minutes prior to gel electrophoresis. Immediately before analysis the slides were stained with SYBRTM Gold solution (Molecular probes Inc.) and viewed with an epifluorescent microscope (Nikon Eclipse E800, Japan). The tail moment was measured on 50 randomly selected cells using Comet assay III software (Perceptive Instruments, UK) and each assay was performed in triplicate.

5.11.3 FACS assay (γ -H₂AX expression and cell cycle analysis)

Conducted in collaboration with Dr Roger Phillips and Dr Qasem Abdallah, Institute of Cancer Therapeutics.

HCT116 p53^{+/+} cells (5×10^5 cells/flask, 10 ml complete RPMI-1640 medium) were incubated for 18 h at 37°C in 5% CO₂, then treated with 10 μ M triplex metallohelix (10 ml in complete RPMI-1640 medium for 24 h). The supernatant, containing any dead cells, was collected and the cells were harvested by trypsinisation. This single cell suspension in trypsin was added to the supernatant and centrifuged at 1500 rpm (300 g) for 5 min. The cells were washed twice with PBS (phosphate buffered saline), re-suspended in ice-cold methanol in PBS (90:10) and incubated in ice for 30 min, then stored at -20°C until required for analysis.

For γ -H₂AX expression the pre-treated cells were washed twice in incubation buffer (PBS containing 0.5 mM BSA) then re-suspended in 100 μ l incubation buffer for 10 min at room temperature. 2 μ l of primary rabbit anti-human phosphor Histone H2AX (Ser 139) antibody (1:50 final dilution) was added and incubated at RT for a further 1 h. This was then washed twice with incubation buffer, re-suspended in 100

µl incubation buffer containing Alexa Fluor conjugated anti-rabbit IgG secondary antibody (1:1000 final dilution) and incubated in the absence of light at room temperature for 30 min then the cells were stored at 0°C until analysis using the FACS. The H2AX expression assay was repeated in triplicate with each compound and the mean expression \pm standard deviation was determined.

For cell cycle analysis 300 µl PBS containing Propidium Iodide (40 µg/ml) and RNase A (200 µg/ml) was added to the pre-treated cells and they were incubated in the absence of light at room temperature for 30 min. 200µl ice-cold PBS was added (final volume of 600 µl) and the cells were placed on ice until analysis using the FACS. The cell cycle assay was repeated four times with each compound and the mean % cells in each phase \pm standard deviation was determined. Red fluorescence was observed at 488 nm excitation by flow cytometry and data analysed using WinMDI2.9 and Cylchred software

5.11.4 Flow cytometry (apoptosis induction)

Conducted by Dr Simon Allison, Institute of Cancer Therapeutics.

HCT116 p53^{+/+} cells (5×10^5 cells/flask, 10 ml complete RPMI-1640 medium) were incubated for 18 h at 37°C in 5% CO₂, then treated with 20 µM triplex metallohelix (10 ml in complete RPMI-1640 medium for 72 h) or fresh media containing no drug (control). The supernatant, containing any dead cells, was collected and the cells were harvested by trypsinisation. This single cell suspension in trypsin was added to the supernatant and centrifuged at 1500 rpm (300 g) for 5 min. The cells were washed with twice with PBS (2 ml) and stained with propidium iodide (100 µl) and Annexin-V-FLUOS labelling solution (100 µl).²⁴ The proportion

of live, early apoptotic and late apoptotic/necrotic cells were then quantified by flow cytometry.²⁵

5.11.5 Cell localisation assay

Conducted in collaboration with Dr Roger Phillips, Institute of Cancer Therapeutics.

Click-iT® reaction buffer (4 ml of component A in 36 ml distilled water) and Click-iT® buffer additive (Component C in 4 ml distilled water) were prepared in advance. Click-iT® reaction buffer (4.4 ml), copper sulphate (100 µL), Click-iT® buffer additive (500 µl) and Alexa Fluor® 555 azide (8.5 µL) were mixed together and the Click-iT® reaction cocktail was used immediately after being prepared. HCT116 p53^{+/+} cells were seeded at 2000 cells per well in complete RPMI-1640 medium (100 µl per well) into Lab-Tek II borosilicate eight-chamber plates and incubated at 37°C, 5% CO₂ for 24 h, prior to drug exposure. All compounds were dissolved in distilled water to give an initial concentration of 100 mM and diluted further with cell media to obtain concentrations ranging from 100 µM – 140 nM. Cell media (200 µl) was added to the reference chamber and differing concentrations of drug solution (100 µl) were added to the remaining chambers. The plates were incubated for a further 24 h at 37°C in an atmosphere of 5% CO₂. The treated cells were fixed with 4% paraformaldehyde in PBS for 10 min, washed with PBS, permeabilised with 0.2% Triton-X 100 in PBS for 5 min, washed with PBS, quenched with 0.1% sodium borohydride in PBS for 5 min and finally washed with PBS three times. The cells were then washed with 2% BSA in PBS, freshly prepared Click-iT® cell reaction cocktail was added (500 µl per well) and the cells were incubated at ambient temperature in the absence of light for 30 min, after which the cells were washed with 2% BSA in PBS. These slides were then analysed by confocal microscopy.

5.12 References

1. O. V. Dolomanov, L. J. Bourhis, R. J. Gildea, J. A. K. Howard and H. Puschmann, *J. Appl. Crystallogr.*, 2009, **42**, 339-341.
2. G. M. Sheldrick, *Acta Crystallogr., Sect. A*, 2008, **64**, 112-122.
3. M. Seredyuk, A. B. Gaspar, V. Ksenofontov, Y. Galyametdinov, J. Kusz and P. Gütllich, *J. Am. Chem. Soc.*, 2008, **130**, 1431-1439.
4. S. M. Bakunova, S. A. Bakunov, T. Wenzler, T. Barszcz, K. A. Werbovetz, R. Brun and R. R. Tidwell, *J. Med. Chem.*, 2009, **52**, 4657-4667.
5. R. Machinek and W. LÜTtke, *Synthesis*, 1975, **1975**, 255-256.
6. R. H. Mitchell and V. S. Iyer, *Synlett*, 1989, **1989**, 55-57.
7. J. S. Zakhari, I. Kinoyama, M. S. Hixon, A. Di Mola, D. Globisch and K. D. Janda, *Bioorgan. Med. Chem.*, 2011, **19**, 6203-6209.
8. Y. Hsiao and L. S. Hegedus, *J. Org. Chem.*, 1997, **62**, 3586-3591.
9. K. Sutowardoyo, M. Emziane and D. Sinou, *Tetrahedron Lett.*, 1989, **30**, 4673-4676.
10. R. N. Bream, S. V. Ley, B. McDermott and P. A. Procopiou, *J. Chem. Soc., Perkin Trans. 1*, 2002, 2237-2242.
11. S. E. Howson, *Ph.D. Thesis, University of Warwick*, 2011.
12. Z. Y. Chang and R. M. Coates, *J. Org. Chem.*, 1990, **55**, 3475-3483.
13. S. E. Howson, A. Bolhuis, V. Brabec, G. J. Clarkson, J. Malina, A. Rodger and P. Scott, *Nat. Chem.*, 2012, **4**, 31-36.
14. P. Das, A. Ghosh, M. K. Kesharwani, V. Ramu, B. Ganguly and A. Das, *Eur. J. Inorg. Chem.*, 2011, **2011**, 3050-3058.
15. C. Dallaire, I. Kolber and M. Gingras, *Org. Synth.*, 2002, **78**, 42.
16. S. Grimme, S. Ehrlich and L. Goerigk, *J. Comput. Chem.*, 2011, **32**, 1456-1465.
17. A. A. Granovsky, *Firefly version 7.1.G*, <http://classic.chem.msu.su/gran/firefly/index.html>, accessed 25/07/2014.
18. M. W. Schmidt, K. K. Baldridge, J. A. Boatz, S. T. Elbert, M. S. Gordon, J. H. Jensen, S. Koseki, N. Matsunaga, K. A. Nguyen, S. Su, T. L. Windus, M. Dupuis and J. A. Montgomery, *J. Comput. Chem.*, 1993, **14**, 1347-1363.
19. R. J. Deeth, A. Anastasi, C. Diedrich and K. Randell, *Coord. Chem. Rev.*, 2009, **253**, 795-816.
20. R. J. Deeth, N. Fey and B. Williams-Hubbard, *J. Comput. Chem.*, 2005, **26**, 123-130.
21. F. Neese, *Wiley Interdiscip. Rev.: Comput. Mol. Sci.*, 2012, **2**, 73-78.
22. A. Klamt, *J. Phys. Chem.*, 1995, **99**, 2224-2235.
23. J. M. Andrews, *J. Antimicrob. Chemother.*, 2001, **48** (suppl 1), 5-16.
24. G. Koopman, C. Reutelingsperger, G. Kuijten, R. Keehnen, S. Pals and M. van Oers, *Blood*, 1994, **84**, 1415-1420.
25. *Apoptosis, Cytotoxicity and Cell Proliferation*, 4th edn., Roche Diagnostics GmbH, Mannheim, Germany, 2008.

Appendix A

A.1 Absorbance spectroscopy

A.1.1 Circular dichroism spectra

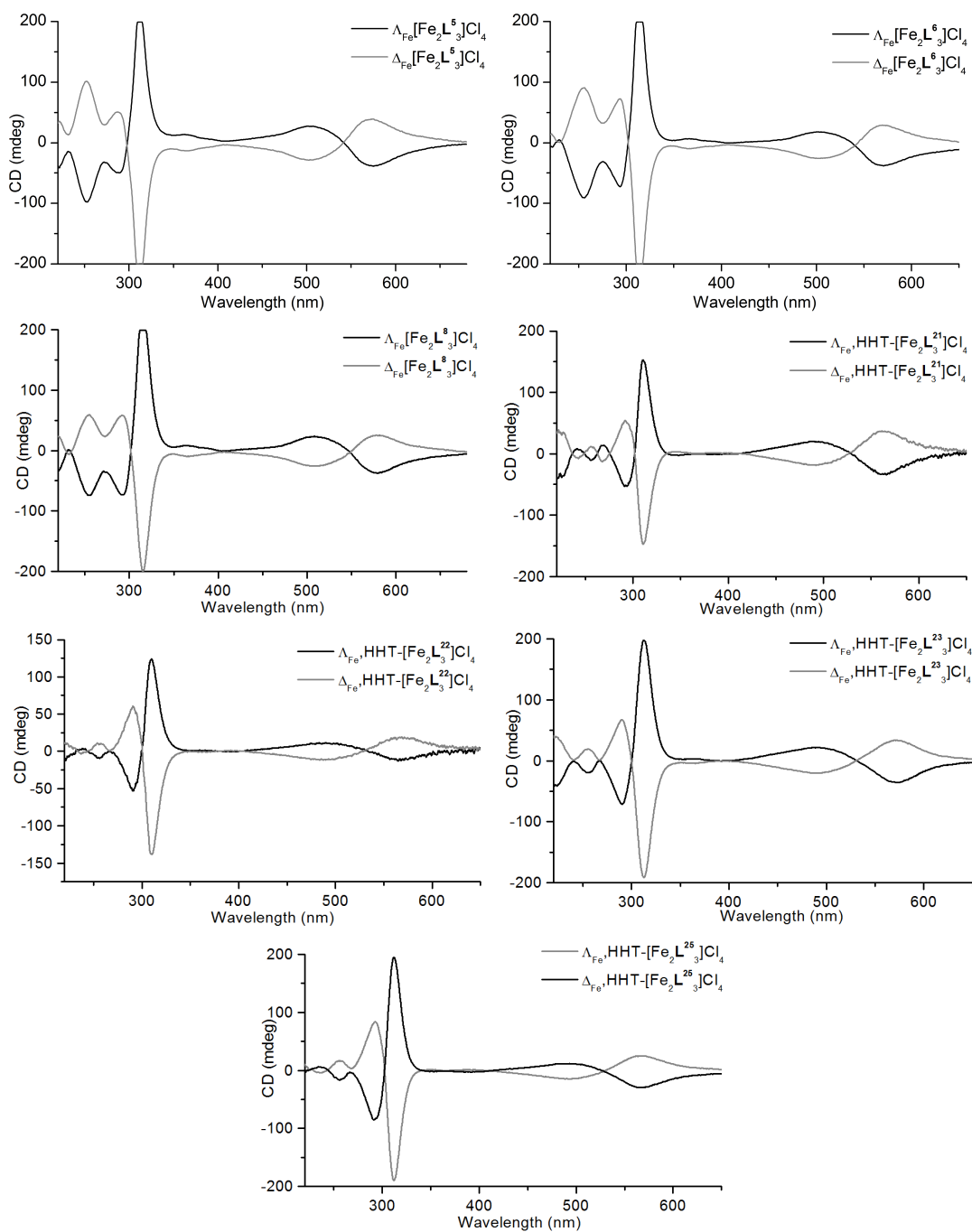


Figure A.1 | Circular Dichroism spectra of each pair of $[\text{Fe}_2\text{L}_3]\text{Cl}_4$ enantiomers in water (0.03 mM).

A.1.2 Water stability studies

The $\ln(\epsilon)$ of absorbance at 540.0 nm (MLCT band) of each iron(II) chloride complex was plotted against time in hours in water (0.03 mM). It can be seen that triplex metallohelices decay with first order rate kinetics. The decay of the complexes was best modelled *via* the following rate equations; k can be calculated from the gradient of a linear fit of $\ln(\epsilon_{540 \text{ nm}})$ vs time. Due to the high experimental error all the iron(II) chloride complexes were investigated in dilute hydrochloric acid.

$$\ln[A] = -kt + \ln[A]_0 \quad t_{1/2} = \frac{\ln(2)}{k}$$

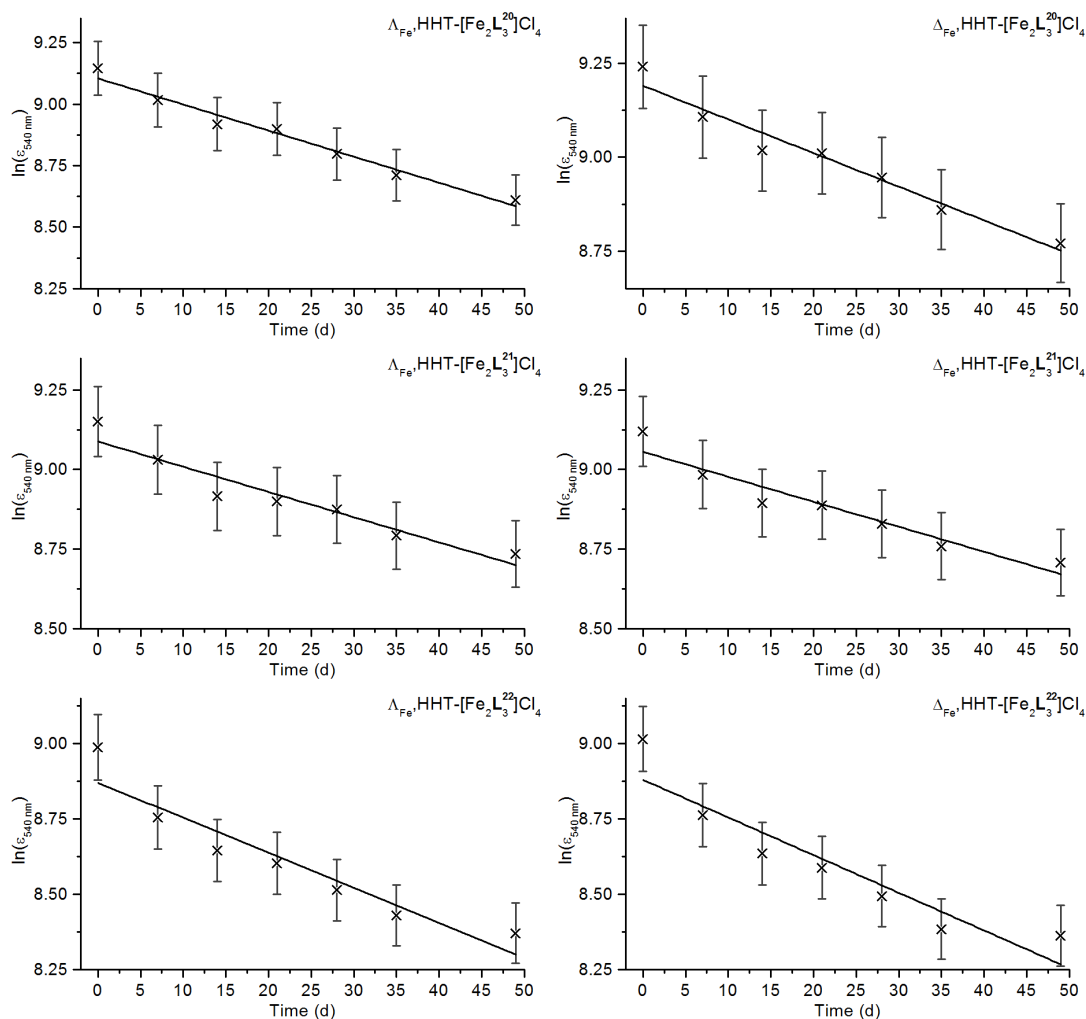
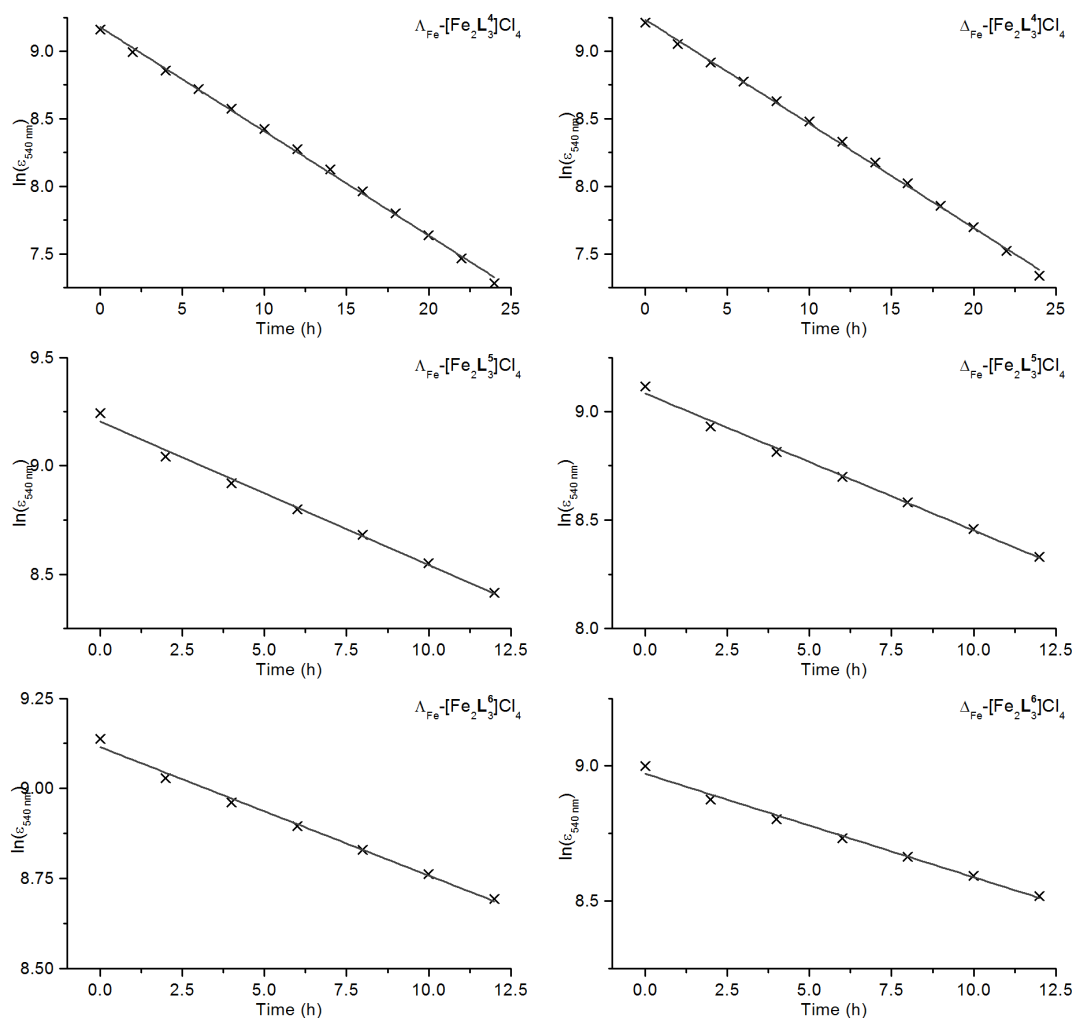


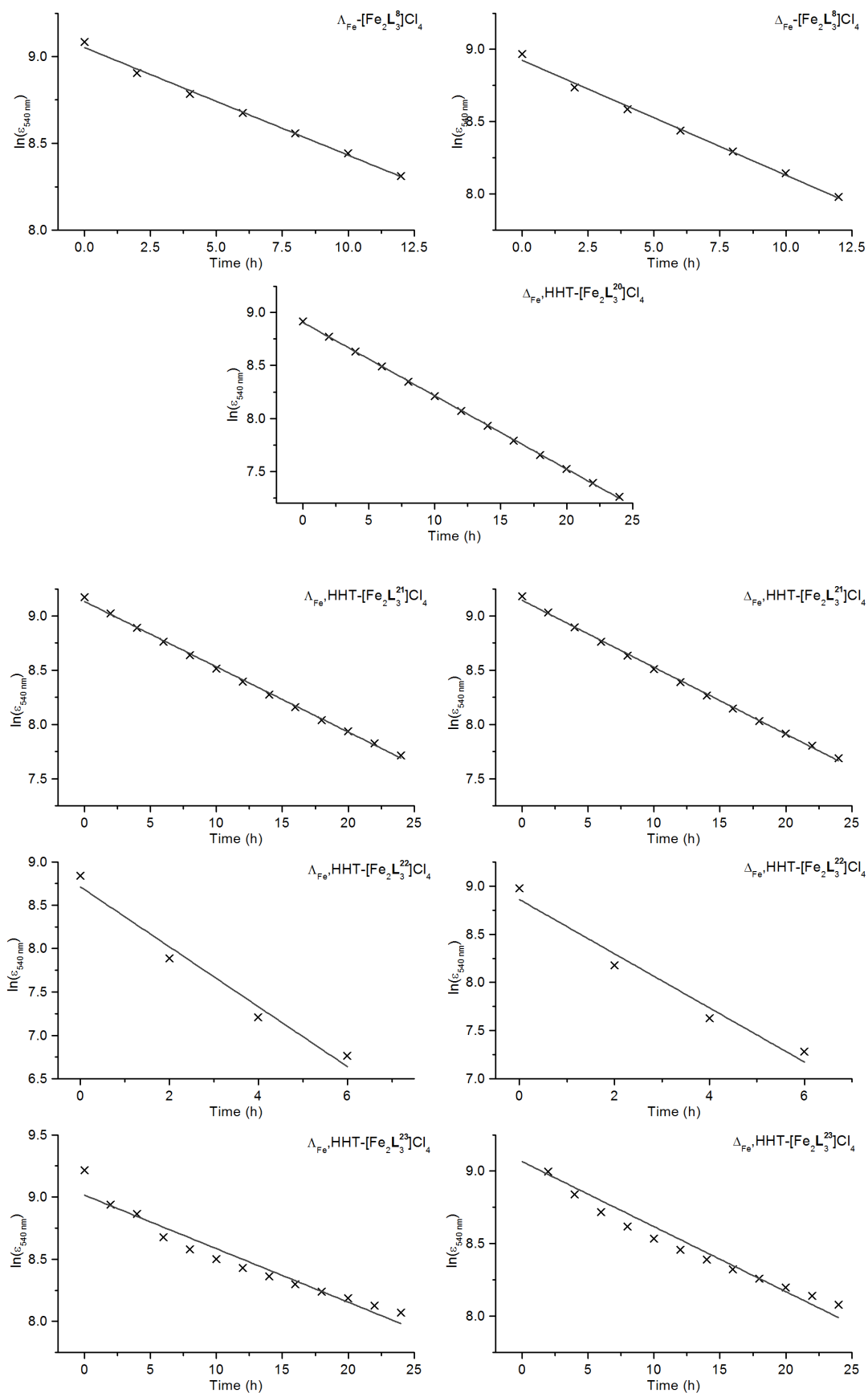
Figure A.2 | $\ln(\epsilon)$ at 540 nm (corresponding to MLCT band) of iron(II) chloride triplex metallohelices (0.03 mM in water).

A.1.3 Dilute acid stability studies

The $\ln(\epsilon)$ of absorbance at 540.0 nm (MLCT band) of each iron(II) chloride complex was plotted against time in hours in dilute hydrochloric acid (0.03 mM). It can be seen that flexicates and triplex metallohelices decay with first order rate kinetics. The complexes all decay *via* the following rate equations; k can be calculated from the gradient of a linear fit of $\ln(\epsilon_{540\text{ nm}})$ vs time.

$$\ln[A] = -kt + \ln[A]_0 \quad t_{1/2} = \frac{\ln(2)}{k}$$





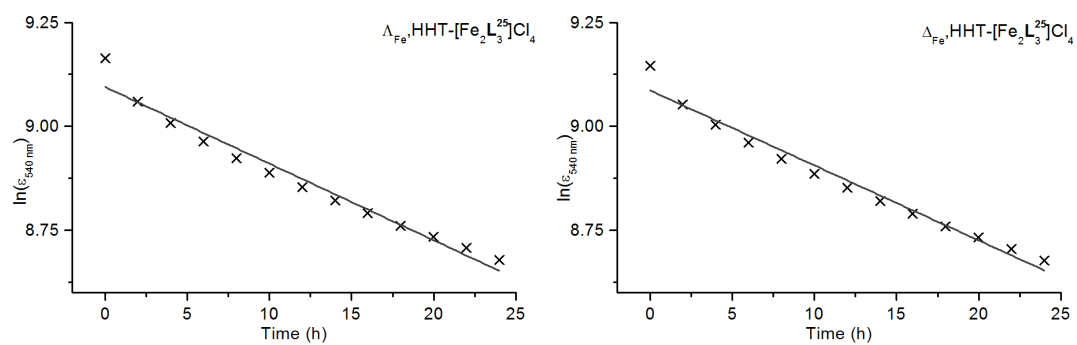


Figure A.3 | $\ln(\epsilon)$ at 540 nm (corresponding to MLCT band) of iron(II) chloride flexicates and triplex metalloheliices (0.03 mM in 0.2 M HCl).

A.2 Thermogravimetric analysis

The % mass lost was plotted against temperature and the % mass loss between ambient temperature and 200°C (loss of water) was recorded. A worked example of $\Delta_{\text{Fe}}\text{-}[\text{Fe}_2\text{L}^4_3]\text{Cl}_4.n\text{H}_2\text{O}$ is shown here (mass lost = 11.4%);

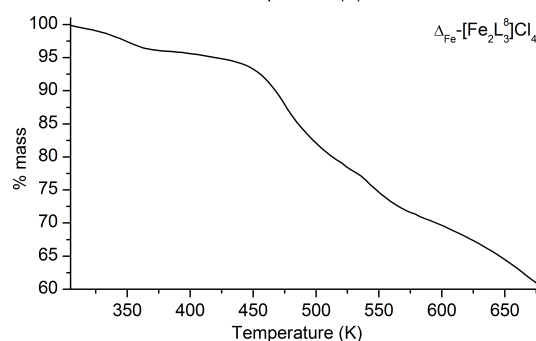
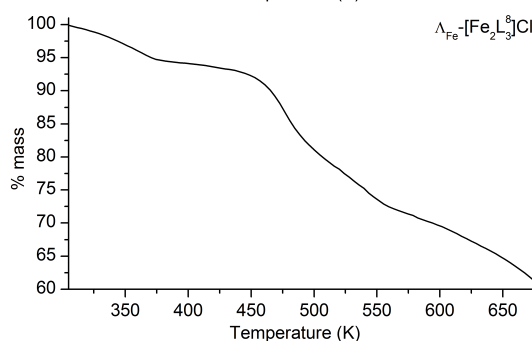
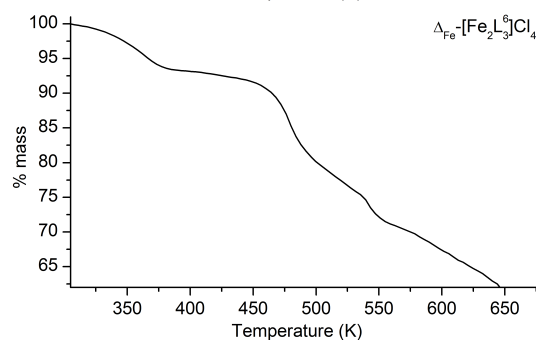
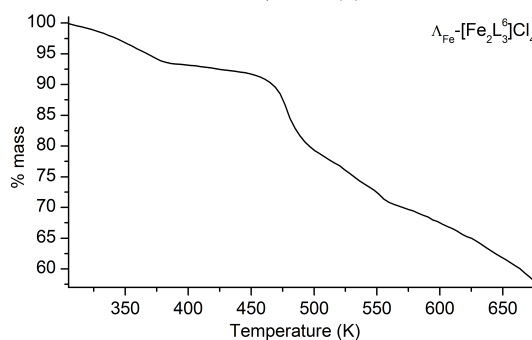
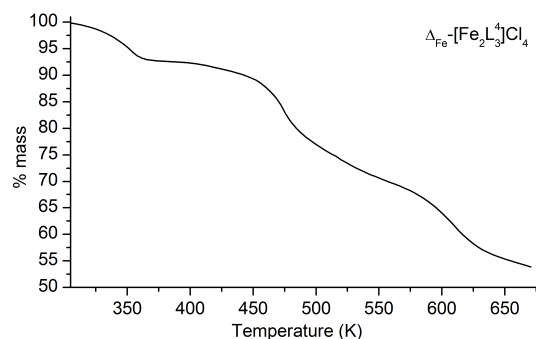
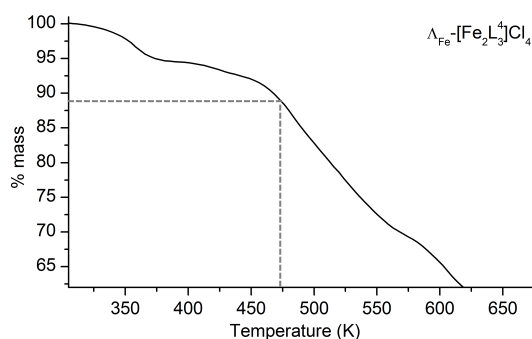
$$n = \frac{m_{\%} \times Mr_{anh}}{18(100 - m_{\%})}$$

n - stoichiometric equivalents of water

$m_{\%}$ - percentage mass loss

Mr_{anh} - anhydrous molecular weight

$$\frac{11.4 \times 1821.44}{18(100 - 1821.44)} = 13$$



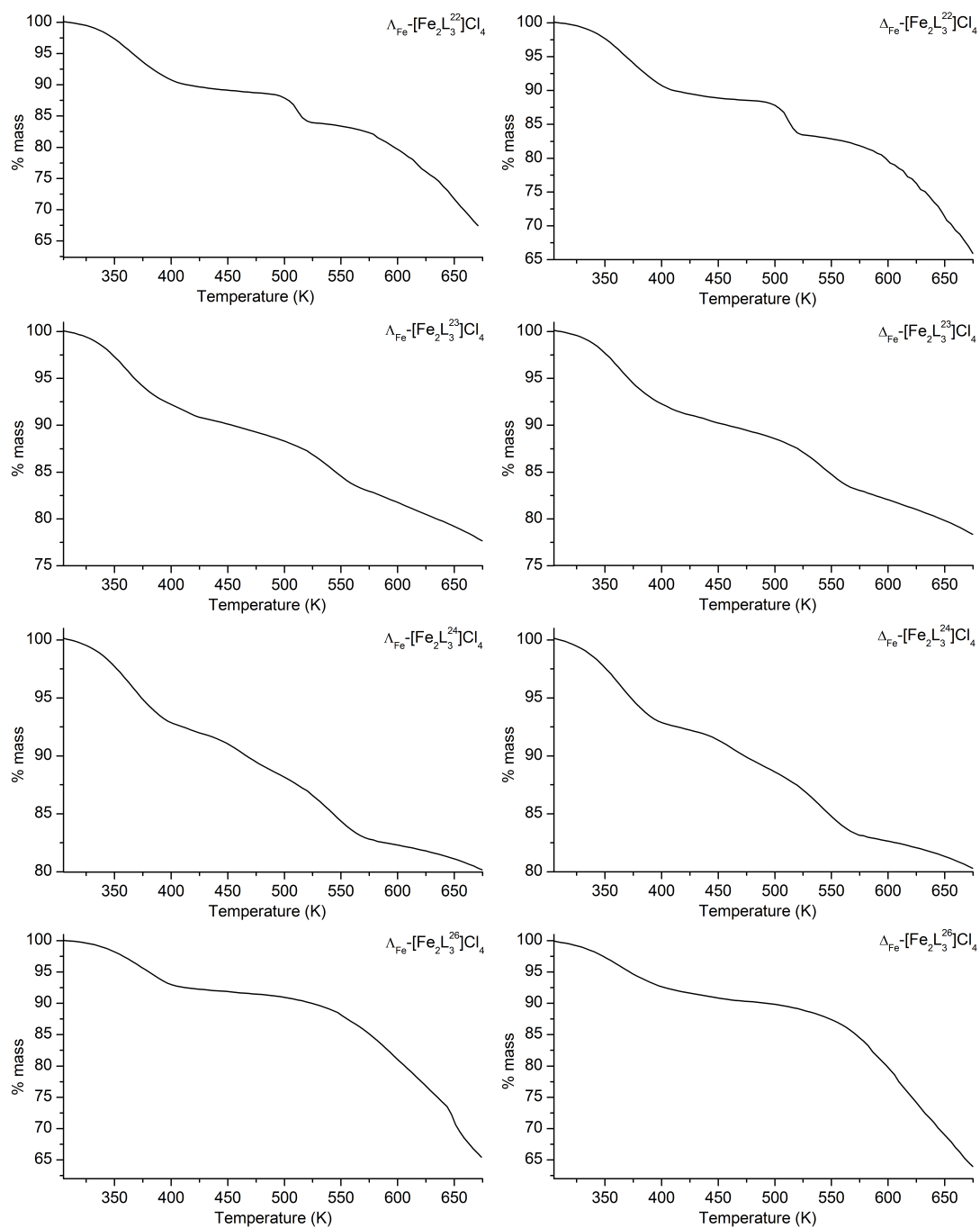


Figure A.4 | Thermogravimetric analysis of iron(II) chloride flexicates and triplex metallohelices, indicating mass lost due to water of crystallisation and thermal decomposition.

A.3 IC₅₀ values

Table A1 | IC₅₀ values of cisplatin, [Fe₂L^H₃]Cl₄ and all iron(II) chloride complexes against MDA-MB-468, HCT116 p53^{+/+}, HCT116 p53^{-/-} and ARPE19 cells over 96 h, and HCT116 p53^{+/+} cells over 24 h.

Complex	MDA-MB-468 /μM (esd)	HCT116 p53 ^{+/+} /μM (esd)	HCT116 p53 ^{-/-} /μM (esd)	ARPE19/μM (esd)	HCT116 p53 ^{+/+} 24h /μM (esd)
cisplatin	2.44 (0.49)	3.51 (1.50)	8.12 (1.83)	3.43 (0.48)	52.18 (3.30)
[Fe ₂ L ^H ₃]Cl ₄	5.29 (1.28)	10.36 (0.60)	14.83 (4.06)	44.54 (2.16)	79.58 (18.61)
Λ _{Fe} ⁻ [Fe ₂ L ^S ₃]Cl ₄	4.06 (0.85)	0.61 (0.31)	0.07 (0.004)	18.69 (2.09)	4.88 (1.36)
Δ _{Fe} ⁻ [Fe ₂ L ^S ₃]Cl ₄	3.72 (0.68)	1.66 (1.05)	0.09 (0.04)	13.90 (1.14)	4.51 (0.67)
Λ _{Fe} ⁻ [Fe ₂ L ^I ₃]Cl ₄	7.29 (0.29)	0.62 (0.08)	0.36 (0.04)	7.00 (0.82)	4.11 (0.85)
Δ _{Fe} ⁻ [Fe ₂ L ^I ₃]Cl ₄	8.36 (0.37)	0.87 (0.13)	0.43 (0.06)	12.06 (0.31)	4.52 (0.84)
Λ _{Fe} ⁻ [Fe ₂ L ⁴ ₃]Cl ₄	0.21 (0.10)	4.29 (1.85)	2.29 (0.32)	-	>100
Δ _{Fe} ⁻ [Fe ₂ L ⁴ ₃]Cl ₄	0.24 (0.07)	0.58 (0.25)	1.44 (0.60)	-	41.60 (13.84)
Λ _{Fe} ⁻ [Fe ₂ L ⁵ ₃]Cl ₄	0.73 (0.22)	3.85 (0.94)	3.37 (1.21)	-	6.42 (1.30)
Δ _{Fe} ⁻ [Fe ₂ L ⁵ ₃]Cl ₄	0.49 (0.01)	3.48 (0.19)	1.71 (0.77)	-	6.50 (0.85)
Λ _{Fe} ⁻ [Fe ₂ L ⁶ ₃]Cl ₄	4.80 (3.27)	3.67 (0.54)	0.41 (0.17)	21.28 (5.47)	22.45 (6.43)
Δ _{Fe} ⁻ [Fe ₂ L ⁶ ₃]Cl ₄	3.59 (1.52)	0.36 (0.05)	0.04 (0.003)	33.42 (8.25)	27.85 (9.02)
Λ _{Fe} ⁻ [Fe ₂ L ⁸ ₃]Cl ₄	0.84 (0.06)	0.27 (0.03)	2.68 (0.49)	-	6.75 (1.66)
Δ _{Fe} ⁻ [Fe ₂ L ⁸ ₃]Cl ₄	0.54 (0.002)	0.48 (0.04)	0.58 (0.18)	-	15.57 (5.86)
Λ _{Fe} ,HHT-[Fe ₂ L ²¹ ₃]Cl ₄	29.27 (13.94)	0.98 (0.60)	0.16 (0.05)	8.03 (0.39)	31.34 (1.89)
Δ _{Fe} ,HHT-[Fe ₂ L ²¹ ₃]Cl ₄	27.34 (4.83)	2.85 (0.37)	0.97 (0.24)	5.79 (1.83)	22.76 (1.86)
Λ _{Fe} ,HHT-[Fe ₂ L ²² ₃]Cl ₄	21.11 (1.73)	1.06 (0.51)	0.37 (0.01)	-	48.96 (3.21)
Δ _{Fe} ,HHT-[Fe ₂ L ²² ₃]Cl ₄	38.43 (9.94)	9.00 (1.59)	2.10 (0.75)	-	42.27 (6.24)
Λ _{Fe} ,HHT-[Fe ₂ L ²³ ₃]Cl ₄	6.44 (1.10)	3.15 (0.79)	0.99 (0.05)	-	7.47 (1.98)
Δ _{Fe} ,HHT-[Fe ₂ L ²³ ₃]Cl ₄	6.52 (0.93)	5.21 (1.04)	1.70 (0.09)	-	22.76 (1.86)
Λ _{Fe} ,HHT-[Fe ₂ L ²⁴ ₃]Cl ₄	7.78 (1.25)	5.28 (0.49)	2.39 (0.44)	-	13.84 (1.48)
Δ _{Fe} ,HHT-[Fe ₂ L ²⁴ ₃]Cl ₄	5.96 (1.10)	10.02 (3.32)	4.23 (0.34)	-	15.67 (2.50)
Λ _{Fe} ,HHT-[Fe ₂ L ²⁶ ₃]Cl ₄	9.47 (0.52)	1.06 (0.13)	0.56 (0.09)	10.75 (3.14)	15.07 (1.03)
Δ _{Fe} ,HHT-[Fe ₂ L ²⁶ ₃]Cl ₄	9.90 (0.64)	1.94 (0.24)	0.77 (0.23)	-	9.44 (1.71)
Λ _{Fe} ,HHT-[Fe ₂ L ^{F1} ₃]Cl ₄	7.06 (2.95)	1.41 (0.78)	-	-	-
Δ _{Fe} ,HHT-[Fe ₂ L ^{F1} ₃]Cl ₄	16.64 (7.82)	0.41 (0.01)	-	-	-
Λ _{Fe} ,HHT-[Fe ₂ L ^{F2} ₃]Cl ₄	58.49 (31.70)	31.08 (9.15)	-	-	-
Δ _{Fe} ,HHT-[Fe ₂ L ^{F2} ₃]Cl ₄	29.10 (6.99)	9.43 (2.85)	-	-	-
Λ _{Fe} ,HHT-[Fe ₂ L ^{F3} ₃]Cl ₄	71.34 (2.58)	4.28 (1.84)	-	-	-
Δ _{Fe} ,HHT-[Fe ₂ L ^{F3} ₃]Cl ₄	16.13 (3.54)	4.83 (2.90)	-	-	-
Λ _{Fe} ,HHT-[Fe ₂ L ^{F4} ₃]Cl ₄	16.72 (3.07)	1.79 (1.45)	-	-	-
Δ _{Fe} ,HHT-[Fe ₂ L ^{F4} ₃]Cl ₄	12.60 (5.83)	1.08 (0.42)	-	-	-
Λ _{Fe} ,HHT-[Fe ₂ L ^{F5} ₃]Cl ₄	18.65 (2.11)	10.36 (3.18)	-	-	-
Δ _{Fe} ,HHT-[Fe ₂ L ^{F5} ₃]Cl ₄	6.61 (2.15)	3.60 (0.35)	-	-	-

Appendix B

B.1 Optically pure heterobimetallic helicates

From “Optically pure heterobimetallic helicates from self-assembly and clock strategies” S. E. Howson, G. J. Clarkson, A. D. Faulkner, R. A. Kaner, M. J. Whitmore & P. Scott, *Dalton Trans*, 2013, **42**, 14967-14981.

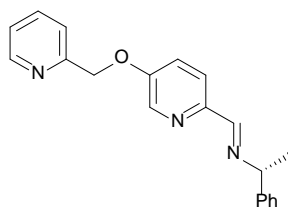


Figure B.1 | Structure of L^{26} designed for formation of a heterobimetallic complex.

The first attempt to synthesise complexes with a reduced symmetry with a ligand based on the chiral iminopyridine unit described previously was to create an optically pure mixed iron (II) copper (I) system with an asymmetric ligand (**AB–C**) containing a pyridine unit bound to the chiral iminopyridine. It is possible to form C_3 helical isomers when the pyridine is bound as a phenylglycinol derived ether, with one copper (I) bound by the three pyridine units. However if the pyridine unit is bound by the pyridine of the chiral part of the ligand this was not successful, probably because in the precursor $[FeL^{26}_3]^{2+}$ complex the three pyridine units sit too far apart to bind a copper (I) cation due to the rigid nature of the coupling of the two parts of the ligand, as can be seen in the single crystal structure of that complex.

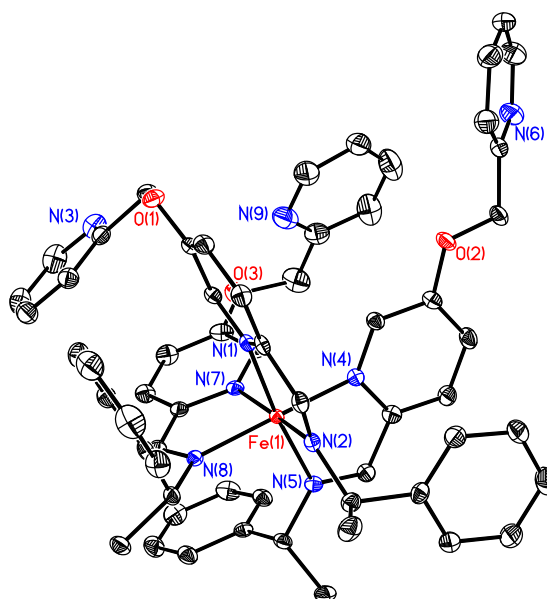
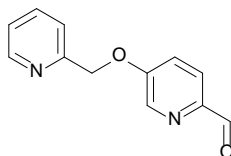


Figure B.2 | Structure of the cation in the asymmetric unit of *fac,Λ*_{Fe}*R*_C-[FeL²⁶](ClO₄)₂·CH₃CN (H atoms, counterions and solvent molecules omitted for clarity). Thermal ellipsoids are shown at 50% probability. Selected bond lengths (Å) and angles (°): Fe(1)-N(1) 1.9745(14), Fe(1)-N(4) 1.9804(15), Fe(1)-N(7) 1.9748(15), Fe(1)-N(2) 1.9788(15), Fe(1)-N(5) 1.9789(15), Fe(1)-N(8) 1.9874(14); N(1)-Fe(1)-N(2) 81.58(6), N(4)-Fe(1)-N(5) 81.16(6), N(7)-Fe(1)-N(8) 81.22(6).

B.2 Experimental details

5-(2-Pyridinyloxy)picolinaldehyde



2-(bromomethyl)pyridine hydrobromide (0.5 g, 1.97 mmol) was dissolved in DMF (10 ml). Potassium carbonate (0.68 g, 4.92 mmol) was added followed by 5-hydroxypicolinaldehyde (0.24 g, 1.97 mmol) and the mixture was stirred at 100 °C for 16 h. The solvent was removed under reduced pressure to give a dark brown solid which was extracted with chloroform (3 × 50 ml), washed with NaOH solution (1M, 3 × 100 ml) and saturated brine solution (3 × 100 ml) and dried over MgSO₄ before evaporation under reduced pressure to give a light brown solid.

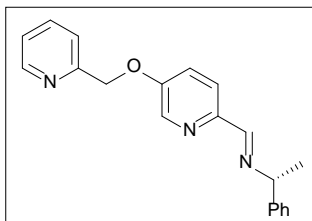
Yield 0.31 g, 73%

¹H NMR (300 MHz, 298 K, CDCl₃) δ_H 9.99 (1H, s, CHO), 8.62 (1H, d, ³J_{HH} = 4.5 Hz), 8.54 (1H, d, ³J_{HH} = 2.5 Hz), 7.94 (1H, d, ³J_{HH} = 8.5 Hz), 7.75 (1H, td, ³J_{HH} = 8.0 Hz, ⁴J_{HH} = 1.5 Hz), 7.51 (1H, d, ³J_{HH} = 8.0 Hz), 7.39 (1H, dd, ³J_{HH} = 8.5 Hz, ⁴J_{HH} = 2.5 Hz), 7.29 (1H, dd, ³J_{HH} = 7.5 Hz, ⁴J_{HH} = 4.5 Hz, Py), 5.33 (2H, s, CH₂).

¹³C{¹H} NMR (101 MHz, 298 K, CDCl₃) δ_C 192.1 (CHO), 158.0, 155.5, 149.7, 146.8, 139.3, 137.2, 123.5, 123.4, 121.7, 121.2 (Py), 71.43 (CH₂)

MS (ESI) m/z 215 [M+H]⁺, 237 [M+Na]⁺

Elemental Analysis found (Calculated for C₁₂H₁₀N₂O₂) % C 66.16 (67.28), H 4.48% (4.70) N 12.86 (13.07).

***fac*,Λ_{Fe},-[FeL²⁶₃](ClO₄)₂.3H₂O**

(*R*)-(+)-α-methylbenzylamine (0.30 ml, 2.33 mmol) was dissolved in acetonitrile (10 ml). 5-(2-Pyridinyloxy)picolinaldehyde (0.5 g, 2.33 mmol) was added, followed by iron (II) perchlorate hexahydrate (0.282 g, 0.78 mmol) to give an immediate colour change to dark pink/purple. After stirring at ambient temperature for 16 h, addition of ethyl acetate (10 ml) caused precipitation of a dark purple powder (0.667 g, 70 %) that contained water of crystallisation according to IR spectroscopy. Single crystals were grown by layering a solution in acetonitrile onto ethyl acetate.

¹H-NMR (300 MHz, 298 K, CD₃CN) δ_H 8.51 (6 H, bs, 6H, CHN/Ar), 7.78 (3H, t, ³J_{HH} = 7.5 Hz), 7.25-7.41 (12H, m), 7.05 (3H, t, ³J_{HH} = 7.0 Hz), 6.92 (3H, t, ³J_{HH} = 7.5 Hz), 6.51 (3H, d, ³J_{HH} = 7.5 Hz), 6.35 (3H, d, ³J_{HH} = 2.0 Hz), 5.05-5.20 (9H, m, CH/CH₂), 1.87 (9H, d, ³J_{HH} = 6.5 Hz, CH₃).

¹³C{¹H} NMR (75 MHz, 298 K, CD₃CN) δ_C 170.3 (CHN), 157.9, 155.7, 152.5, 150.5, 143.0, 141.1, 138.2, 130.8, 130.0, 128.3, 125.4, 124.6, 124.5, 123.2, 72.2 (CH₂), 69.3 (CH)

MS (ESI) *m/z* 345 [FeL₂]²⁺, 503 [FeL₃]²⁺, 789 [FeL₂.ClO₄]⁺

Elemental analysis found (calculated for C₆₀H₅₇Cl₂FeN₉O₁₁.3H₂O) % C 57.16 (57.15), H 4.58 (5.04), N 9.79 (10.00).

The crystal data for *fac*, $\Lambda_{\text{Fe},R_{\text{C}}}$ -[FeL²⁷₃](ClO₄)₂ (CCDC 947142) was collected using an Xcalibur Gemini diffractometer with a Ruby CCD area detector using CuK $_{\alpha}$ (λ = 1.54184 Å) radiation source. The structures were solved with the XS structure solution program using Direct Methods and refined with the ShelXL¹ refinement package using Least Squares minimisation.

1. G. M. Sheldrick, *Acta Crystallogr., Sect. A*, 2008, **64**, 112-122.